[redacted]

NASA-CR-72517

GA-8974

[redacted] Unclassified)

STUDIES OF THERMIONIC MATERIALS FOR SPACE POWER APPLICATIONS

SUMMARY REPORT

NOVEMBER 23, 1965 THROUGH SEPTEMBER 30, 1968

by

Members of the Direct Conversion Project

Prepared for
National Aeronautics and Space Administration
Lewis Research Center
under Contract NAS 3-6471

[redacted]

[redacted]

Gulf General Atomic
Incorporated
P. O. Box 608, San Diego, California 92112

Issued: June 3, 1969

[redacted]

NOTICE

This report was prepared as an account of Government sponsored work. Neither the United States, nor the National Aeronautics and Space Administration (NASA), nor any person acting on behalf of NASA:

A. Makes any warranty or representation, expressed or implied, with respect to the accuracy, completeness, or usefulness of the information contained in this report, or that the use of any information, apparatus, method, or process disclosed in this report may not infringe privately owned rights; or

B. Assumes any liabilities with respect to the use of, or for damages resulting from the use of any information, apparatus, method or process disclosed in this report.

As used above, "person acting on behalf of NASA" includes any employee or contractor of NASA, or employee of such contractor, to the extent that such employee or contractor of NASA, or employee of such contractor prepares, disseminates, or provides access to, any information pursuant to his employment or contract with NASA, or his employment with such contractor.

Requests for copies of this report should be referred to

National Aeronautics and Space Administration
Office of Scientific and Technical Information
Attention: AFSS-A
Washington, D. C. 20546

[redacted] C69-2004

Gulf General Atomic
Incorporated
P. O. Box 608, San Diego, California 92112

NASA-CR-72517
GA-8974
Copy No. [illegible]

(Title Unclassified)

STUDIES OF THERMIONIC MATERIALS FOR SPACE POWER APPLICATIONS

SUMMARY REPORT

NOVEMBER 23, 1965 THROUGH SEPTEMBER 30, 1968

by

Members of the Direct Conversion Project

Sponsored by
National Aeronautics and Space Administration
Lewis Research Center

Technical Management
NASA-Lewis Research Center
Reactor Irradiation Branch
J. W. R. Creagh and J. R. Smith

During the period of this report, the following "reportable items" as defined by the article "Report of New Technology" evolved: Methods for fabricating a multi-wire high temperature thermocouple using a swageable hot junction.

[redacted]

[redacted]

Contract: NAS 3-6471

Issued: June 3, 1969

[redacted]

[redacted]

PREVIOUS SUMMARY REPORTS IN THIS SERIES

Contract NAS 5-1253	GA-3523, Final Report for the Period Ending August 31, 1962. (U)
Contract NAS 3-2301	GA-3642, Final Report for the Period Ending August 31, 1962. (U)
Contract NAS 3-2532	GA-4769, Final Report for the Period Ending August 31, 1963. Part I (U), Part II (C/RD)
Contract NAS 3-4165	NASA CR-54322, GA-5665, Summary Report for the Period September 1, 1963 through August 31, 1964. (C/RD)
Contract NAS 3-6471	NASA CR-54980, GA-6860, Summary Report for the Period September 1, 1964 through November 23, 1965. (C/RD)
Contract NAS 3-8504	NASA CR-72315, GA-7682, Summary Report for the Period November 23, 1965 through January 31, 1967 (C/RD)
Contract NAS 3-8504	NASA CR-72327, GA-7745, Semi-Annual Report for the Period February 1, 1967 through July 31, 1967. (C/RD)

[redacted]

(This page is Unclassified)

[redacted]

[redacted]

CONTENTS

[redacted]

FIGURES

Figures (continued)

[redacted]

Figures (continued)

[redacted]

[redacted]

Figures (continued)

[redacted]

[redacted]

Figures (continued)

TABLES

[redacted]

SUMMARY

(U) Post-operation examinations of LC-1 and LC-2 converters were completed and the results obtained were presented in a topical report.[1]

(U) Four life-test converters, LC-6, LC-7, LC-8 and LC-9 were fabricated. LC-6 and LC-8 were fueled with 50UC-50ZrC and 90UC-10ZrC respectively; while LC-7 and LC-9 were unfueled, with one (LC-7) containing a fluoride tungsten emitter of {100} preferred crystal orientation and the other (LC-9) containing a chloride tungsten emitter of {110} preferred crystal orientation on a fluoride tungsten substrate. Details were given on developments and processing of component materials, emitter characterization and converter assembly procedures.

(U) Capsules V-2A and V-2B were irradiated at NASA Plum Brook Reactor Facility for two cycles before the test was terminated because of the malfunction of the capsule positioning mechanism. A parametric analysis of the relationship among fuel temperature, fission power density and thermal bond temperature was carried out, taking into account the uncertainty limits in the various thermal and mechanical parameters of the capsule design. The results were used to evaluate the observed fuel temperature versus thermal bond temperature relationship, and to deduce the fuel temperature, the fission power density, and the uncertainty ranges of these quantities as a function of irradiation time.

(U) A new capsule design was established for the study of the irradiation properties of fluoride tungsten clad UC-ZrC samples in a configuration similar to that of a fueled emitter in a thermionic fuel element. Fabrication developments, including joining and bonding of metal components, fabrication and evaluation of tungsten-rhenium high temperature thermocouples, and preparation of Inconel surface of stable and high emittance were carried out. 90UC-10ZrC and 50UC-50ZrC samples of various surface

INTRODUCTION

(U) This report describes the work carried out from November 23, 1965 through September 30, 1968, the completion date for Contract NAS 3-6471. Two subjects were included under this contract during the reporting period specified above. These are:

1. Fabrication and post-operation examination of out-of-pile converters.
2. Irradiation studies of thermionic materials.

Studies of other subjects of nuclear thermionic interest are being pursued concurrently with these two subjects under Contracts NAS 3-8504 and NAS 3-11822. A list of summary reports issued under previous NASA contracts related to thermionic materials development at Gulf General Atomic is shown at the front of this report.

area to volume ratios, containing about 4 wt% of tungsten and having a carbon to uranium ratio of 1.03 to 1.05, were prepared. Two capsules, V-2C and V-2D, containing the 90UC-10ZrC and the 50UC-50ZrC samples respectively, were assembled and delivered to NASA Plum Brook Reactor Facility for irradiation at a cladding temperature of 1650°C.

[redacted]

PART I. FABRICATION AND POST-OPERATION EXAMINATION OF OUT-OF-PILE CONVERTERS

(U) The work included in Part I of Contract NAS 3-6471 during this reporting period consists of:

1. Post-operation examination of LC-1 and LC-2 converters.
2. Fabrication of LC-6, LC-7, LC-8 and LC-9 converters.

The detail description and discussion of results of the post operation examination of LC-1 and LC-2 converters have been given in a topical report[1] and therefore are not repeated in this report. The specific features of LC-6 through LC-9 converters and their fabrication procedures are described below.

1.1. CONVERTER DESIGN AND SPECIFIC FEATURES

(C-RD)(Gp-1) Of the four converters fabricated during this reporting period, LC-6 and LC-8 are fueled with 50UC-50ZrC and 90UC-10ZrC respectively, while LC-7 and LC-9 are unfueled. The essential design features of the LC series life test converters and their accessories have been described previously for converters LC-1 through LC-5.[2] No change was introduced to these design features when converter LC-6 was fabricated. Some modifications, however, were made in the design of the accessories of LC-7, LC-8 and LC-9 converters. The two major aspects are:

(1) Improvement of the designs of the electron bombardment filament and filament holder. Previously a double helix filament was used and no guide was available in the filament holder to allow the filament to be positioned reproducibly at the center of the emitter cavity. Filament sagging and mis-positioning affected the filament life and performance and tended to change the

[redacted]

temperature profile of the emitter surface. To overcome these difficulties, a single helix filament wound around a thick tungsten central post was used. The lower terminal of the filament was welded to the lower end of the tungsten central post. In addition, the filament holder was attached to the top of the tantalum transition piece of the emitter by a tapered joint which helped to locate the filament at the center of the emitter cavity.

(2) Adoption of a collector heat sink incorporating a variable thermal conductance gas gap. Previously the collector and the cooling water coil were separated by metal webs the thermal conductance of which was fixed. The use of a variable thermal conductance gas gap lends flexibility to collector heat flux handling and thus facilitates converter operation and converter performance mapping.

(C-RD)(Gp-1) In addition to these design modifications, several significant changes were made in the component materials of converters LC-7, LC-8 and LC-9. These are:

(1) The use of niobium instead of molybdenum as collector material, since the thermal expansion of niobium matches more closely with the Al_2O_3 in the sheath insulator of a thermionic fuel element.

(2) The use of carbon rich (a few mole percent) 90UC-10ZrC containing tungsten addition (~4 wt%) as the fuel material in LC-8 emitter, because the excess carbon is believed necessary to maintain emitter work function stability and the tungsten addition is needed to prevent the dissolution of tungsten cladding by the carbide fuel. Previously near-stoichiometric carbide fuels containing no tungsten addition were used.

(3) The use of a duplex tungsten emitter in LC-9, which consists of a partially {110} oriented chloride tungsten* emitting layer of 12.5 mil thickness deposited on a 27.5 mil thick fluoride tungsten* substrate. This chloride tungsten emitter layer had a vacuum work function of 4.8 eV, as compared to 4.5 eV for a fluoride tungsten emitter. It was anticipated that converters containing such emitters of higher vacuum work functions would perform better than those containing fluoride tungsten emitters.

(U) Figure 1.1 shows the modified converter design and Table 1.1 lists the materials used for the major components of these converters. The emitters of LC-7, LC-8 and LC-9 all have a diameter of 0.625 inch and an active length of 1.25 inch. The interelectrode spacing was 0.009 inch (hot) for all these converters.

1.2. CONVERTER FABRICATION

(U) The assembly of LC-6 converter was completed during the previous contractual year but its final bakeout was carried out in this contractual period. Information on its assembly can be found in the previous summary report.(2) The following describes the fabrication methods for LC-7, LC-8 and LC-9 converters and the final bakeout data for LC-6 converter.

1.2.1. Assembly Sequence

(U) Figure 1.2 shows the converter components before assembly. Figure 1.3 describes the assembly sequence. The important steps involved are elaborated in more detail in the following sections.

---

*Chloride tungsten = tungsten formed by the hydrogen reduction of tungsten chlorides. Fluoride tungsten = tungsten formed by the hydrogen reduction of tungsten hexafluoride.

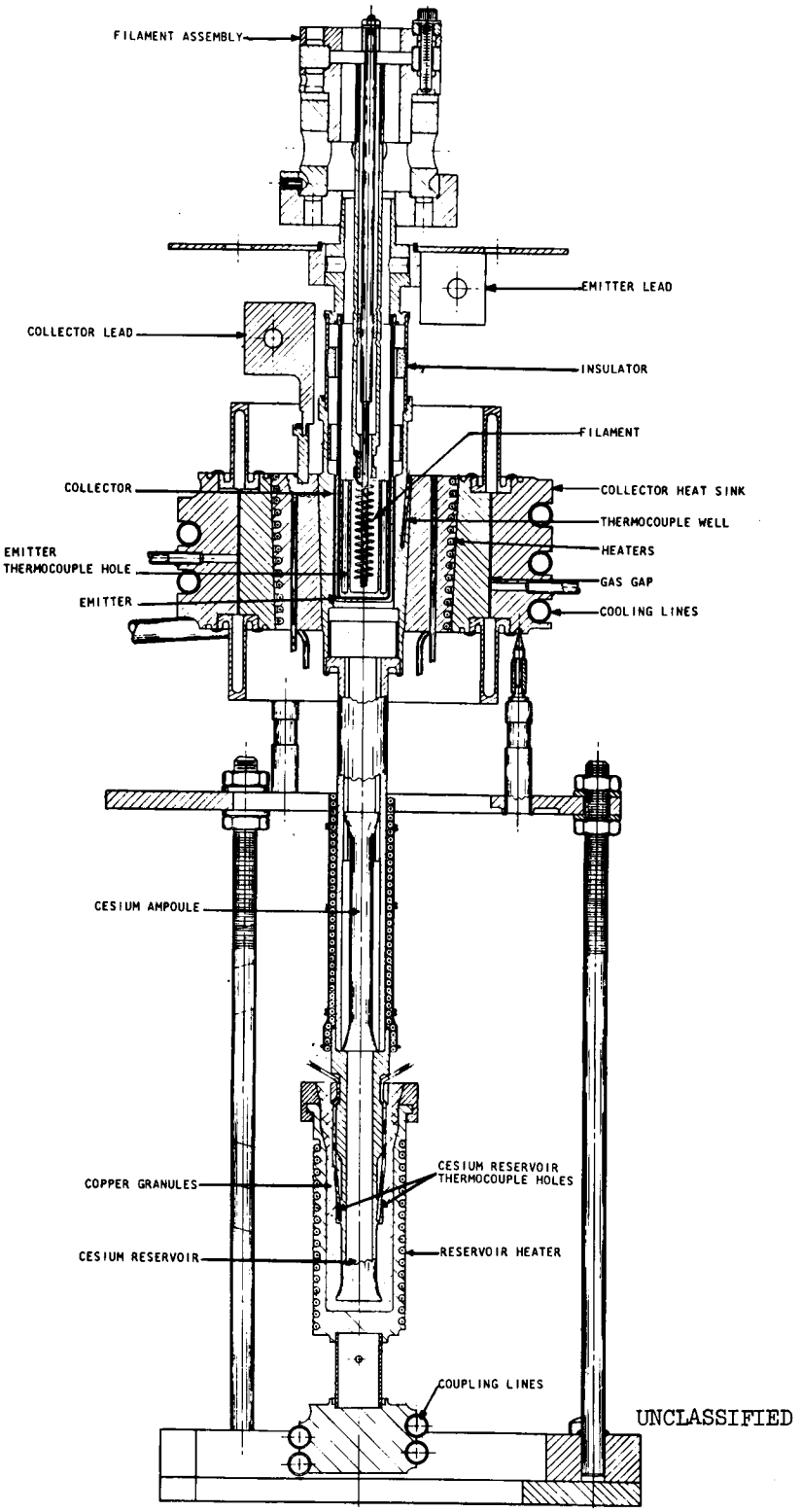

Fig. 1.1--(U) Converter design

(This page is Unclassified)

[redacted]

Table 1.1

(U) CONVERTER COMPONENT MATERIALS

(This table is classified Confidential-Restricted Data-Group 1)

Component	Material
Emitter	Chemically vapor-deposited tungsten - duplex tungsten for LC-9; fluoride tungsten for the rest.
Collector	Molybdenum for LC-6; electron beam melted niobium for the rest.
Cesium lead tube	Electron beam melted niobium.
Cesium ampoule	Vacuum melted Kovar.
Insulator	
Skirt material	Niobium
Ceramic	Al_2O_3 (Lucalox)
Braze	Cu-10% Ni
Metallizing	GGA modified version of Litton composition
Cesium reservoir	OFHC copper
Transition piece	Electron beam melted tantalum
Emitter-to-transition piece braze	Vanadium
Collector-to-insulator skirt braze	Copper-titanium

[redacted]

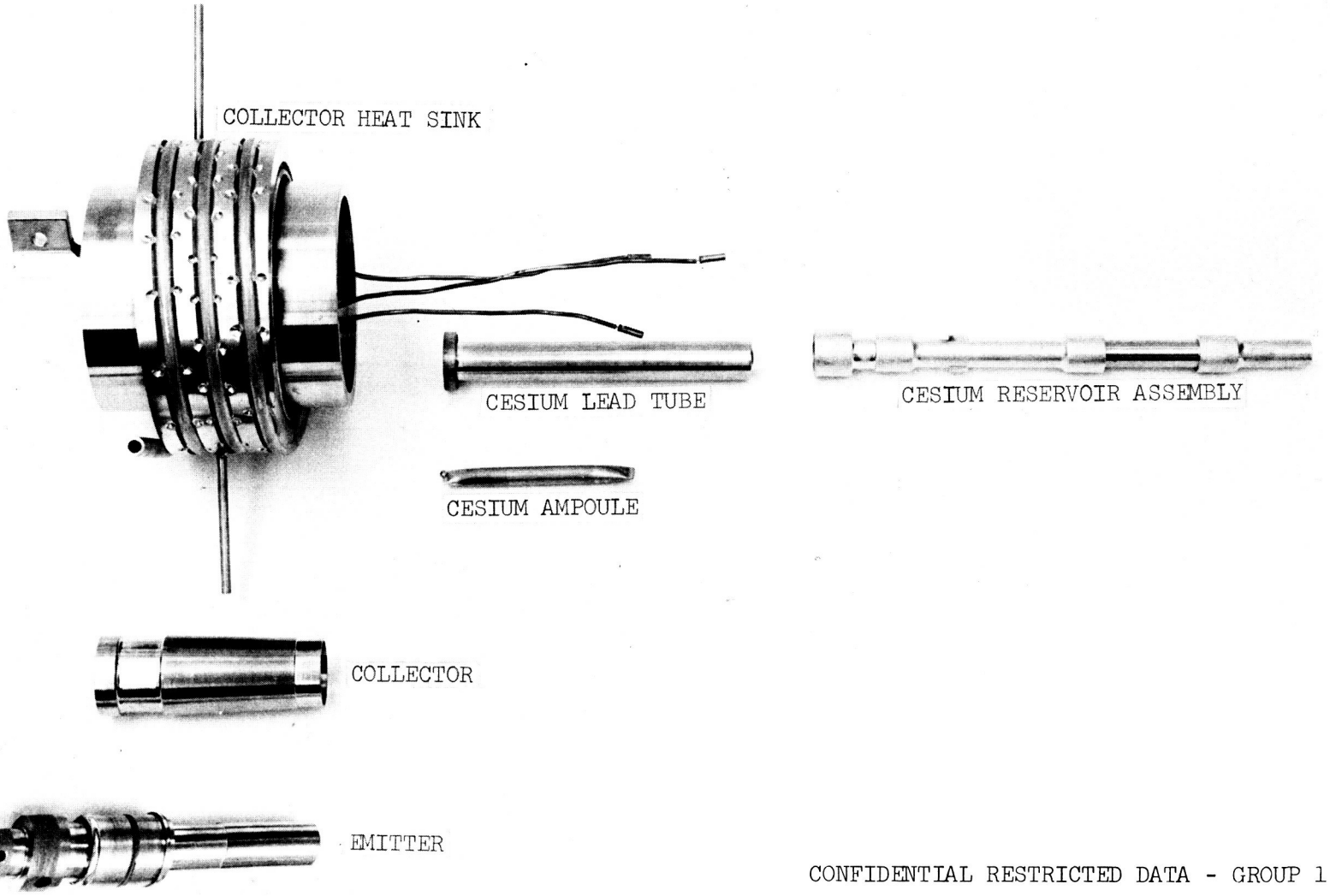

CONFIDENTIAL RESTRICTED DATA - GROUP 1

Fig. 1.2--(U) Converter components before assembly

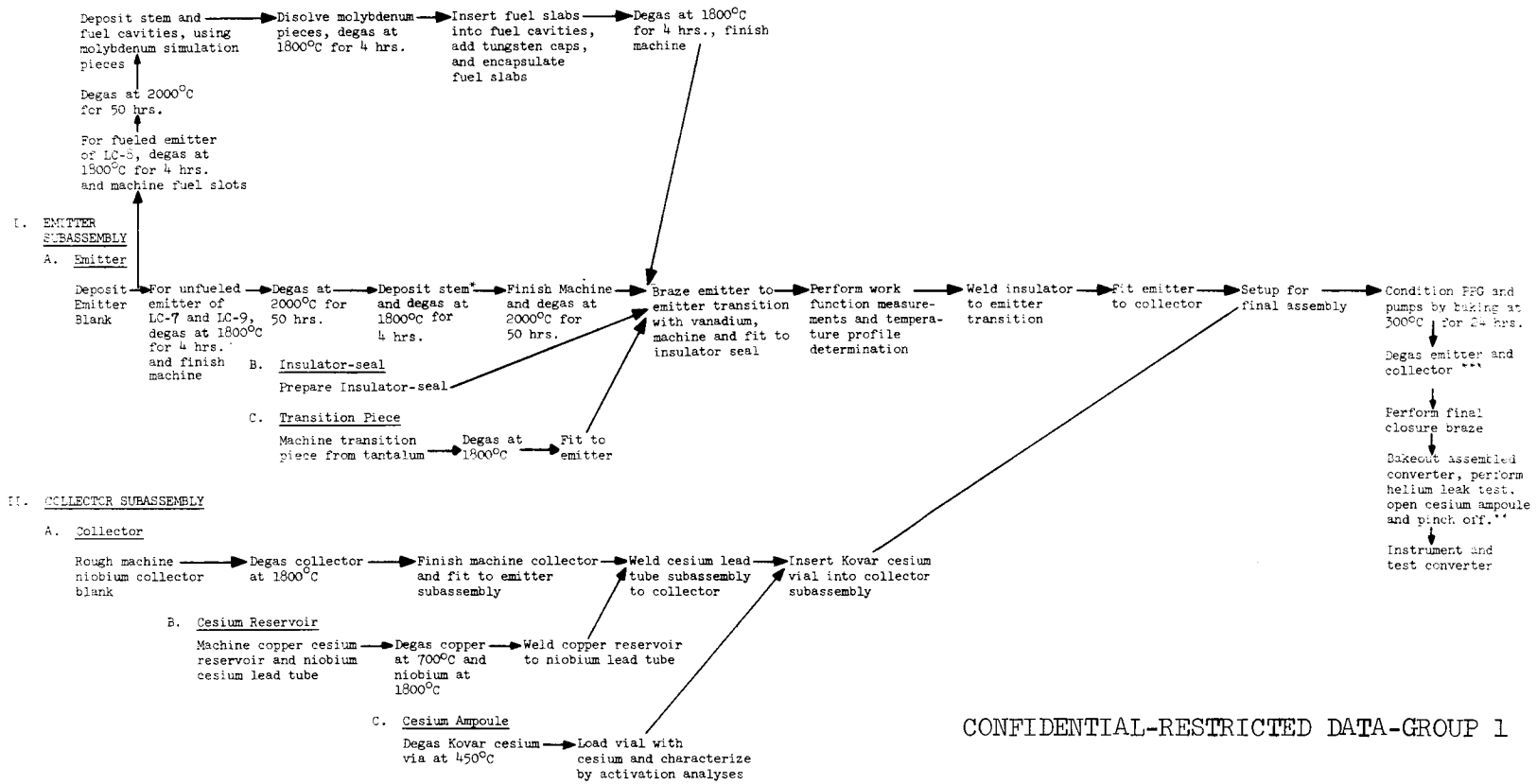

CONFIDENTIAL-RESTRICTED DATA-GROUP 1

*For LC-9, an additional deposition of tungsten (from the hexachloride) was performed and finish machined at this point.

**For LC-6, the cesium ampoule was opened after the converter was pinched off.

***See section 1.2.6 for temperature and time

Fig. 1.3--(U) Assembly sequence

1.2.2. Component Bulk Bakeout

(C-RD)(Gp-1) Bulk bakeout of rough machined active metal components (the niobium collectors and cesium lead tubes, and the tantalum transition pieces) was accomplished by electron bombardment in an ion-pumped, all metal sealed vacuum chamber.

(C-RD)(Gp-1) The emitters, copper cesium reservoirs and the Kovar cesium ampoules were bulk baked out by electron bombardment in cold-trapped diffusion pumped vacuum systems or furnaces except for the final bakeout of the LC-8 and the LC-9 emitters which were accomplished in a Vac-Ion pumped, all metal sealed resistance furnace. The bulk bakeout temperatures, times and maximum pressures are shown in the following table:

Table 1.2

(U) CONDITIONS FOR BULK OUTGASSING OF CONVERTER COMPONENTS
(This table is classified Confidential-Restricted Data-Group 1)

	Temp	Time	Maximum Total Pressure of Active Gases (N_2 Equivalents)
Tungsten	2000°C	50 hrs	10^{-8} torr range
Niobium	1800°C	4 hrs	10^{-8} torr range
Tantalum	1800°C	4 hrs	10^{-8} torr range
Copper	700°C	50 hrs	10^{-7} torr range
Kovar	450°C	50 hrs	10^{-7} torr range

During bakeout of the niobium and tantalum converter components, the chamber pressure and constitution were monitored with a Varian Associates Partial Pressure Gauge. A typical residual gas analysis (taken during bakeout of the collectors) is shown below:

Table 1.3

(U) RESIDUAL GAS ANALYSIS OF CHAMBER WITH NIOBIUM COLLECTORS AT 1800°C AFTER 4 HOURS

(This table is classified Confidential-Restricted Data-Group 1)

Gas	True Partial Pressure (torr)
H_2	2.39×10^{-7} (67% of gas load)
CH_4	6.07×10^{-9}
H_2O	5.46×10^{-8}
CO, N_2	1.4×10^{-8}
Ar	2.79×10^{-8}
CO_2	1.99×10^{-8}
Calculated Total Pressure	3.62×10^{-7}

[redacted]

1.2.3. Preparation of Fueled Emitter

1.2.3.1. Fuel Material

(C-RD)(Gp-1) Preparation of the 50UC-50ZrC fuel slabs for LC-6 followed the same procedures described in a previous topical report.[3] The finished fuel slabs had a composition of $U_{0.49}Zr_{0.51}C_{1.00}$ after final outgassing.

(C-RD)(Gp-1) The 90UC-10ZrC fuel material for LC-8 converter differs from that used in previous out-of-pile and in-pile converter tests in two respects, namely, the addition of tungsten and the close control of carbon to metal ratio to insure hyperstoichiometry in carbon.

(C-RD)(Gp-1) The addition of tungsten is motivated by the fact that a few percent of dissolved tungsten was found in 90UC-10ZrC which had been in contact with tungsten cladding for thousands of hours at 1800°C-1900°C.[1],[4] The dissolved tungsten, if not allowed its carbon share, may raise the uranium activity of the fuel and the uranium diffusion flux through the tungsten cladding, and thus may affect the electron emission properties of an emitter. Moreover, dissolution of the tungsten cladding by the fuel material impairs the mechanical stability of the cladding, especially if the fuel to cladding weight ratio is high and the dissolution occurs non-uniformly.

(C-RD)(Gp-1) The necessity of using carbon-rich carbide fuel has been established in previous diffusion-emission studies.[2] Tungsten clad 90UC-10ZrC containing a few mole percent of excess carbon has been shown to be able to maintain vacuum emission stability at 1900°C for 1000 hours, and at 1800°C for 10,000 hours. While the need of a few mole percent of excess carbon in the carbide fuel is recognized, it is not known, however, how high the carbon to metal ratio of the fuel can be before the fuel will carburize the tungsten cladding.

(C-RD)(Gp-1) Efforts were therefore made to develop techniques for preparing 90UC-10ZrC fuel materials containing about 3-4 wt% of tungsten and various amounts of excess carbon and to study the compatibility of these fuel materials with arc-cast tungsten (20 ppm C, complete analysis of

impurity content, see Reference (2) at 1800°C. The fabrication methods and the compatibility results are described as follows.

Sample Preparation

(C-RD)(Gp-1) The carbide samples for the compatibility studies, unless otherwise stated, are prepared according to the following procedures. Special attention is paid to minimizing the loss of carbon by atmospheric contamination.

(1) Arc-melt weighed amounts of U, Zr, and C into carbide buttons in an argon atmosphere.

(2) Grind the carbide button to -44μ size, in an argon atmosphere in a glove box, the moisture content of which is kept below 10 ppm.

(3) Blend the required amount (~4 wt%) of W powder with the carbide powder in an argon atmosphere in a glove box.

(4) Isostatic vacuum press the blended powder mixture in an elastomer die at 90,000 psi.

(5) Sinter and homogenize the pressed body in vacuum at 2285°C for 6 hours.

(6) Grind the sintered body to the required dimensions, with special attention paid to avoid atmospheric contamination by handling the carbide pieces under an argon atmosphere in a glove box and impregnating them with a removable hydrocarbon oil before grinding.

(7) Remove the impregnated oil from the finished carbide pieces by repeated rinsing with xylene, ultrasonic cleaning, and evacuating.

(8) Anneal the ground carbide pieces at 1800°C for 48 hours.

(9) Analyze the U, Zr, W and C contents and examine the microstructures of the annealed carbide.

Compatibiltiy Results

(C-RD)(Gp-1) Gross diffusion tests were carried out at 1800°C in an experimental arrangement similar to that employed in previous compatibility studies.(5) Carbide samples were sandwiched between tungsten samples in a tantalum die lined with tungsten foil. Table 1.4 summarizes the compositions of the carbide samples studied and the durations of the tests. Figures 1.4 through 1.8 show the appearances of the carbide samples and the tungsten samples after the diffusion runs. It can be seen that for carbide samples with a C/U ratio of about 1.05 or less (allowing one C atom for each Zr atom and one carbon atom for every two W atoms) no formation of tungsten carbide phase occurred. X-ray studies of carbide sample 10088 B-2 showed the presence of UC-ZrC, UWC_2 and a very small amount of free W. On the basis of these findings and the previous diffusion-emission results, it seems that a $\frac{C}{U}$ ratio of 1.03 to 1.05 should be considered safe from the point of view of maintaining emission stability and preventing carburization of the tungsten cladding.

(C-RD)(Gp-1) Fuel slugs needed for LC-8 were prepared according to the procedures described above in Step (1) to Step (5). The sintered and homogenized fuel slugs were then ground to -44 μ powder, which was isostatically cold-pressed at 90,000 psi and sintered at 2175°C for 16 hours. Fuel slabs were machined from the sintered slugs and outgassed at 1800°C for 48 hours prior to insertion into the fuel slots of LC-8 emitter. The finished pieces had a composition of $U_{0.85}Zr_{0.10}W_{0.05}C_{1.01}$, with a C/U ratio of 1.039.

1.2.3.2. Encapsulation of Fuel Slabs in Emitter

(C-RD)(Gp-1) Encapsulation of the 50UC-50ZrC fuel slabs in the fluoride tungsten emitter for LC-6 was carried out at San Fernando Laboratories, following the same procedures as that used for LC-5.(1) Encapsulation of the 90UC-90ZrC fuel slabs in the fluoride tungsten emitter for LC-8 was carried out at Gulf General Atomic at a temperature of 450°C, using the same type of experiment arrangements as that for LC-5.

Table 1.4

(C-RD)(Gp-1) CARBIDE COMPOSITIONS AND DIFFUSION TEST DURATIONS AT 1800°C

(This table is classified Confidential-Restricted Data-Group 1)

Carbide Sample No.	Composition (Duplicate Analysis)	C/U Ratio With One C Atom Allowed for Each Zr Atom and One C Atom Allowed for Every Two W Atoms		Diffusion Time (hr)
10087-1	$U_{0.858}\ Zr_{0.0905}\ W_{0.0472}\ C_{1.095}$ $U_{0.853}\ Zr_{0.0918}\ W_{0.0528}\ C_{1.072}$	1.138 1.115	1.127 Average	150
10088A	$U_{0.853}\ Zr_{0.0948}\ W_{0.0533}\ C_{1.054}$ $U_{0.854}\ Zr_{0.0920}\ W_{0.0532}\ C_{1.056}$	1.093 1.095	1.094 Average	93
10088B-1	$U_{0.863}\ Zr_{0.0945}\ W_{0.0417}\ C_{1.040}$ $U_{0.864}\ Zr_{0.0940}\ W_{0.0414}\ C_{1.038}$	1.068 1.065	1.057 Average	150
10088B-2	$U_{0.857}\ Zr_{0.0950}\ W_{0.0482}\ C_{1.030}$ $U_{0.854}\ Zr_{0.0952}\ W_{0.0507}\ C_{1.010}$	1.064 1.042	1.053 Average	150
50001C*	$U_{0.858}\ Zr_{0.0935}\ W_{0.0450}\ C_{0.970}$ $U_{0.862}\ Zr_{0.0955}\ W_{0.0448}\ C_{0.965}$	0.990 0.976	0.983 Average	150

*Homogenized at 2285°C for 6 hours, ground to -44 μ /+20 μ, isostatically cold-pressed at 90,000 psi, sintered at 2175°C for 16 hours and annealed at 1800°C for 24 hours. Analysis of the composition was performed after the 1800°C annealing treatment.

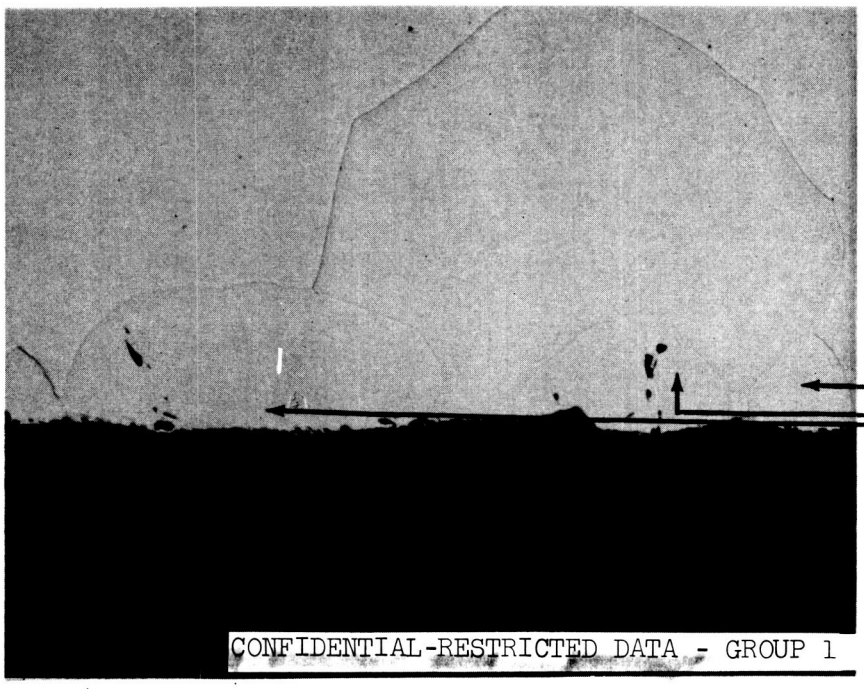

BP-224 100X

(a) W surface in contact with carbide. Note carburization and formation of cracks

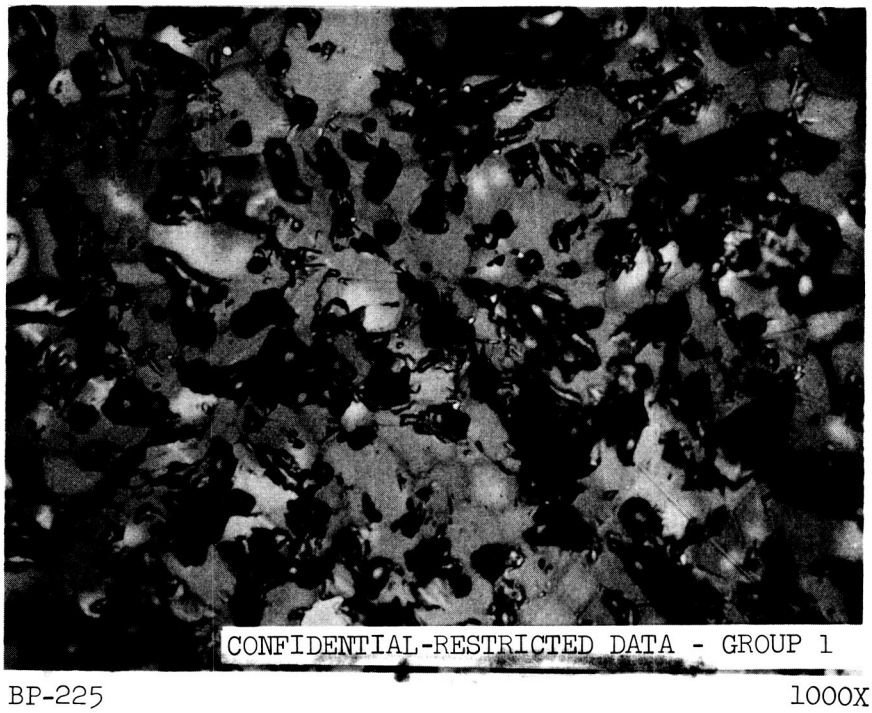

BP-225 1000X

(b) Carbide microstructure

Fig. 1.4--(C-RD)(Gp-1) Appearance of carbide and tungsten after diffusion test at 1800°C for 150 hours. (Carbide Sample 10087-1, C/U = 1.127)

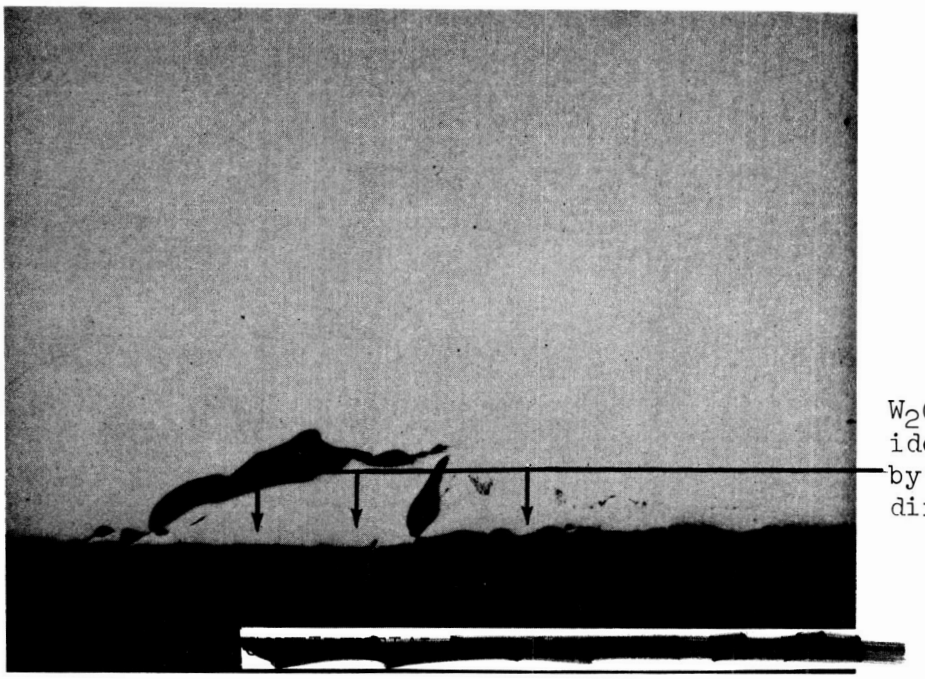

BP-226 100X

(a) W surface in contact with carbide. Note carburization and formation of cracks

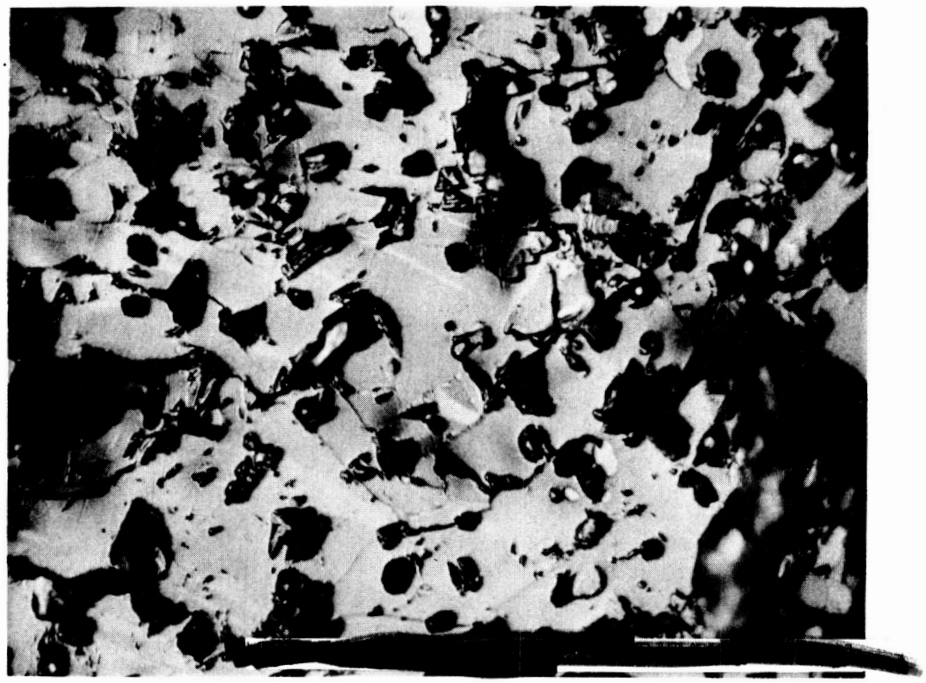

BP-227 1000X

(b) Carbide microstructure

Fig. 1.5--(C-RD)(Gp-1) Appearance of carbide and tungsten after diffusion test at 1800°C for 93 hours. (Carbide Sample 10088 A, C/U=1.094)

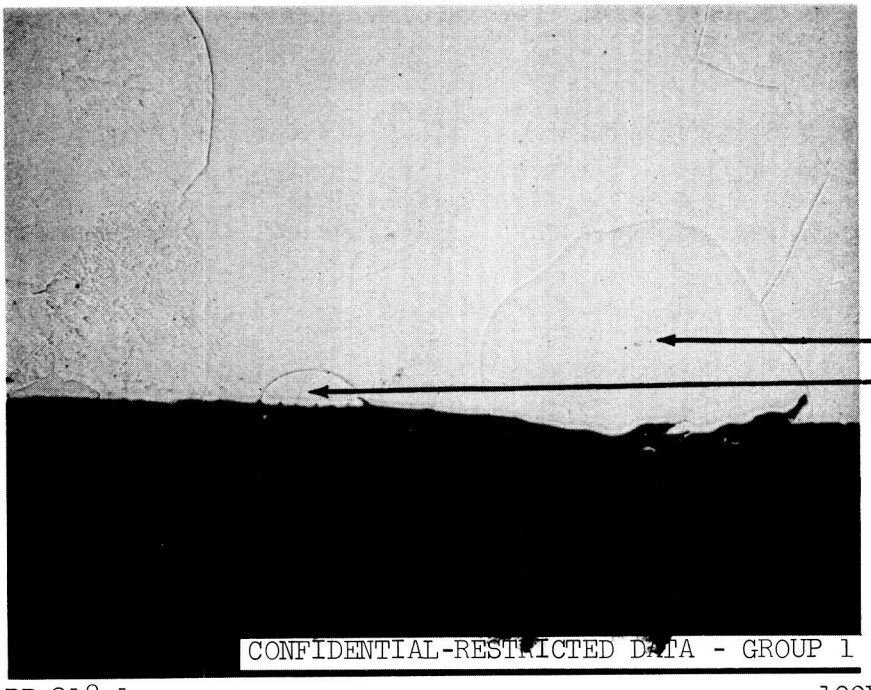

BP-218-1 100X

(a) W surface in contact with carbide. Note carburization and formation of cracks

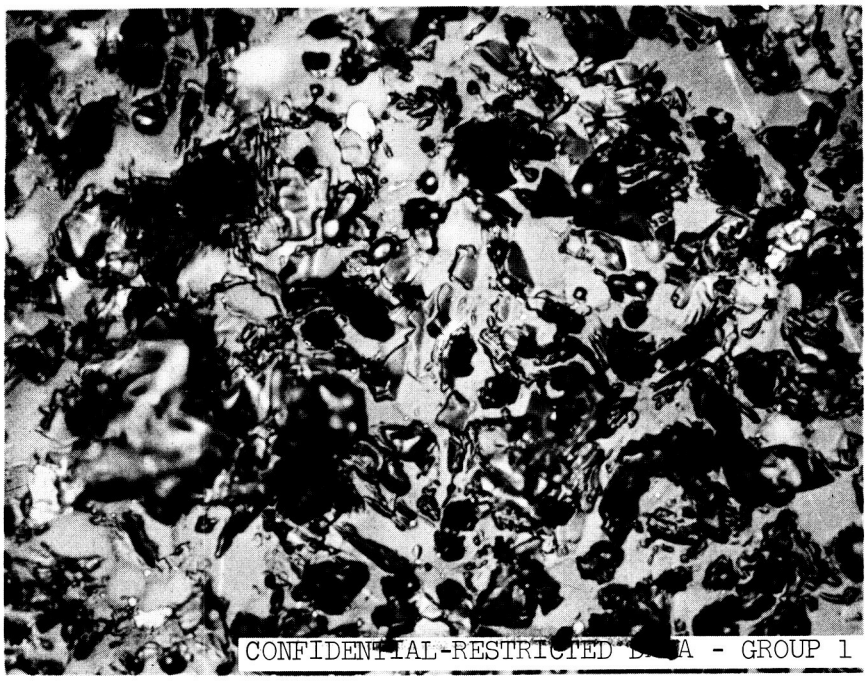

BP-219-1 1000X

(b) Carbide microstructure

Fig. 1.6--(C-RD)(Gp-1) Appearance of carbide and tungsten after diffusion test at 1800°C for 150 hours. (Carbide Sample 10088 B-1, C/U=1.067)

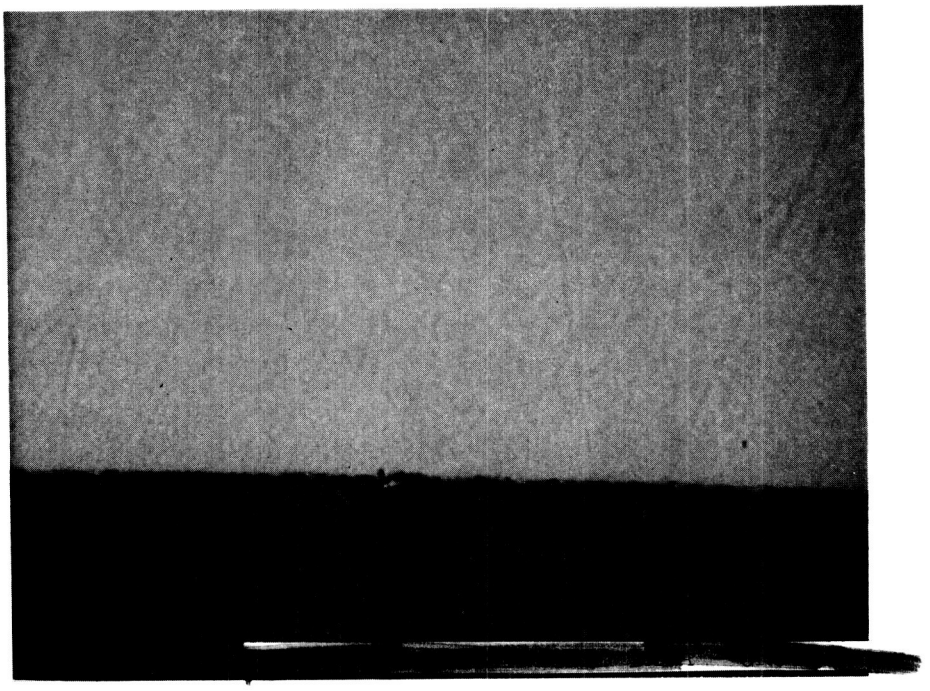

BP-220-1 1000X

(a) W surface in contact with carbide. Note absence of carburization and cracks

BP-221-1 1000X

(b) Carbide microstructure

Fig. 1.7--(C-RD)(Gp-1) Appearance of carbide and tungsten after diffusion test at 1800°C for 150 hours. (Carbide Sample 10088 B-2, C/U=1.053)

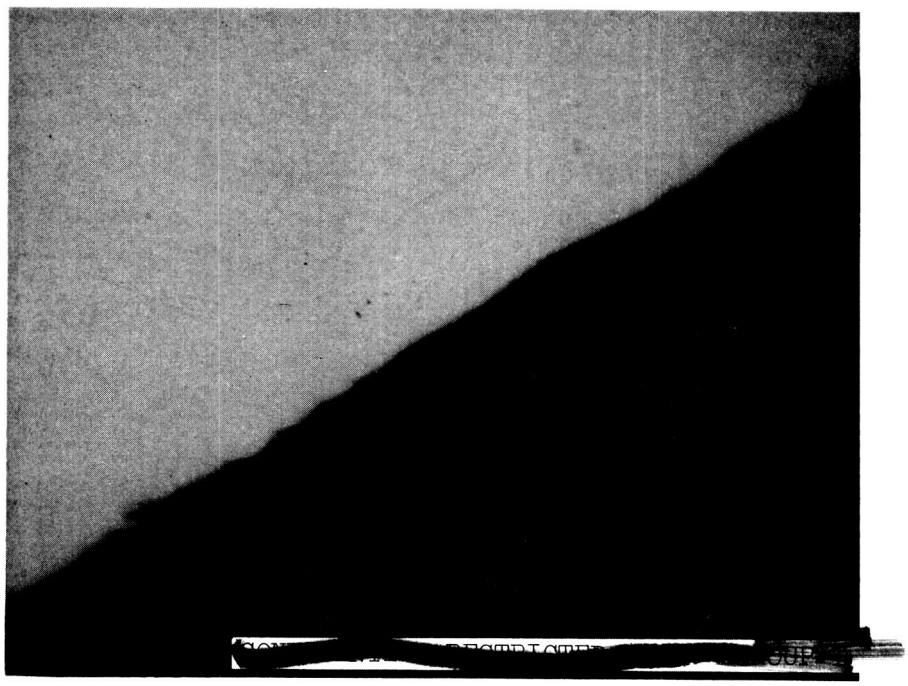

BP-222-3 1000X

(a) W surface in contact with carbide. Note absence of carburization and cracks

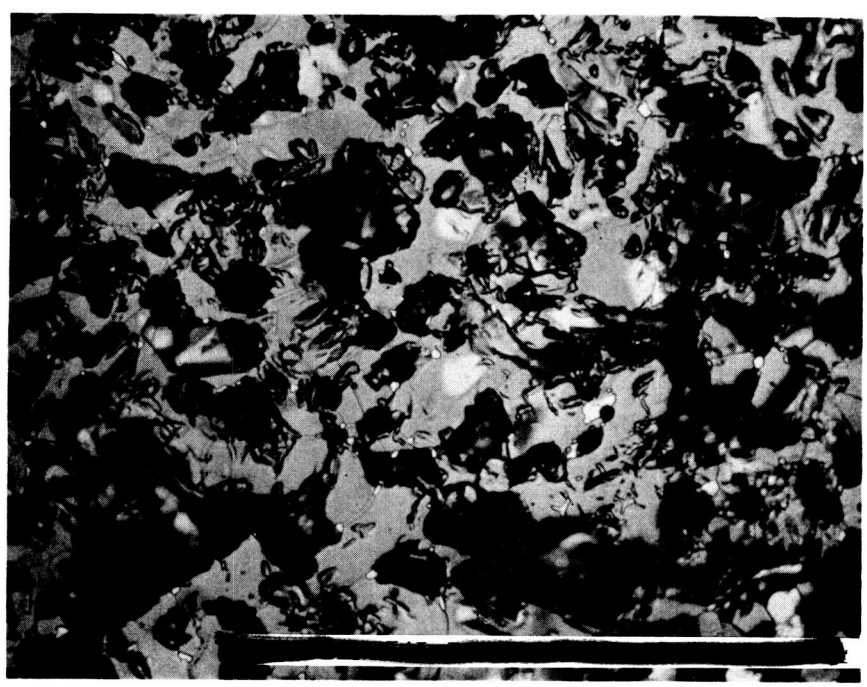

BP-223-3 1000X

(b) Carbide microstructure

Fig. 1.8--(C-RD)(Gp-1) Appearance of carbide and tungsten after diffusion test at 1800°C for 150 hours. (Carbide Sample 50001 C, C/U=0.983)

1.2.4. Preparation of Duplex Tungsten Emitter for LC-9

(C-RD)(Gp-1) The duplex tungsten emitter for LC-9 was prepared by depositing a chloride tungsten layer over the fluoride tungsten emitter blank at 1100°C after the latter had been ground to a 4-8 RMS finish, cleaned with a mixture of nitric and hydrofluoric acids in water, heated to 1800°C in vacuum for 4 hours and subsequently heat treated in hydrogen for 1 hour at 1000°C just prior to the chloride tungsten deposition. The emitter had a chloride tungsten layer of 12.5 mil thickness over a fluoride tungsten substrate of 27.5 mil thickness after a finish machining.

1.2.5. Emitter Characterization

(C-RD)(Gp-1) Prior to final converter assembly, measurements of emitter effective work function and emitter temperature distribution were conducted for LC-7, LC-8 and LC-9 emitters in the experimental arrangement shown in Fig. 1.9. A niobium cylinder which had three sets of eleven optical pyrometry sight holes set at 120° was used as the collector. The emitter-collector gap was 0.020 inch and the outer diameter of the niobium cylinder was 1.5 inch. Stainless steel air lines brazed to the cylinder provided collector cooling. An alumina insulator separated the collector from the emitter support plate. The emitter hung within the collector from the support plate. The emitter in turn supported the filament assembly. The filament assembly and lead cooling collar are the same as those used during life testing of LC-7, LC-8 and LC-9.

(C-RD)(Gp-1) The complete assembly was enclosed in an ion pumped glass bell jar vacuum system. A partial pressure gauge was added to the vacuum system to measure the residual oxygen pressure. The total pressure during the experiments was maintained below 5×10^{-7} torr; the oxygen pressure was less than 10^{-9} torr.

(C-RD)(Gp-1) Effective work functions were determined from extrapolated short circuit currents and Richardson's equation using A = 120 $A/cm^2/°K$. Axial temperature profiles of the emitter surface were obtained by pyrometry using the sighting holes in the collector. Figure 1.10 shows the emitter

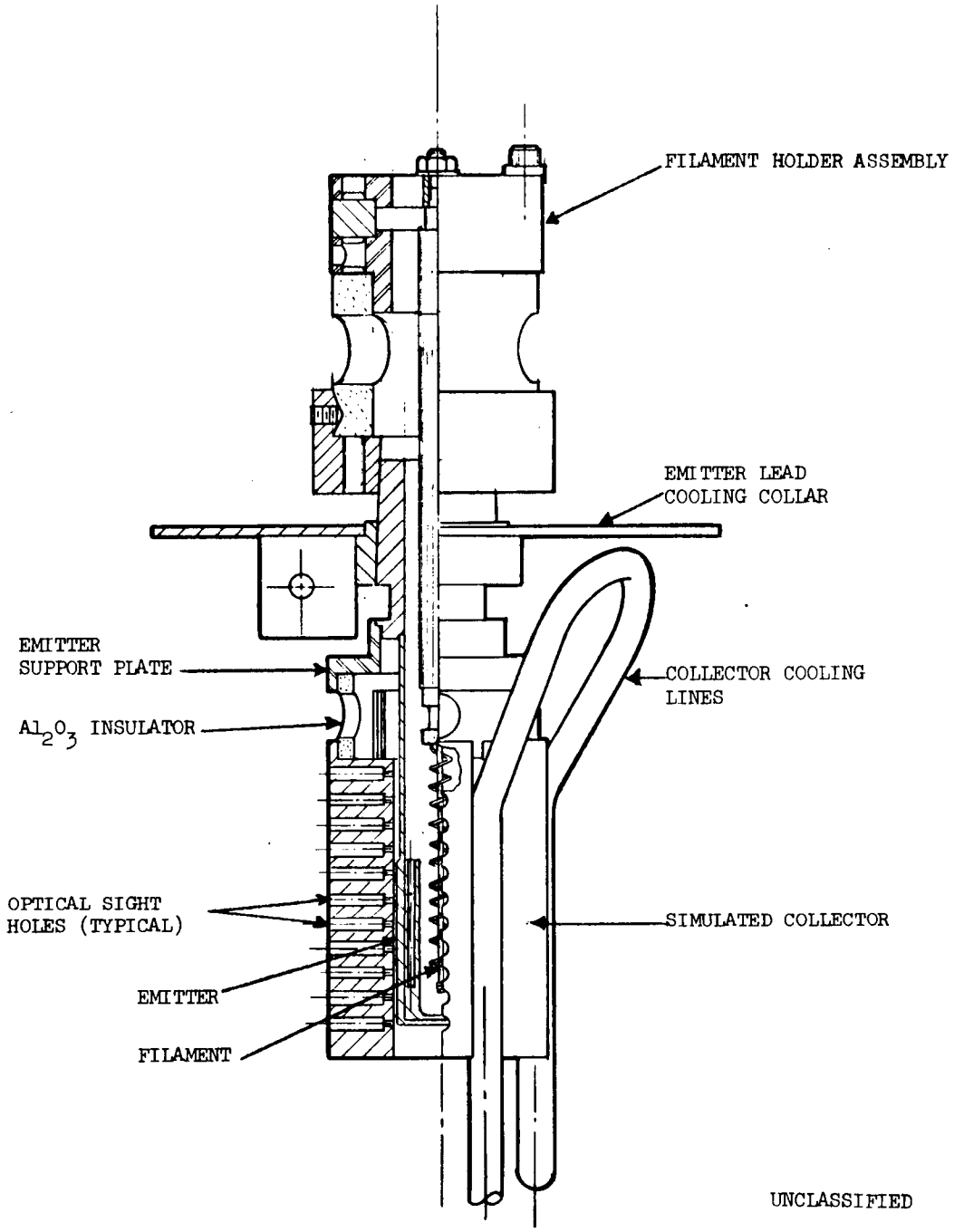

Fig. 1.9--(U) Vacuum emission test assembly

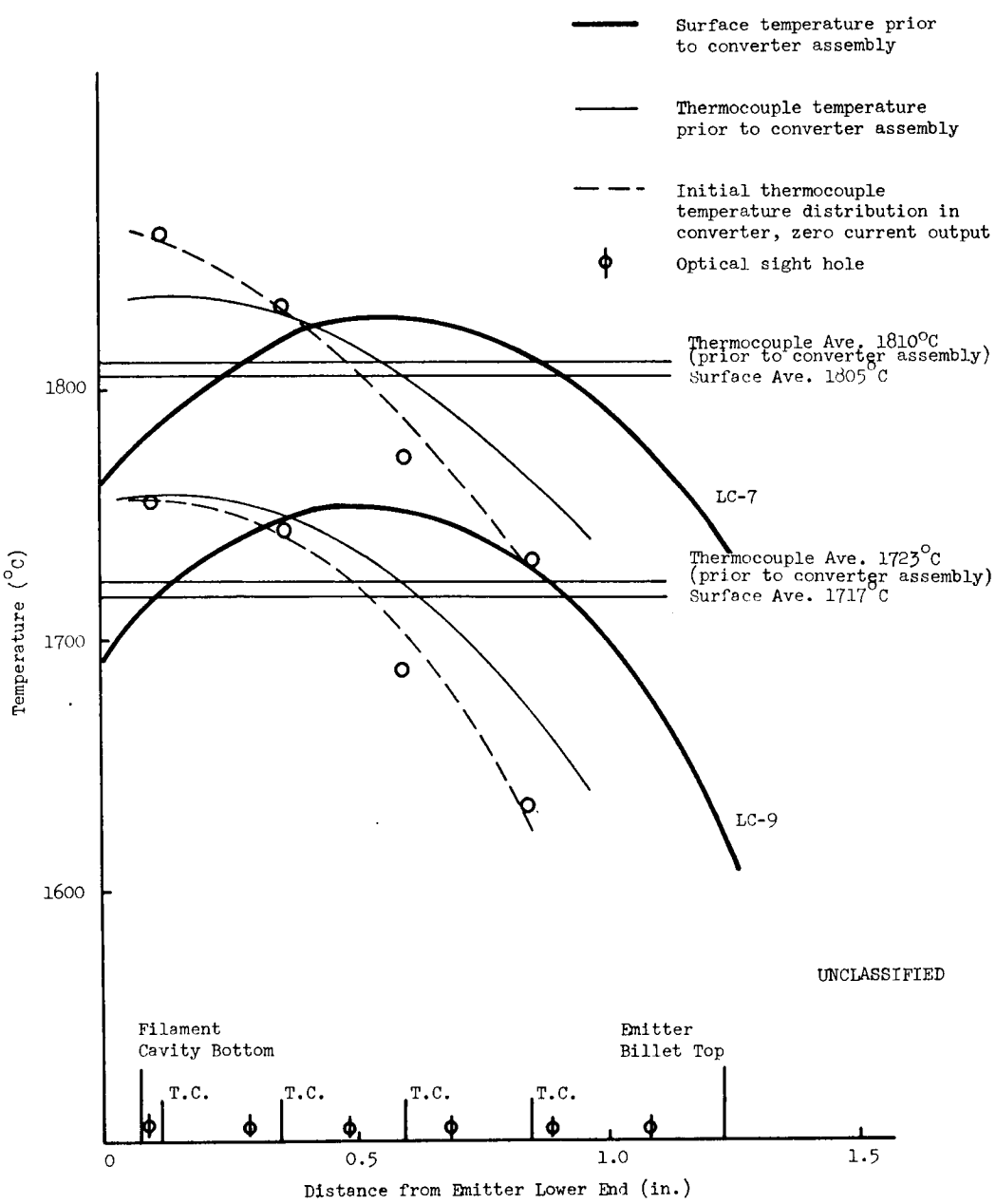

Fig. 1.10--(U) LC-7 and LC-9 emitter temperature profile

temperature profiles measured on LC-7 and LC-9 during the study. The difference between maximum and average temperatures is seen to be 30° to 35°C, and 86% of the surface is within ±35°C of the average temperature for both emitters. Figure 1.11 shows the emitter temperature profile measured on LC-8 for three different temperatures. The difference between maximum and average temperatures is between 30° to 55°C, and about 80% of the surface is within ±30°, ±40° and ±55°C for the three emitter temperatures shown. The average surface temperature determined from the profile was used for effective work function calculations. The collector temperature, measured at the outside surface of the niobium cylinder, was maintained below 200°C during vacuum emission measurements. The effective work functions for LC-7, LC-8 and LC-9 were 4.55 eV, 4.71 eV and 4.78 eV respectively. Errors in the determination of the work function due to experimental uncertainties was estimated to be ± 0.03 eV.

In addition to work function determinations the vacuum emission apparatus provided a correlation between the emitter surface temperature profile and emitter thermocouple temperature distribution. Both LC-7 and LC-9 converters were instrumented with four emitter thermocouples positioned along the emitter axis. As shown in Fig. 1.10 the average surface temperature and the thermocouple average were within 10°C. Also shown in Fig. 1.10 is the open circuit thermocouple distribution obtained at the start of converter life testing. The maximum deviation between converter open circuit and vacuum emission thermocouple profiles was 30°C, which made it possible to use the average thermocouple temperature to estimate the average surface temperature of the converter during diagnostic measurements. When the converter was operating in the power mode the agreement between the converter thermocouple temperature distribution and the vacuum emission thermocouple distribution improved because of the resistance heating of the stem at high currents. For LC-8 converter which was fueled and instrumented with only two high temperature thermocouples at the same axial location, the readings of thermocouples T_{E1} or T_{E2} were used to estimate the average temperature of the emitter surface in the converter, assuming the observed relationships between these thermocouple readings and the average temperature of the emitter surface remained unchanged after the emitter was incorporated into the converter.

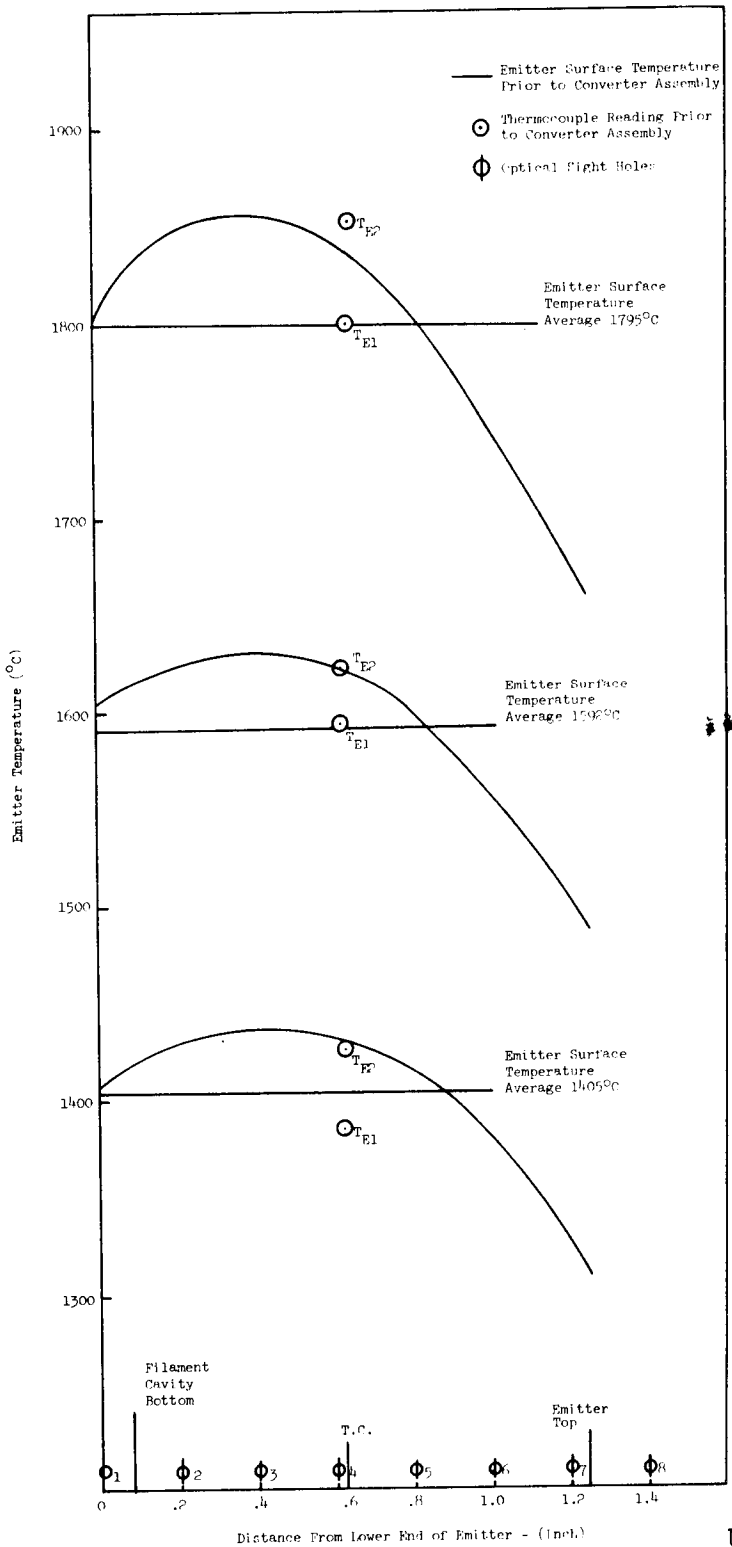

Fig. 1.11--(U) LC-8 emitter temperature profile and thermocouple reading prior to converter assembly

1.2.6. Converter Final Assembly and Bakeout

(C-RD)(Gp-1) Remote assembly techniques that have been described elsewhere[2] were used for the converter final assembly. A Varian Associates partial pressure gauge (PPG) was provided in the cell exhaust tubulation during LC-7, LC-8 and LC-9 assembly so that the partial pressures of active gases could be determined before and after the converter final assembly sequence. Vacuum valving was provided so that the PPG and pumps could be isolated and baked if necessary. The cell assembly cycle was initiated by baking the PPG and other cell exhaust hardware at > 300°C for 24 hours, then cooling to 150°C for electrode bakeout and assembly procedures. Electrode bakeout data prior to final closure brazing, are shown below:

Converter	Temperature °C		Chamber Pressure Torr	PPG Torr	Time
	Collector	Emitter			
LC-7	750 ± 25°C	1600 ± 25°C	4×10^{-7}	8×10^{-7}	2.0 hours
LC-8	750 ± 25°C	1755 ± 25°C	5×10^{-7}	4×10^{-7}	2.0 hours
LC-9	750 ± 25°C	1755 ± 25°C	5×10^{-7}	3×10^{-7}	2.2 hours

(C-RD)(Gp-1) The assembled converters received final bakeout in a vacuum station equipped with a heat sink and ancillary instrumentation required to approximate converter component temperatures experienced during normal operation. Table 1.5 and Fig. 1.12 describe the LC-6 final bakeout data. Helium leak check yielded a leakage rate of 7×10^{-14} std c.c./sec. The converter was pinched off at a residual gas pressure of $< 1 \times 10^{-9}$ torr. The cesium ampoule was then opened before the converter was installed on the test stand. Figure 1.13 illustrates the time-pressure relationship during the final bakeout of LC-8. The cesium ampoule remained intact during the bakeout. Table 1.6 gives the partial pressures of residual gases at various stages of the final bakeout. The helium leakage rate measured was 9.5×10^{-14} std c.c./sec. The cesium ampoule was opened after the helium leak rate determination and the converter was then pinched off. The pressure history for LC-9 final bakeout is shown in Fig. 1.14 and is representative of LC-7

Table 1.5

(U) LC-6 FINAL BAKEOUT DATA

(This table is classified Confidential-Restricted Data-Group 1)

Date/Time	Emitter Temperature		Insulator Temperature		Collector Temperature	Converter Pressure (mmHg)	Vacuum System Pressure (mmHg)	
	Thermocouple	Pyrometer	Top Skirt	Bottom Skirt			Upper Gauge	Lower Gauge
Outgassing Started: 2/14/66	1745(c)	1620(a)	762(b)	750(b)	775(b)	9×10^{-8}	8×10^{-8}	1.7×10^{-7}
Outgassing Finished: 2/23/66	1745(c)	1655(a)	745(b)	745(b)	750(b)	9×10^{-9}	5.2×10^{-8}	6×10^{-8}

(a) The significant deviation from the thermocouple emitter temperature readings is attributed to a deviation from blackbody conditions of the thermocouple hole monitored, and to asymmetry in emitter heating.

(b) Insulator and collector temperature measurements were made with an Ircon Series 300T radiation thermometer. Thermocouples used for initial monitoring of these temperatures proved to be inaccurate because of poor thermal contact. Corrections for spectral emissivity and sight port reflectance were made for the Ircon. The instrument calibration accuracy is ± 2%.

(c) An error limit of ± 20°C is ascribed to the thermocouple readings.

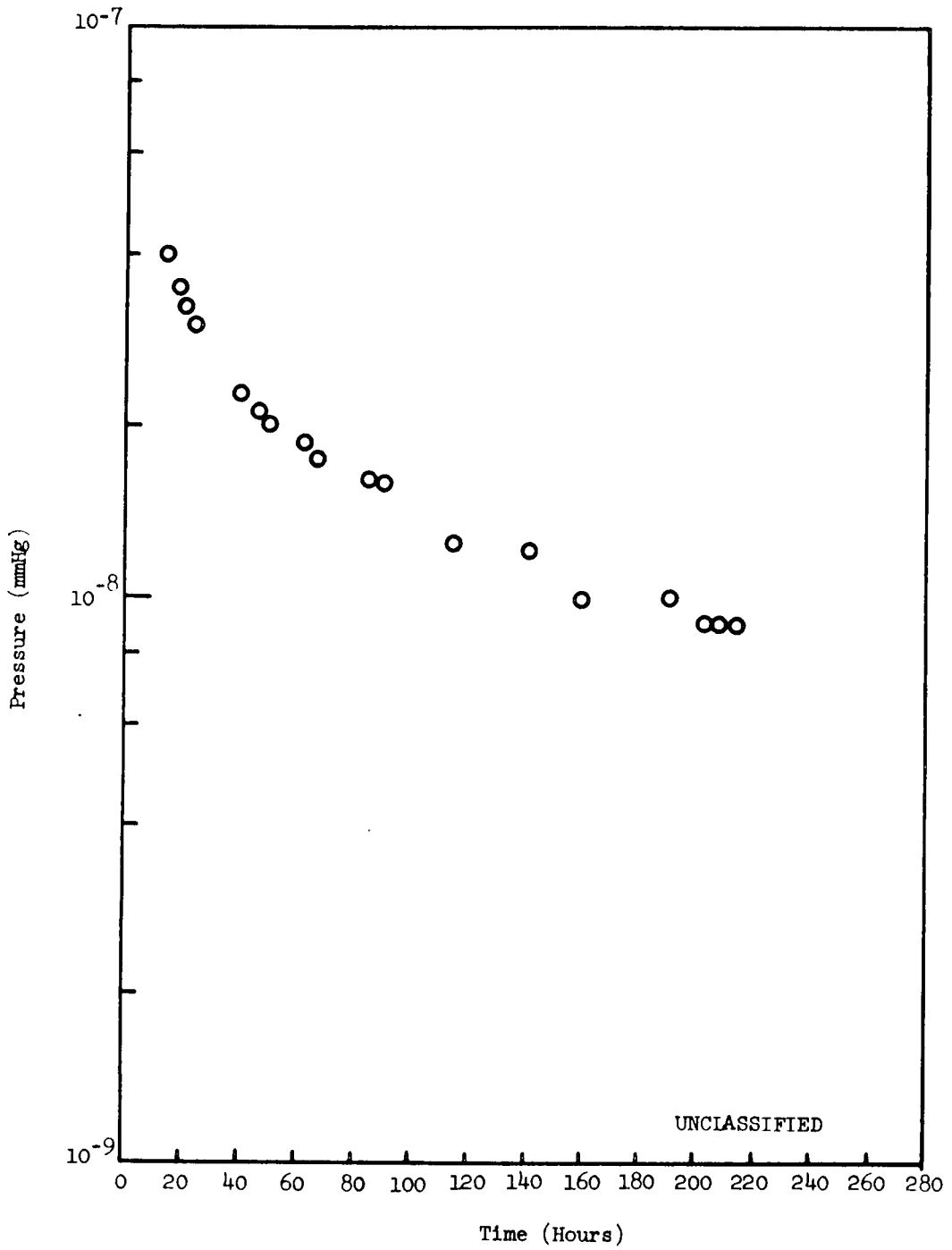

Fig. 1.12--(U) Internal pressure vs. time during LC-6 converter final bakeout

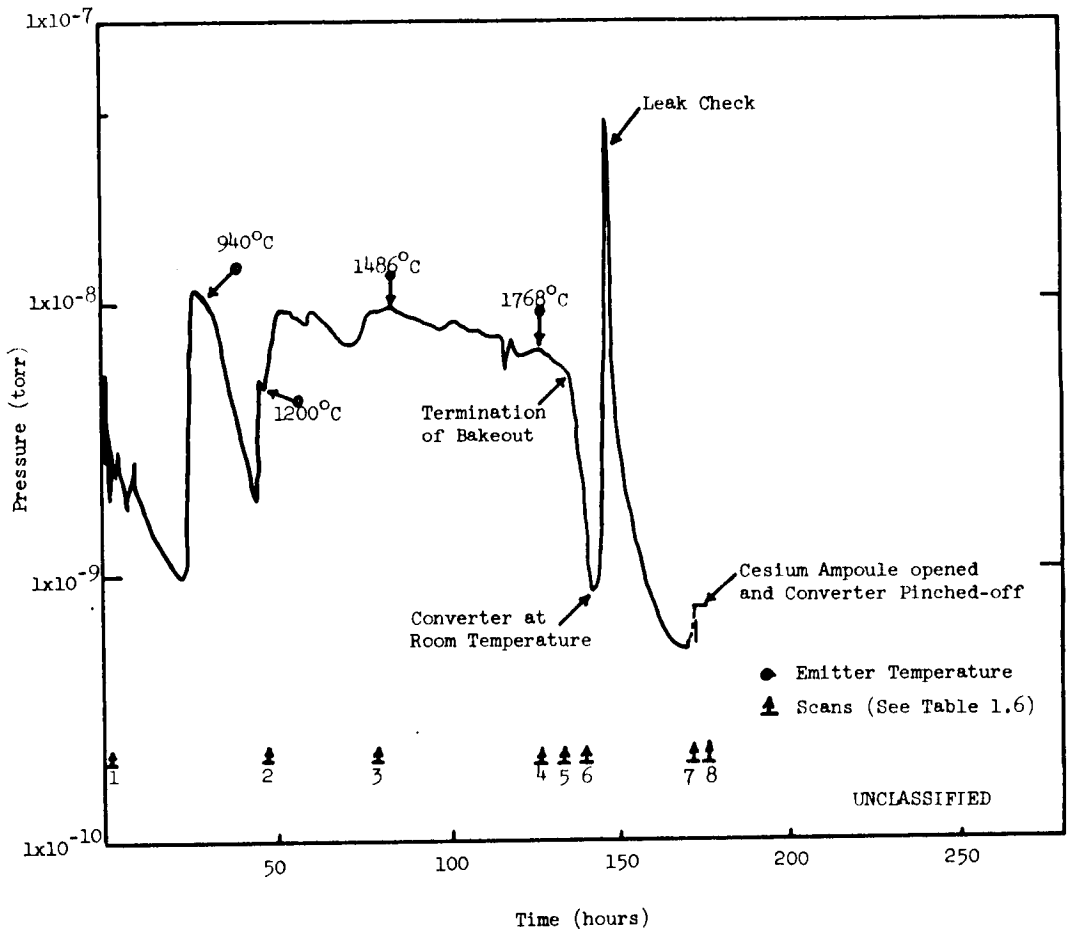

Fig. 1.13--(U) LC-8 pressure history during final bakeout

Table 1.6

(U) RESIDUAL GAS PARTIAL PRESSURES READINGS DURING LC-8 CONVERTER FINAL BAKEOUT

(This table is Unclassified)

Scan No.	Conditions	Total Gauge Pressure (torr)	True Pressure (torr)	Partial Pressures - torr					
				AMU - 2	16	18	28	40	44
				Gas - H_2	CH_4	H_2O	CO & N_2	A	CO_2
1	Prior to start of bakeout. Converter at 23°C	2.4×10^{-9}	3.91×10^{-9}	2.32×10^{-9}	2×10^{-11}	1.9×10^{-10}	1.26×10^{-9}	-	1.2×10^{-10}
2	Emitter temperature at 1200°C	4.7×10^{-9}	8.13×10^{-9}	5.2×10^{-9}	2×10^{-11}	7.5×10^{-10}	1.91×10^{-9}	-	2.4×10^{-10}
3	Emitter temperature at 1486°C	9.6×10^{-9}	1.89×10^{-8}	1.39×10^{-8}	8×10^{-11}	1.60×10^{-9}	2.83×10^{-9}	-	4.1×10^{-10}
4	Emitter temperature at 1768°C	6.7×10^{-9}	1.3×10^{-8}	9.88×10^{-9}	4×10^{-11}	9.6×10^{-10}	2.23×10^{-9}	-	2.0×10^{-10}
5	Following ≅ 12 hours at 1768°C	5.6×10^{-9}	1.15×10^{-8}	8.8×10^{-9}	4×10^{-11}	7.9×10^{-10}	1.72×10^{-9}	-	1.5×10^{-10}
6	Converter at room temperature prior to leak check	8.3×10^{-10}	1.64×10^{-9}	1.2×10^{-9}	1.1×10^{-11}	8.1×10^{-11}	3.13×10^{-10}	-	2.1×10^{-11}
7	Prior to opening of cesium ampoule	7.5×10^{-10}	1.37×10^{-9}	9.47×10^{-10}	8×10^{-12}	5.6×10^{-11}	3.43×10^{-10}	-	2.4×10^{-11}
8	After open of ampoule just prior to pinch-off	7.5×10^{-10}	1.36×10^{-9}	9.25×10^{-10}	8×10^{-12}	5.7×10^{-4}	3.48×10^{-10}	-	2.4×10^{-11}

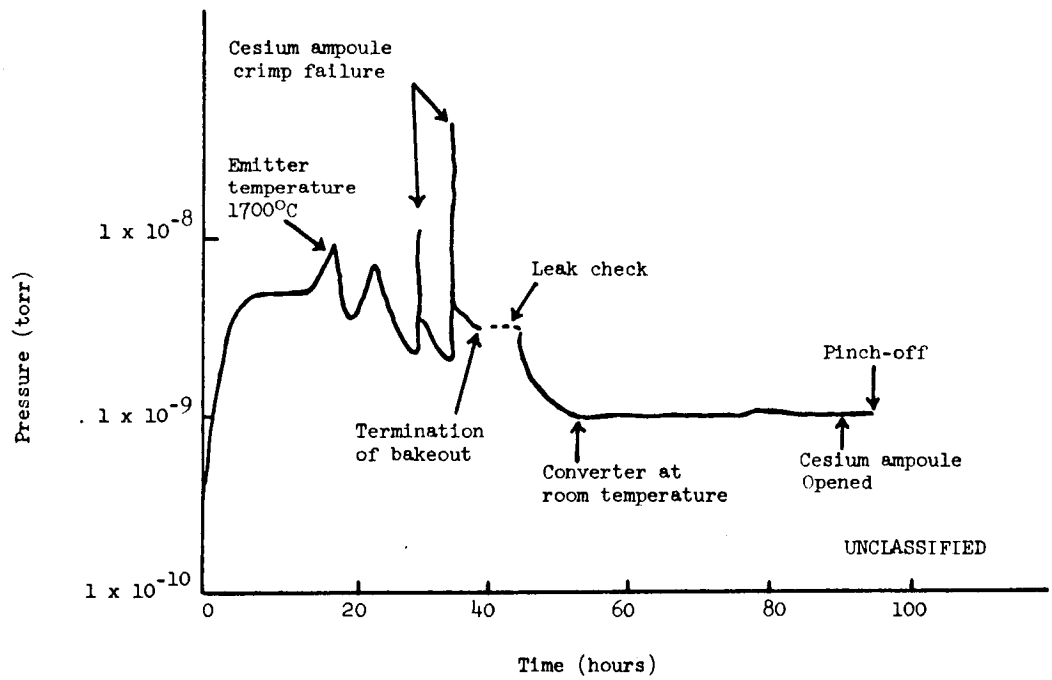

Fig. 1.14--(U) LC-9 pressure history during final bakeout

bakeout history. The partial pressures of residual gases are listed in Table 1.7. Both LC-7 and LC-9 bakeouts were terminated prematurely because of failures of the cesium ampoule which leaked cesium into the converters. However, as noted in Fig. 1.14, prior to cesium ampoule failure the total pressure at an emitter temperature of 1700°C was $\cong 2 \times 10^{-9}$ torr with hydrogen as the major constituent. Following termination of bakeout and with the converter at room temperature the helium leakage rate was determined. The envelope of the converter was subjected to one atmosphere of helium while monitoring the helium peak on a partial pressure gauge. The leakage rate was determined to be 5.5×10^{-14} std. c.c./sec. Following leak rate determination the converter was pinched off.

Table 1.7

(U) RESIDUAL GAS PRESSURE READINGS DURING LC-9 CONVERTER FINAL BAKEOUT

(This table is Unclassified)

Scan No.	Conditions	Total Gauge Pressure (torr)	True Pressure (torr)	Partial Pressures - torr							
				AMU - 2	16	18	28	32	40	44	
				Gas - H_2	CH_4	H_2O	CO & N_2	O_2	A	CO_2	Other
1	Prior to start of outgassing. Converter at 23°C	3.8×10^{-10}	8.51×10^{-10}	5.95×10^{-10}	8.71×10^{-11}	1.22×10^{-11}	1.207×10^{-10}	1.92×10^{-11}	1.07×10^{-11}	5.97×10^{-12}	
2	Start of outgassing. Emitter temperature 1700°C	8×10^{-9}	1.26×10^{-8}	7.5×10^{-9}	1.57×10^{-10}	2.2×10^{-10}	3.92×10^{-9}	6.98×10^{-11}	6.55×10^{-10}	5.33×10^{-11}	
3	Following suspected opening of cesium ampoule	4×10^{-8}	8.48×10^{-8}	6.89×10^{-8}	2.39×10^{-9}	1.2×10^{-8}	8.71×10^{-9}	-	2.45×10^{-9}	1.2×10^{-9}	3 peaks above 44 AMU. Total pp = 1×10^{-9} torr
4	Prior to final pinch-off converter at 23°C	1×10^{-9}	1.65×10^{-9}	1.02×10^{-9}	2.89×11^{-11}	1.35×10^{-11}	3.88×10^{-10}	3.78×10^{-11}	1.42×10^{-10}	1.92×10^{-11}	

REFERENCES

(1) Horner, M. H., "Post-Operation Examination of Thermionic Life Cells LC-1 and LC-2 (U)," National Aeronautics and Space Administration Report NASA CR-72050, General Dynamics, General Atomic Division, May 15, 1967. (C/RD).

(2) "Studies of Thermionic Materials for Space Power Applications, Annual Summary Report for the Period September 1, 1963 through August 31, 1964 (U)," National Aeronautics and Space Administration Report NASA CR-54322, General Dynamics, General Atomic Division, August 17, 1965. (C/RD).

(3) Lindgren, J. R., and A. F. Weinberg, "Fabrication Development of U-ZrC Fuels (U)," National Aeronautics and Space Administration Report NASA CR-54381, General Dynamics, General Atomic Division, n.d. (C/RD).

(4) "Studies of Thermionic Materials for Space Power Applications, Summary Report for the Period September 1, 1964 through November 23, 1965 (U)," National Aeronautics and Space Administration Report NASA CR-54980, General Dynamics, General Atomic Division, May 6, 1966. (C/RD).

(5) Weinberg, A. F., et al., "Investigations of Carbides as Cathodes for Thermionic Space Reactors, Final Report for the Period May 15, 1961 through August 31, 1962," National Aeronautics and Space Administration Report GA-3523, General Dynamics, General Atomic Division, n.d. (U).

PART II. IRRADIATION STUDIES OF THERMIONIC MATERIALS

(U) Two subtasks were involved during this reporting period. The first is concerned with the irradiation of two capsules, designated as V-2A and V-2B, in the V-2 tube position of NASA Plum Brook Reactor Facility (PBRF); both the capsules and the capsule positioning mechanism (CPM) were fabricated during the previous contractual period.(1) The second is concerned with the design and fabrication of Capsules V-2C and V-2D for irradiation studies in the same V-2 tube position of PBRF, using a new capsule positioning mechanism. Details of the work carried out are described as follows.

2.1. IRRADIATION OF CAPSULES V-2A AND V-2B

2.1.1. Description of the Capsule

(U) Capsules V-2A and V-2B are two identical capsules, designed for the study of the irradiation behaviors of vapor deposited tungsten clad UC-ZrC and cermet fuel materials at 1800°C to fission densities of 8×10^{19} and 1.76×10^{20} fission/cm^3 respectively. The design of the capsule is similar to that used previously for the irradiation of refractory metal and alloy clad fuel samples in the General Electric Test Reactor (GETR) under Contract NAS 3-2532.(2) Owing to the shorter core length of the Plum Brook Reactor (24 inch versus 36 inch for GETR), however, the length of the fuel zone of the capsule was reduced in order to minimize axial temperature variation. Forty irradiation samples were divided into two similar portions and contained in these two identical capsules for irradiation side by side in the 8 inch diameter V-tube. There were two fuel pins in each capsule — one containing ten vapor-deposited tungsten clad UC-ZrC fuel samples and the other containing ten vapor-deposited tungsten clad cermet fuel samples. Each sample consisted of a doughnut-shaped fuel piece enclosed by

vapor-deposited tungsten cladding with a built-in void volume in the cladding envelope. The cladding had a thickness of 20 mils around the cylindrical surfaces of the fuel piece and 40 mils at the top and bottom. To minimize fuel redistribution by vaporization; two 0.002 inch thick tungsten baffles were placed on top of the carbide fuel bodies, while the cermet fuel pieces were all coated with 0.0025 inch thick vapor-deposited tungsten. A hole was drilled through the cap of the cladding in order to vent the fission gases released from the fuel body. The cap was brazed with a small amount of platinum to the cladding envelope to hold the cap in place during the handling of the capsule. Table 2.1 describes the characteristics of the fuel samples. Table 2.2 shows the fuel sample arrangements in each fuel pin; six of the fuel samples in the middle portion of each fuel pin are the test samples, while the two top and the two bottom fuel samples in each fuel pin were used as thermal shields. Two W-5% Re versus W-26% Re high temperature thermocouples were used to monitor the fuel temperatures. The thermocouple wires were insulated with BeO and contained in a 60 wt% Mo-40 wt% Re alloy sheath in the high temperature region (~ 2 inch long). The whole assembly was then enclosed in a tantalum sheath. The use of a duplex sheath in the high temperature region was for the purpose of avoiding any interaction between the tantalum sheath and the BeO insulation. Figure 2.1 shows schematically the longitudinal cross section of a fuel pin and the locations of the high temperature thermocouples. The fabrication procedures for the fuel samples were given in the Annual Summary Report for Contract NAS 3-4165.[3] Detail design, and thermal, nuclear and stress analysis of the capsule were described in the "Experimental Design Manual and Hazard Analysis, Plum Brook Reactor Experiment No. 62-13-R1."[4]

2.1.2. Capsule Positioning Mechanism

(U) The Capsule Positioning System consists of a carriage mounted on two rails and driven by a hydraulic cylinder. The rails and cylinder are attached to a frame, which, in turn is mounted in the "holding fixture" portion of the V-tube. The carriage assembly consists of an aluminum carriage block in which are mounted two 1-1/4 inch I.D. tubes that serve the dual purpose of holding the capsules and providing a coolant annulus, and two stainless steel precision Thompson linear bearings to provide

Table 2.1

(U) CHARACTERISTICS OF FUEL BODIES OF IRRADIATION SAMPLES[a]

(This table is classified Confidential-Restricted Data-Group 1)

Number of Samples	Fuel	Density (% T.D.)	SRF[b]	Carbon Content of Fuel	Stoichiometric Carbon Content
4	UC	80-85	188	5.0	4.85
4	90UC-10ZrC	80-85	400	5.15	5.11
12	50UC-50ZrC	80-85	400	6.95	6.80
4	W-60 vol-% UC	92-97	---	4.95	4.85
4	W-60 vol-% (90UC-10ZrC)	93-97	---	5.15	5.11
12	W-60 vol-% UO_2	90-95	---	----	---

[a]Enrichment same as that used for the GETR clad capsule (29.4×10^{20} U^{235} atoms/cm^3 for the carbides and 34.6×10^{20} U^{235} atoms/cm^3 for the cermets) (Ref. 1).

[b]Surface roughness factor = ratio of true surface area to geometric surface area.

Table 2.2

(U) FUEL SAMPLE ARRANGEMENT IN PLUM BROOK V-2A AND V-2B CAPSULES

(This table is Unclassified)

Capsule 213-1 (V-2A)	Capsule 213-2 (V-2B)
Cermet Pin 213-3	Cermet Pin 213-4
$W\text{-}UO_2$	$W\text{-}UO_2$
$W\text{-}UO_2$	$W\text{-}UO_2$
$W\text{-}UO_2$	$W\text{-}UO_2$
W-UC	W(90UC-10ZrC)
W(90UC-10ZrC)	
	W-UC
$W\text{-}UO_2$	$W\text{-}UO_2$
W-UC	W-UC
W(90UC-10ZrC)	W(90UC-10ZrC)
$W\text{-}UO_2$	$W\text{-}UO_2$
$W\text{-}UO_2$	$W\text{-}UO_2$
Carbide Pin 213-5	Carbide Pin 213-6
50UC-50ZrC	50UC-50ZrC
50UC-50ZrC	50UC-50ZrC
90UC-10ZrC	90UC-10ZrC
50UC-50ZrC	50UC-50ZrC
UC	UC
90UC-10ZrC	90UC-10ZrC
UC	UC
50UC-50ZrC	50UC-50ZrC
50UC-50ZrC	50UC-50ZrC
50UC-50ZrC	50UC-50ZrC

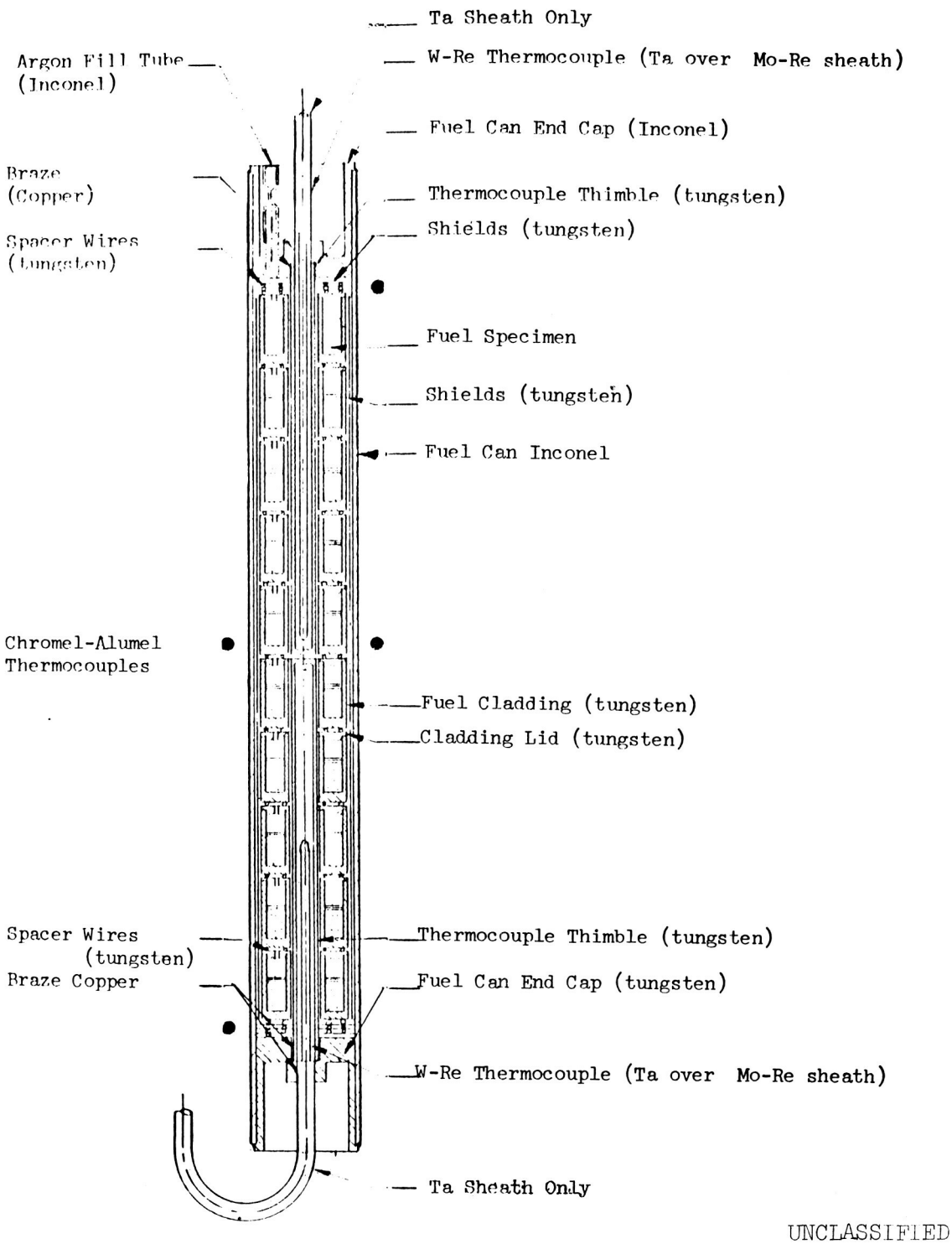

Fig. 2.1--(U) Longitudinal cross section of fuel pin in V-2A and V-2B capsules

alignment of the carriage on its rails. The hydraulic cylinder is fabricated of 17-4PH steel, hardened to condition H-1100. It is built without seals at the rod penetrations, and the clearance at these points is such that a good sliding fit is obtained with minimum leakage through the bearing. Piston sealing and concentricity requirements are met by using a pair of expanding metal seal rings. In operation, full reactor tank pressure is applied to both ends of the cylinder during a "hold" condition and leakage cannot contribute to unwanted movement of the piston. When a movement of the piston is desired, one end of the cylinder is opened to the "hot" drain (at approximate atmospheric pressure) through a throttling valve to provide the desired rate of travel. These throttling valves are bypassed when a "fast out" condition is required. The hydraulic system has provisions for purging the system of air at installation and to "flush the cylinder periodically as an aid in preventing corrosion. A flow switch is installed in the flushing line. Details of the design and the instrumentation are described in the "Experimental Design Manual and Hazard Analysis, Plum Brook Reactor Experiment No. 62-13-R1."(4)

2.1.3. Operating History

(U) Irradiation experiment No. 62-13-R1 started on Cycle 42-P on January 3, 1966. The reactor was held at several power levels while temperature versus position data were taken for the two capsules. Only one of the eight fuel thermocouples responded properly during startup; another two indicated temperatures several hundred degrees lower; while the remaining five indicated shorting to the sheath. On the basis of the reading of the one good fuel thermocouple, the graphite thermal bond temperature was about 100°C lower than that predicated by the design calculation.

(U) Cycle 43-P started on January 18th and the capsule temperatures showed good agreement with those from the previous cycle. The CPM did not function properly during this cycle as the normal "In" motion could not always be initiated. A mechanical stop was then designed to limit the "In" travel of the CPM and would thus allow faster travel speeds which would hopefully eliminate the problem of the CPM not moving.

(U) During the routine check-out of the CPM prior to start of Cycle 44-P, the CPM stuck and would not move in either direction. The hydraulic pressure was increased to 300 psig, which did free the CPM, but it subsequently stuck again. The reactor cycle was completed with the CPM immovable at a position about 1.4 inch out from the V-tube centerline.

(U) Following reactor shutdown, further attempts to move the CPM were not successful. It was decided to remove the experiment from the reactor and attempt to repair or replace the malfunctioning parts. The capsules were first discharged following the normal procedure. The handling tools present were not adequate but did not greatly endanger the safety of the capsules. A resistance check of the thermocouples after discharge indicated all thermocouples, except one of the shorted fuel thermocouples, still retained continuity.

(U) The V-tube was removed from the reactor and transferred via an underwater cart to the hot cell area. It was decided that the activity levels, 20 R at 2' from the bottom of the V-tube to 5 R at the cylinder, would allow manual disassembly behind some portable shielding. The cylinder was thus removed and disassembled. It was found that the piston shaft was frozen into one of the cylinder end plates and showed visible signs of galling. Also present in the cylinder was an appreciable amount of fine metal particles. A sample of these particles was collected, photographed, and analyzed. They were identified as a 300 series stainless steel, probably 304. Since the cylinder was fabricated from 17-4 PH the particles must have originated elsewhere and were subsequently deposited in the cylinder by primary water circulation. Similar but larger metal particles plus miscellaneous organic matter was found in the turbine flow meter filter. The CPM carriage did not move as freely as it should have, so it also was disassembled. The 440-C steel tracks were removed and showed signs of wear similar to those previously noted on softer material. It was apparent that a new CPM design was needed to insure the proper positioning of the capsule during the irradiation. Since the accumulated burn-up was rather low, no hot cell examinations of these capsules were performed.

2.1.4. Temperature Record

(U) Figure 2.2 shows schematically the locations and the designations of the fuel pods and thermocouples. Shown in the same figure are also a set of temperature readings of these thermocouples during the initial startup. While all of the low temperature Chromel-Alumel thermocouples (No. 1, 12, 2, 15, 2, 14, 4 and 16) used for the indication of the capsule thermal bond temperatures performed satisfactorily throughout the two reactor cycles, only two high temperature W-Re thermocouples (No. 5 and 8) used for measuring the fuel temperatures recorded reasonable readings (1730°C by T/C No. 8 in fuel pod 213-6 and 1618°C by T/C No. 5 in fuel pod 213-3). These two thermocouples provided believable readings only during a portion of the first reactor power cycle. Figure 2.3 shows the experimentally determined relationship between the readings of the high temperature thermocouple No. 8 and the corresponding average thermal bond temperatures (average of T/C No. 4 and T/C No. 16 readings) of fuel pod 213-6 during the initial startup. Figure 2.4 contains the chronological records of the average thermal bond temperature of each of the four fuel pods during the two reactor cycles. The experiment was terminated after the second cycle irradiation because of the malfunction of the capsule-positioning mechanism.

2.1.5. Evaluation of Fuel Temperature and Fission Power Density

(U) The purpose of the present evaluation is to provide a means for estimating the fuel temperatures and the fission power densities prevailing in each of the four irradiated fuel pods as a function of irradiation time. The evaluation was based on the experimental data shown in Figs. 2.2, 2.3 and 2.4.

(U) The procedures adopted consist of the following:

(1) Establish the parameters which determine the relationship among fuel temperature, fission power density and thermal bond temperature.

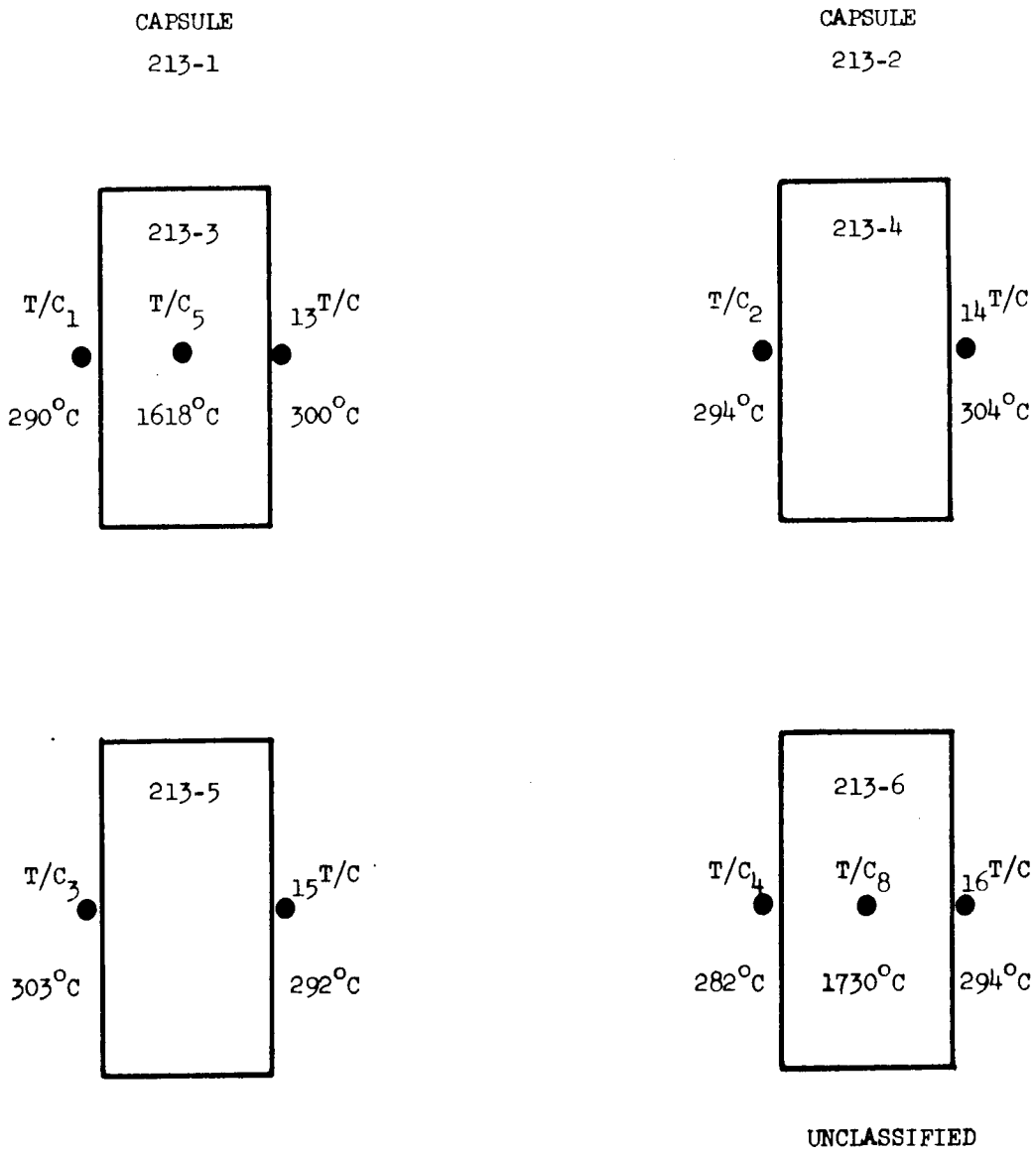

Fig. 2.2--(U) Schematic of fuel pods and thermocouple locations The temperatures indicated represent thermocouple readings during the initial startup

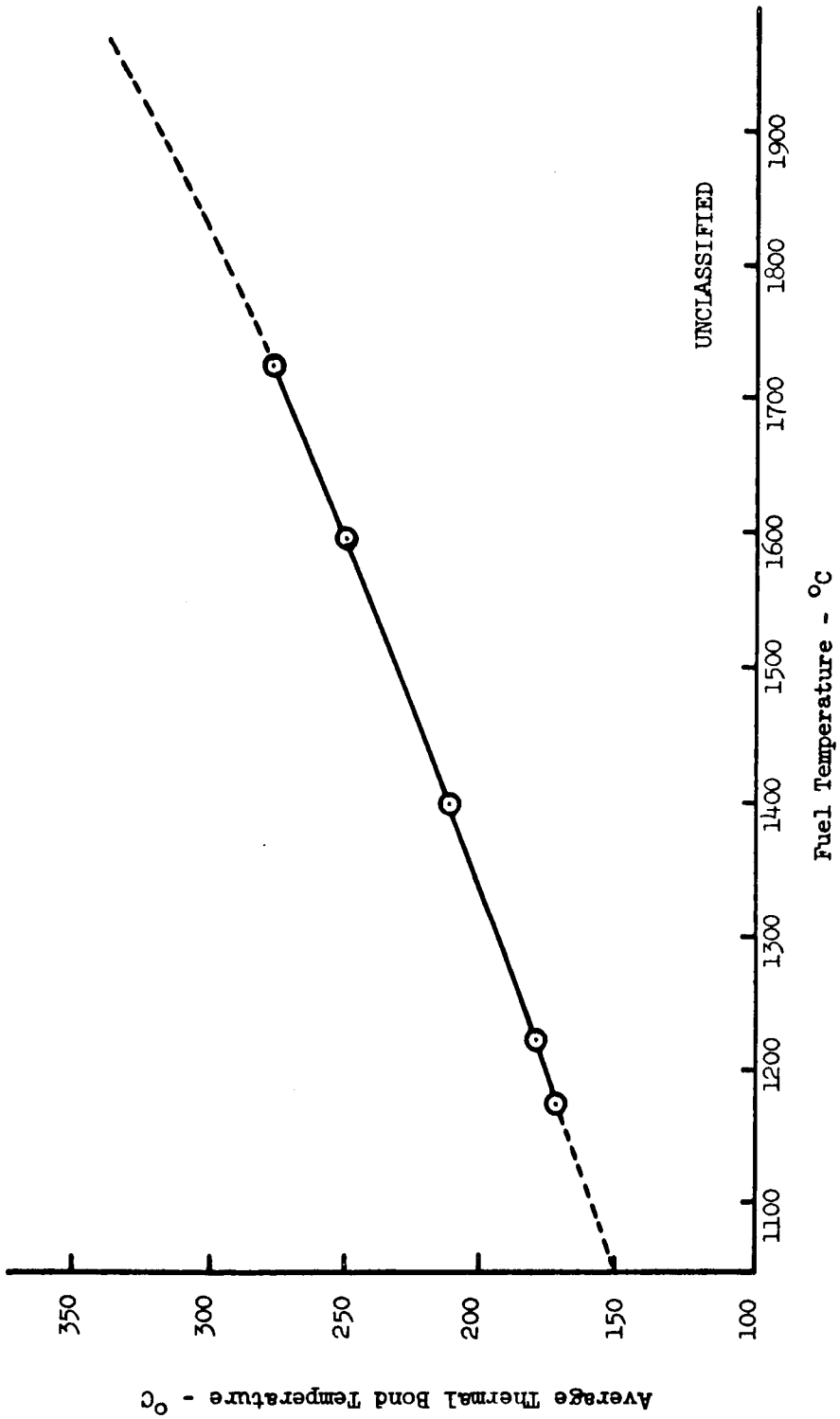

Fig. 2.3--(U) Observed relationship between fuel temperature and average thermal bond temperature for fuel pod 213-6 during initial start-up. Data taken at 60 MW on 1-3-66

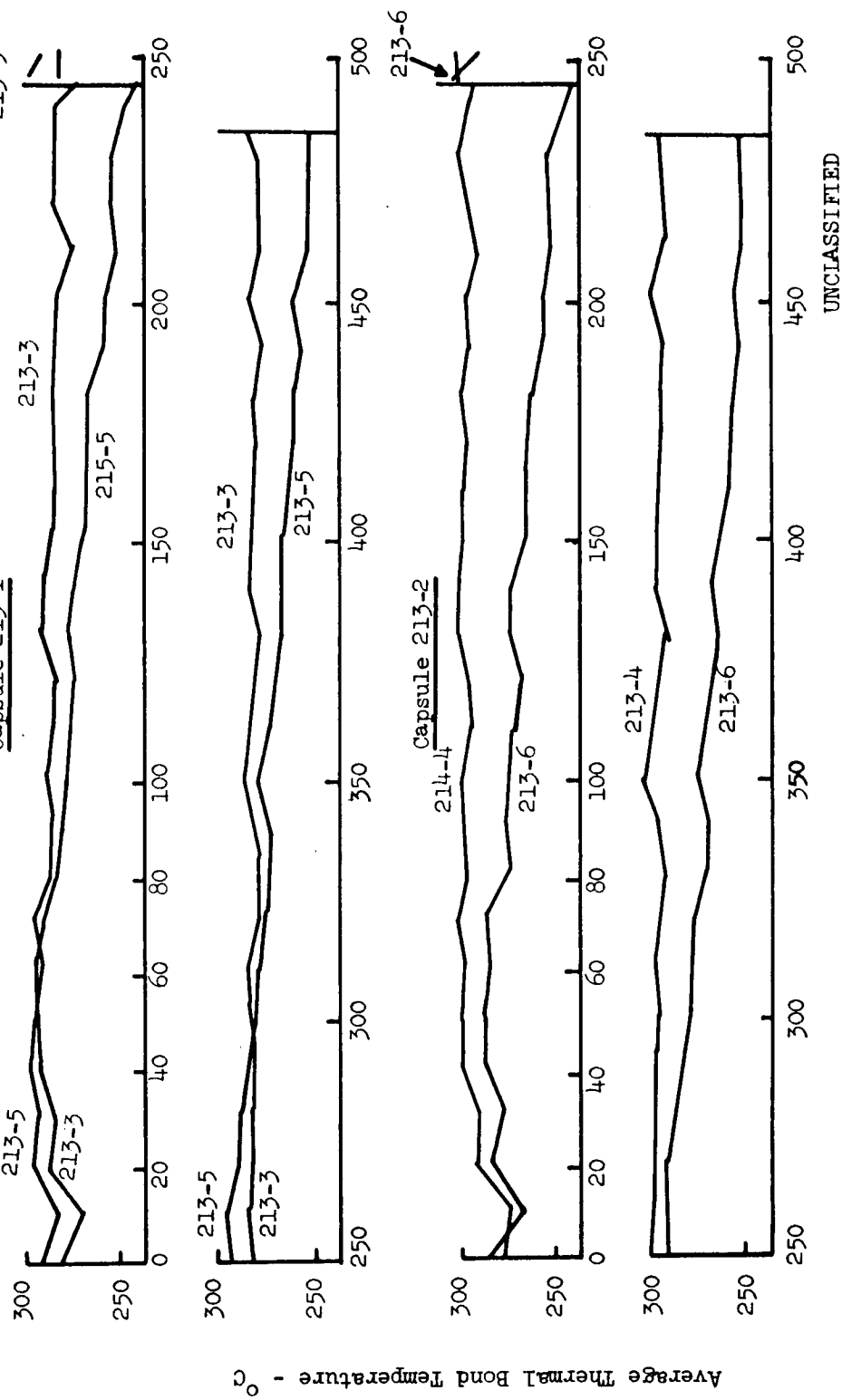

Fig. 2.4--(U) Average thermal bond temperatures of the four fuel pods as a function of irradiation time

(2) Estimate the uncertainty limits of the values of these parameters, as set by design tolerances or specifications, or chosen by judgement and experience.

(3) Perform parametric analysis of the relationships among fuel temperature, fission power density, thermal bond temperature by using the "RAT" heat transfer code taking into account these uncertainty limits.

(4) Correlate the experimentally determined fuel temperature versus thermal bond temperature relationships for fuel pods 213-6 and 213-3 (see Figs. 2.2 and 2.3) with parametric analysis results obtained in (3) in order to check the credibility of the observed relationships.

(5) Deduce the fuel temperatures and fission power densities for the four fuel pods as a function of time on the basis of the results obtained in (3) and (4).

Selection of Parameters

(U) Figure 2.5 illustrates schematically the cross section of the capsule. For the configuration shown, the following parameters control the relationship among fuel temperature, fission power density and thermal bond temperature:

(1) Helium gap size
(2) Argon gap size
(3) Total thermal emittance of Inconel
(4) Total thermal emittance of tungsten
(5) γ heating rate
(6) Coolant flow rate
(7) Coolant temperature

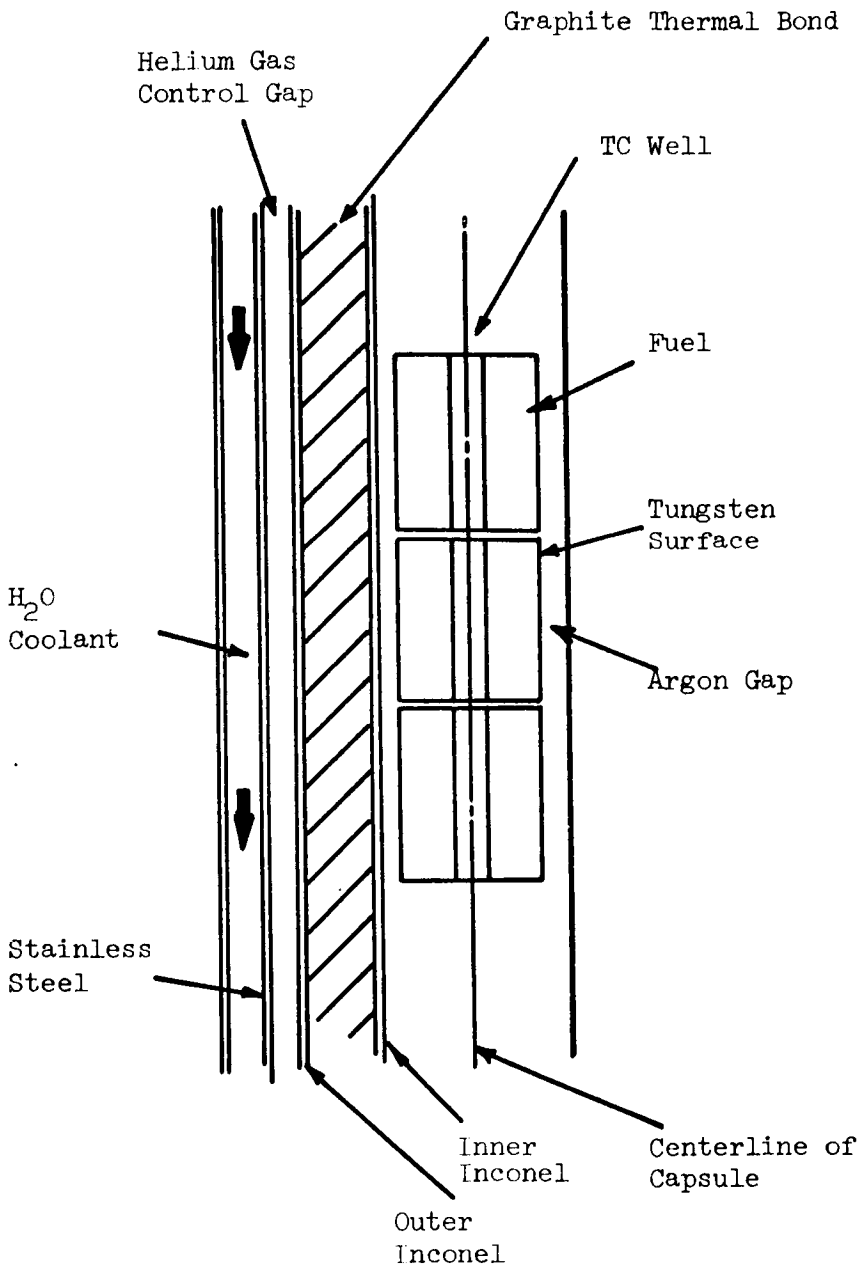

Fig. 2.5--(U) Capsule schematic cross-section

Determination of Uncertainty Limits of Each Parameter

(1) Helium gap size: 0.017 - 0.019 inch (room temperature), treated as a function of temperature in calculation.

The variation in helium gap size is due to fabrication tolerance.

(2) Argon gap size: 0.0185 inch (room temperature), treated as a function of temperature in calculation.

The diameter of the sample and the diameter of the Inconel are machined and measured to achieve the argon gap; therefore there is no uncertainty in this room temperature gap size. The thermal conductivity data of argon are shown in Fig. 2.6. The data from Ref. 2 are the most recent and were used in the calculation.

(3) Inconel emittance: 0.15

The capsule design specifies at 16 micro-inch finish on the Inconel primary containment can, which is a polished surface. For small diameter tubing, honing is the usual process by which close dimensional control and a low surface roughness may be obtained. Handbook values for the emittance of polished Inconel vary somewhat as a function of temperature but show negligible differences in the temperature region of interest (see Fig. 2.7). The value is ~ 0.15 at ~ 300°C from either Ref. (7) or Ref. (8) but in actual manipulation of the Gulf General Atomic RAT code for heat transfer calculation, the emittance curve from Ref. (7) may be inserted as an equation with temperature dependence.

(4) Tungsten emittance: 0.26

The value of 0.26 for the emittance of tungsten was selected on the basis of both handbook data (see Fig. 2.8) and measurements made at Gulf General Atomic on emitter structures. The selected handbook values (Ref. 9) and the measured data agree quite well. The tungsten emittance may also be treated as a function of temperature in code usage.

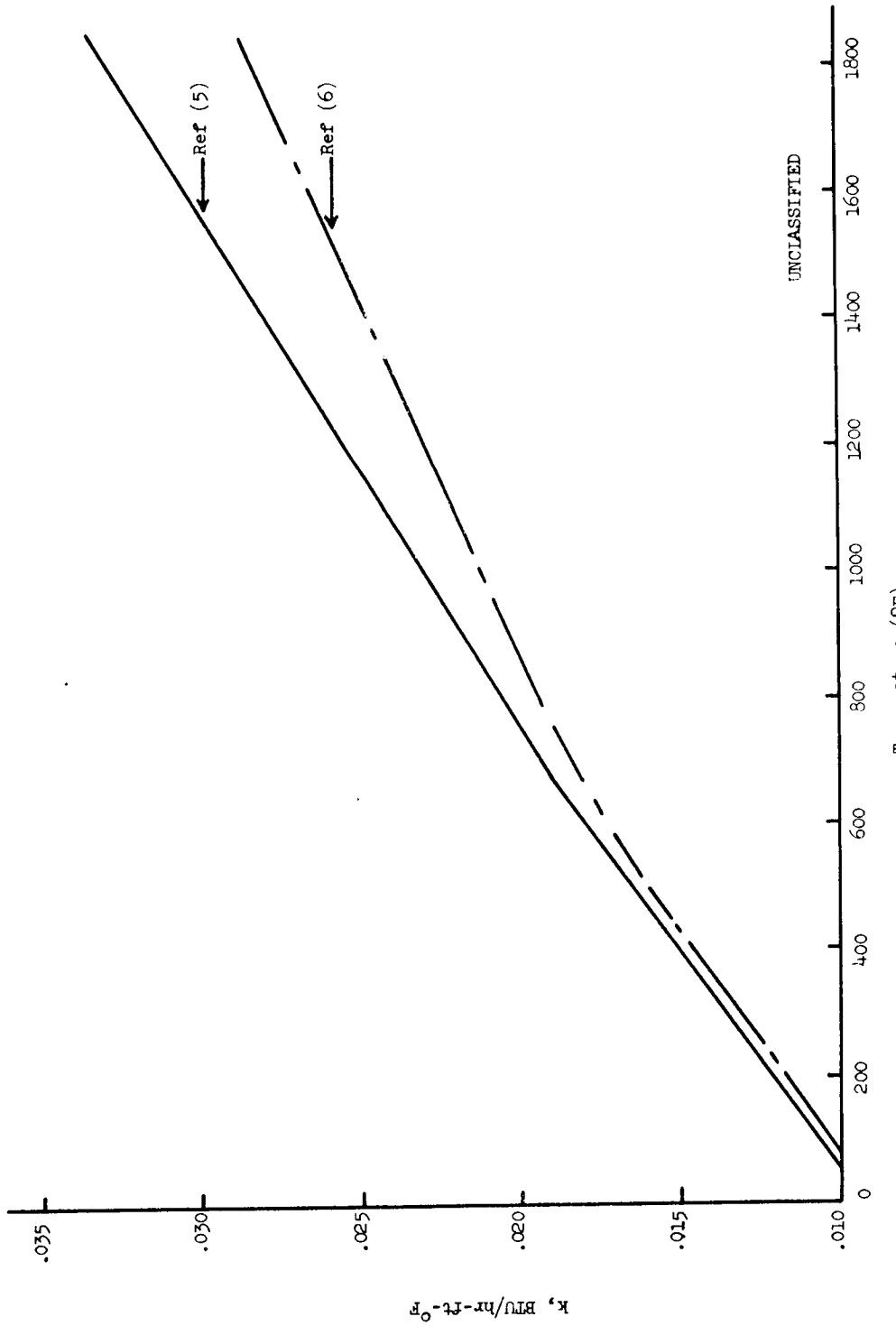

Fig. 2.6--(U) Thermal conductivity of argon

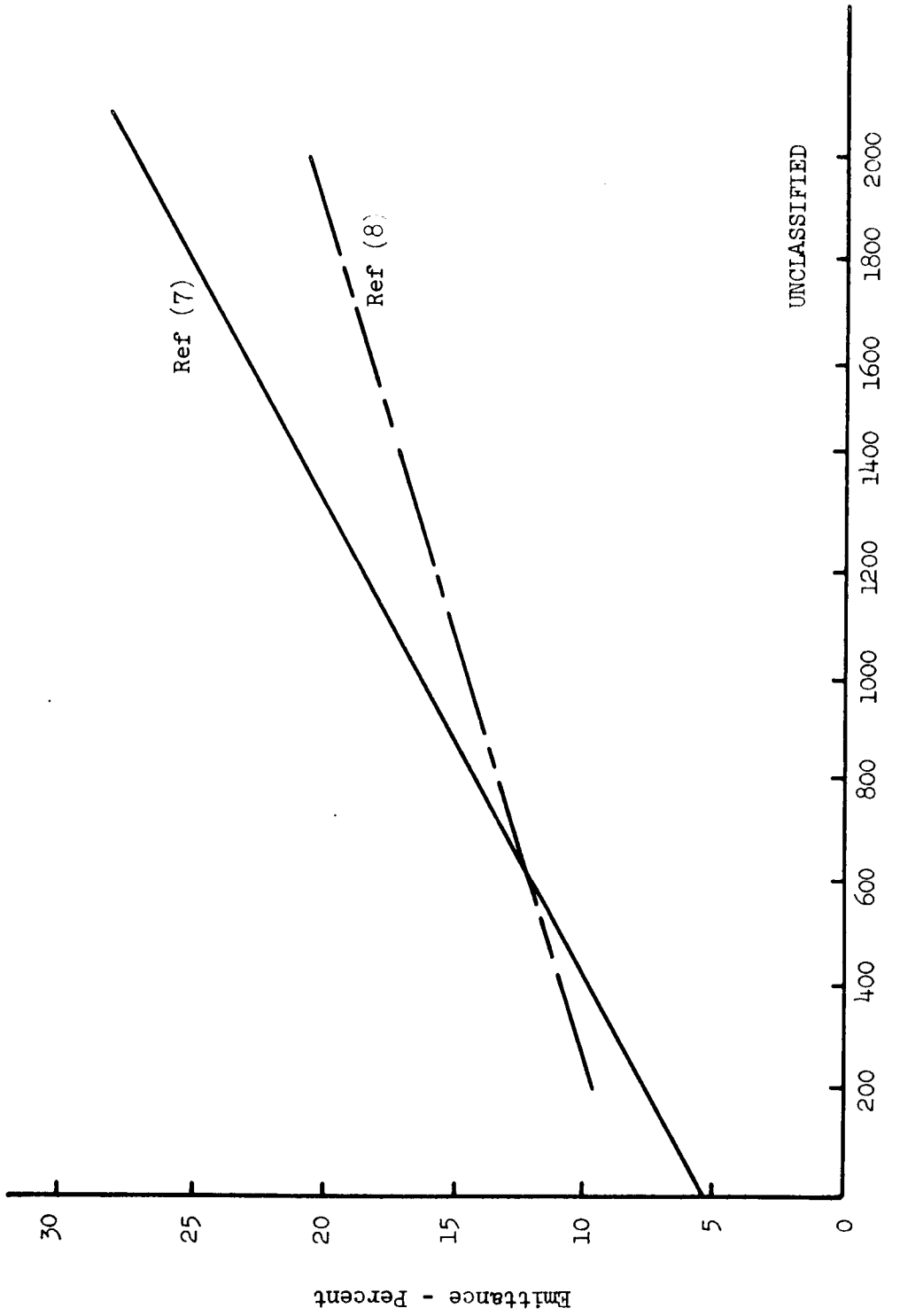

Fig. 2.7--(U) Emittance of polished Inconel

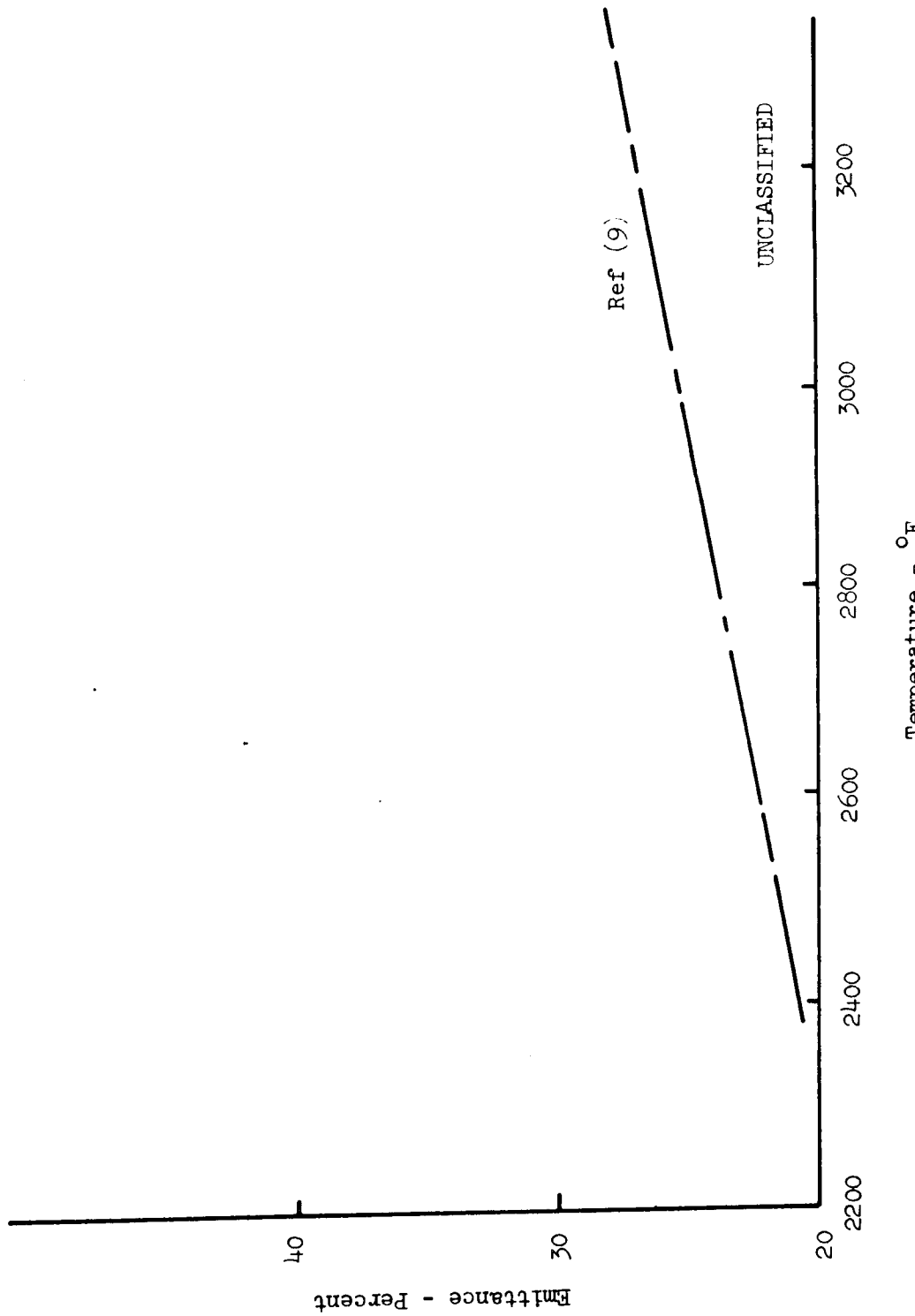

Fig. 2.8--(U) Emittance of polished tungsten

(5) γ heating rate: 0.5 - 1.0 w/gr

This is consistent with the range of interest in the V-2 tube region.

(6) Coolant flow rate: 4 - 7 GPM

This covers the range measured during the experiment.

(7) Coolant temperature: 125 - 135°F

These represent the temperature of the reactor inlet water and the temperature of the reactor outlet water.

Parametric Analysis

(U) The radial-axial heat transfer code, "RAT", was used to conduct the analysis. Figure 2.9 shows the fuel temperature-thermal bond temperature relationship obtained as a function of γ heating rate, fission power density, helium gap size, and coolant capacity, with the Inconel emittance, the tungsten emittance and the argon gap size considered to be dependent on their respective temperatures as described previously. Using these curves, one can deduce the uncertainty limits of fuel temperature and fission power density from the observed thermal bond temperature if the values of these parameters vary in the ranges indicated in the figure. Table 2.3 shows the changes in the fuel temperature and the thermal bond temperature when each of the parameters shown varies independently from its base value by the indicated amount, with the other parameters staying constant. It can be seen from Table 2.3 that the size of the helium gap and the γ heating rate are influential in changing the thermal bond temperature, (and fission power density values deduced therefrom) while the fuel temperature is strongly dependent upon the Inconel emittance and the fission power density.

Correlation Between Analytical and Experimental Results

(U) Fuel pod 213-6 exhibited the fuel temperature-thermal bond temperature relationship shown in Fig. 2.3 during the initial startup. At an average thermal bond temperature of 288°C, the observed fuel temperature was 1730°C. One of the data points for fuel pod 213-3 which contains the

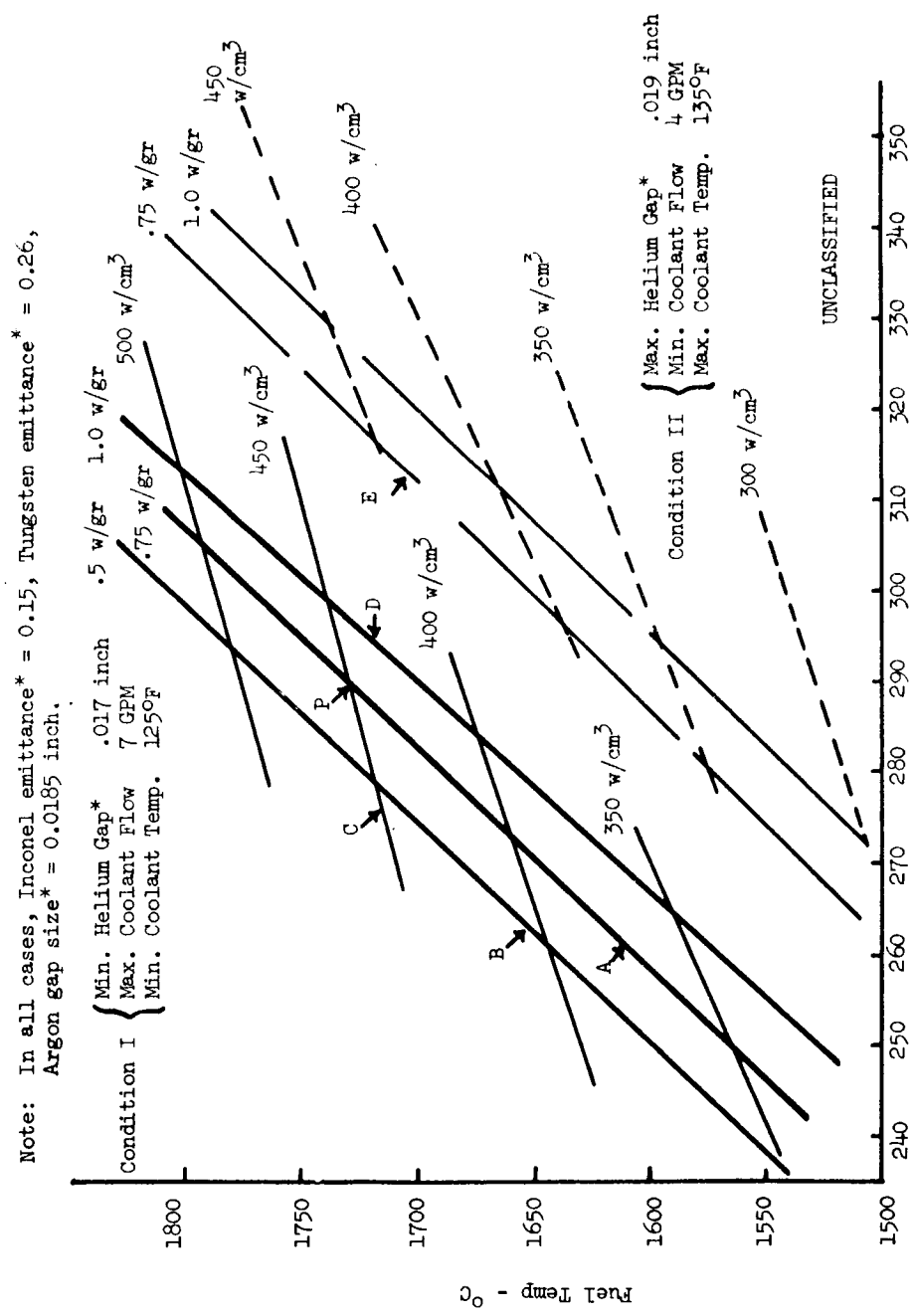

*These are room temperature values. In computation, they are fed in as a function of temperature.

Fig. 2.9--(U) Parametric analysis of the fuel temperature vs. thermal bond temperature relationship

Table 2.3

(U) CHANGES IN FUEL TEMPERATURE AND THERMAL BOND TEMPERATURE WITH CHANGES OF THE VALUES OF SOME PARAMETERS

(This table is Unclassified)

Independent Variables	Base	Variation From Base		Change in Fuel Temp.		Change in Thermal Bond Temp.	
		Amount	%	Degrees Cent.	%*	Degrees Cent.	%*
Helium Gap	.017"	+.002"	+11%	+3°	0.18%	+20°	8.4%
Argon Gap	.0185"	+.0015"	+8.1%	+32°	+1.9%	0	0
Gamma Heat	.75 w/gr	+.25	+33%	+13°	+0.77%	+10°	4.2%
Fuel Fission Power	440 w/cm^3	+110	+25%	+147°	+8.7%	+37°	+15.5%
		-110	-25%	-127°	-7.5%	-40°	-16.8%
Inconel Emittance	≅ .15	+.25	+167%	-140°	-8.3%	0	0

*Percent changes in temperature are based on temperatures above coolant temperature. For the fuel temperature the base was (1730 - 50) = 1680°C, and for the thermal bond the base was (288 - 50) = 238°C.

Tungsten emittance = 0.26

Coolant flow rate = 7 GPM

Coolant temperature = 125°F

other functioning high temperature thermocouple showed a fuel temperature of 1618°C at an average thermal bond temperature of 295°C. In order to ascertain which of the two "fuel temperature-thermal bond temperature" relationships is the more probable one and whether it could be used for establishing the fuel temperature and the fission power density in all the four fuel pods during their two cycle irradiation, comparisons were made between these experimental results and the analytical data. Using Fig. 2.9, the calculated maximum and minimum fuel temperature for conditions I and II at gamma heating rates of 0.5 and 1.0 W/gm respectively were determined for thermal bond temperatures of 288°C and 295°C. These values are compared with the observed fuel temperatures in Table 2.4. It can be seen that the observed fuel temperatures in both fuel pods (i.e. 1730°C and 1618°C) fall within the ranges (i.e. 1575-1762°C and 1604-1794°C), of the calculated values. The fission power density obtained from nuclear calculation based on data presented in the Design and Hazards Manual and assuming a γ heating rate of 1 W/gr is also shown.

(U) Although the above comparisons do not lead to a definite conclusion as to whether the fuel temperature - thermal bond temperature relationship in one fuel pod is more credible than that in the other, the following correlation analysis indicates that the relationship established for fuel pod 213-6 during the initial startup is more believable. In Fig. 2.10, the experimentally determined relationship is compared with the calculated ones for the parametric conditions indicated on the figure (which are identical with condition I of Fig. 2.9), with the γ heating rate as a variable (0.5, 0.75 and 1.0 W/gr.). It can be seen that the agreement is excellent at a γ heating rate of 0.75 W/gr. In fact, further changes of the parametric conditions within the allowable ranges do not lead to any better agreement. Figure 2.11 gives the calculated thermal bond temperature versus fission power density relationship for fuel pod 213-6 for the same parametric conditions as that shown in Fig. 2.10. The correlation analysis was therefore believed useful for deducing the fuel temperature and the fission power density from the more reliable thermal bond temperature reading if the capsule operates under the conditions specified in Fig. 2.10 and at a γ heating rate of 0.75 W/gr.

Table 2.4

(U) COMPARISON OF CALCULATED AND EXPERIMENTAL FUEL TEMPERATURE IN FUEL PODS 213-6 AND 213-3

(This table is Unclassified)

	Thermal Calc.		Experimental Values	
	Pod 213-6	Pod 213-3	Pod 213-6	Pod 213-3
Parameters				
He gap size, inch	.017-.019	.017-.019	--	--
Ar gap size, inch	.0185	.0185	--	--
Y heating rate, W/gr.	0.5-1.0	0.5-1.0	--	--
Inconel emittance	0.15	0.15	--	--
Tungsten emittance	0.26	0.26	--	--
Coolant flow rate GPM	4-7	4-7	6-7	6-7
Coolant temperature ^{o}F	125-135	125-135		
Location in PBR V-2 tube facility	---	---	0.2" E of centerline	0.2" E of centerline
Thermal bond temperature ^{o}C	288	295	288 ±.75%*	295 ±.75%*
Fuel Temperature ^{o}C	1575-1762	1604-1794	1730 ± 1%*	1618 ± 1%*
Fission power density W/cm^3	340-480	360-505	--	--

*Calibration accuracy when thermocouple is functioning

Design Point: He gap size, 017-.019 inch; Ar gap size, .0185 inch; Y heating rate, 1 W/gr; Inconel emittance 0.58; Tungsten emittance, 0.26; Coolant flow rate, 5 GPM; Coolant temperature, 125°F; Location in PBR V-2 tube facility, ~1" E of centerline; Thermal bond temperature, 420°C; Fuel temperature, 1800°C; Fission power density, 650 W/cm^3.

Nuclear Calc. from Reference (4): Y heating rate, 1 W/gr; Location in PBR V-2 tube facility, 0.2" E of centerline; Fission power density W/cm^3, 350 ± 35%.

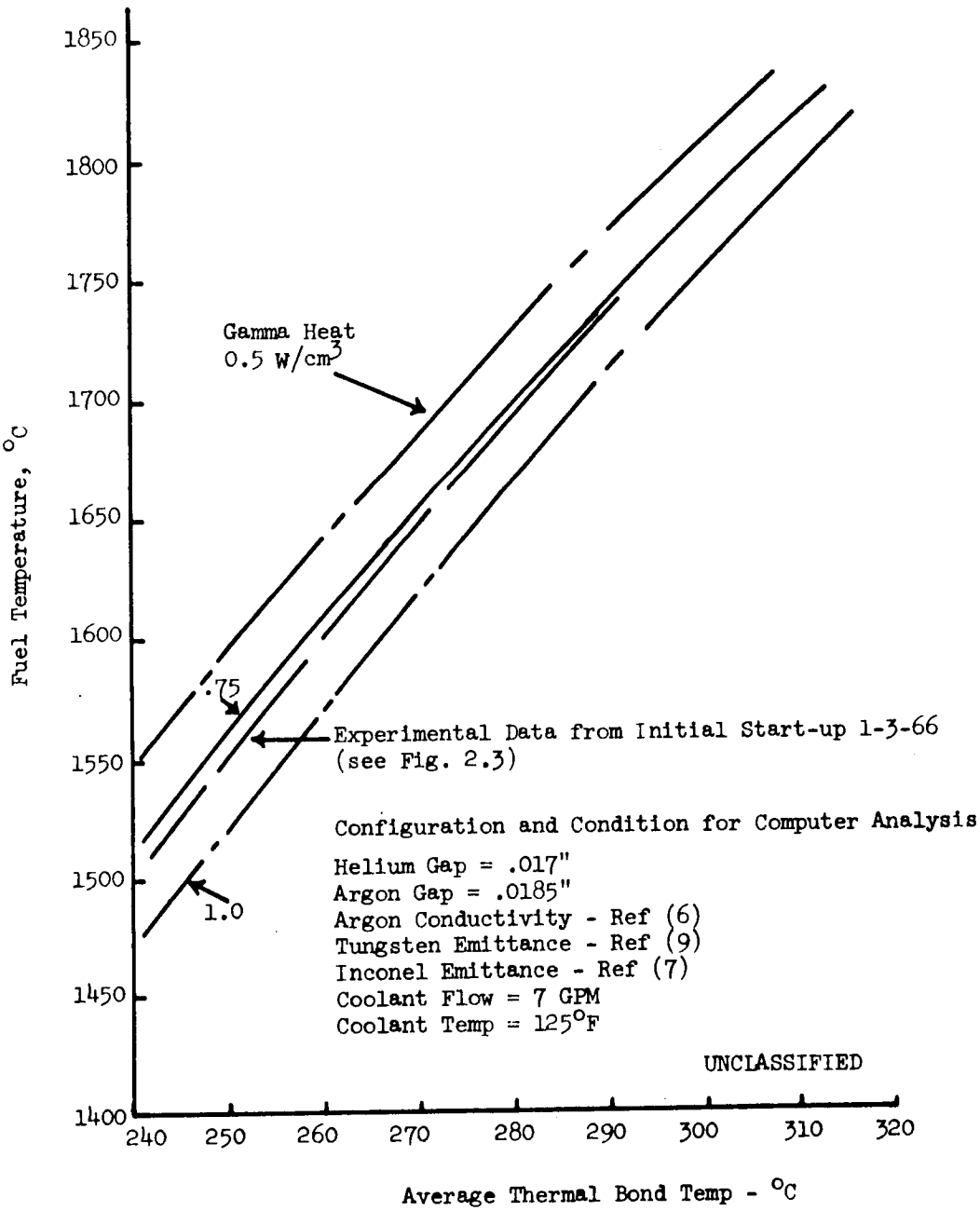

Fig. 2.10--(U) Thermal bond temperature vs. fuel temperature relationship for fuel pod 213-6

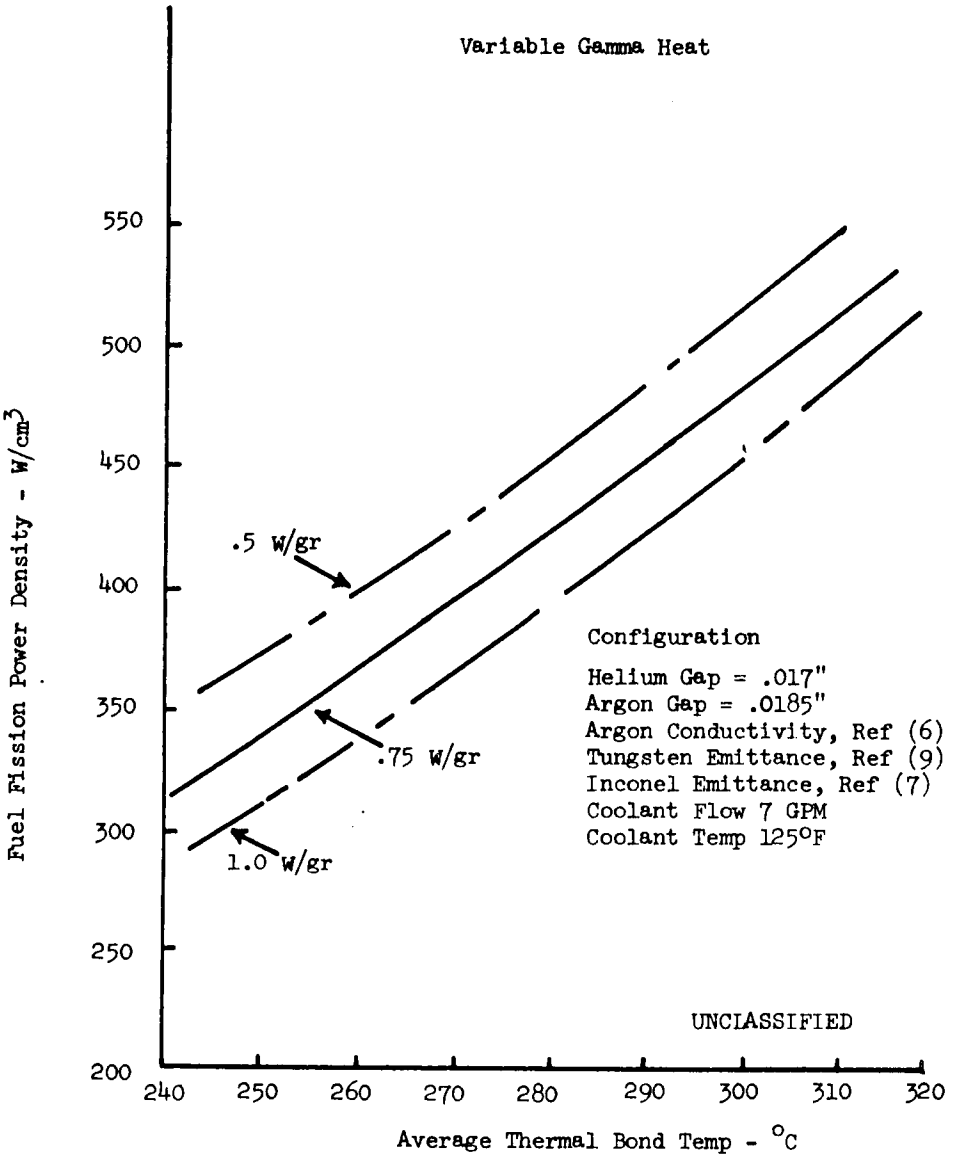

Fig. 2.11--(U) Analytical thermal bond temperature vs. fuel fission power density relationship for conditions specified on Fig. 2.10

(U) Similar comparison between experimental and analytical results was carried out using the previously mentioned data point for fuel pod 213-3 (1618°C fuel temperature versus 295°C average thermal bond temperature). Figures 2.12 and 2.13 summarize the results obtained. It can be seen that good correlation can be obtained only by assuming a high γ heating rate (1 W/gr.) in conjunction with a low fission power density (350 W/cm^3) for the parametric conditions defined in Fig. 2.12, or by assuming a high Inconel emittance (0.40) for the parametric conditions defined in Fig. 2.13. From these results it was concluded that the observed temperature relationship during the startup of fuel pod 213-3 (i.e. the 1618°C high temperature thermocouple reading versus the 295°C for the average thermal bond thermocouple reading) does not represent a true fuel temperature versus thermal bond temperature relationship for the following reasons.

(1) During the startup, fuel pods 213-3 and 213-6 were located in regions of about equal neutron flux. Therefore the fuel temperature on pod 213-3 should be expected to be about the same as that in pod 213-6. The experimental results, however, indicated otherwise; the high temperature thermocouple in pod 213-3 read 1618°C while the high temperature thermocouple in pod 213-6 read 1730°C. Since thermocouples rarely read higher but can read lower than the true temperature because of an electrical shortage upstream from the hot junction, it is believed that the 1618°C reading rather than the 1730°C reading is in error.

(2) Compared with fuel pod 213-6 for which good correlation between experimental and calculated results was obtained, the γ heating rate has to be higher (1 W/gr. versus 0.75 W/gr.) and the fission power density has to be lower (350 W/cm^3 versus 450 W/cm^3) in fuel pod 213-3 in order to achieve good correlation. This is contradictory to the fact that in the V-2 region, the γ flux and the neutron flux show changes in a similar rather than opposite direction. (+33% change in γ heating rate accompanied by a -22% change in effective thermal neutron flux.)

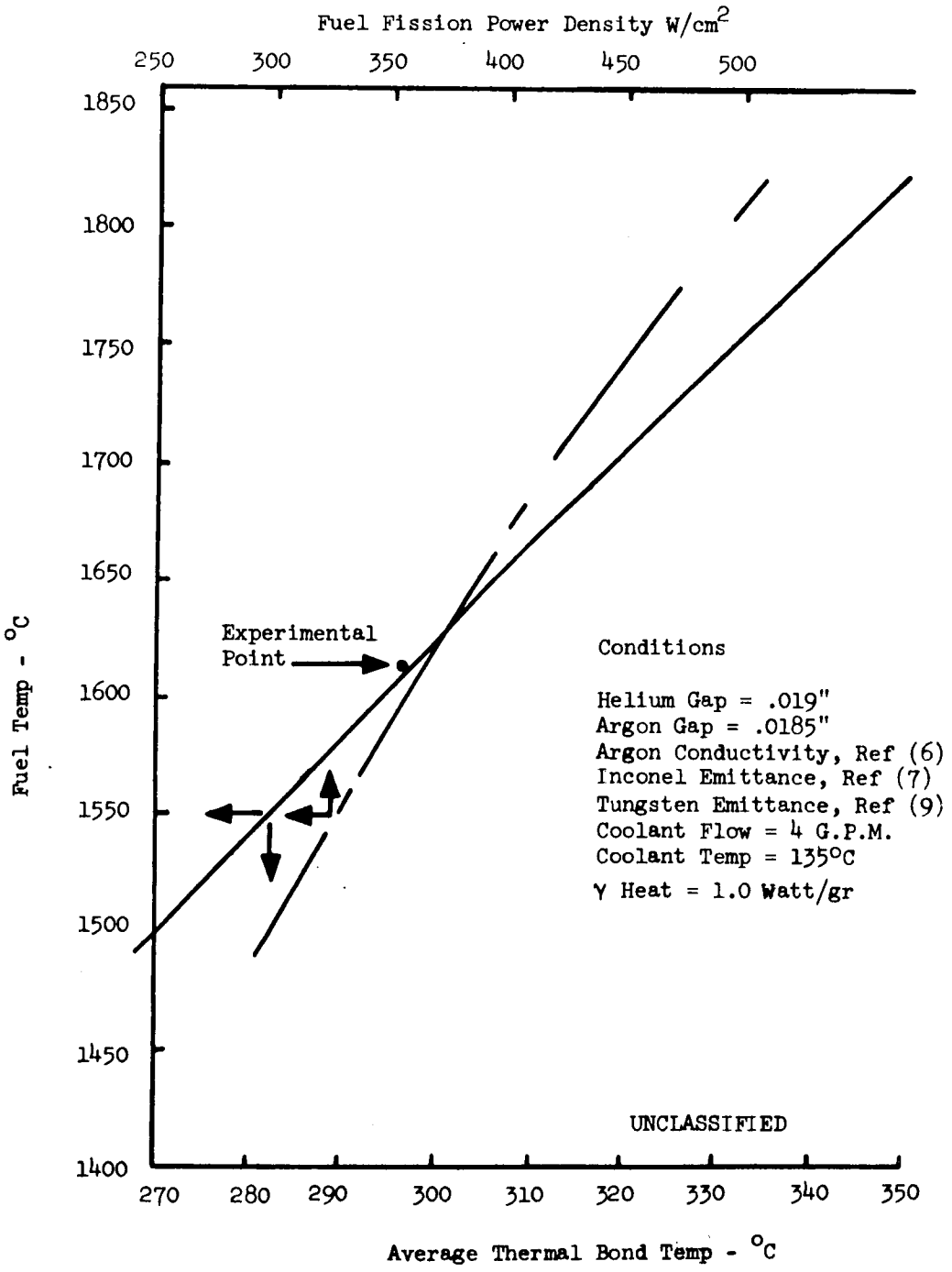

Fig. 2.12--(U) Thermal bond temperature vs. fuel temperature relationship for fuel pod 213-3

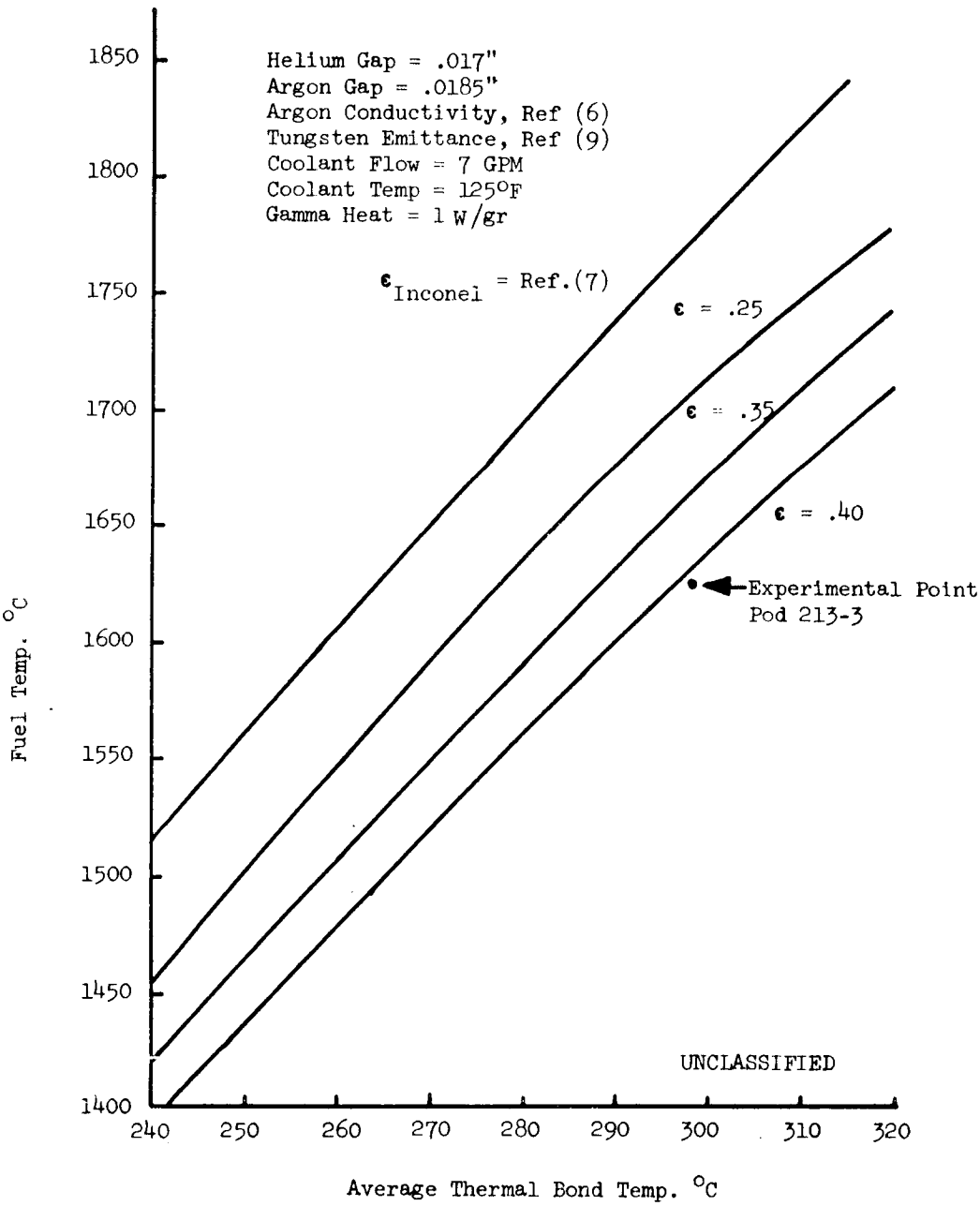

Fig. 2.13--(U) Thermal bond temperature vs. fuel temperature relationship for fuel pod 213-3, with Inconel emittance as variable

(3) The high Inconel emittance required (0.40) for good correlation is inconsistent with the polished finish of the Inconel surface. It is doubtful that enough deposit could have been accumulated during the initial startup period to increase the emittance from 0.15 to 0.40.

(U) Thus the above analysis indicates that a good correlation exists between the experimental and the calculated fuel temperatures versus average thermal bond temperature relationship during the initial startup for fuel pod 213-6, but not for fuel pod 213-3. The relationship established for fuel pod 213-6 and the parametric curves of Fig. 2.9 are used below to evaluate the fuel temperatures and the fission power densities in the four fuel pods as a function of irradiation time.

Evaluation of Fuel Temperatures and Fission Power Densities in Irradiated Fuel Pods as a Function of Irradiation Time

(U) The fuel temperatures and the fission power densities in the four irradiated fuel pods were deduced from their average thermal bond temperature history (Fig. 2.3) by using the relationships shown in Fig. 2.10 and Fig. 2.11. The results obtained are shown in Figs. 2.14(a) and (b). Such deductions were made by assuming that the conditions prevailing in each fuel pod were the same as that specified in Fig. 2.10 throughout the two irradiation cycles. Since this is not exactly true, the results shown in Figs. 2.14(a) and (b) are subjected to various degrees of uncertainties. These uncertainties are analyzed below for each fuel pod on the basis of the allowable variations in the values of the parameters involved, the parametric curves in Fig. 2.9 and the guiding principle that at any time during the irradiation the γ heating rates and the neutron flux densities in these fuel pods can shift from the initial values in fuel pod 213-6 only in the same direction, i.e. both are bigger or both are smaller but not one is bigger and the other is smaller than the initial values in fuel pod 213-6.

(1) Fuel pod 213-6. The good agreement between the experimental and the calculated fuel temperature versus average thermal bond

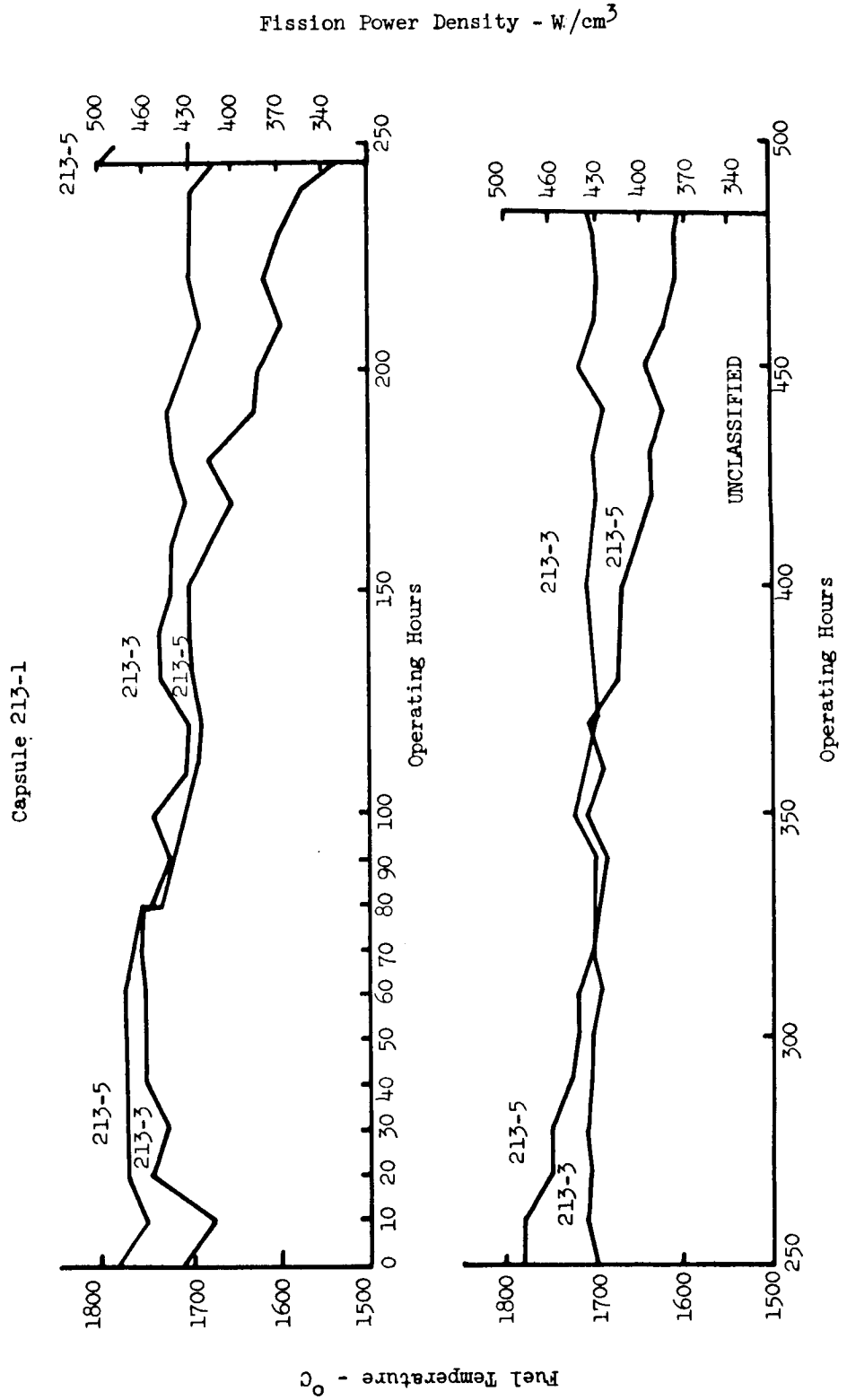

Fig. 2.14 (a)--(U) Fuel temperature and fission power densities in fuel pods as a function of irradiation time

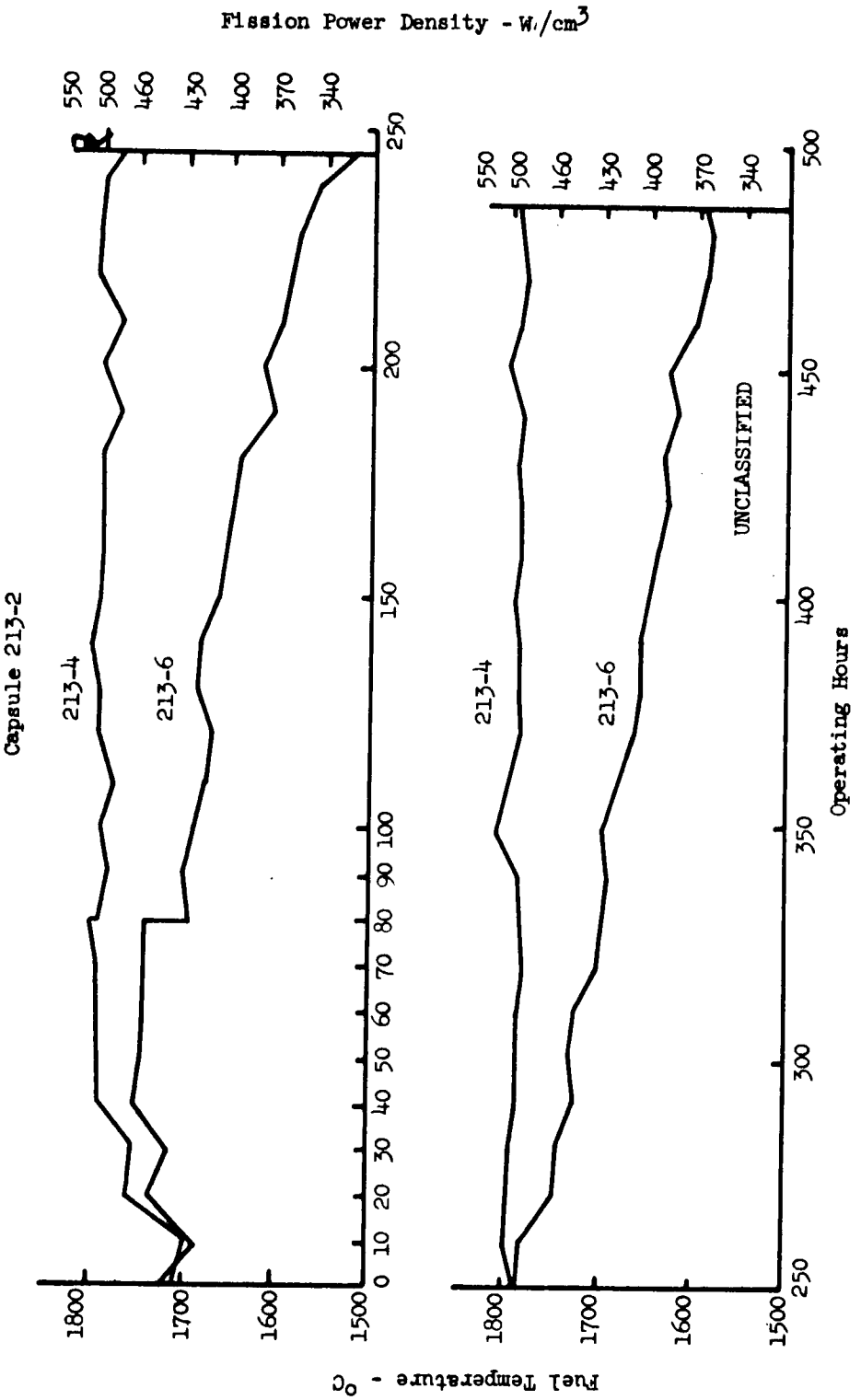

Fig. 2.14 (b)--(U) Fuel temperatures and fission power densities in fuel pods as a function of irradiation time

temperature relationship shown in Fig. 2.10 indicates that the initial fuel temperatures and fission power densities shown in Fig. 2.14 (b) should involve very little uncertainties. However, as the irradiation proceeds, it is expected that the major perturbation is the change of the γ heating rate and the neutron flux density, which alters the relationship among the thermal bond temperature, the fuel temperature and the fission power density, although the other parameters may remain essentially unchanged from those specified in condition I of Fig. 2.9. Since the γ heating rate and the neutron flux density have to both increase or both decrease from the initial values in the fuel pod 213-6 (defined by point P in Fig. 2.9), therefore for a given observed thermal bond temperature, the point defining the fuel temperature and the fission power density in Fig. 2.9, when shifted from the original reference line A, can move only within certain areas. If the γ heating rate and the fission power density both become lower than the initial value defined by point P, then this area is bounded by the lines A, B and C to the left of point P. On the other hand, if both the γ heating rate and the fission power density become higher than the initial values defined by the point P, then this area is bounded by the lines A, C and D to the right of point P. The reason that line B and line D form the bounds of these areas is based on the assumption that the γ heating rate in the V-2 tube is limited to 0.5 - 1.0 W/gr. Since the data shown in Fig. 2.4 indicate that the average thermal bond temperature for fuel pod 213-6 is less than 293°C throughout the two irradiation cycles, it can be seen from Fig. 2.9 that the maximum uncertainties in fuel temperature and fission power density, as represented by the maximum vertical distance in the above described areas of uncertainty for these thermal bond temperatures, are defined by the vertical distance between line A and line B, which amounts to ~30°C for the fuel temperature and ~30 W/cm^3 for the fission power density.

(2) Other fuel pods. For the other three fuel pods, the uncertainties in the fuel temperatures and fission power densities shown in Fig. 2.14 are due to the differences in both the Y heating rate and the values of the other parameters from the reference values of line A shown in Fig. 2.9. A similar analysis by invoking the same guiding principle described above but with operation possible in both condition I and condition II indicates that for the observed average thermal bond temperatures shown in Fig. 2.4, the maximum uncertainties on fuel temperatures and fission power densities in these fuel pods are defined by the vertical distance between the reference line A and the line E. Below line E the Y heating rate increases but the fission power density decrease, i.e. the guiding principle is not obeyed. These uncertainties amount to ~120°C for the fuel temperature and ~70 W/cm^3 for the fission power density.

Conclusions

(U) The calculated fuel temperature and fission power density ranges during the two irradiation cycles are taken from Fig. 2.14 and shown in Table 2.5. The uncertainties in these ranges due to possible variations in dimensions and gamma heating rate are also indicated here.

Table 2.5
(U) SUMMARY OF RESULTS
(This table is Unclassified)

Fuel Pod Number	Fuel Temperature Range °C	Fission Power Density Range, W/cm^3	Uncertainties	
			Fuel Temp. °C	Fission Power Density W/cm^3
Capsule 213-3	1675-1750	410-464	120	70
213-1 213-5	1540-1785	333-488	120	70
Capsule 213-4	1690-1815	418-510	120	70
213-2 213-6	1520-1810	329-507	30	30

(U) In the above treatment, the Inconel emittance is assumed to be uniform from pod to pod and to remain constant during the two reactor cycles. While this is probably true, as indicated by the similarity among the average thermal bond temperature histories of the fuel pods, no projection can be made of the change in the fuel temperature-thermal bond temperature correlation with time due to possible Inconel emittance changes.

(U) As shown in Fig. 2.4, there is good agreement in thermal bond temperature between the two top fuel pods and between the two bottom fuel pods, which indicates that the neutron flux conditions in the two capsules are symmetrical with respect to the reactor core. The decrease in temperature of the two lower fuel pods with control rod withdrawal indicates that the axial location of the capsules in the V-2 tube was lower than optimum. It appears that an adjustment in location upward of 2-4 inches could reduce the temperature variation in the lower pods at the expense of a small temperature variation in the upper pods. This would give the smallest maximum and smallest average temperature variation for all specimens.

2.2. DESIGN AND FABRICATION OF CAPSULES V-2C AND V-2D

(U) Following the termination of the irradiation test of Capsules V-2A and V-2B, efforts were initiated for modifying the designs of the capsule and the CPM in order to overcome the difficulties encountered during the irradiation of these capsules in PBRF. The final design layout and fabrication of the CPM (capsule positioning mechanism) and its associated instrumentation were subsequently carried out by Lewis Research Center. The final capsule design was firmed up after a series of discussions and reviews with NASA Lewis Research Center and PBRF personnels. On the basis of the new capsule design, several aspects on component fabrication, such as the bonding and joining of refractory metal and Inconel parts, the fabrication and evaluation of high temperature thermocouples, and the preparation of Inconel surface of high stable emittance, were investigated. Porous UC-ZrC fuel samples of controlled stoichiometry and containing tungsten additions were prepared according to the procedures developed under Part I of this contract and the high temperature stability of the

open pore structures of these fuel materials were demonstrated in work carried out under Contract NAS 3-8504.[10] Two capsules, V-2C and V-2D, containing vapor-deposited fluoride tungsten clad 90UC-10ZrC and 50UC-50ZrC fuel samples respectively, were assembled and delivered to PBRF for the study of the irradiation behaviors of these improved fuel materials. The irradiation experiment, designated as Experiment No. 62-13R2, is aiming at a cladding temperature of 1650°C and an integral burnup of 2×10^{20} fission/cm^3. These capsules are being irradiated in the V-2 tube position of NASA Plum Brook reactor. Details about capsule design, fabrication development, fuel sample preparation and capsule assembly and shipping are described below.

2.2.1. Capsule Design

2.2.1.1. Ground Rules for the Design

(U) The design of the capsule was based on the following ground rules:

(1) The nominal fuel cladding temperature shall be 1650°C and the nominal fission power density in the fuel material shall be about 200 Watt/cm^3.

(2) The fuel temperature shall be measured or otherwise deduced to an accuracy of ±100°C or better.

(3) The configuration of the test sample shall be similar to that of a fueled emitter in a thermionic fuel element.

(4) High temperature fuel thermocouples shall be used, with provisions to otherwise determine the fuel temperature if the fuel thermocouples should fail.

(5) A gamma heat meter shall be included in an attempt to measure the gamma heat generated in the capsule.

(6) The heat transfer system shall allow the measurement of the fission heat generation rate in the fuel by means of radial calorimeter.

2.2.1.2. Design Description

2.2.1.2.1. Design Criteria. – (U) The capsule was designed to provide thermionic fuel material irradiation information and to contain the fission gases inside the capsule during the irradiation. It was built to the intent of the ASME pressure vessel code but the code was not strictly adhered to in the welds and bonds because of the use of thin wall materials. However, the safety of the experiment and thus a remote hazard to the reactor was the prime factor.

(U) All metals used were certified and the welds were made by a qualified welder. All welds, and brazed and diffusion bonded joints were meticulously inspected and leak tested at each step during capsule assembly, using a Veeco Model MS9AB mass spectrometer-type helium leak detector. Any joint that was found to exhibit detectable leakge (10^{-8} std. cc/sec or greater) was repaired or the defective parts were replaced. The capsule was also X-rayed at each step of the assembly to verify the location of the fuel specimens and the thermocouples.

(U) Thermocouple leads were sealed at a transition joint with Hysol epoxy resin. This joint from metal-sheathed thermocouple to glass-asbestos covered wire was approximately 10 feet above the hot junction. This type of joint has been used extensively at Gulf General Atomic and has proven very successful. The terminals of all thermocouples were joined to a hermetically-sealed Cannon plug.

(U) The outer containment of the capsule was constructed of stainless steel and all joints exposed to reactor primary coolant were TIG welded. All portions of the capsule outer containment were pneumatically tested internally to pressures exceeding 1.5 times the primary system operating pressure (150 psig) with no evidence of leakage or distortion. It should be noted that the flexible portion of the lead tube could not withstand external overpressure; however, precautionary measures were taken in design and operational procedures to prevent such an occurrence.

(U) Instrument failures, loss of power and other hazard conditions are discussed in Appendix A.

[redacted]

2.2.1.2.2. Fuel Sample Design. - [redacted] Each capsule contained nine donut-shaped fuel samples, six of which were test samples and three of which were thermal shields. The six test samples were of three different configurations which were designed for the study of the variation of fuel swelling property with the surface area to volume ratio of the fuel body. The configurations, differing by the number and size of axial vent holes drilled into the fuel body while maintaining radial and circumferential grooves of the same size on one of the flat surfaces,* will be described in more detail in the section on fuel sample fabrication. The purpose of the axial vent holes and the grooves and the variation of the number and size of the vent holes are:

(1) The axial venting holes and grooves allowed the passage of fission gases released from all the fuel samples into a chamber for the containment of fission gases.

(2) The various sizes and numbers of vent holes in different test samples provided a range of surface area to volume ratios for the study.

In the design of the configuration of the vent hole, the principal nuclear constraint was that the void volume should not exceed ten percent of the volume of the fuel body. Other practical design constraints included the minimum diameter (~ 0.020 inch) of hole, which could be drilled into the carbide fuel body in large number (32) with a reasonable chance of success. The configuration of the three thermal shields was the same as that of the test samples of the largest surface area to volume ratio.

2.2.1.2.3. Fuel Sample Containment. - (U) The fuel containment assembly shown in Fig. 2.15 contained the fuel samples, the high temperature fuel thermocouple well, three sets of four-wire high temperature fuel thermocouples, two low temperature Chromel-Alumel thermocouples and the fission product storage chamber. The fuel was contained in a chemically

*Except for the top thermal shield which had grooves on both of its flat surfaces.

[redacted]

vapor deposited fluoride tungsten cup which was diffusion bonded to a tantalum transition piece. The thickness of the cup was 40 mils in the region in contact with the fuel samples. The high temperature thermocouples consisted of W-3 wt% Re versus W-25 wt% Re wires, the details of which will be described in the section on Fabrication Development. Two remote Chromel-Alumel thermocouples were embedded in a tantalum transition piece which was diffusion-bonded to the tungsten high temperature fuel thermocouple well and electron-beam welded to the tantalum transition piece of the fuel cup. Further description and the purpose of the transition remote thermocouples follows in the section on Capsule Instrumentation. An Inconel fission product chamber, copper brazed to the tantalum transition piece of the tungsten fuel cup, completed the fuel containment, with the thermocouples being sealed at the top end. This subassembly was outgassed during fabrication processing and then back-filled with argon gas. The copper pinchoff tube was then pinched off and backwelded shut.

2.2.1.2.4. Primary Containment. – (U) The fuel containment subassembly described above was contained in an Inconel primary containment tube, as shown in Fig. 2.16. This subassembly also contained the gamma heat calorimeter and its radiation heat shields, and the inner group of Chromel-Alumel thermocouples for the radial calorimeter, which were embedded in the wall of the Inconel primary containment for the determination of fission heat generation rate and the deduction of fuel temperature if the fuel thermocouple should fail. The gamma heat calorimeter is described in more detail in the section on Capsule Instrumentation. An annular neon gas gap was provided between the fuel cup and the Inconel primary containment with the radial spacing maintained by tungsten stand-off pins. The nominal gap dimension was 0.031 inch. All thermocouples were fed through a metal flange and sealed at the top of this subassembly. The subassembly was outgassed by heating and evacuating and backfilled with neon gas. The copper evacuation tube was pinched off than then backwelded.

2.2.1.2.5. Outer Containment. – (U) Final closure of the capsule was provided by the 321 stainless steel outer containment. This subassembly, shown in Fig. 2.17 contained the fuel containment and primary containment

subassemblies, and the outer group of Chromel-Alumel thermocouples for the radial calorimeter, which were embedded in the wall of the stainless steel outer containment tube. These thermocouples were separated from the inner group of Chromel-Alumel thermocouples in the wall of the Inconel primary containment by a helium gas gap of 0.013 inch width. All thermocouples were fed through a metal flange and sealed at the top of this subassembly. This containment was outgassed by heating and evacuating and backfilled with helium. The evacuation valve was then closed and welded shut.

2.2.1.2.6. Lead Tube. – (U) All capsule instrumentation was brought out of the outer containment and out of the reactor through a lead tube which incorporated a flexible section to provide freedom of capsule movement in the positioning mechanism.

(U) In pressure tests conducted at Gulf General Atomic it was determined that the flexible lead tube portion would contract about 7-3/4 inches over the entire length if an external pressure of 150 psi greater than the internal pressure were imposed upon it. Recovery could be made by an internal pressure excess of ~225 psi. Over-stretching could not occur since the criss-cross overbraid prevented such extension. A check valve was installed in the inlet gas pressurization line inside the lead termination to prohibit the loss of internal pressure in the event of a failure of the lead tube pressurization system. Another check valve was installed in series with the first valve in the inlet line outside the lead tube termination. The valves crack open at ~0.3 to 0.5 psi differential.

(U) The lower end of the lead tube was attached to the capsule by welding to the outer containment tube. Welded to the upper end of the lead tube was a multi-pin electrical connector for all instrumentation leads. The reactor vessel feed through assembly, shown in Fig. 2.18, also allowed angular rotation and about 2 inches vertical positioning in either direction of the capsule in the CPM. Two tubing connections were provided for purging and pressurizing the lead tube with helium to a pressure of 225 psig. The lifting adapter was used during manipulation of the capsule outside the reactor. It also provided protection for the multi-pin

connector until the final connections were mde. The complete capsule assembly and the lead tube are shown in Fig. 2.18.

2.2.1.2.7. Capsule Internal Instrumentation. – (U) Several new design features have been incorporated into the V-2C and V-2D capsules which were not in the original V-2A and V-2B capsules of Experiment 62-13-R1.

(U) High temperature fuel thermocouples. – Three high temperature thermocouple assemblies were located at three axial positions in the well to sense the fuel centerline temperatures (Fig. 2.19). Each sheathed thermocouple assembly contained two W-3 wt% Re versus two W-25 wt% Re wires formed into a common junction. The hot end of the thermocouple assembly contained hard-fired high purity BeO insulation inside an unswaged sheath of W-26 wt% Re. By using the common junction, breakage of a single wire would not cause the loss of both thermocouples in each assembly, and by using the remaining three wires there would still be two thermocouples functioning. The fabrication development and evaluation of these thermocouples are described in the section on Fabrication Development.

(U) Gamma calorimeter. – This instrument, shown in Fig. 2.16, consisted of a thick-walled aluminum cylinder with an electrical heater located at the center, and two Chromel-Alumel thermocouples embedded in the aluminum wall. The electrical heater consisted of nichrome wires insulated with MgO and sheathed with Inconel. This type of heater has been used with long life expectancy in Gulf General Atomic's TRIGA reactor for all in-pile tests. Two additional Chromel-Alumel thermocouples spaced correspondingly in the Inconel primary containment allowed measurement of the temperature gradient across a 0.040 inch neon gas gap. This calorimeter was expected to be a heat meter for determining gamma, or non-fissioning heat flux generated in the aluminum during capsule irradiation. The calculated heat flux value, together with the high temperature fuel thermocouple reading, provides a relationship between the Chromel-Alumel thermocouple readings and the fuel temperature. Also, the data from this calorimeter could be used as an indicator of any change in the thermal conductance of the neon gas gap during irradiation, caused by the leakage

of helium gas from the outer containment or argon gas from the fuel containment into the neon gas space. The information may also be used for other diagnostic purpose to evaluate capsule performance.

(U) Low temperature thermocouples. – In order to provide redundancy in determining the fuel temperature, Chromel-Alumel thermocouples were placed at a number of locations in the capsule.

(U) Two were located in the tantalum transition piece of the tungsten thermocouple well in the fuel containment subassembly (Fig. 2.15). A correlation can be established between the readings of these more reliable thermocouples and that of the fuel thermocouples by analytical means or by calibration of the beginning of the irradiation experiment. In the event of failure of the fuel thermocouples, the fuel temperature may be deduced from the readings of these low temperature thermocouples. However, since the axial expansion of the fuel samples due to swelling and the change of the thermal conductivity of the tungsten stem by neutron irradiation (see Section 2.2.1.3) affect the correlation, caution must be excercised in using this method to deduce fuel temperatures.

(U) Twelve Chromel-Alumel thermocouples were located in the wall of the Inconel primary containment as shown in Fig. 2.16. Again, the relationship between the readings of these thermocouples and that of the high temperature fuel thermocouples can be established first by calculation and then by calibration during irradiation. The uncertainty in the fuel temperature deduced from these temperatures was calculated and is discussed in Section 2.2.1.5.

(U) Three Chromel-Alumel thermocouples were located in the wall of the stainless steel outer containment for the determination of the fission power density in the fuel. Uncertainty calculations made for these thermocouples is given in Section 2.2.1.5.

2.2.1.2.8. Cooling Water. – (U) The experiment cooling system is shown in the line schematic of Fig. 2.20. The cooling water for the experiment is taken directly from the reactor primary coolant through a

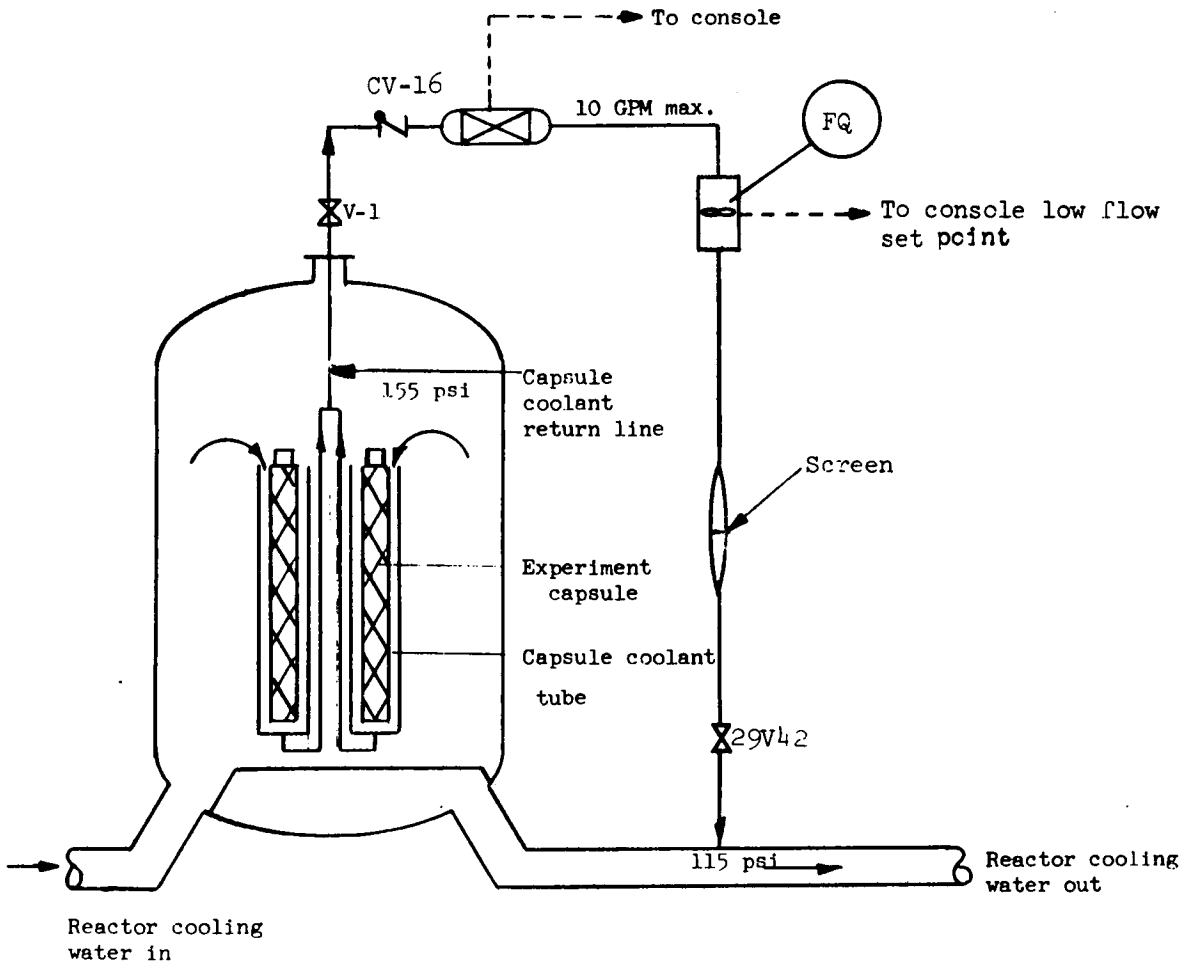

UNCLASSIFIED

Fig. 2.20--(U) Capsule coolant water flow diagram
Experiment 62-13R2

longitudinal slot, approximately 4 inches wide by 10 feet long, cut in the side of the V-tube. The coolant enters the top of the capsule facility tube and flows down the annular space between the tube and capsule. The coolant water is then returned to the reactor primary coolant system via lines which run from the bottom of the facility tubes, up along and inside the V-tube, through the V-tube housing to the return lines. The maximum water temperature is 150°F.

2.2.1.2.9. Capsule Positioning Mechanism (CPM). – (U) The irradiation experiment requires close control of the specimen temperature throughout each reactor cycle. In order to accomplish this objective, a system utilizing radial displacement of the capsules to modify the neutron and gamma flux seen by the specimens and thus to control the fuel temperature has been designed. Furthermore, the portion of the facility (V-2) in which the axial flux deviations are minimal has been selected for the nominal experiment position. Nuclear calculations indicate that the lower half of the core length exhibits the best flux profiles throughout the reactor cycle.

(U) The CPM consists of a movable, vertical beam pivoted about its midpoint inside a modified V-tube (see Fig. 2.21). The capsules are located at the lower end of the beam inside two 1-1/2 inch I.D. tubes that serve the dual purpose of holding the capsules and providing a coolant annulus. The swinging movement of the beam about the pivot bearing moves the capsules toward or away from the reactor core box, thus providing neutron flux variations for temperature control.

(U) At the upper end of the beam are the drive and positioning devices as shown in Fig. 2.21. A Jactuator, which provides the push-pull movement of the upper end of the beam, is driven by a variable speed, electric motor and gear box. Total movement of the beam (and capsules) is 5-3/8 inches. The Jactuator shaft penetrates the V-tube via a moving pressure seal made with a double "V" ring packing. A remote linear position indicator is provided so that the capsule position, with respect to the V-tube centerline, can be noted at the control console, from where the CPM is operated.

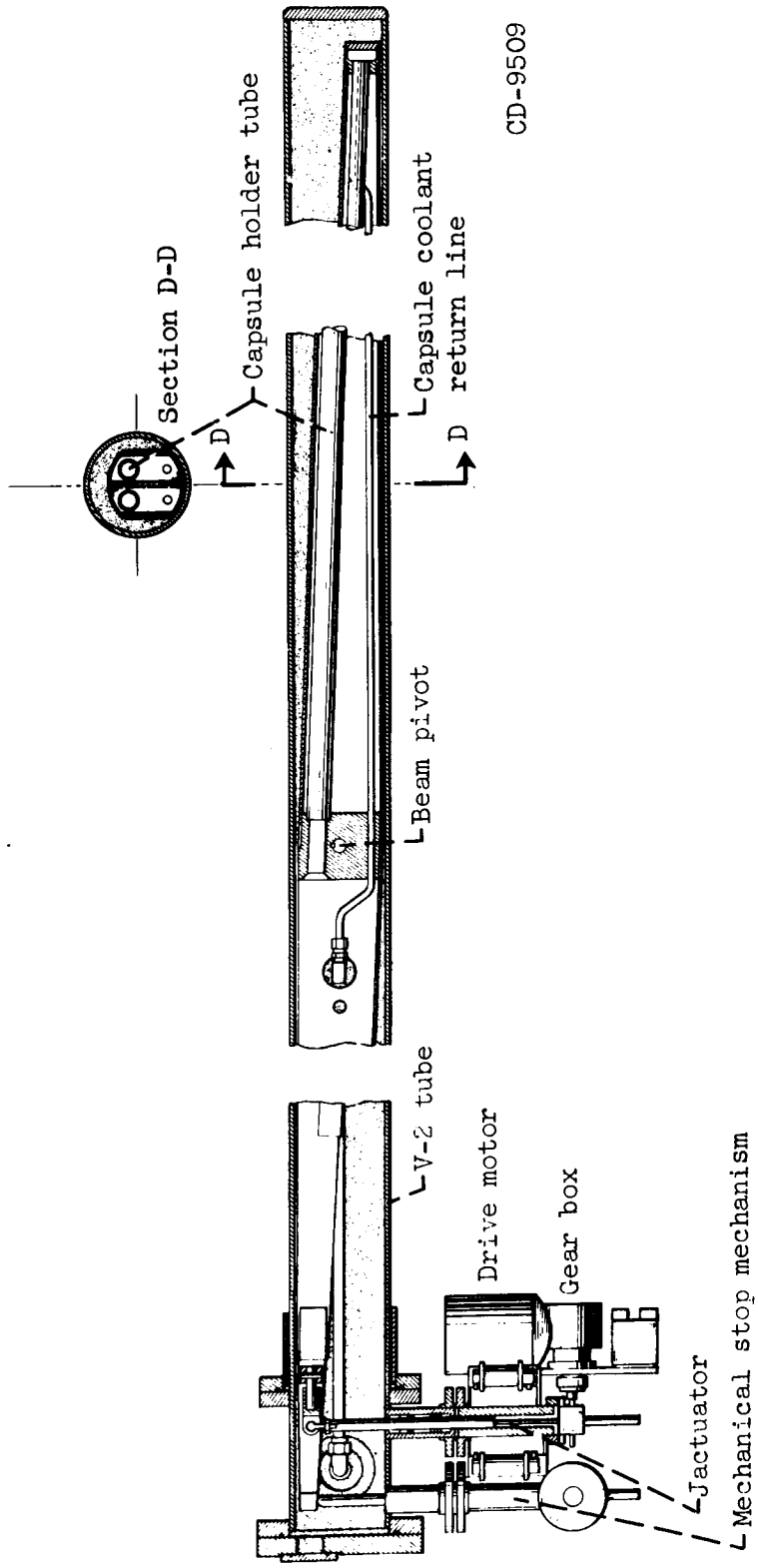

Fig. 2.21--(U) Capsule position mechanism

(U) Manual operation of the CPM is required to move the capsules in the flux field to attain the desired operating temperatures. The inward travel (toward the core) of the mechanism is normally restricted by a limit switch. If this fails, a second limit switch in conjunction with an adjustable mechanical stop prevents further motion. Either of the two switches will de-energize the drive motor. However, if both fail in this function and the motor continues to operate, a slipping clutch will allow the motor to rotate with the beam against the stop. Similarly, two limit switches detect the CPM out limit, but without a mechanical stop. All limit switches operate a light on the control console.

(U) A remote linear position indicator is provided so that the capsule position with respect to the V-tube centerline can be noted at the control console, from where the CPM is operated. Limit switches electrically restrict the travel of the beam toward or away from the core by opening the motor circuit as they are actuated by adjustable cams on the Jactuator shaft.

2.2.1.3. Thermal Analysis

(U) A thermal analysis was performed in which the temperature field was calculated throughout the irradiation capsule. This analysis was performed using the RAT, two-dimensional heat transfer program. The following assumptions apply to the calculation:

(1) The average surface heat flux at the outside of the fuel container is 45 W/cm^2.

(2) The nominal temperature of the fuel container is 1650°C.

(3) The gamma heating rate in the capsule components if uniform at 1 W/gram.

(4) The fuel and fuel container are in perfect thermal contact.

(5) The primary containment can (Inconel 600) is filled with 1 atm of neon gas.

(6) The secondary containment can (stainless steel) is filled with 1 atm of helium gas.

(7) The Inconel surfaces in the fueled region are oxidized to produce uniform radiation properties with an equivalent emissivity of 0.9756. This is based upon a non-gray, thermal radiation analysis.

(8) The coolant water has a film coefficient of 1910 Btu/hr-ft^2-$^\circ$F on the outside of the capsule.

(U) A typical temperature map is given in Fig. 2.22.

2.2.1.3.1. Transient Analysis. – (U) The RAT program was used to calculate the temperature field within the capsule components at 120% and 150% of design power for steady state operation. The results are that the fuel container temperature is nominally 1760°C at 120% power and 1950°C at 150% power.

2.2.1.3.2. "Remote" Thermocouple Correlation. – The "remote" thermocouple is mounted on the capsule fuel clad structure at a position where the temperature is considerably less than that of the fuel. It was intended that the remote temperature reading be correlated with the fuel temperature early in the life of the capsule.

(U) The correlation between the remote thermocouple and the fuel temperature can be affected by at least three mechanisms. These are gamma heating, fuel axial expansion and changes in tungsten thermal conductivity.

(U) The remote thermocouple temperature was calculated for variable fuel fission power and constant gamma heating. The result is shown in Fig. 2.23 where the remote reading is plotted versus the maximum fuel clad temperature.

(U) The next series of calculations* were made to explore the effects of constant fission power and variable gamma heating. The results are shown in Figs. 2.24 and 2.25. It can be seen that for the expected range of gamma

*These calculations were for a constant fission power which yields a nominal cladding temperature of 1800°C at a gamma heating of 1 W/gm.

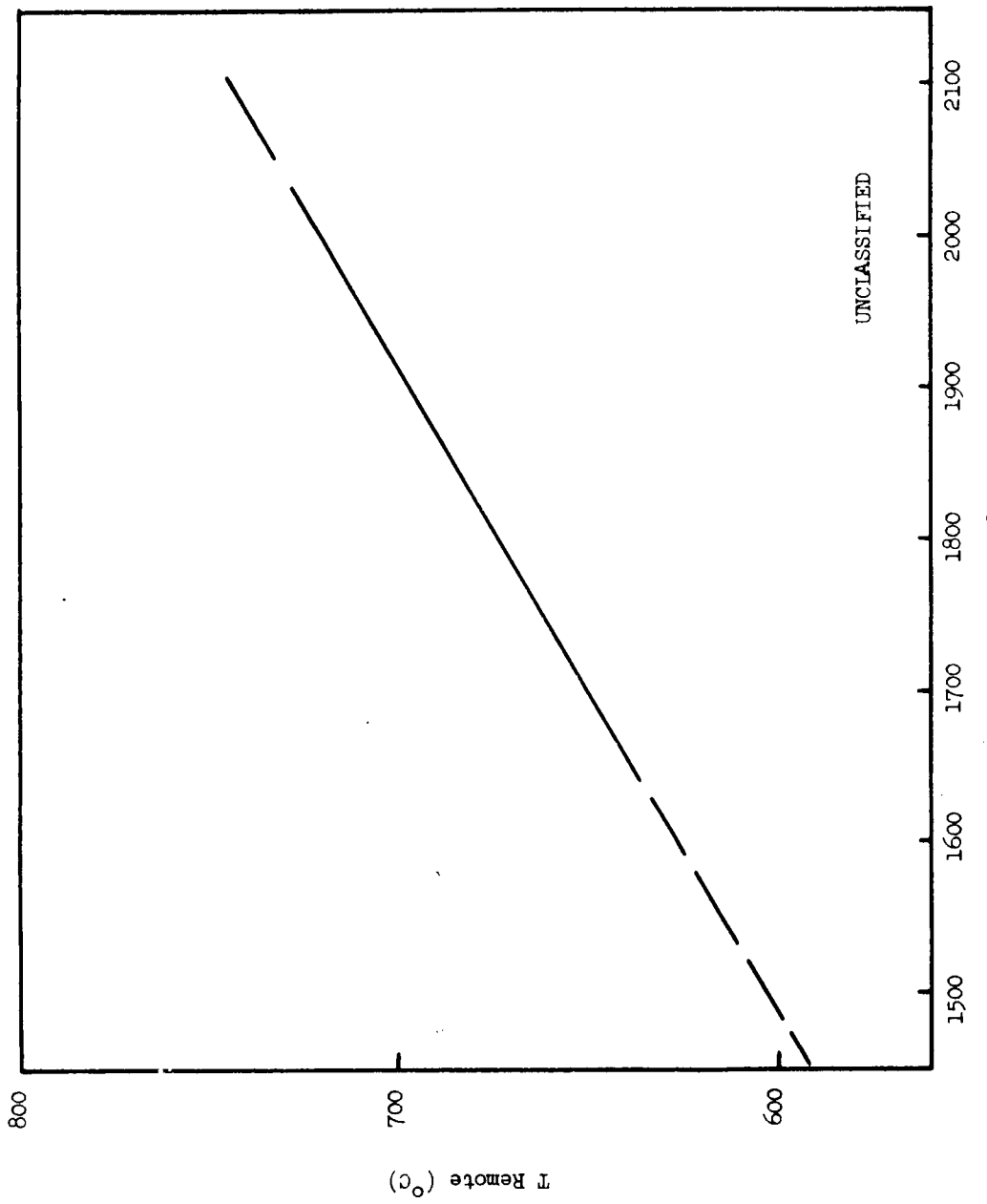

Fig. 2.23--(U) Remote thermocouple temperature reading versus clad temperature for variable fission power

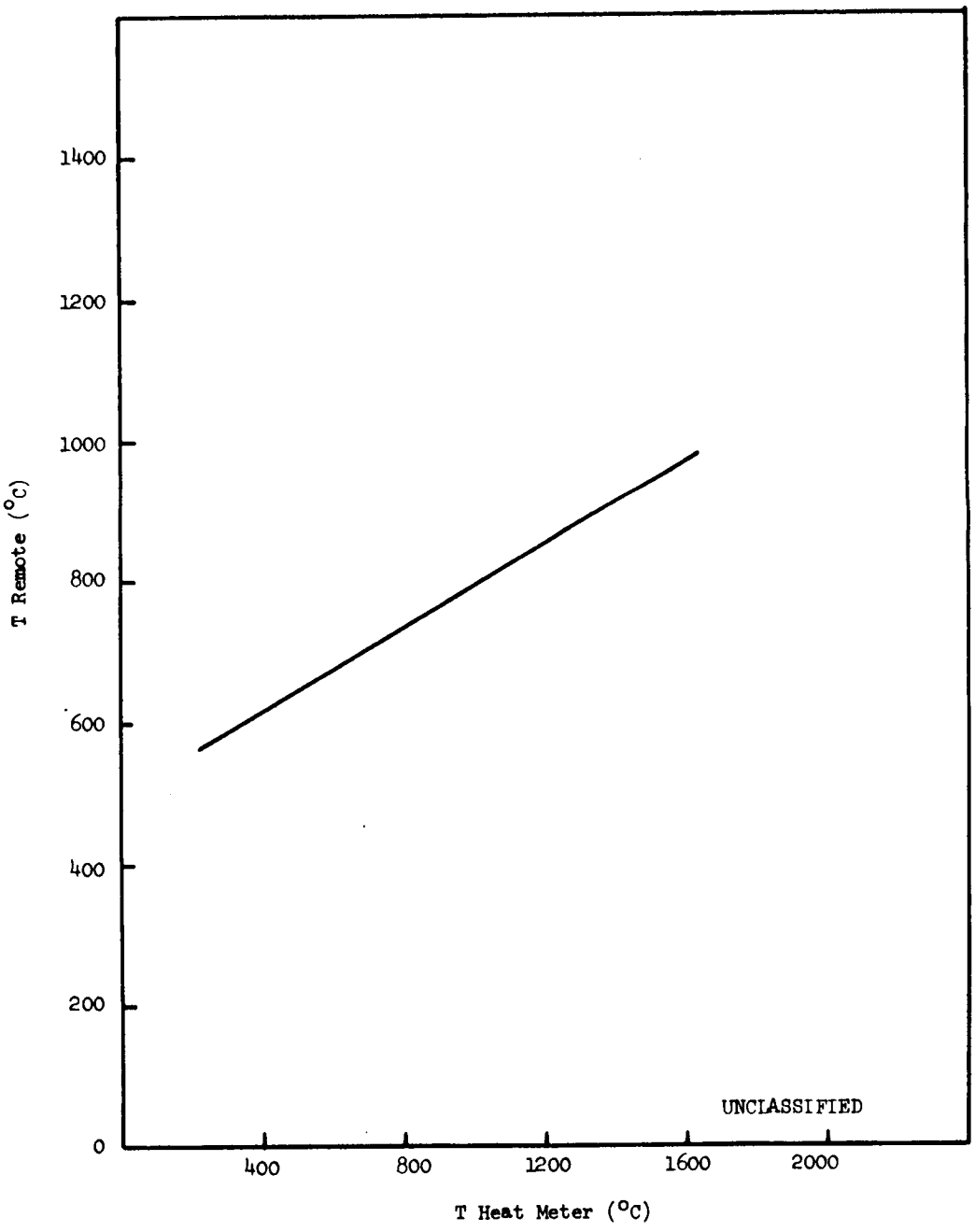

Fig. 2.24--(U) Remote thermocouple temperature versus heat meter temperature for constant fission power

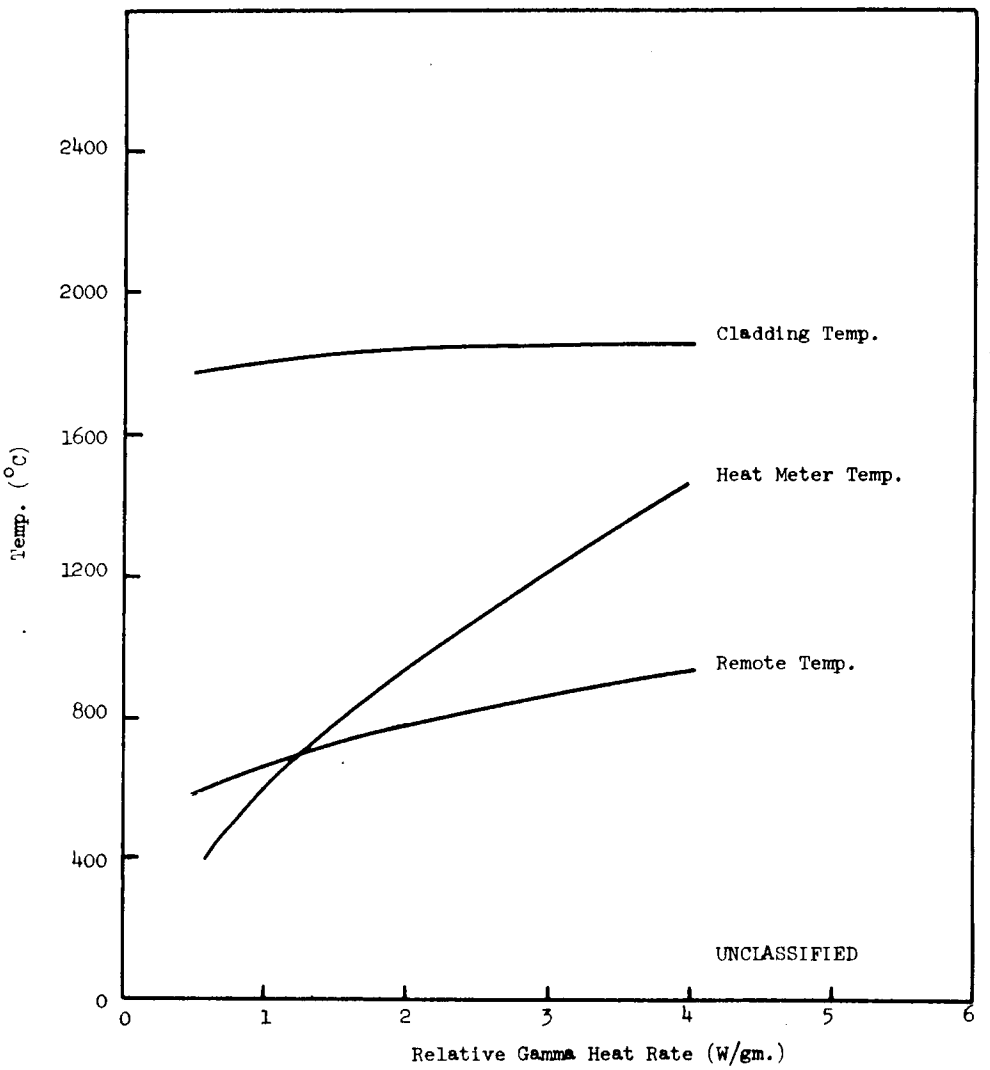

Fig. 2.25--(U) Gamma heat effects at constant fission power

heating in the Plum Brook V-tube, 0.5 to 1.5 W/gm, the variation in remote thermocouple reading is from 590° to 730°C. This corresponds to a variation in fuel clad temperature of 1450° to 2050°C according to Fig. 2.23. It is obvious that a usable correlation of the remote temperature with that of the fuel requires allowance for the influence of changes in gamma heating rate.

(U) Calculations* were then made to investigate the effect of variation of thermal resistance between the fuel and the remote thermocouple location. The major changes are a decrease of thermal conductivity during irradiation causing increased thermal resistance and a net decrease of tungsten thermal conductance length due to fuel expansion which results in decreased thermal resistance. The resulting effects are shown in Figs. 2.26 and 2.27. It is noted that the two changes tend to be compensating. That is, a 20 percent increase in fuel length results in a remote temperature increase of 100°C which would compensate for a tungsten thermal conductivity decrease of 30 percent.

2.2.1.3.3. Gamma Heating Effects. – (U) Gamma heating of the tungsten fuel clad due to activation by thermal neutrons (with no flux depression), followed by self absorption, amounts to about 3.1% of the surface heat flux with a half life at 24 hours for the only important isotope formed (W^{187}). At design operating conditions, gamma heating at 1 W/gm accounts for 18% of the total capsule power in the fueled region.

2.2.1.4. Nuclear Analysis

2.2.1.4.1. Fission Power Distribution. – (U) A nuclear analysis was conducted on the capsule design to determine the fission power distribution in the fuel sample. The relative radial distribution of fission power is shown in Fig. 2.28. This is a plot through the center line of a fuel pellet as a function of distance from the reactor core. The power in the capsule is normalized to an average of 1.0 such that the peak-to-average may be read directly from the curve. It is noted that the flux in the region near the core is about twice that of the region away from the core.

*These calculations were for a constant fission power which yields a nominal cladding temperature of 1800°C at a gamma heating of 1 W/gm.

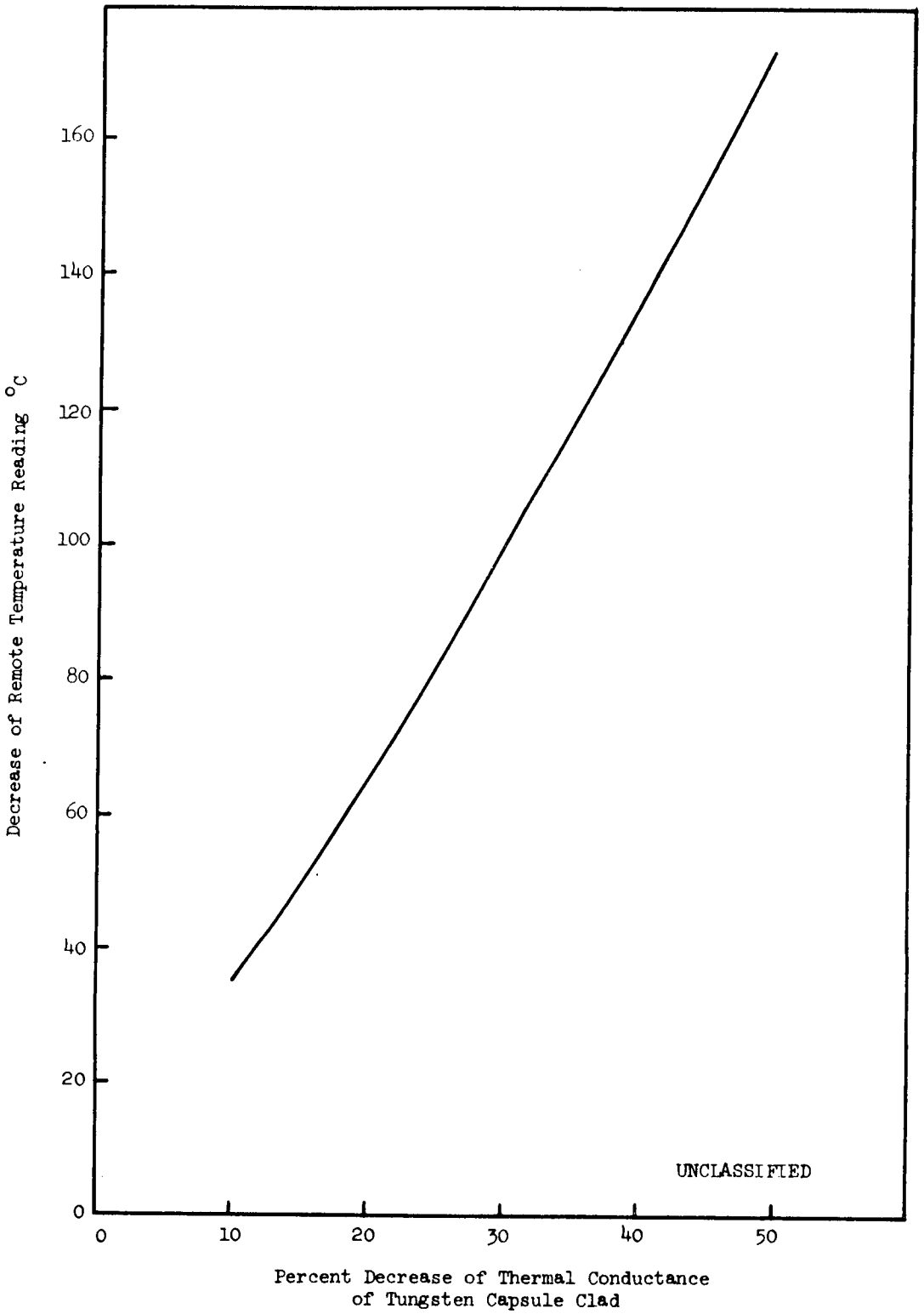

Fig. 2.26--(U) Decrease of remote thermocouple temperature as a function of tungsten thermal conductivity decrease

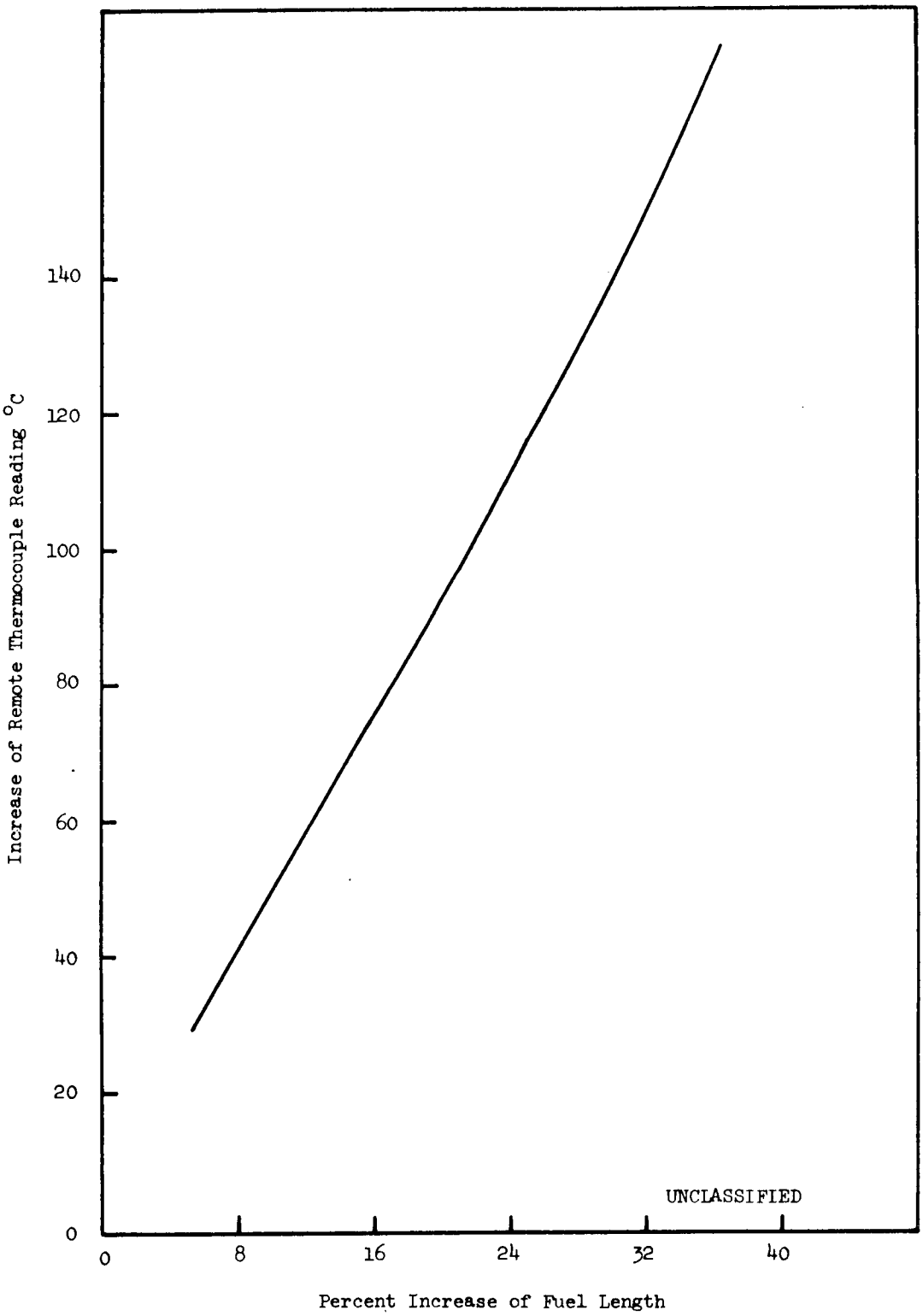

Fig. 2.27--(U) Increase of remote thermocouple temperature as a function of fuel length increase

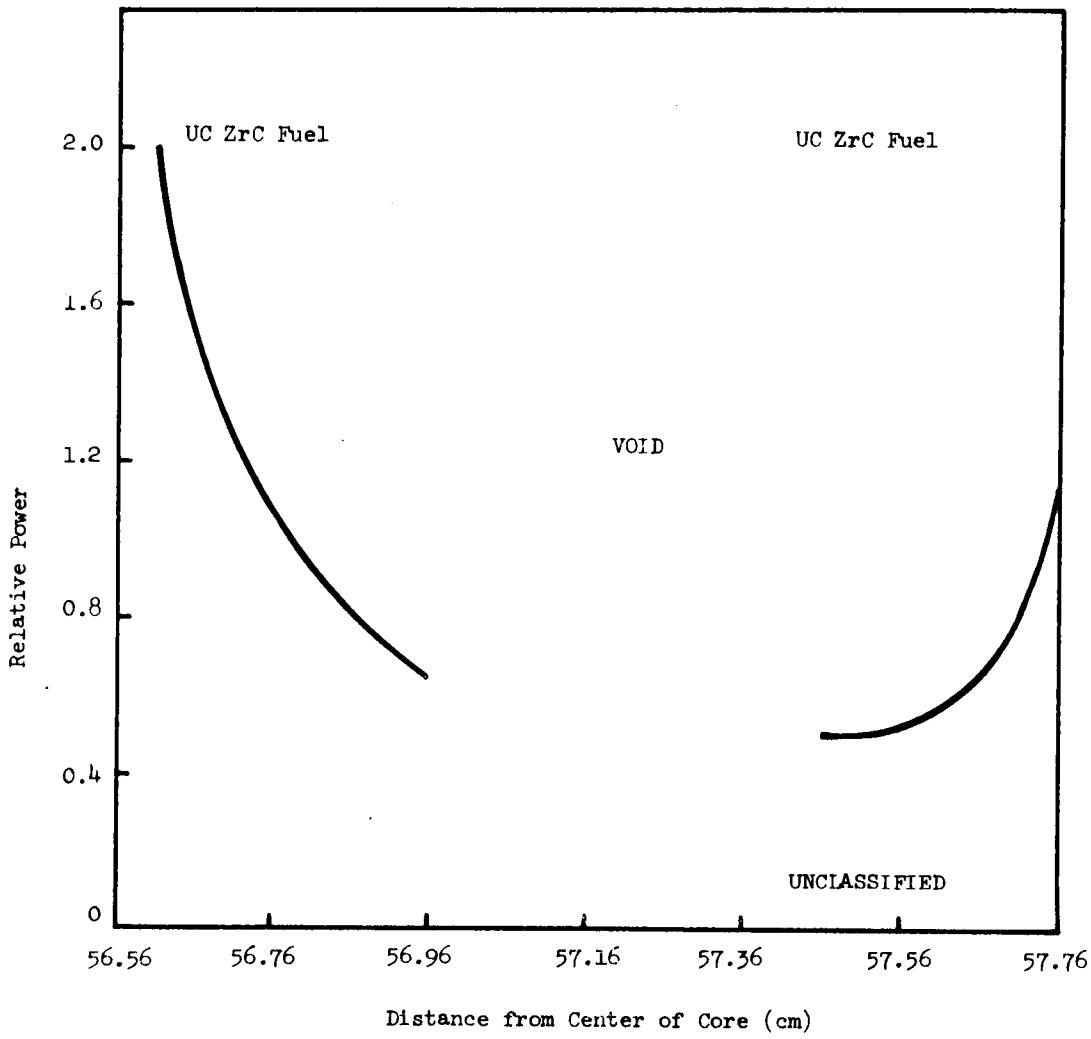

Fig. 2.28--(U) Relative radial power distribution in capsule

(U) The relative axial power distribution in the fuel as a function of radial position is shown in Fig. 2.29. The power distribution is normalized to an average of 1.0 in the capsule. It is seen that the axial peaking is greater towards the center of the capsule. The axial peak to average varies from 1.40 at the center of the capsule to about 1.2 at the outer edge.

2.2.1.4.2. Gamma Distribution. – (U) The amount and the distribution of heat that is attributable to the gamma ray flux were calculated. This is important for the assessment of the total fission power and burnup in the fuel. The sources of gamma rays considered were:

(1) Prompt fission - gamma rays emitted essentially in coincidence with the fission process.

(2) Fission products - gamma rays emitted essentially in decay of radioactive fission products.

(3) Capture - gamma rays emitted in the (n, γ) reaction.

(4) Activation - gamma rays emitted from active nuclei produced in a neutron reaction.

(U) The total radial gamma heating distribution through the capsule is shown by the solid line in Fig. 2.30. The dotted line shows the gamma heating due to the core and reflector. It is noted that about 65 percent of the gamma heating in the fuel and about 80 percent of gamma heating in the non-fuel regions is due to gamma rays originating outside of the capsule. The gamma heating varies across the fuel from about 1.3 watt/gm to 0.8 watt/gm.

(U) The axial gamma heating distribution through the capsule is shown in Fig. 2.31. This distribution is typical of all radial positions through the fuel. The axial variation in the fuel is from about 1 watt/gm to 0.8 watt/gm.

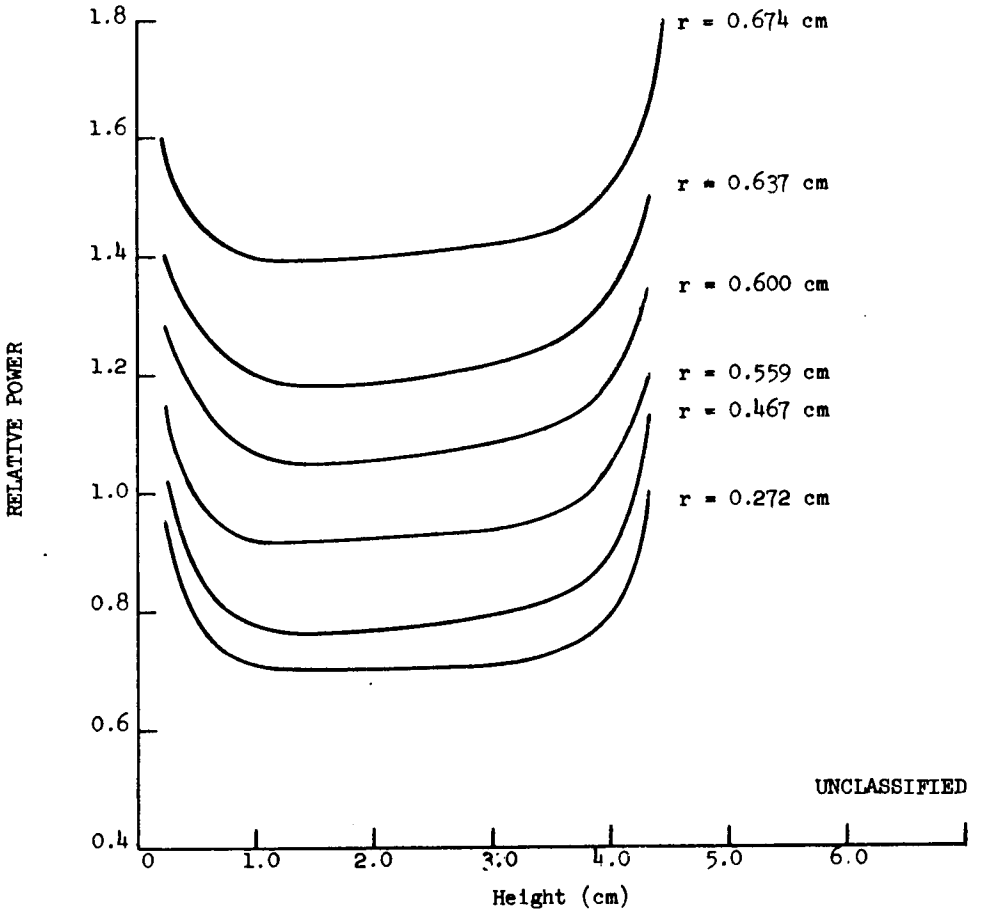

Fig. 2.29--(U) Axial power distribution as a function of radial position in capsule

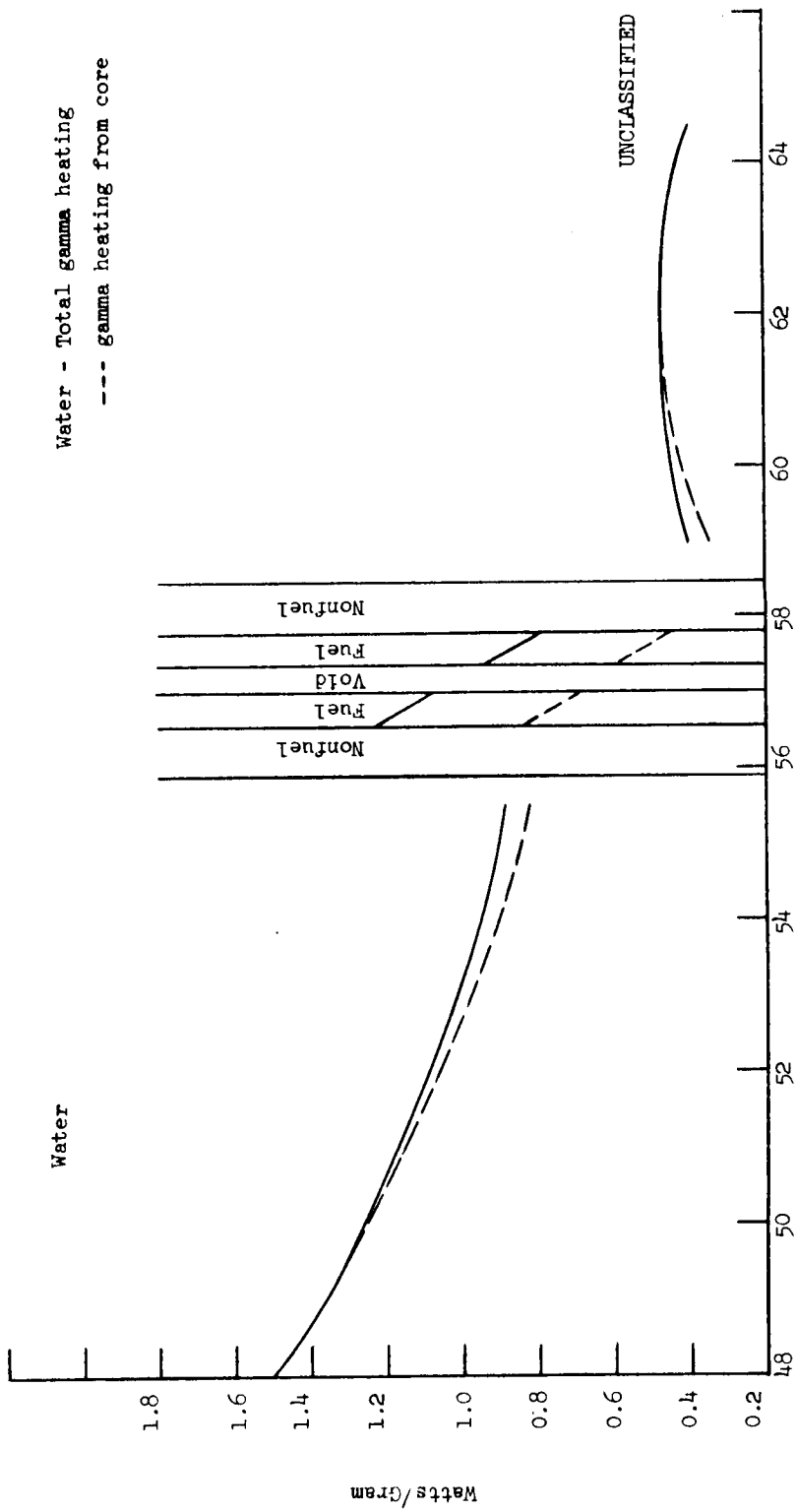

Fig. 2.30--(U) Radial gamma heating distribution in capsule V-2C

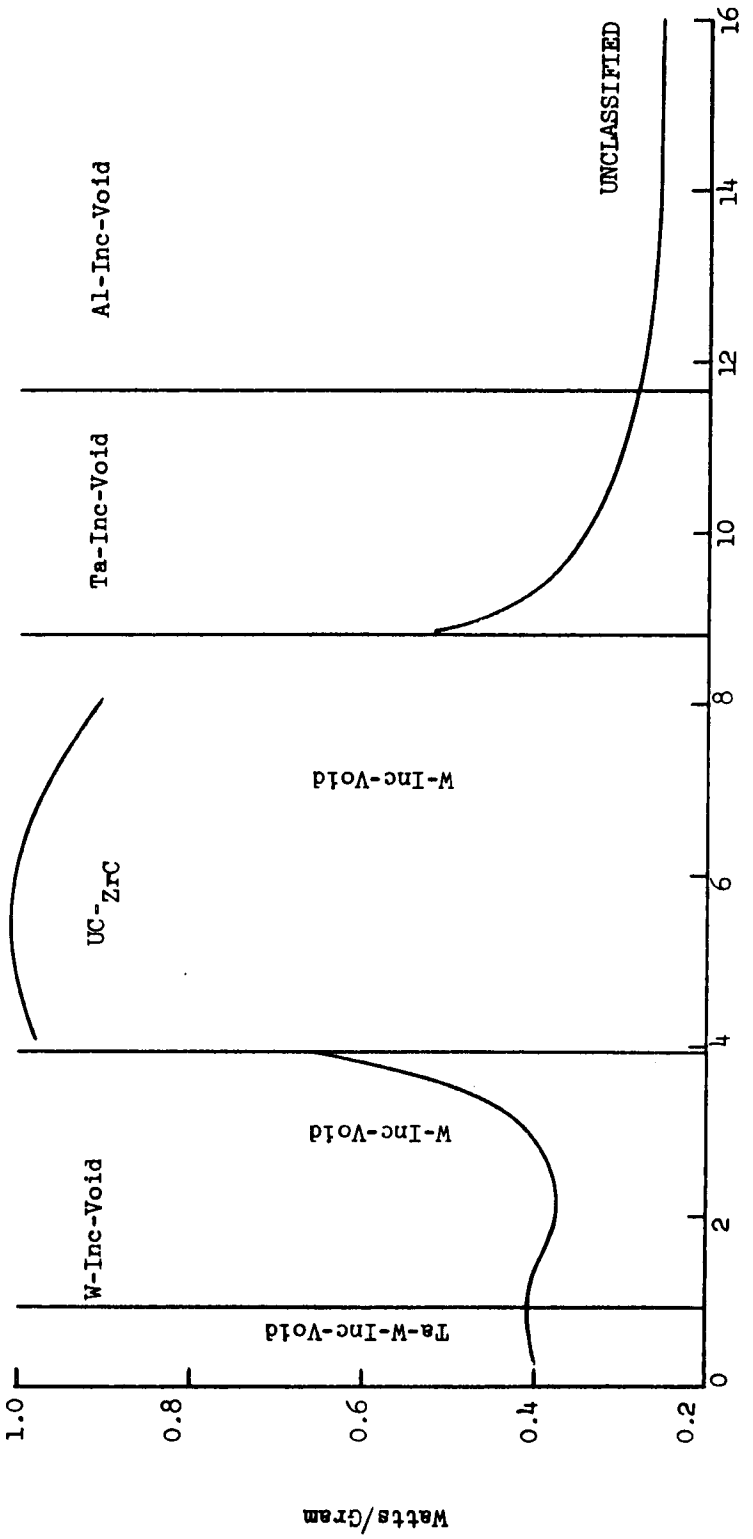

Fig. 2.31--(U) Axial gamma heating distribution in capsule V-2C

2.2.1.5. Uncertainty Analysis

(U) The experimental data obtained from the capsule irradiation experiment are primarily that concerned with the correlation of fuel temperature, fission power and irradiation time. It is generally assumed that the irradiation time can be determined to sufficient accuracy. However, there are a larger number of error sources associated with the experimental determination of fuel temperature and fission power. The phenomena that contribute to these uncertainties of measurement are listed below.

2.2.1.5.1. Sources of Fuel Temperature Error. – (U) These sources are:

(1) Fuel thermocouple calibration and stability.

(2) Capsule heat meter thermocouples sensitivity and stability.

(3) Change in thermal radiation properties of the helium or neon gap.

(4) Change in gas composition due to leakage between compartments at the sensitivity level of the helium mass spectrometer used in inspection.

(5) Angular variations in gas gap spacing.

(6) Mode of averaging axial and radial temperature gradients.

(7) Axial heat flow in the Inconel can affects the heat flux measured at helium gap.

(U) Items (1) and (6) above apply to the case when the fuel thermocouple is apparently operating in a satisfactory manner. All items apply if the fuel thermocouple is used to calibrate the fuel temperature versus radial heat meter readings and then this calibration is used to deduce fuel temperature, following complete failure of the fuel thermocouples.

2.2.1.5.2. Sources of Fission Power Error. – (U) These sources are:

(1) Capsule heat meter thermocouple sensitivity and stability.

(2) Uncertainty in heat transfer gap width due to manufacturing tolerances and uncertainties in thermal expansion, and eccentricity.

(3) Uncertainty in the gap transport properties including thermal radiation properties and gas thermal conductivity.

(4) Gamma heat meter uncertainties in electric power measurement, gap temperature measurement, gap properties, activation level, and relationship of gamma flux at capsule to gamma flux at the gamma heat meter.

(5) Uncertainty in relationship between gamma heating rate in the capsule materials and in the gamma heat meter due to geometry, mass, cross section, and activation.

(6) Uncertainty in axial heat losses as a portion of total fission power.

(7) Mode of averaging the heat meter readings to get integrated power in the presence of axial and radial temperature gradients.

(U) A linear error analysis was performed to estimate the uncertainty of measurement of fuel temperature and fission power in the PBRF irradiation capsule as defined by Figs. 2.15 through 2.19.

(U) Contributions to the total estimated uncertainty from each of various sources listed above are estimated based upon linear perturbation theory with second order effects being ignored in many cases. This is justified on the basis of the accuracy of the individual estimates and upon the method of combination of the individual error quantities into an overall uncertainty estimated. The method of combination of these quantities is that of Kline and McClintock,[11] which is a root-mean-square averaging.

(U) For the operative fuel thermocouple, the root mean square, or overall uncertainty is:

$$\epsilon = \pm 89^{\circ}C.$$

(U) For the inoperative fuel thermocouple, the root mean square, or overall, uncertainty is:

$$\varepsilon = \pm 87^{\circ}C.$$

(U) The distinction between the operative and inoperative fuel thermocouple cases is a time factor. In both cases the fuel thermocouple is operative for a sufficient period to calibrate the fuel temperature against the capsule heat meter thermocouple readings. The uncertainty in fuel temperature for the operative thermocouple includes the effect of long-term calibration drift, assumed here to be 5% of the nominal reading.

(U) The results for the two cases indicate that the fuel temperature uncertainty is less if the fuel thermocouples become inoperative early in the irradiation period and the heat meter readings are used as a measure of fuel temperature. This conclusion may be invalid in that it is the consequence of a somewhat arbitrary assumption regarding calibration drift. It seems more acceptable to adopt the philosophy that the fuel thermocouple readings be used as long as possible; switching to operation on the heat meter readings when necessary; with the overall uncertainty in fuel temperature being about $90^{\circ}C$ throughout the operation.

(U) The details of the fuel temperature uncertainty analysis are given in Appendix B.I. The estimated fuel temperature measurement uncertainties are summarized in Table 2.6.

(U) The details of the uncertainty analysis of fission power are given in Appendix B.II. The estimated fission power uncertainties are summarized in Table 2.7.

Table 2.6

(U) FUEL TEMPERATURE MEASUREMENT UNCERTAINTY

(This table is Unclassified)

Source of Uncertainty	Uncertainty	
	Operative Fuel Thermocouple	Inoperative Fuel Thermocouple
Fuel thermocouple calibration and drift	± 89°C	± 25°C (calibration only)
Heat meter thermocouple calibration and drift:		
Inconel -	---	± 12.6
Stainless Steel -	---	± 9.6
Outer gap radiation properties	---	± 23.0
Inner gap radiation properties	---	± 64.0
Gas composition change	---	0
Angular gap variations	---	0
Radial heat flux averaging	0	0
Axial heat flux averaging	± 1.0	± 1.0
Axial heat flow in Inconel	---	± 23.0
Thermocouple radial location in Inconel	---	± 20.0
Thermocouple radial location in stainless	---	± 20.0
Fuel thermocouple gamma heating	+ 8.0	+ 8.0
Fuel thermal conductivity uncertainty	---	± 23.0

Table 2.7

(U) FISSION POWER MEASUREMENT UNCERTAINTY

(This table is Unclassified)

Source of Uncertainty	Uncertainty (%)
Heat meter thermocouple calibration and drift	± 1.2
Helium gap dimensions	± 9.1
Helium gap radiation properties	± 1.5
Gamma meter electrical input measurement	± 1.3
Temperature recorder reproducibility	± 1.6
Gamma meter activation	± 1.7
Axial heat flow in Inconel	± 2.1
Axial heat flow from capsule	± 6.4
Radial locations of heat meter thermocouples	± 1.7
Gamma absorption variations with composition (η, α) and β activation, estimated	± 1.2

The overall, root-mean-square, uncertainty is given by the root mean square method as: $\epsilon = \pm 11.9\%$. That is the fission power can be determined to an accuracy of about 88 percent.

2.2.2. Fabrication Development

2.2.2.1. Metal Components

(U) Thermocouple well and fuel cap bonding and machining. – Because of the reliability demonstrated by tungsten-to-tantalum diffusion bonds in similar applications, diffusion bonding (1800°C, 2000 psi for 2 hours) was the preferred method of attaching the tungsten fuel cup and the thermocouple well to their respective tantalum transition pieces. Bonding, finish machining of a practice fuel cup and a thermocouple well assembly were successfully accomplished. Figure 2.32 shows the finished fuel cup after an 1800°C outgassing treatment. The thermocouple well assembly is shown in Fig. 2.33.

(U) Thermal contact welding between the fuel cup tantalum transition and thermocouple well tantalum transition. – Satisfactory joints were obtained on practice samples by electron beam welding. Microstructures of one of the practice samples are shown in Fig. 2.34.

(U) Tantalum-to-Inconel transition brazing. – Practice samples of tantalum and Inconel 600 were copper brazed and thermal cycled to 800°C (400°C higher than the design temperature). Figure 2.35 shows the excellent structure of the joint.

(U) Tungsten centering pin insertion techniques. – Fuel cup centering pins were placed into the Inconel 600 center sleeve mock-up sample, tightened by pressing into their locking tapers, and then permanently fixed to the sleeve wall by cover welding with Inconel filler. The pins were successfully ground to a common I.D. radius. The procedure was considered satisfactory for capsule fabrication.

(U) Inconel primary containment. – Drilling of the thermocouple and heater lead holes through the Inconel primary containment presents a major fabrication problem. Various avenues of approach were explored. Satisfactory results were finally obtained by Allied Pacific Manufacturing of Compton, California by using electrical discharge machining. The drilled pieces were then finished machined at Gulf General Atomic. The center sleeve hole problem was thus resolved.

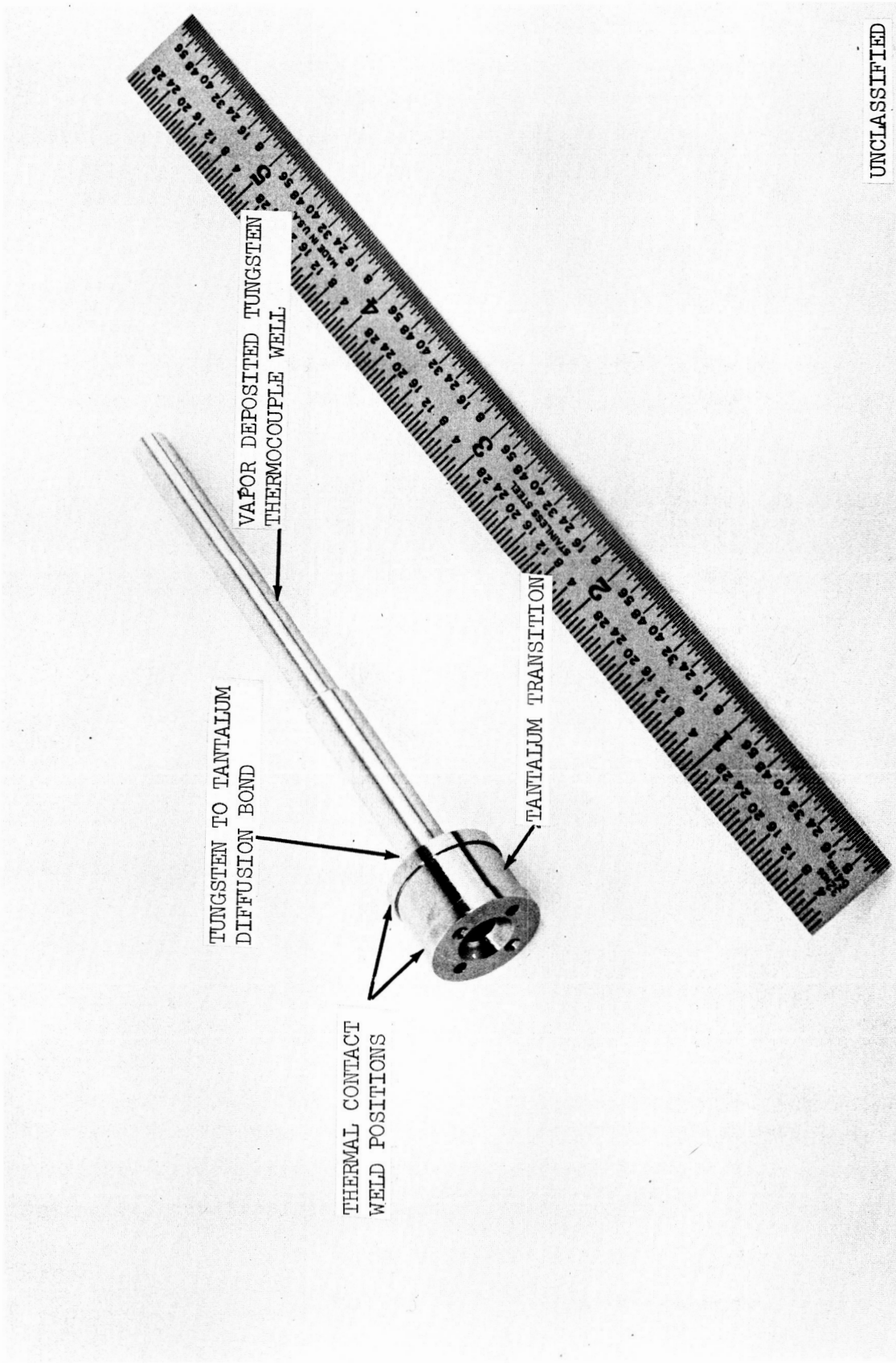

Fig. 2.32--(U) Fuel cup. Tantalum to vapor deposited tungsten diffusion bonded and machined assembly

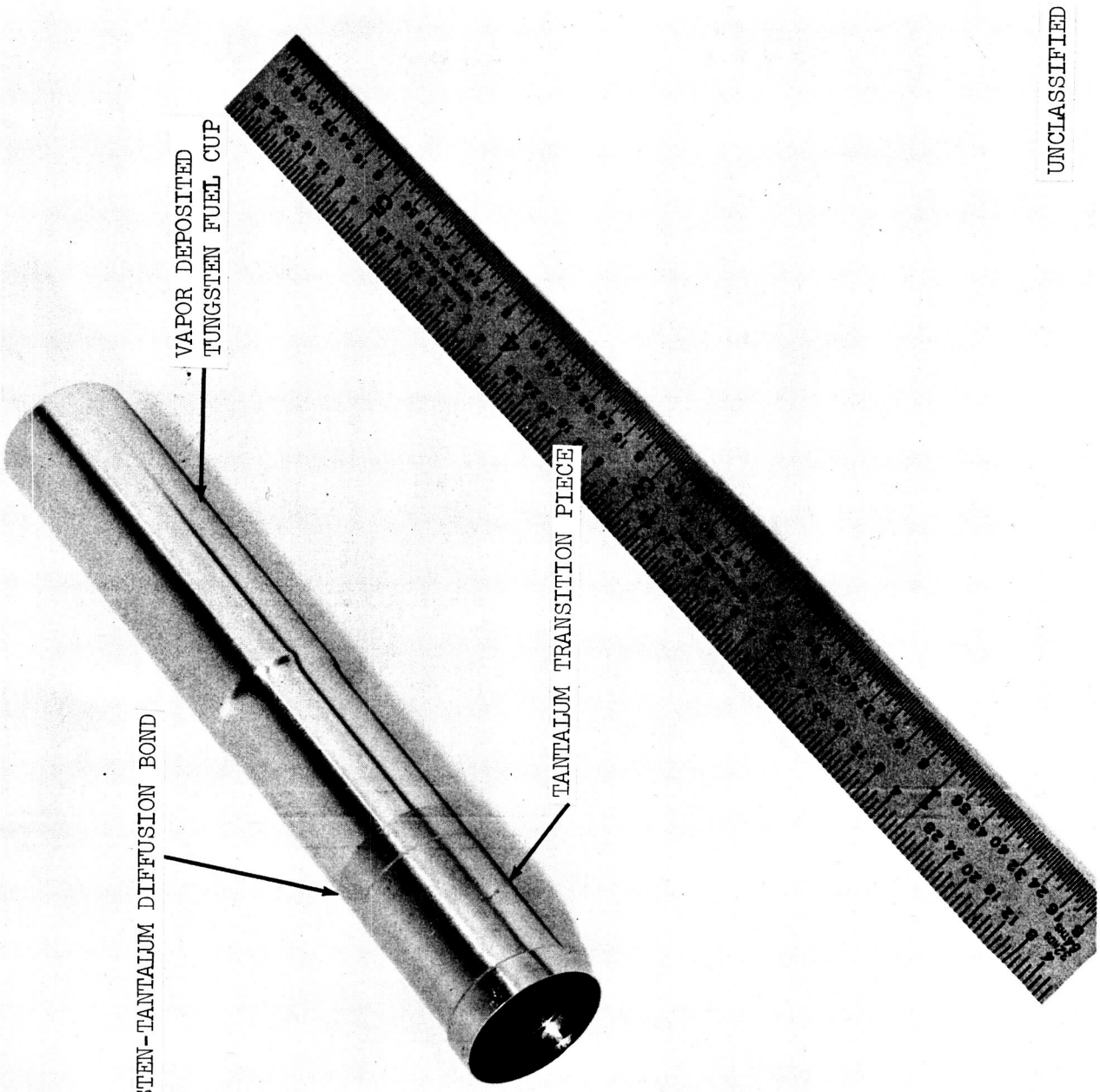

Fig. 2.33--(U) Thermocouple well assembly. Tantalum to tungsten diffusion bonded and machined assembly. Note: Thermal contact weld position

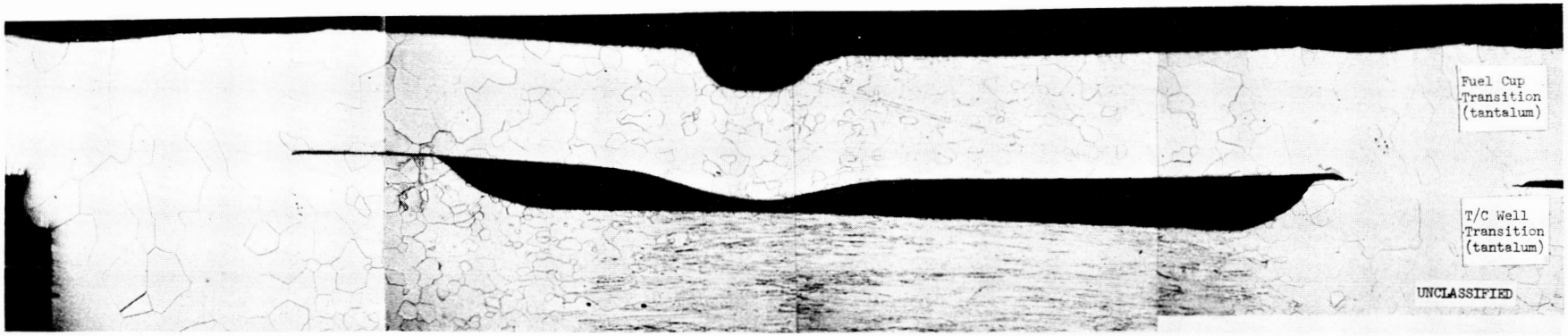

M-21291-1 through -4

~25X

Fig. 2.34--(U) Fuel cup to thermocouple well tantalum transition piece weld section

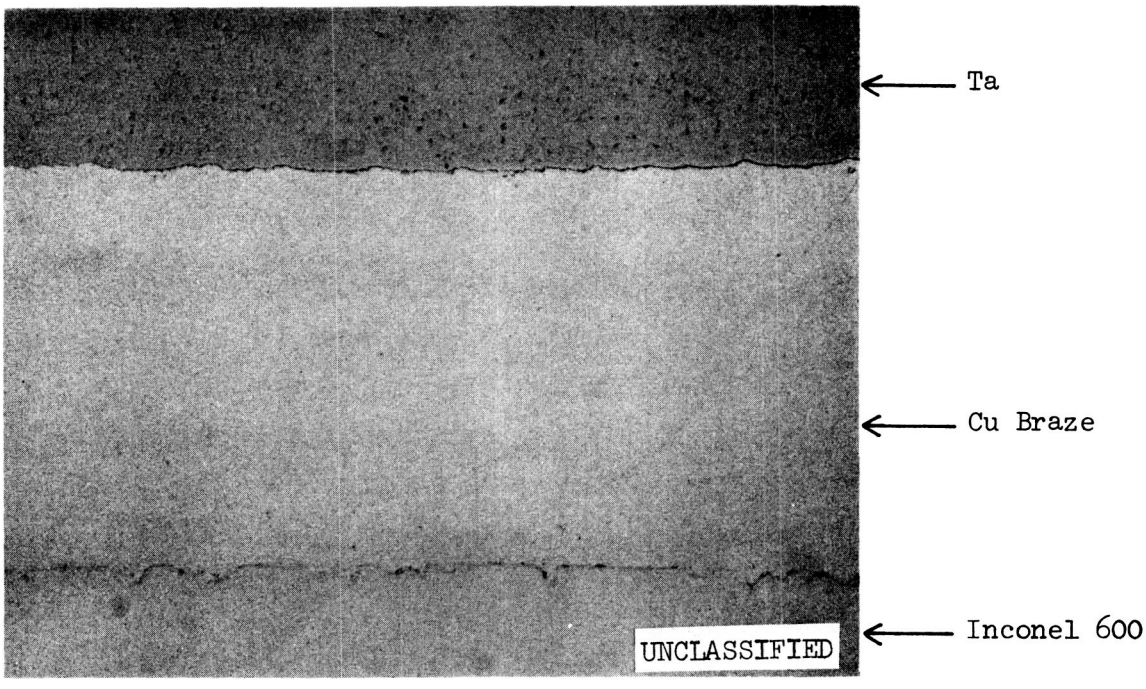

M-21292-1 500X

Fig. 2.35--(U) Tantalum-to-Inconel fuel cup transition piece extension braze

(U) Emissive coating of Inconel primary containment center sleeves. – The inside diameter of polished Inconel 600 tubes was vapor blasted to prepare the surfaces for emissive coating by air oxidation according to the procedures described in the next section on emissive coating development. Satisfactory coating was obtained and the coating process did not affect the dimensions of the tubes. Such a stable emissive coating was needed to facilitate the transfer of heat from the tungsten clad fuel samples in a reproducible fashion.

(U) Fuel cup outgassing. – Assembly of the fuel into the fuel cup was facilitated by attachment of a removeable copper pinch-off to the fuel cup Inconel transition piece. The fuel and T/C well were loaded through the pinch-off and fixed into position by a clip. After loading the fuel, the fuel cup was outgassed and pinched off prior to thermal contact welding of the fuel cup tantalum transition to the thermocouple well tantalum transition. The pinched off and outgassed fuel cup assembly provided a satisfactory storage capsule for the fuel in case assembly of the fission product chamber was delayed. The pinch-off was simply removed prior to attachment of the fission product chamber. Practicing pieces were made for brazing the copper pinch-off to the Inconel transition of the fuel cup by Ni-Au alloy. The copper pinch-off piece was subsequently removed mechanically. All the experimental operations were satisfactorily demonstrated.

(U) Welding of Inconel primary containment center sleeve to Inconel transition piece of fuel cup. – The welding operation was successfully demonstrated after two iterations of the weld joint design.

2.2.2.2. High Temperature Thermocouples

(U) To insure the success and the reliability of the performance of high temperature W-Re thermocouples used for monitoring the fuel temperature during irradiation in PBRF, a program on fabrication development and evaluation on W-Re thermocouples was carried out.

(U) Thermocouple and sheath fabrication development. – The sheaths in which the thermocouples were inserted were fabricated from vapor deposited W-26 wt% Re tubes of 1/16 inch O.D., .010 inch wall thickness and 6 inch length. Prior to closing the end of the cylinder by welding in a controlled inert gas atmosphere, the tubes were degreased, etched in a solution of 20 parts of latic acid, 3 parts of nitric acid, 1 pard of hydrofluoric acid and 25 parts of water, and thoroughly washed in distilled water and dried. The weld and the length of each tube were then leak checked, using a mass spectrometer leak detector with a sensitivity of 2×10^{-10} std. cc/sec.

(U) The thermocouples consist of .005 inch diameter W-5 wt% Re and W-26 wt% Re wires from the same lots inserted into holes in a tantalum plug, with the plug swaged to form the hot junction. Two hole or four hole hard fired beryllia insulator beads were strung over the thermocouple wires from the hot junction to a point past the end of the sheath. This assembly was then inserted into the sheath.

(U) Three types of tantalum plug design were used; a single .013 inch diameter hole on center, two .013 inch diameter holes equally spaced on an .017 inch bolt circle, and four equally spaced .007 inch wide slots of .015 inch depth. Slots were used in the last case to simplify the fabrication of the plug. All these plugs were 0.040 inch in diameter and 3/32 inch in length prior to the swaged operation. These three designs are shown in Fig. 2.36. Five thermocouple assemblies were fabricated, they were given identification numbers as follows:

C-116	two dissimilar wires in a one hole plug (Fig. 2.36(a))
C-117,118	two dissimilar wires per hole in a two hole plug (Fig. 2.36(b))
C-119,120	one wire per slot in a four slot plug (Fig. 2.36(c))

Within these 5 units there was a total of 9 separate thermocouples. The reason for the four wire thermocouple design is that if one of the thermocouple wires is lost, there still are two functioning thermocouples, using the three remaining wires.

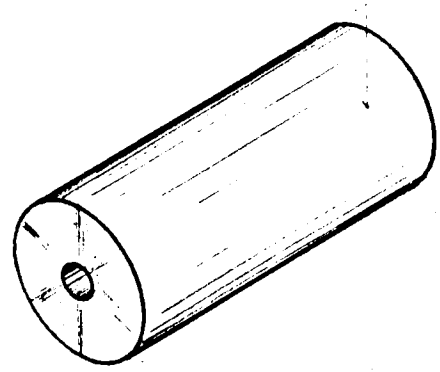

(a)

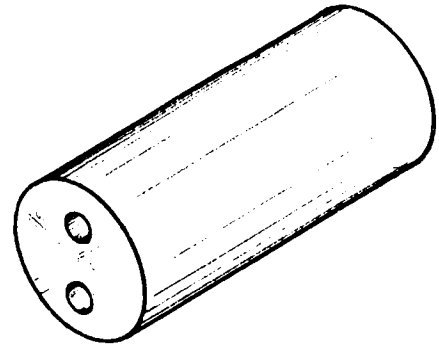

(b)

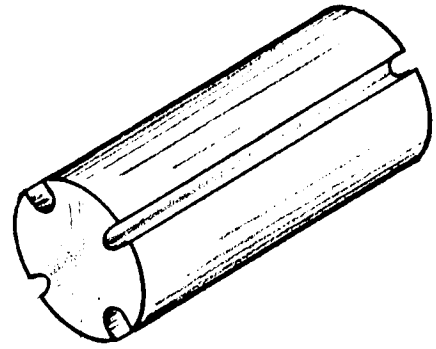

(c)

UNCLASSIFIED

Approximately 20X

Fig. 2.36--(U) Thermocouple junction crimp plugs

(U) Apparatus for evaluating thermal cycling effect and the stability of the thermal emf at 1650°C. – The thermocouples prepared were evaluated for the effect of thermal cycling and time at 1650°C on their thermal emf values. The apparatus (Fig. 2.37) was designed primarily for thermocouple calibrations at temperatures ranging from 1000 to 2000°C at a pressure of 1×10^{-6} torr. A closed end tungsten cylinder horizontally mounted and heated by electron bombardment from an internal filament is externally radiation shielded with five layers of tantalum. There are thirteen 3/4 inch deep holes in the cylinder annulus in which the sheathed thermocouples are inserted. Holes 1/32 inch diameter by 0.34 inch long are drilled through the closed end so that the temperature at the hot junction area of the thermocouple sheath may be read by using an optical pyrometer. The vacuum containment and pumping system consists of an 18 inch glass bell jar, a stainless steel base plate with feed-throughs, an ion gauge, a water cooled chevron baffle and an oil diffusion pump. The thermocouple wire feed-through consists of continuous W-5wt% Re and W-26 wt% Re wires from inside the vacuum chamber to a terminal strip at room temperature outside of the vacuum system at which point 205/260 compensated leads are joined for the run to the instrumentation. A digital voltmeter, with room temperature compensation added, is used to measure the thermocouple millivolt output. A movable shield is located between the hot tungsten cylinder and the viewing window to forestall condensation of materials vaporized from the hot cylinder to the window. Such a coating of the window would give incorrect pyrometer temperature readings.

(U) Evaluation results. – Prior to starting the test and again at the end of the test, window calibration curves were run to check any changes that might have occurred due to the possible deposition of materials from the hot test cylinder onto the window. No differences were noticed between the two window calibrations (see Fig. 2.38).

(U) The five thermocouple assemblies were inserted in appropriate holes in the test cylinder and connected to the thermocouple output measuring instrumentation. The test chamber was then evacuated to a pressure of 1×10^{-6} torr and the thermocouples heated to a temperature of 1800°C and aged for 3 hours. At the end of 3 hours a calibration (calibration No. 1,

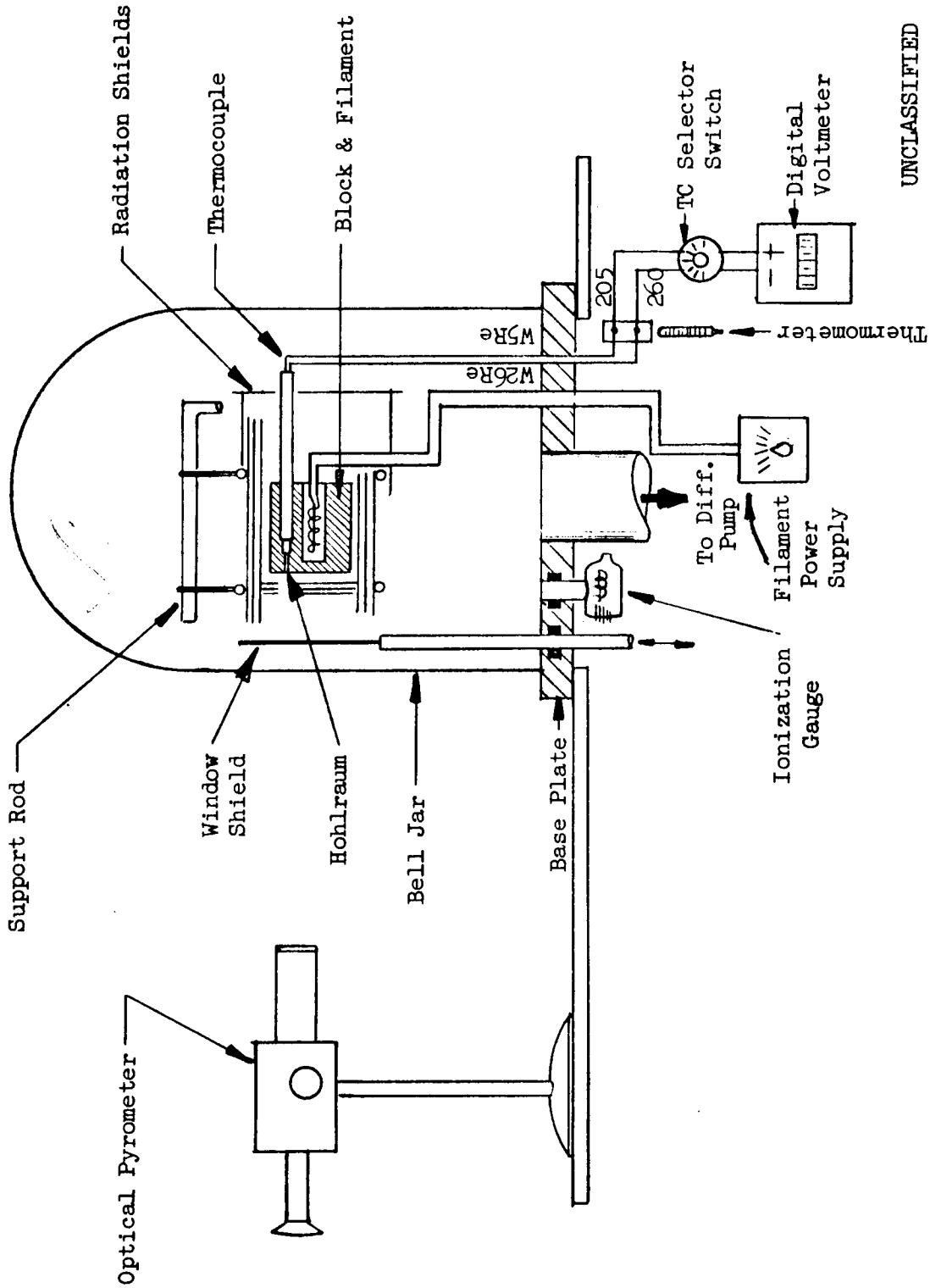

Fig. 2.37--(U) Calibration and test assembly schematic

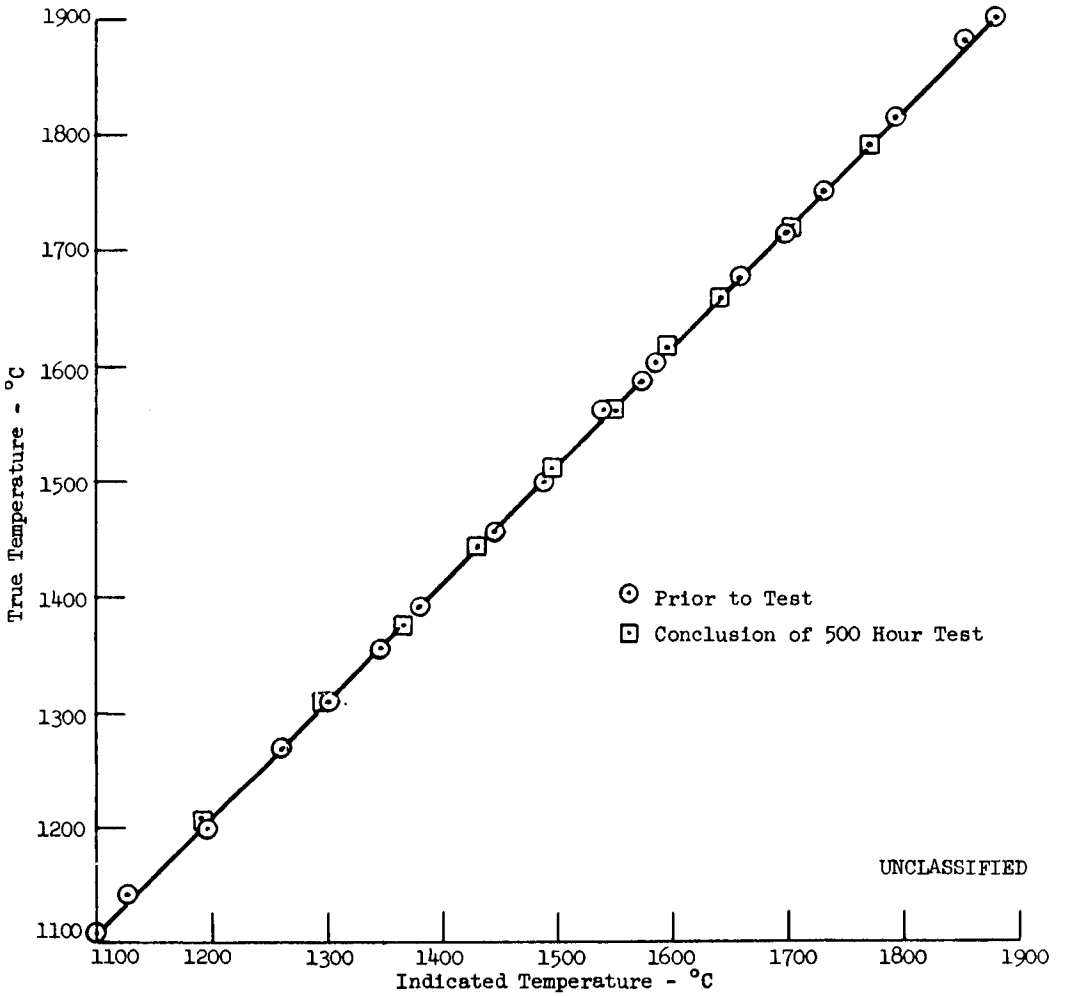

Fig. 2.38--(U) Optical window correction

Fig.s 2.39 through 2.43) curve was run on each thermocouple from approximately 1800° to 1300°C at intervals of 100°C. No differences in millivolt outputs were noted among thermocouples common to one tantalum plug. The room temperature at the transition between the thermocouple wire and the compensated lead wire was 23° ± 2°C during the test and appropriate compensation was applied to the thermocouple millivolt output.

(U) The cycling part of the test was then started and the thermocouples were thermally cycled 40 times from < 500°to 1800°C and then back to < 500°C with a total cycle time of approximately 45 minutes. All heater power was removed to start the 15 minute decreasing part of the cycle from 1800°C to about 350°C. The temperature was then brought back up to 1800°C over a period of 15 minutes and allowed 15 minutes to stabilize at 1800°C before starting another cycle. The thermocouples were brought to room temperature at the conclusion of each day during the cycling part of the test. At the completion of the thermal cycling test all nine of the thermocouples were again calibrated (calibration No. 2, Figs. 2.39 through 2.43) from 1800° to 1300°C. No appreciable changes were noted when the points were plotted and compared to the standard curve.

(U) The 500 hour life test at 1650°C was then started and data were taken once a day. No special attempt was made to maintain the temperature other than normal control. Checks throughout the test showed that the temperature remained at 1650°C ± 25°C. The steady state test data for each thermocouple, plotted in Figs. 2.39 through 2.43 showed no apparent drift, within experimental errors, from the calibration curves. No differences were noted in the millivolt outputs of the thermocouples common to one tantalum plug until 320 hours. At this time it was noted that between the dissimilar wire pairs common to one tantalum swaged hot junction had an 0.02 millivolt difference which remained until the test ended at 500 hours. The thermocouples were again calibrated at the end of the 500 hour test and the data are also shown in Figs. 2.39 through 2.43 (calibration 3, Figs. 2.39 through 2.43). No set pattern of change was noticed. The temperature difference was never greater than 5°C for any thermocouple common to the same plug.

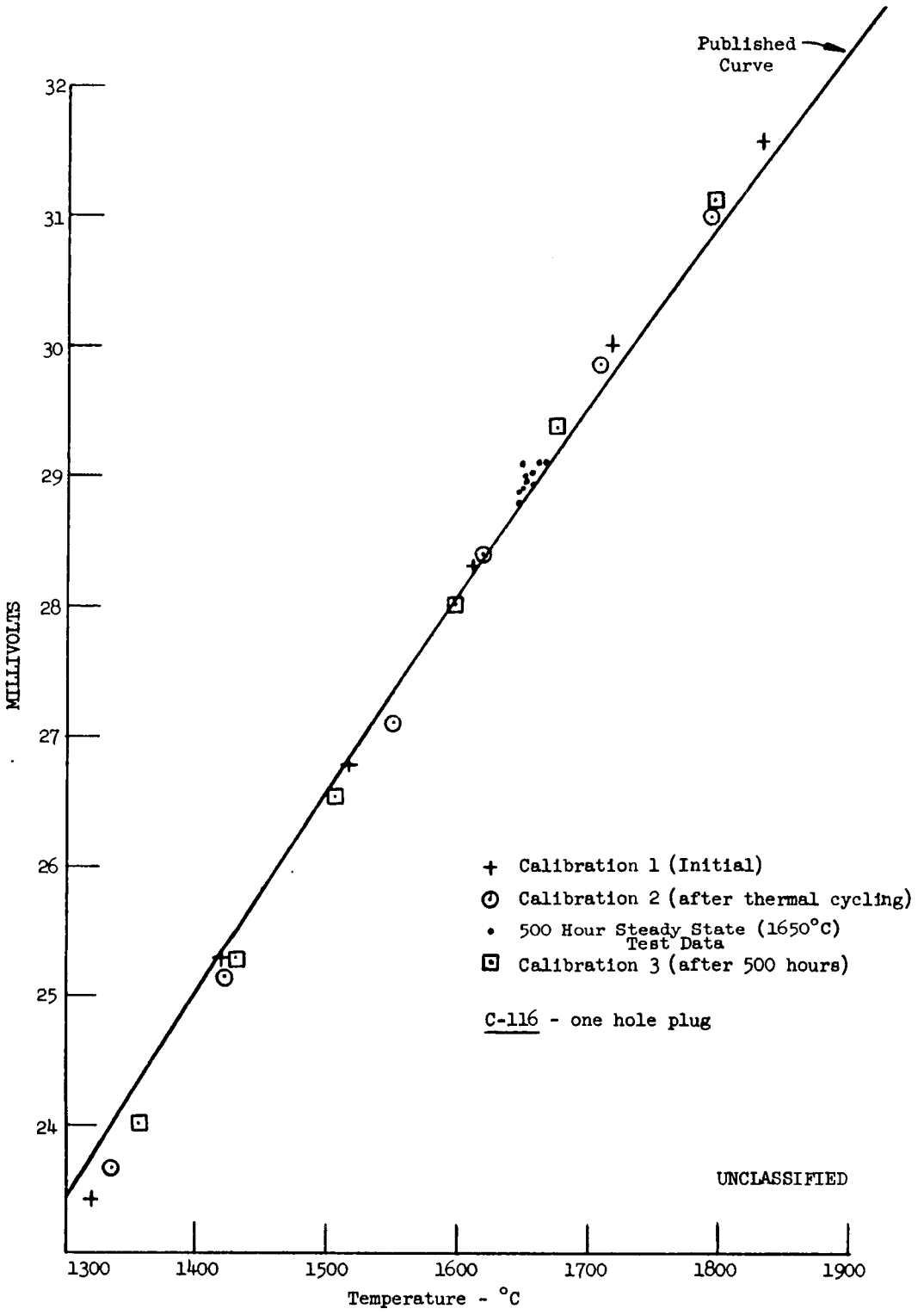

Fig. 2.39--(U) Test results on C-116

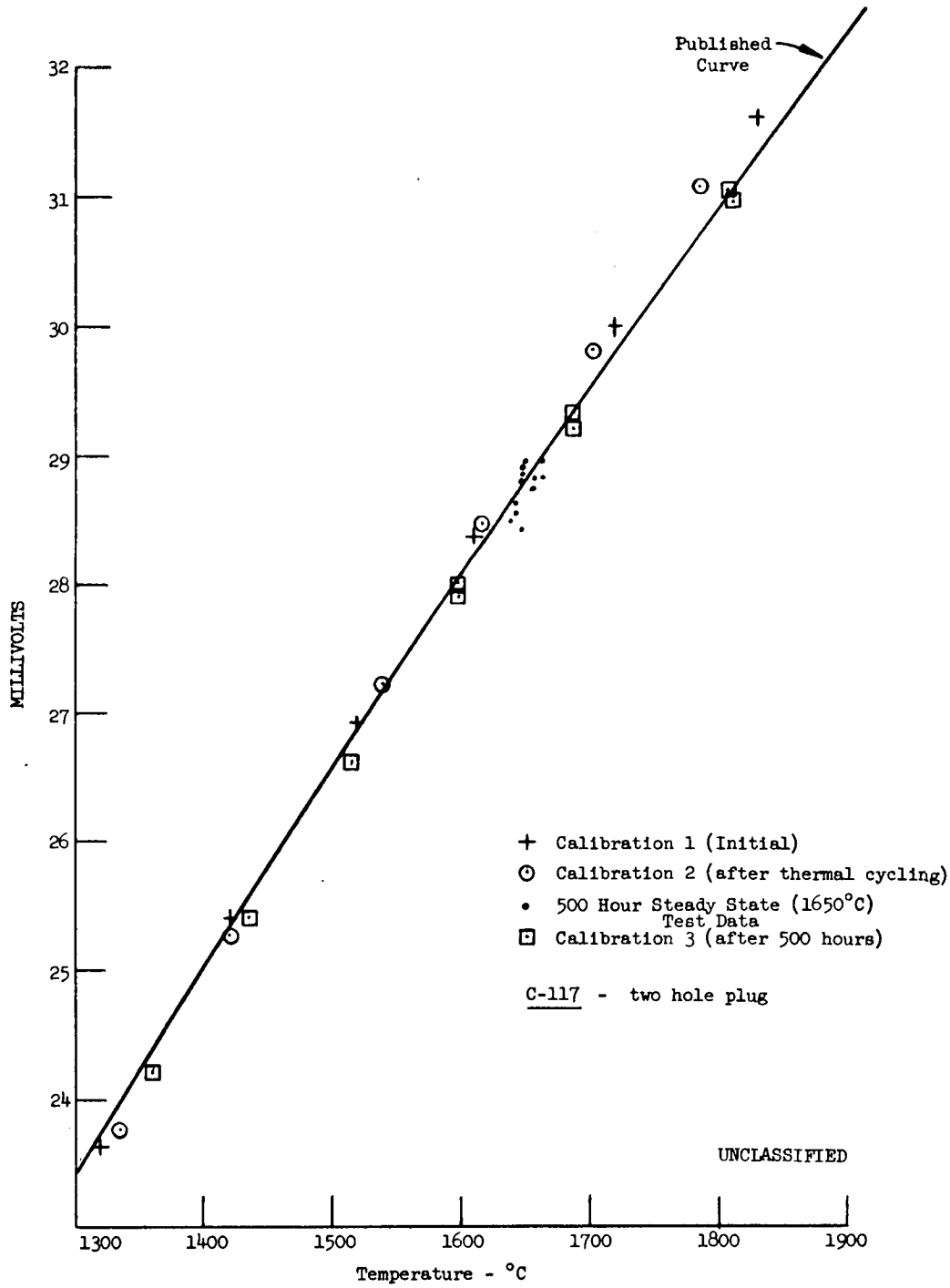

Fig. 2.40--(U) Test results on C-117

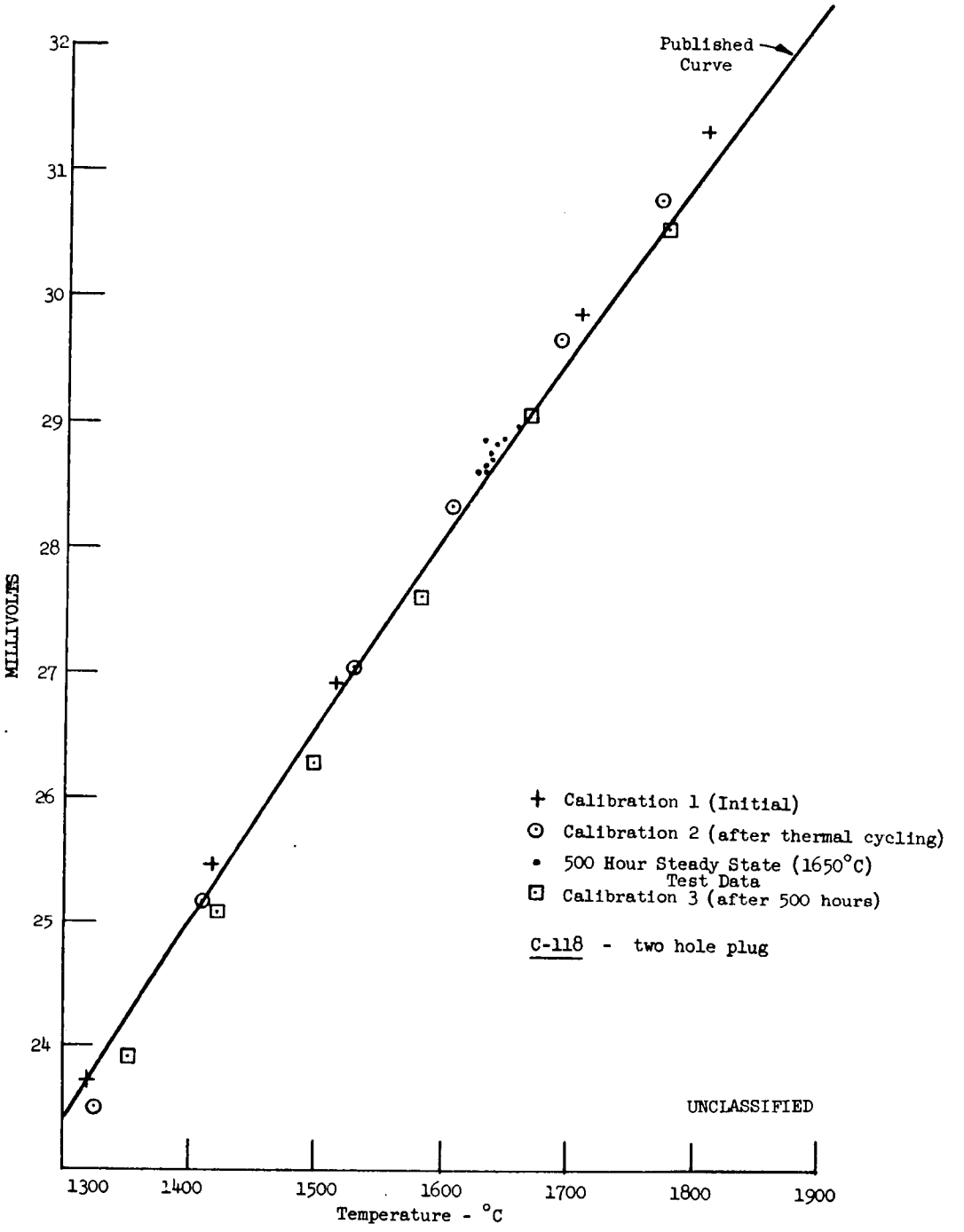

Fig. 2.41--(U) Test results on C-118

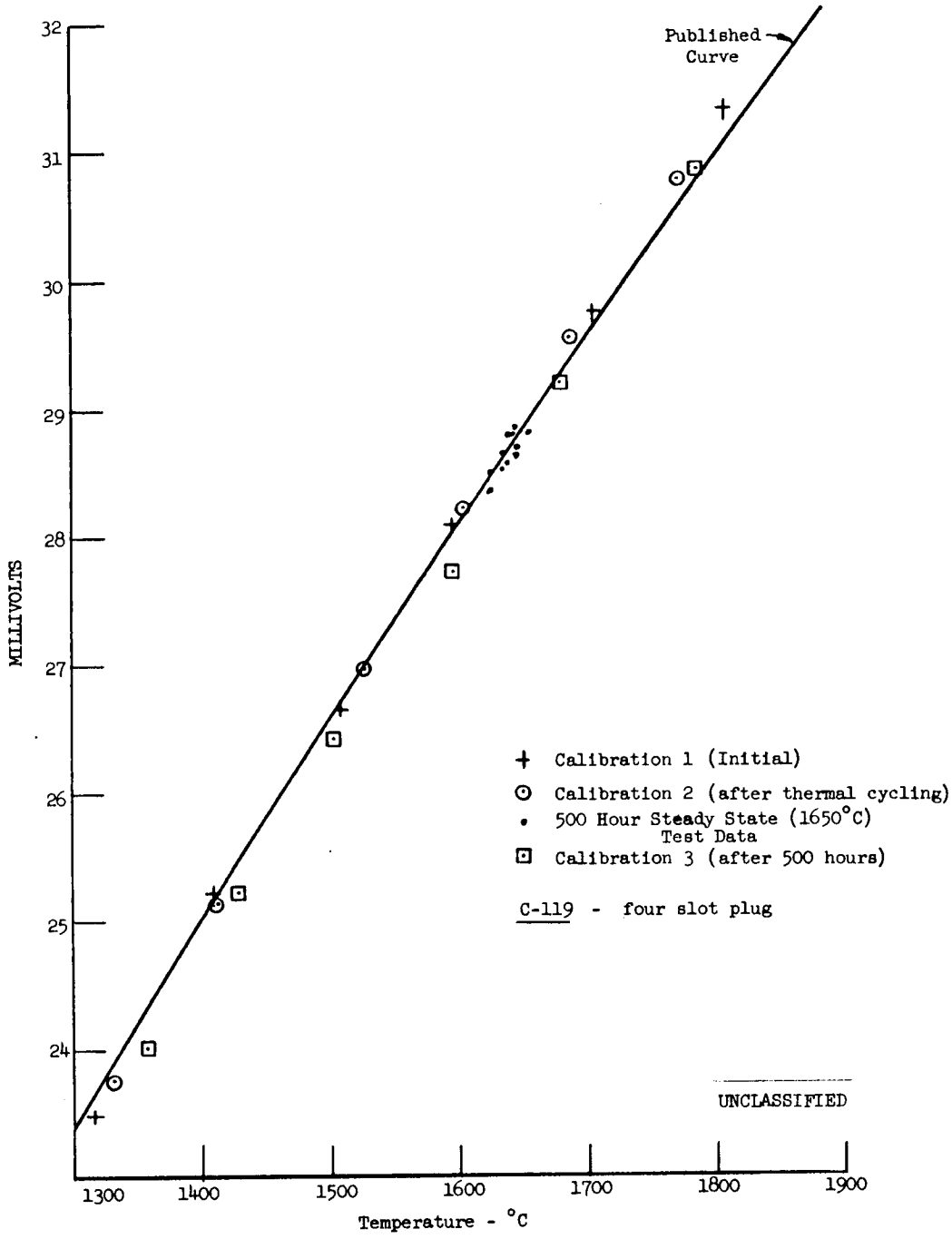

Fig. 2.42--(U) Test results on C-119

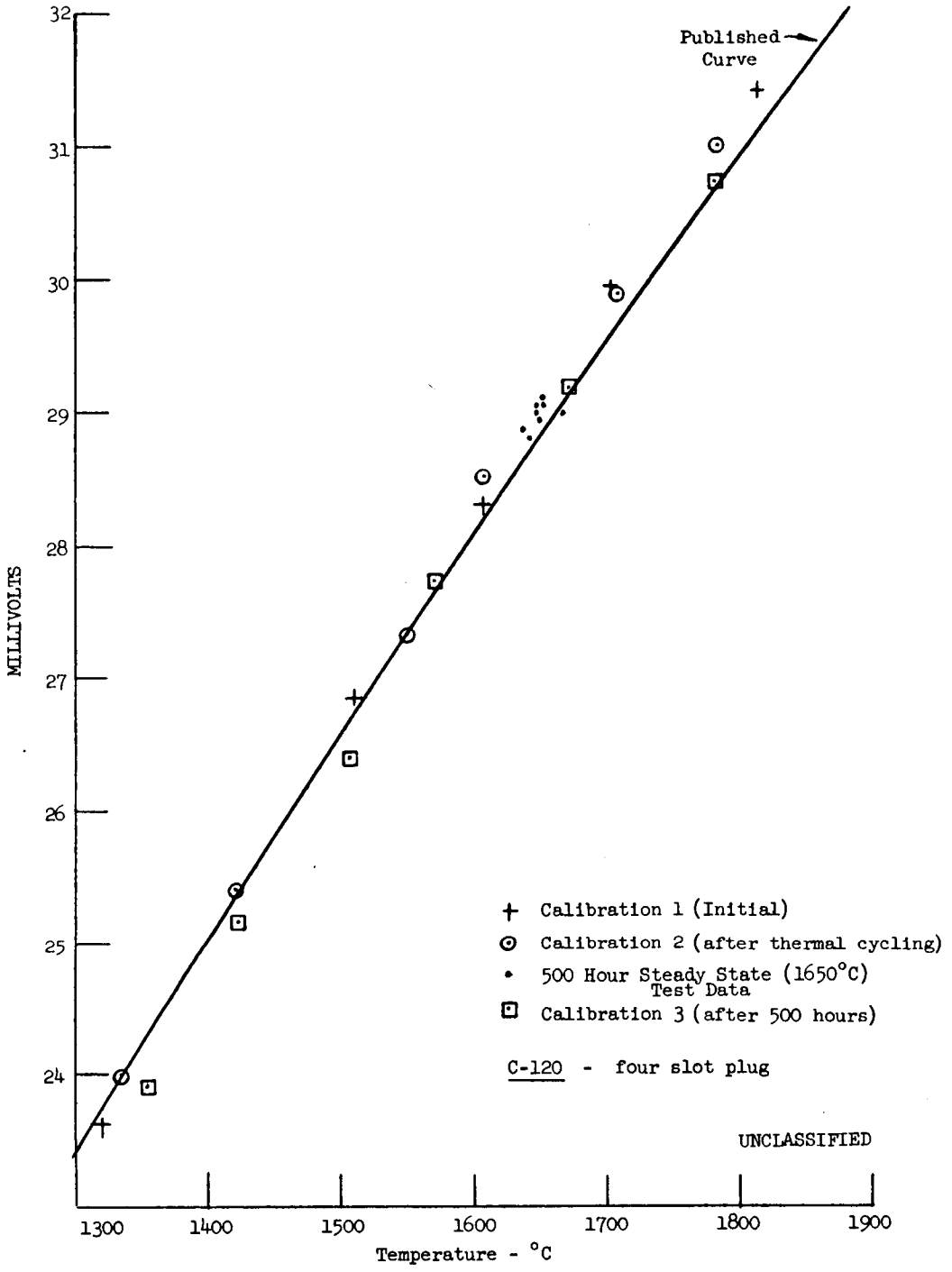

Fig. 2.43--(U) Test results on C-120

(U) Figure 2.44 is a plot of all the data presented as calibrations 1, 2 and 3 on Figs. 2.39 through 2.43. It can be seen that from 1300°C to 1800°C the deviations are in the order of ±25°C.

(U) Post-test visual inspection and chemical analysis. – The thermocouples were carefully removed from the test block and visually inspected (Fig. 2.45(a)). All W-26 wt% Re sheaths were bright where they had been inserted into the test cylinder and had been subjected to high temperatures. There was a light brownish discoloration from where the sheath left the block going into a darker discoloration at a point of 3-3/8 inches from the welded tip. This was the point at which the rear radiation shield was installed and the darkening was probably due to material transport from the hot filament and block to the cooler areas. The sheaths from all the thermocouples, except C-119, were helium leak checked and found to be leak tight. The sheath of C-119 had been broken 3/4 inch from the welded end; this could have occurred during a required filament change near the end of the test. The sheaths are quite brittle after being heated to 1800° and a slight bump could have broken it. The C-116, 119, and 120 thermocouple assemblies were easily removed from the sheath. The tantalum plug on assemblies C-117 and 118 had bonded to the sheath. C-117 was broken away from the sheath by pulling on the wires. C-118 was left for further examination if necessary at a later date.

(U) Upon disassembly of the thermocouples it was found that the beryllia used for C-116 (two hole) was slightly discolored for the first 1-5/8 inches from the hot end and then went into a very shiny black discoloration for the next 1-5/8 inches. The remaining 2-3/4 inches was just off white. The beryllia used for thermocouples C-117 through C-120 (four hole) was white with some light gray areas for the first 1-3/8 inches from the hot end and then changed into a flat black color for about 1/2 inch with a definite white deposit build-up. The remainder of the insulator length was dark gray (Fig. 2.45 (b)).

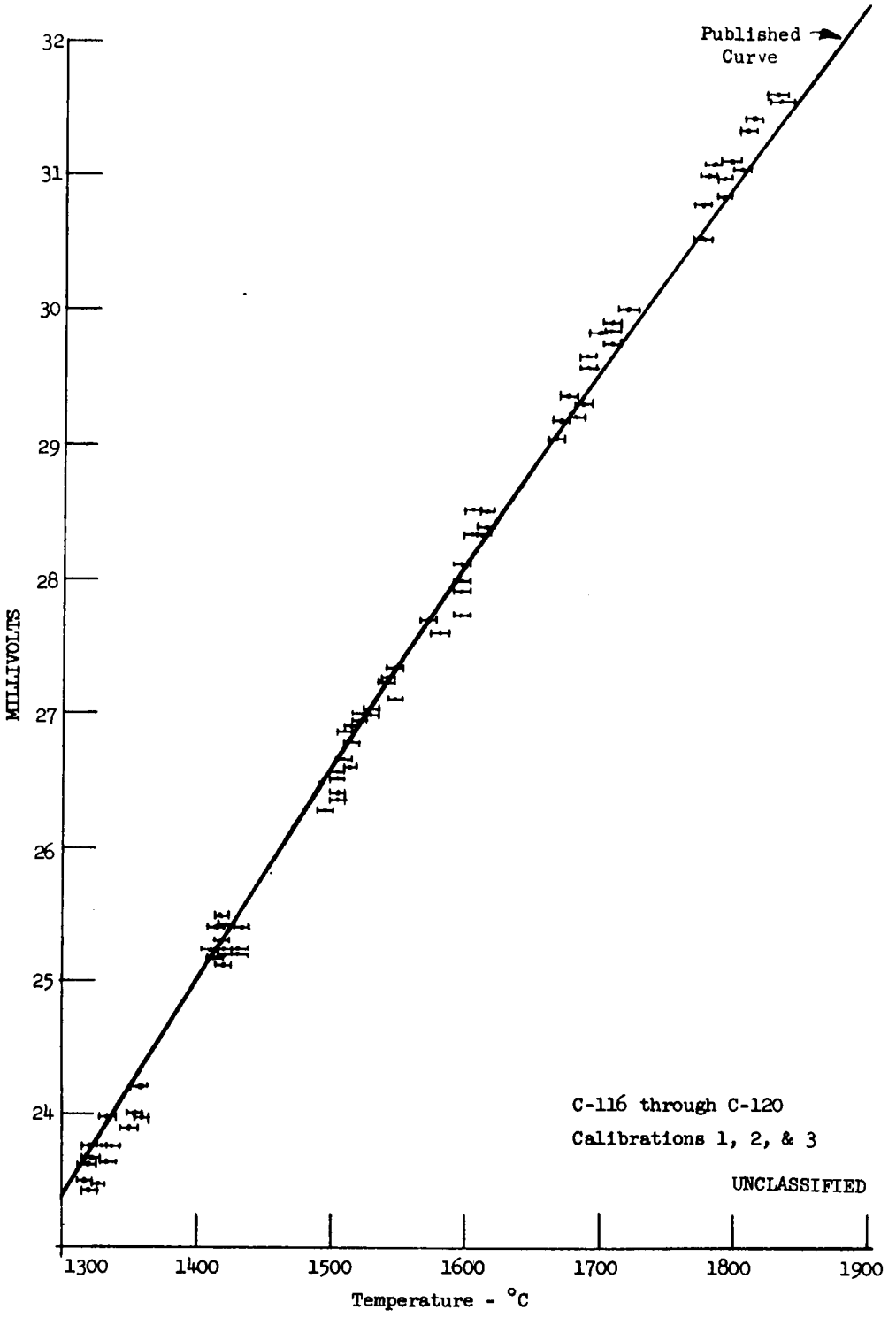

Fig. 2.44--(U) Summary plot of the test results

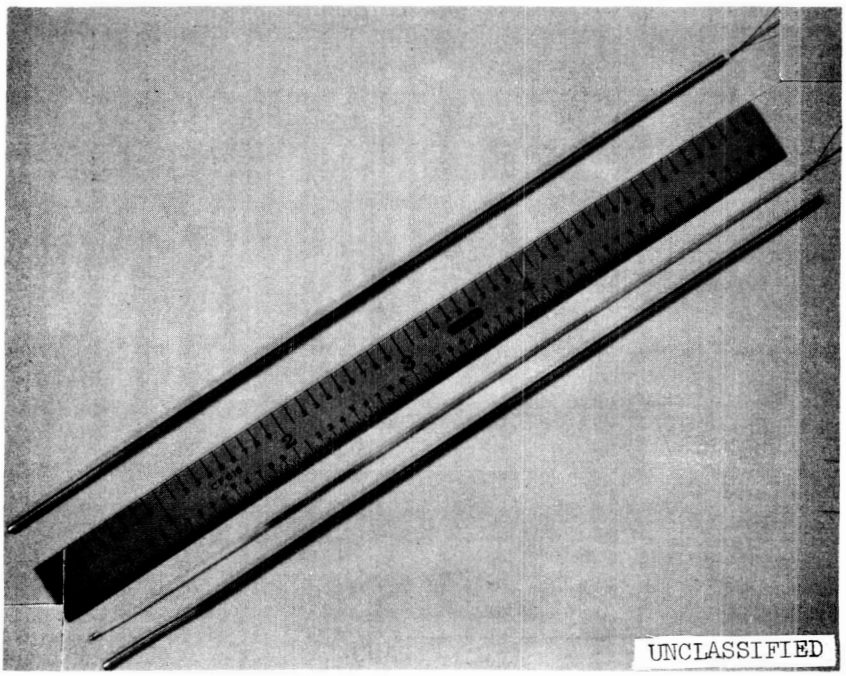

Fig. 2.45(a)--(U) Thermocouple assembly of C-120

Section above the scale shows the complete test assembly while below the scale is the thermocouple assembly consisting of the sensor wires, tantalum swaged hot junction and the beryllia insulating beads showing the deposit as described for C-119. Also shown is the W_{74} Re_{26} sheath.

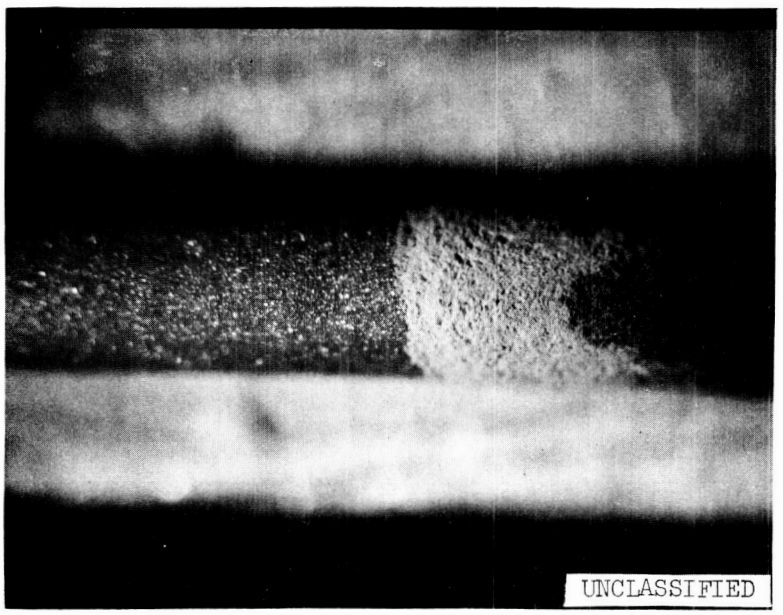

Fig. 2.45(b)--(U) White deposit buildup on beryllia beads of thermocouple C-119. Hot junction end was to left of picture

(U) The following are the chemical analysis results (in ppm) of the 2 hole and the 4 hole beryllia beads:

	2 hole	4 hole		2 hole	4 hole
Al	90	> 1000	Mg	880	> 1000
Fe	25	8	Zn	< 20	ND
Mn	< 2	< 10	Si	110	400
Cr	3	< 100	Ti	< 2	ND
Ni	3	< 40	Cd	ND	< 100
B	< 1	4	Ag	< 1	< 5
Co	< 1	< 40	Mo	< 3	< 10
Cu	< 2	< 10	Na	50	< 600
Li	< 1	< 1000	Pb	< 2	< 80
Ca	60	400	C	80	-

The two hole beryllia was purchased as 99.8% purity with a certified chemical analysis from one supplier and the four hole beryllia was purchased from another supplier as 99.9% purity but without a chemical analysis. The chemical analysis of the four hole beryllia was done here at Gulf General Atomic. The analysis, though not as complete as that for the two hole beryllia, is acceptable for comparison purposes and shows that the four hole beryllia is not as pure as the two hole beryllia. A later order for the four hole beryllia was made from the same vendor, with the supplied chemical analysis data in agreement with that obtained at Gulf General Atomic.

(U) Samples of the deposits from C-116 and C-119 were sent for electron microprobe analysis. Excerpts from the analysis are as follows:

(i) Specimen C-116 (Two hole beryllia). – Carbon was just detected and had no particular pattern of distribution. It was borderline in conductivity depending on the beam current used. Magnesium was found in the dark grains but was not detected in the white colored grains at the hot end. Going away from the hot junction the magnesium gradually increased in amount and was found more frequently until magnesium was present in all of the grains. Aluminum was detected only occasionally and only in that half

of the specimen, which was away from the hot junction. Silicon was detected only occasionally and was usually present at some very low levels except for some very small high silicon specks. Chromium was very rare. Iron was detected in very small amounts in very small areas. Nickel was not detected as the sulfur, chlorine, potassium, calcium, titanium, tungsten, vanadium, manganese, cobalt, copper, and zinc. A complete spectral scan for all elements heavier than sodium was made on one of the dark grains with only chromium being detected.

(ii) Specimen C-119 (Four hole beryllia). — Carbon was found to be very high in the black ring and increased from this very high value to an even higher value as the hotter end was approached. Going in the other direction from the black ring, carbon decreased but always could be found. This specimen was found to be highly conductive. Magnesium was only occasionally detected in the portion from the black ring away from the hot junction end. Aluminum was sought specifically. There was no aluminum in the white material. Aluminum was very low in the gray area approaching the black ring and increased steadily until large amounts were found in the gray area past the black ring, beyond which it decreased again to very small amounts. Silicon was not detected in the white material or in the gray material approaching the black ring. Silicon began to appear in the black ring and throughout the gray material following the black ring and then decreased to zero. Chromium was not detected over the entire length. Iron in very small amounts was detected only in the black ring. Nickel occurred only rarely as small specks but was always present. Elements sought specifically over the whole surface and not detected were silicon, chlorine, potassium, calcium, titanium, tungsten, vanadium, manganese, cobalt, copper, and zinc. A complete spectral scan was made on the black ring and only silicon and iron were detected. A complete spectral scan for all elements heavier than sodium was made on the white deposit and only

aluminum and nickel were detected. Visual examination with a bench microscope indicated that the white deposit has substantial thickness. Microprobe analysis indicated that this material must be an element or elements below magnesium in the periodic table, including a large amount of carbon as already noted.

(U) Post-test metallographic examinations. – Figure 2.45(c) shows the post-test appearance of the tantalum plugs of the one hole, two hole and four-slot configurations. Figures 2.46, 2.47 and 2.48 show respectively the microstructures of the cross sections of these plugs. From these photographs, the following conclusions can be drawn:

(i) The tantalum has a very clean grain structure, indicating no significant contamination has occurred during the test.

(ii) There are pores and voids around each thermocouple wire on all three configurations. Some of them could have originated from the gap existing between the thermocouple wire and the wall of the cavity; the others may be due to the Kirkendall effect associated with the interdiffusion of metallic components. The thicknesses of the diffusion layers between the tantalum and the thermocouple wires, as estimated from these figures, are of the order of 1/2 to 1 mil. In spite of these voids and pores, the test data indicated that good contact existed among the thermocouple wires. This good contact is evident from the fact that interdiffusion between the thermocouple wires has occurred for the configurations where the two wires are in direct contact.

(iii) Electron microprobe studies indicate that the diffusion layer between the tantalum and the thermocouple wires has a high concentration of tantalum plus some tungsten and rhenium. It is interesting to see that the diffusion layer is present where no direct contact between tantalum and thermocouple wires exist. Perhaps the tantalum reached there either by vapor transport or by surface diffusion.

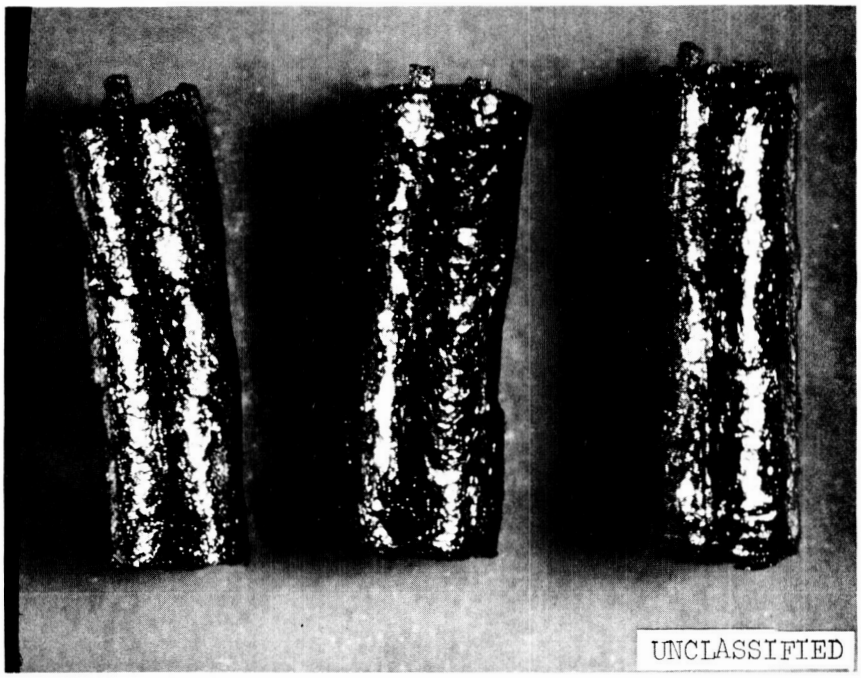

C-116 C-117 C-119

24X

Fig. 2.45 (c)--(U) Appearance of tantalum plugs after the test

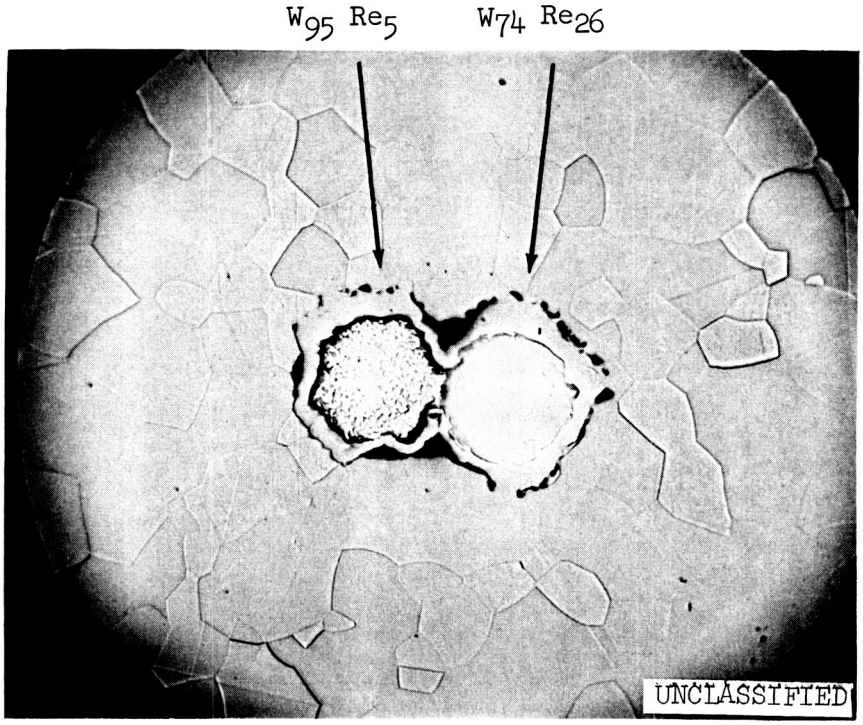

150X

Fig. 2.46--(U) Microstructures of the cross section of C-116

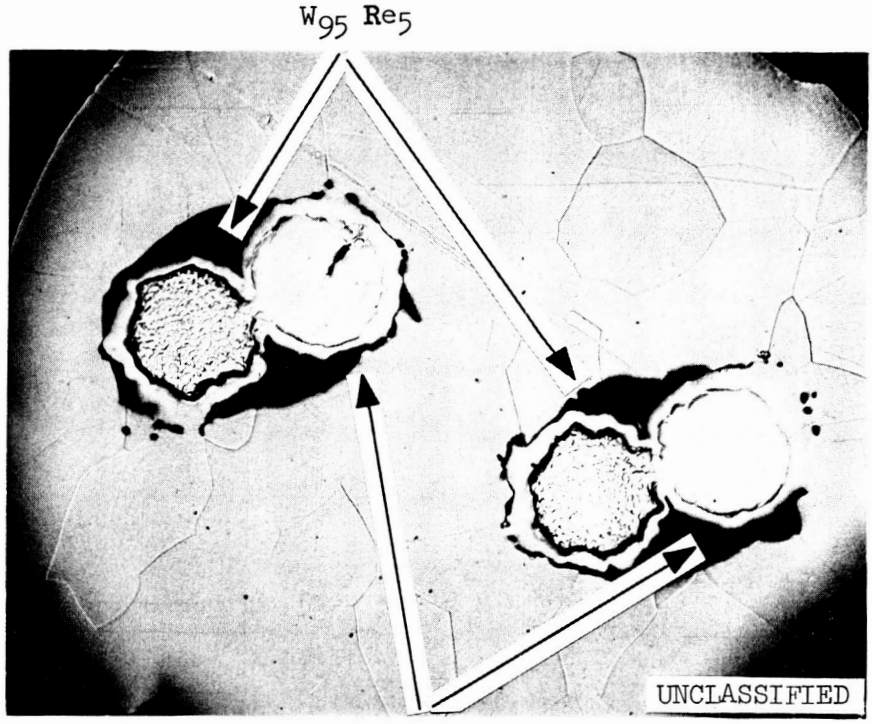

Fig. 2.47--(U) Microstructures of the cross section of C-117

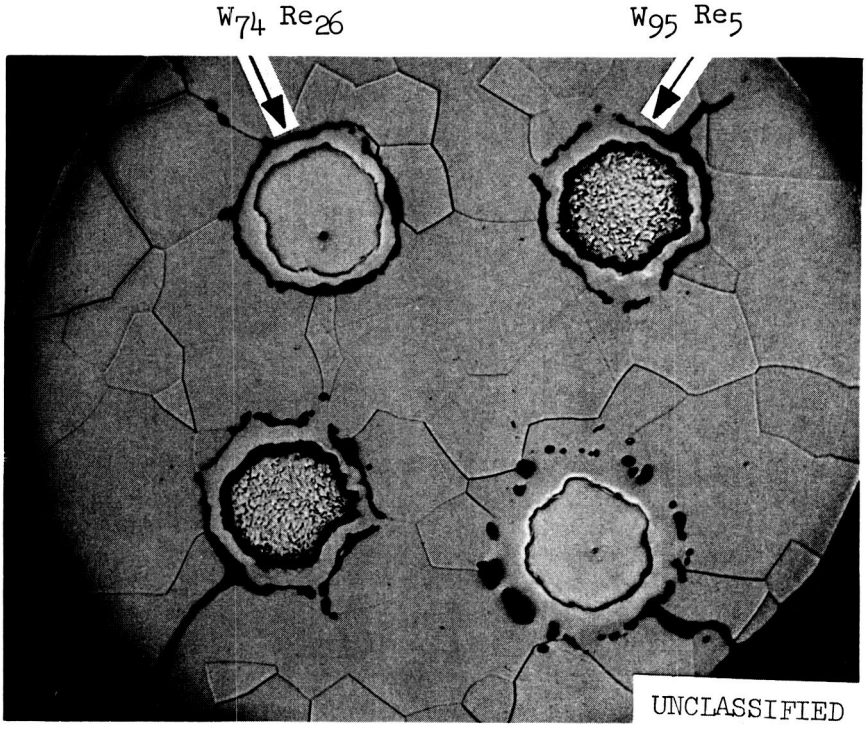

150X

Fig. 2.48--(U) Microstructures of the cross section of C-119. Note: Remnants of the slots in the tantalum

(U) Test results on W-3 wt% Re versus W-25 wt% Re. – At a later date it was decided to substitute W-3 wt% Re versus W-25 wt% Re for the W-5 wt% Re versus W-26 wt% Re previously tested. The reason for this change was because it is generally thought that the W-3 wt% Re versus W-25 wt% Re thermocouple is more reliable at elevated temperatures. W-5 wt% Re versus W-26 wt% Re has been used as fuel temperature thermocouples for thousands of hours in the Gulf General Atomic TRIGA reactor. Some apparent downward drift of thermocouple temperature has been noted when compared with calculated temperatures.

(U) During the fabrication of the actual four wire thermocouple (2 + 2) to be used in the irradiation, extensions of the thermocouple wires were removed and the common ends junctioned using the four slot (Fig. 2.36(c)) tantalum swage as in test pieces C-119 and C-120. These test thermocouples were identified as C-121, C-122, C-123. They were installed in the calibration apparatus previously described. It was decided to forego the thermal cycling and to shorten the total number of hours at temperature as it was felt that nothing new could be realized over the first test. A second set of similar thermocouples was fabricated and again sections were removed, identified as C-124, C-125, and C-126. These in turn were tested. The test hours for the two sets were 155 and 100 hours, respectively, at 1650 ± 25°C. The test calibration data are shown in Fig. 2.49 and Fig. 2.50. The results from these short term tests are in general agreement with that observed for W-5 wt% Re versus W-25 wt% Re thermocouples.

2.2.2.3. Preparation and Evaluation of Inconel Surface of High and Stable Emittance

(U) In the design of the capsule, the tungsten cladding of the fuel samples transfers part of the heat generated by radiation to the oxidized surface of the Inconel primary containment at about 600°C in a neon environment. Oxidized Inconel surface was recommended because of its high emittance which facilitates the radiative heat transfer. A test was therefore carried out to evaluate the stability of the absorptance of an oxidized Inconel 600 surface in neon at 600°C for radiation from a tungsten surface at 1800°C. Since the test was not intended to measure the absolute value of the

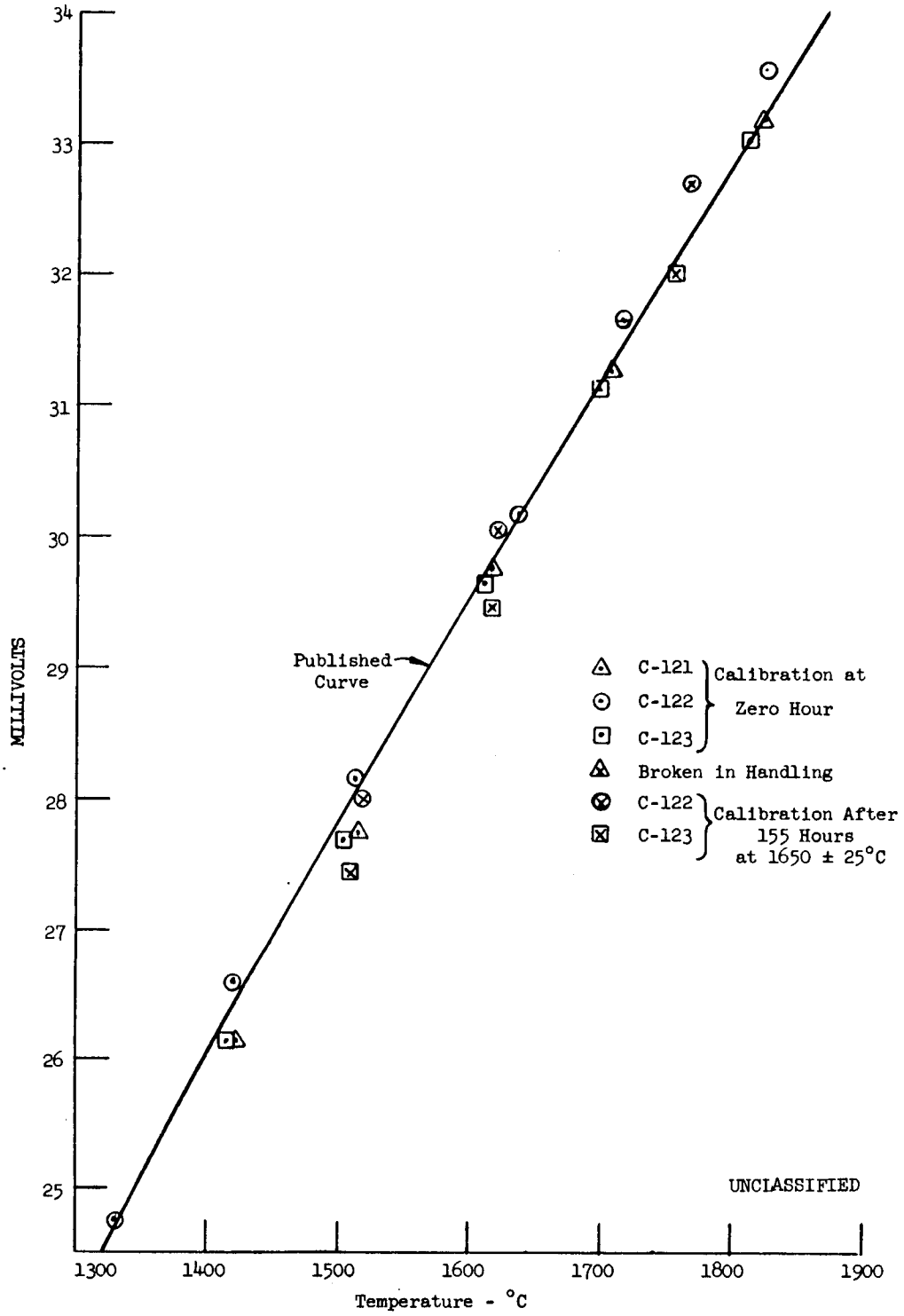

Fig. 2.49--(U) Test results for W-3 wt% Re vs. W-25 Re thermocouples C-121, C-122 and C-123

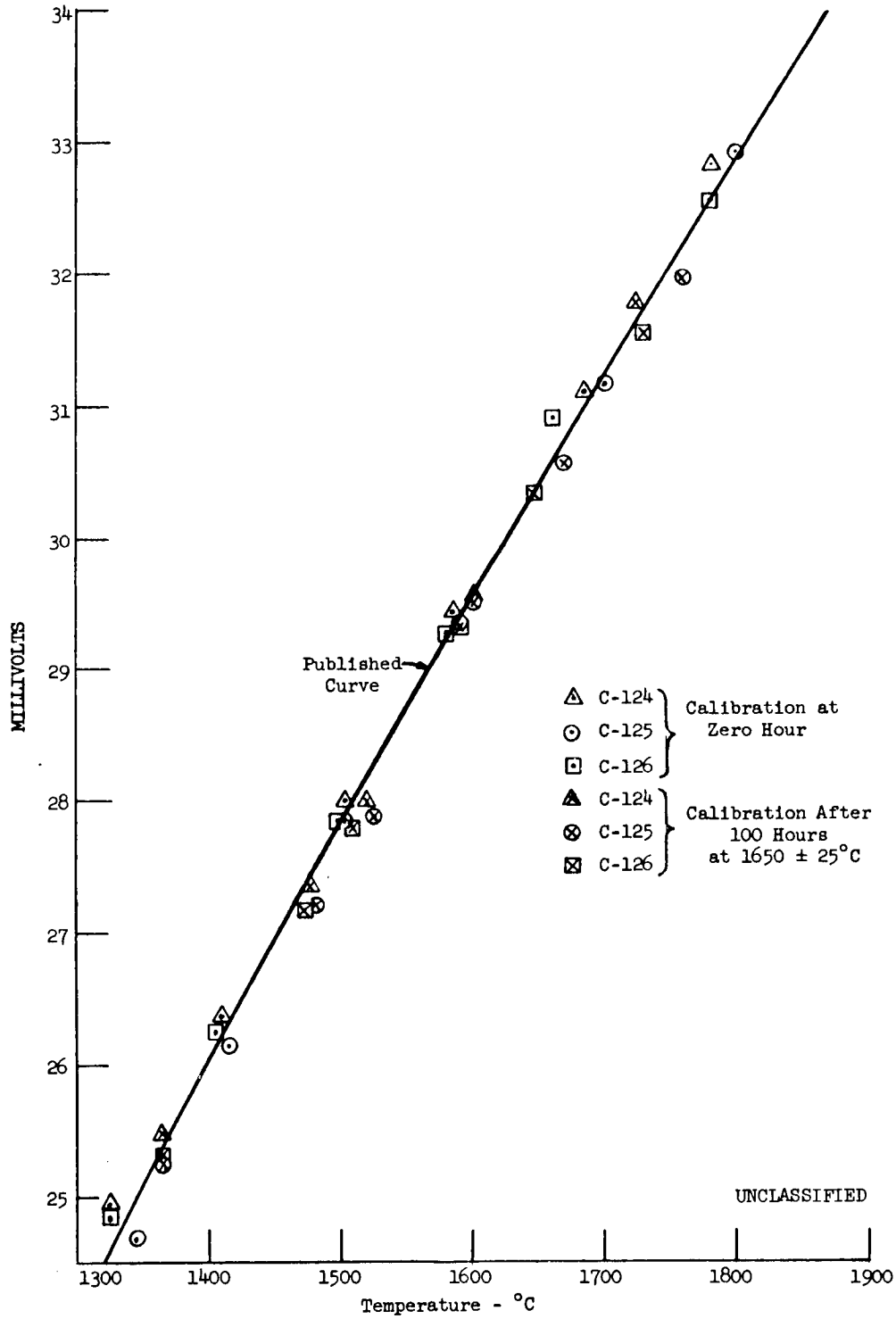

Fig. 2.50--(U) Test results for W-3 wt% Re vs. W-25 wt% Re thermocouples C-124, C-125 and C-126

absorptance of the oxidized surface but to determine the change that occurred, it was believed that such information should throw lights on the stability of the radial heat transfer characteristics of the capsule, even though the tungsten cladding was designed to operate at 1650°C instead of 1800°C. The experimental procedures and results are described as follows.

(U) Sample preparation. — A total of eight samples (Numbers 0, 1, 3, 4, 5, 6, 7, and 8) of Inconel 600 were fabricated from 1/8 inch sheet into 15/16 inch diameter discs. One surface of the disc was stamped for identification while the other side was polished and then vapor-blasted to produce a smooth matte surface. The samples were then ultrasonically cleaned in acetone, passivated in a mixture of 10% nitric acid and 1% hydrochloric acid for 5 minutes at room temperature, rinsed in distilled water, and then in acetone. The cleaned samples were placed in a muffle furnace in air and supported on ceramic supports on the hearth of the furnace. The furnace was brought to 1067°C and held for 24 hours, then dropped to 827°C and held for an additional 24 hours. The samples were allowed to cool before removal from the furnace.

(U) Determination of initial absorptance. — After removal from the furnace, the spectral reflectance (R_λ) of the oxidized surface was measured at room temperature over the wave length range of 1.0-32.0 microns.

(U) The spectral absorptance α_λ is deduced from the spectral reflectance R_λ from the formula: Absorptance = 1 − reflectance. The total absorptance α is evaluated from the formula

$$\alpha = \frac{\int_{\lambda_1}^{\lambda_2} \varepsilon_\lambda E_\lambda (1 - R_\lambda)\, d\lambda}{\int_{\lambda_1}^{\lambda_2} \varepsilon_\lambda E_\lambda\, d\lambda} \qquad (1)$$

where

ε_λ = spectral emittance of tungsten at 1800°C[12]

E_λ = rate of energy emission at 1800°C from a blackbody for wave length λ.

i.e. $\epsilon_\lambda E_\lambda = E_{w\lambda}$ = rate of energy emission from tungsten at 1800°C for wave length λ.

(U) In practice, both the denominator and the numerator of the above equation can be evaluated by taking summations over given small wave length increments for the wave length range λ_1 to λ_2.

(U) Experimental arrangement and procedures for evaluating the stability of absorptance. — The test container and arrangement is shown schematically in Fig. 2.51. The samples were spot welded to the Inconel thermocouple well inside the Inconel can. The nickel tube was then pinched off and seal-welded. Tantalum pieces were installed in the Inconel can to simulate the conditions in the irradiation capsule. The can was then welded, leak checked, evacuated, and outgassed at 650°C and 3×10^{-6} torr for 24 hours before being cooled to room temperature and backfilled to 200 mm with purified neon.

(U) Two samples (No. 1 and No. 3) were placed in the first test can and after outgassing and backfilling, were removed and their reflectance remeasured to determine the effects of the test assembly preparation.

(U) Four samples (No. 5, 6, 7, and 8) were subsequently welded into a second test can and after pinch-off and seal welding, were heated at 600°C for 1000 hours. The samples were then removed and their reflectance remeasured.

(U) Experimental results. — Table 2.8 contains the pre-test and the post-test reflectance data for all the samples studied. The adsorptance data for these samples, calculated by use of equation (1) are summarized in Table 2.9. It seems that all the observed changes occurred during the outgassing stage. Such an oxidized Inconel surface therefore should be able to maintain stable radial heat transfer characteristics in the capsule.

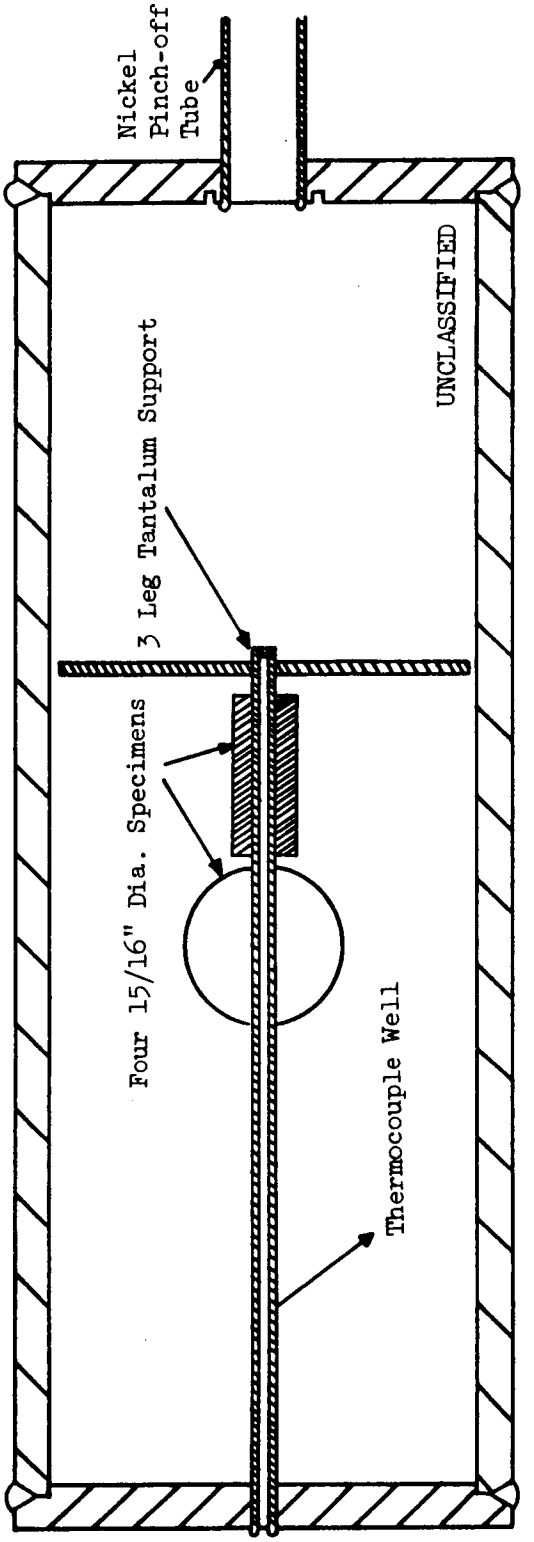

Fig. 2.51--(U) Test capsule

Table 2.8

(U) SPECTRAL REFLECTANCE AT ROOM TEMPERATURE

(This table is Unclassified)

Wave Length Microns	Spectral Reflectance at Room Temperature												
	#1*	#1-A	#3	#3-A	#4	#5	#5-A	#6	#6-A	#7	#7-A	#8	#8-A	#0
1.0	.220	.120	.220	.120	.220	.220	.150	.220	.160	.220	.155	.220	.150	.220
1.1	.220	.120	.220	.120	.220	.220	.150	.220	.160	.220	.155	.220	.150	.220
1.2	.220	.120	.220	.120	.220	.220	.150	.220	.160	.220	.155	.220	.150	.220
1.3	.220	.120	.220	.120	.220	.220	.150	.220	.160	.220	.155	.220	.150	.220
1.4	.220	.125	.210	.120	.215	.220	.150	.230	.160	.230	.155	.220	.150	.240
1.5	.220	.140	.215	.130	.220	.220	.160	.240	.170	.240	.165	.225	.165	.240
1.6	.220	.145	.220	.135	.220	.230	.170	.240	.175	.240	.170	.230	.165	.245
1.7	.225	.145	.225	.145	.220	.230	.170	.240	.175	.245	.170	.230	.165	.245
1.8	.225	.145	.220	.140	.225	.230	.180	.240	.175	.240	.175	.235	.180	.240
2.0	.220	.150	.215	.145	.210	.225	.170	.230	.175	.230	.170	.230	.170	.240
2.5	.225	.165	.225	.145	.230	.230	.185	.240	.175	.240	.175	.240	.180	.245
3.0	.240	.180	.240	.180	.235	.230	.200	.250	.195	.245	.200	.235	.195	.245
3.5	.240	.200	.240	.205	.240	.245	.200	.255	.200	.245	.205	.250	.200	.250
4.0	.255	.225	.255	.225	.245	.260	.220	.255	.220	.265	.220	.265	.220	.255
4.5	.245	.220	.250	.225	.245	.255	.240	.245	.230	.250	.240	.255	.230	.255
5.0	.245	.230	.255	.230	.250	.255	.240	.245	.225	.250	.225	.255	.240	.260
5.5	.255	.250	.255	.235	.255	.260	.250	.255	.230	.260	.235	.265	.240	.260
6.0	.255	.240	.250	.235	.255	.255	.250	.240	.230	.250	.240	.265	.250	.255
6.5	.155	.165	.165	.170	.150	.145	.210	.140	.200	.145	.210	.150	.210	.145
7.0	.140	.155	.125	.155	.140	.135	.140	.130	.135	.135	.135	.135	.145	.135
7.5	.155	.145	.130	.145	.155	.160	.150	.150	.135	.155	.145	.165	.150	.155
8.0	.080	.090	.078	.090	.075	.085	.120	.080	.090	.065	.110	.085	.110	.080
8.5	.080	.080	.067	.075	.075	.085	.075	.065	.065	.070	.060	.080	.070	.075
9.0	.090	.090	.067	.085	.085	.085	.070	.080	.060	.080	.055	.085	.065	.080
9.5	.145	.120	.110	.110	.115	.145	.100	.135	.090	.135	.100	.150	.110	.155
10.0	.150	.135	.130	.115	.165	.145	.130	.140	.110	.145	.115	.155	.130	.155
10.5	.145	.145	.120	.120	.145	.135	.130	.120	.115	.135	.125	.140	.130	.140
11.0	.165	.155	.125	.130	.175	.165	.150	.150	.130	.155	.135	.165	.150	.165
11.5	.160	.150	.145	.140	.180	.160	.160	.145	.135	.150	.145	.165	.160	.165
12.0	.130	.130	.115	.110	.135	.130	.130	.110	.120	.120	.120	.130	.140	.125
12.5	.115	.105	.095	.080	.125	.110	.090	.090	.080	.100	.090	.110	.090	.110
13.0	.090	.100	.067	.080	.100	.090	.100	.075	.080	.065	.090	.085	.095	.080
14.0	.245	.220	.190	.170	.220	.265	.210	.220	.180	.210	.190	.245	.210	.245
15.0	.280	.255	.250	.245	.280	.300	.275	.250	.230	.245	.235	.270	.265	.270
16.0	.310	.275	.285	.285	.315	.325	.310	.290	.270	.270	.280	.300	.310	.290
17.0	.225	.205	.185	.190	.215	.220	.185	.190	.150	.170	.155	.200	.165	.190
18.0	.300	.320	.220	.250	.290	.290	.300	.260	.240	.270	.260	.310	.310	.300
19.0	.270	.275	.220	.245	.290	.270	.280	.250	.240	.245	.250	.270	.285	.270
20.0	.320	.300	.275	.290	.330	.305	.290	.290	.275	.295	.270	.305	.300	.310
21.0	.300	.290	.265	.280	.300	.285	.285	.265	.265	.280	.275	.295	.320	.285
22.0	.265	.245	.255	.250	.270	.260	.250	.240	.230	.245	.240	.265	.265	.255
23.0	.235	.220	.225	.220	.240	.235	.230	.205	.210	.210	.220	.235	.250	.220
24.0	.175	.165	.175	.180	.190	.180	.165	.155	.155	.155	.155	.165	.165	.155
25.0	.260	.260	.250	.250	.275	.260	.250	.240	.220	.240	.225	.280	.250	.265
26.0	.245	.250	.220	.230	.250	.235	.225	.250	.200	.225	.210	.250	.240	.235
27.0	.240	.245	.225	.235	.250	.250	.230	.210	.210	.220	.220	.260	.250	.240
28.0	.240	.230	.220	.235	.250	.245	.210	.310	.205	.230	.230	.245	.255	.230
29.0	.220	.225	.220	.233	.245	.240	.220	.220	.195	.225	.205	.220	.220	.225
30.0	.225	.230	.225	.225	.245	.240	.225	.240	.210	.230	.210	.235	.230	.245
31.0	.230	.225	.230	.235	.250	.250	.225	.235	.210	.235	.205	.240	.225	.230
32.0	.225	.220	.235	.235	.250	.245	.220	.235	.210	.230	.210	.230	.225	.230

Data for #1, 3, 4, 5, 6, 7, 8 and 0 represent initial reflectance.
Data for #1-A, 3-A, 5-A, 6-A, 7-A and 8-A represent post-test reflectance.

Table 2.9

(U) TOTAL ABSORPTANCE CALCULATED BY EQUATION (1) FOR ALL THE OXIDIZED INCONEL SAMPLES STUDIED

(This table is Unclassified)

Samples	As Oxidized	After 24 Hours at 650°C	After 1000 Hours at 600°C	Percent Change
1	.78	.85		9.0
3	.78	.90		15.4
4	.78			
5	.77		.83	7.8
6	.77		.83	7.8
7	.77		.83	7.8
8	.77		.83	7.8
0	.76			

2.2.3. Preparation of Fuel Cup and Fuel Samples

2.2.3.1. Tungsten Fuel Cup

(U) The tungsten fuel cup was prepared by the deposition of tungsten formed by the hydrogen reduction of WF_6 on a molybdenum mandrel which was subsequently removed by dissolution in a mixture of HNO_3 + H_2SO_4. The conditions for the acceptance of the sample prepared included

(i) A fluorine content in the range of 10 to 20 ppm

(ii) No dimensional change after 6 hours at 2200°C

(iii) No bubble detected at 250X magnification under a microscope after 6 hours at 2000°C.

The qualified fuel cup was then outgassed at 1800°C for 50 hours, ground to smooth finish (including about 5 mils from the surface in contact with the molybdenum mandrel to prevent initiation of grain growth) diffusion-bonded to the tantalum transition piece, and then machined to the required dimensions. The fueled region has a thickness of 40 mils.

2.2.3.2. Fuel Samples

(C-RD)(Gp-1) Requirements. – 90UC-10ZrC and 50UC-50ZrC were to be irradiated in Capsule V-2C and Capsule V-2D respectively. Both types of fuel samples were required to satisfy the following conditions:

(i) Each fuel sample should contain about 4 wt% of tungsten to prevent the dissolution of the tungsten cladding by the fuel materials and to insure the stability of the open pore structures in the fuel materials at high temperatures.

(ii) The carbon to uranium ratio in each fuel sample should fall in the range of 1.03 to 1.05, after allowing one carbon atom to each zirconium atom and one carbon atom to every two tungsten atoms present in the fuel materials, to insure electron work function stability and to prevent the carburization of the tungsten cladding.

(iii) Each fuel sample should possess a high specific surface area to encourage the release of fission gas so that fuel swelling due to fission gas pressure buildup could be minimized. The high specific surface area was achieved in two ways. The first was to select the fabrication conditions so that a high degree of open porosity was incorporated into the microstructures of the fuel sample. The degree of open porosity was characterized by measuring the true open surface area of a fuel sample by low pressure krypton adsorption, and the ratio of the true open surface area to the geometric surface area (surface ratio factor, or SRF) was chosen as the index for comparing the degree of open porosity of fuel samples of a given geometry. The second was to increase the geometric surface area A to volume V ratio of the fuel sample by machining macroscopic channels into the fuel body. These macroscopic channels could provide alternative escaping routes for the fission gas in case some of the microporosities leading to the exterior surfaces of the fuel sample became blocked. On the basis of previous post-irradiation annealing studies of fission gas release rates,[3] hot cell examinations of irradiated UC-ZrC samples,[13] and results obtained on tungsten containing UC-ZrC in fabrication development (see Part I of this report), it was decided that both the 90UC-10ZrC and the 50UC-50ZrC samples used in this irradiation experiment should have densities of 75-80% of the theoretical values, a SRF values of at least 150 and a geometric surface area to volume ratio greater than five. The latter was achieved by machining venting holes and grooves into the carbide fuel samples. To evaluate the effect of A/V on the dimensional stability of the fuel samples, three fuel configurations were selected for each of the two fuel compositions. These fuel configurations, as shown in Figs. 2.52(a), (b) and (c), have A/V values of 5.70, 6.36 and 6.91 respectively.

(C-RD)(Gp-1) Fabrication. – The fuel samples were prepared according to the following procedures.

(i) Arc-melt weighed amounts of U, Zr, and C into carbide buttons in an argon atmosphere.

(ii) Grind the carbide buttons to -44 micron size in an argon atmosphere in a glove box, the moisture content of which was kept below 10 ppm.

(iii) Blend the required amount (~4 wt%) of W powder with the carbide powder in an argon atmosphere in the glove box used in (ii).

(iv) Cold press the blended powder to carbide cylinders in a steel die and homogenize the pressed carbide cylinders at 2285°C for 6 hours in vacuum.

(v) Analyze the composition of the homogenized carbide cylinder to insure that it contained the required uranium to carbon atom ratio.

(vi) Grind the homogenized carbide cylinder and sieve out the -44/+20 micron size powder in argon in the glove box used in (ii).

(vii) Isostatically cold press the sieved out carbide powder fraction at 90,000 psi and sinter the pressed body for 16 hours at 2070°C for 90UC-10ZrC and 2285°C for 50UC-50ZrC.

(viii) Grind and cut the sintered carbide body to the dimensions needed, with special attention paid to avoiding atmospheric contamination by impregnating it with a removable hydrocarbon oil before grinding and cutting.

(ix) Remove the impregnated oil from the finished carbide pieces by repeated rinsing with xylene, ultrasonic cleaning, and evacuating.

(x) Outgas the finished carbide pieces at 1800°C for 24 hours in vacuum.

(xi) Analyze the composition of one of the outgassed carbide pieces and determine the SRF value of another.

(xii) If the results obtained in (xi) are satisfactory (C/U = 1.03-1.05, SRF $\geq$ 350), the carbide pieces are again impregnated with hydrocarbon oil and electrical-discharge machined into the configurations shown in Fig. 2.52.

(xiii) Repeat procedures (ix), (x) and (xi).

(xiv) If the results obtained on the stoichiometry and the SRF value of the finish-machined carbide pieces are satisfactory (C/U = 1.03-1.05, SRF $\geq$ 150), they are sealed in glass ampoules before incorporation into the fuel pins.

(C-RD)(Gp-1) Techniques for determining the open surface area of UC-ZrC samples by the low pressure krypton adsorption method were described in the annual summary report for Contract NAS 3-4165.(3) For each composition, nine samples were required for the irradiation experiment, three pieces of configuration (c) of Fig. 2.52 as thermal shields and six pieces (two of configuration (c), two of configuration (b) and two of configuration (a) of Fig. 2.52 as duplicates) as test samples. In addition, samples were needed for each fuel configuration for the determination of chemical composition and SRF value, both before and after the machining of the holes and the grooves. The duplicate of each test sample, the chemistry sample and the sample for surface area determination, were always obtained from the same fuel cylinder.

(C-RD)(Gp-1) While the fabrication of the 90UC-10ZrC samples proceeded quite smoothly, the fabrication of the 50UC-50ZrC samples has encountered some difficulties in stoichiometry control, mainly because of the higher specific surface area of the 50UC-50ZrC samples and the longer time needed for electrical-discharge-machining holes and grooves in 50UC-50ZrC samples. Contamination by oxygen and moisture during the lengthy machining of the highly porous structures led to the loss of carbon content so that the carbon to uranium ratios became lower than the specified values (1.03 to 1.05). Remedies for this situation were sought in two ways.

PLUMBROOK FUEL PELLET

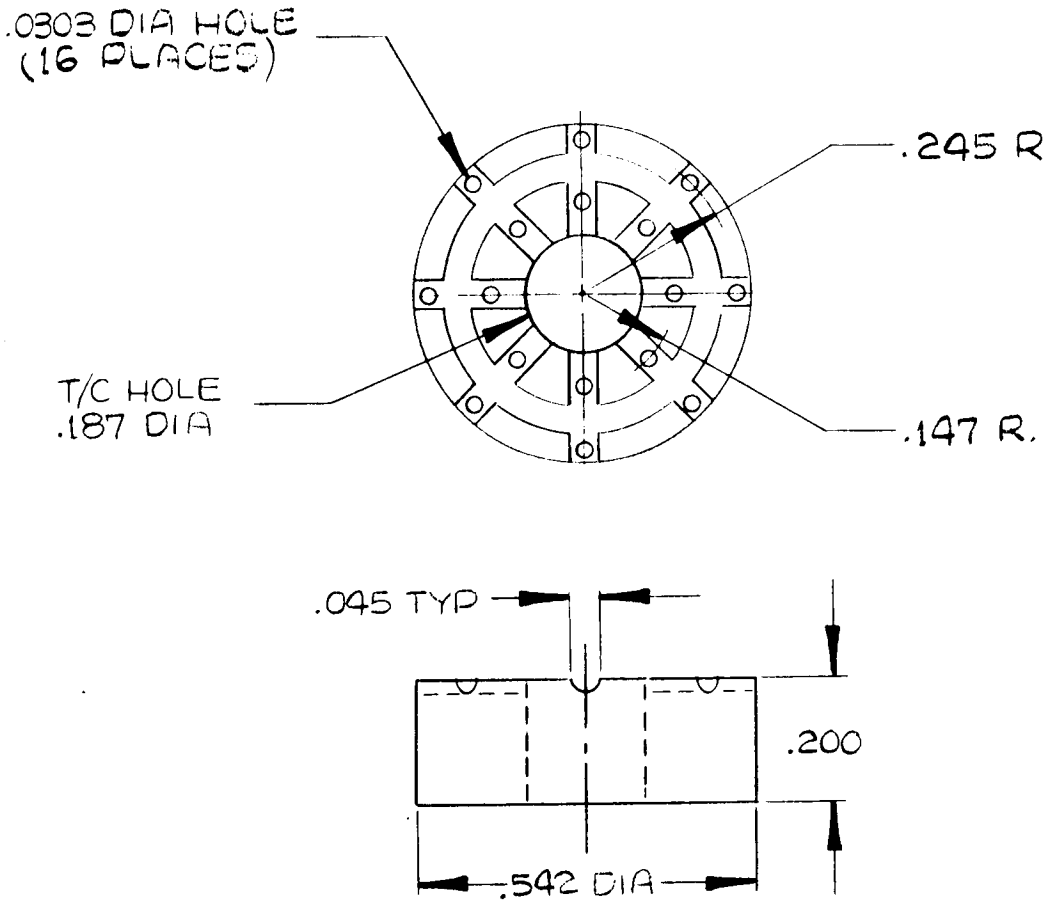

$$\frac{A}{V} = 14.4875 \text{ IN.}^{-1} \text{ OR } 5.7037 \text{ CM.}^{-1}$$

A = Surface area of grooves, vent holes and area adjacent to grooves on neighboring pellet. The outer cylindrical surface area in contact with the tungsten cladding and the inner cylindrical surface area in contact with the thermocouple well are not included.

V = Volume of remaining mass only.

Note: All grooves are of the same size for all three fuel configurations.

Fig. 2.52 (a)--(C-RD) (Gp-1) Fuel configurations used in experiment No. 62-13-R2

PLUMBROOK FUEL PELLET

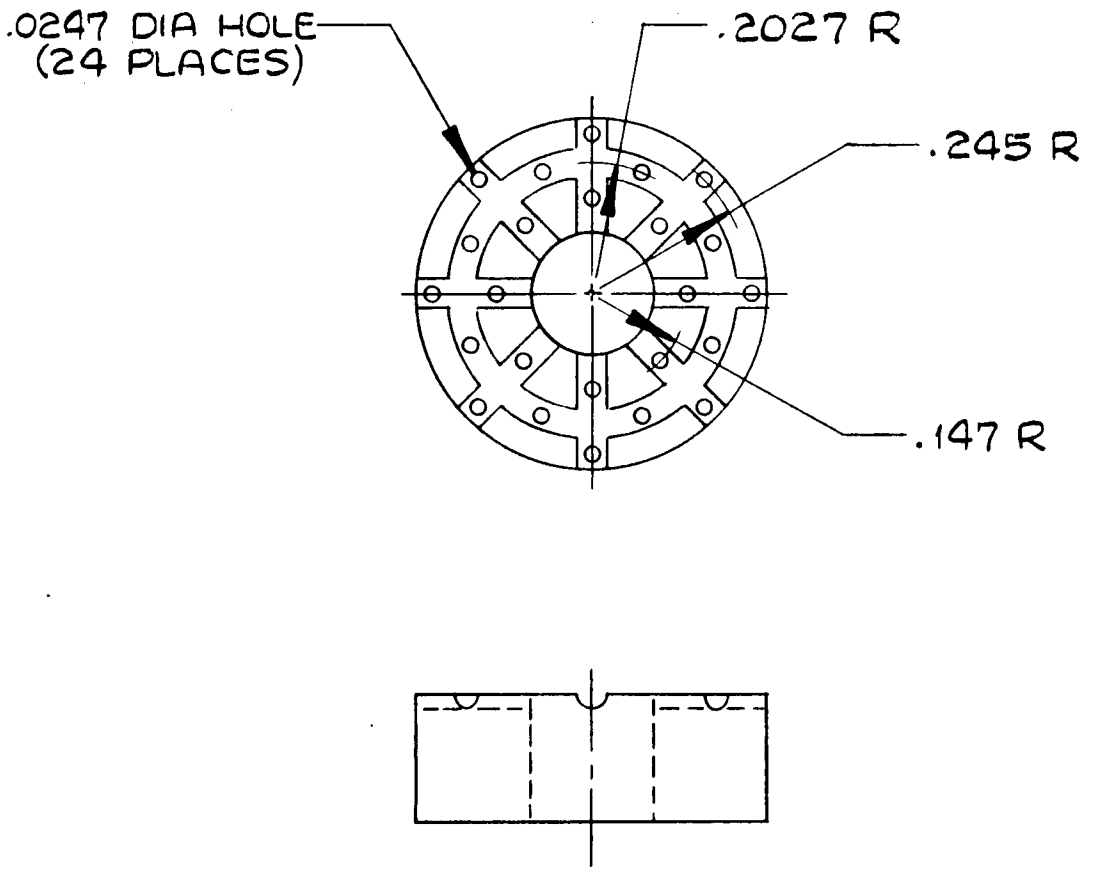

$$\frac{A}{V} = 16.1554 \text{ IN.}^{-1} \text{ OR } 6.3604 \text{ CM.}^{-1}$$

Fig. 2.52 (b)--(C-RD)(Gp-1) Fuel configurations used in experiment No. 62-13-R2

PLUMBROOK FUEL PELLET

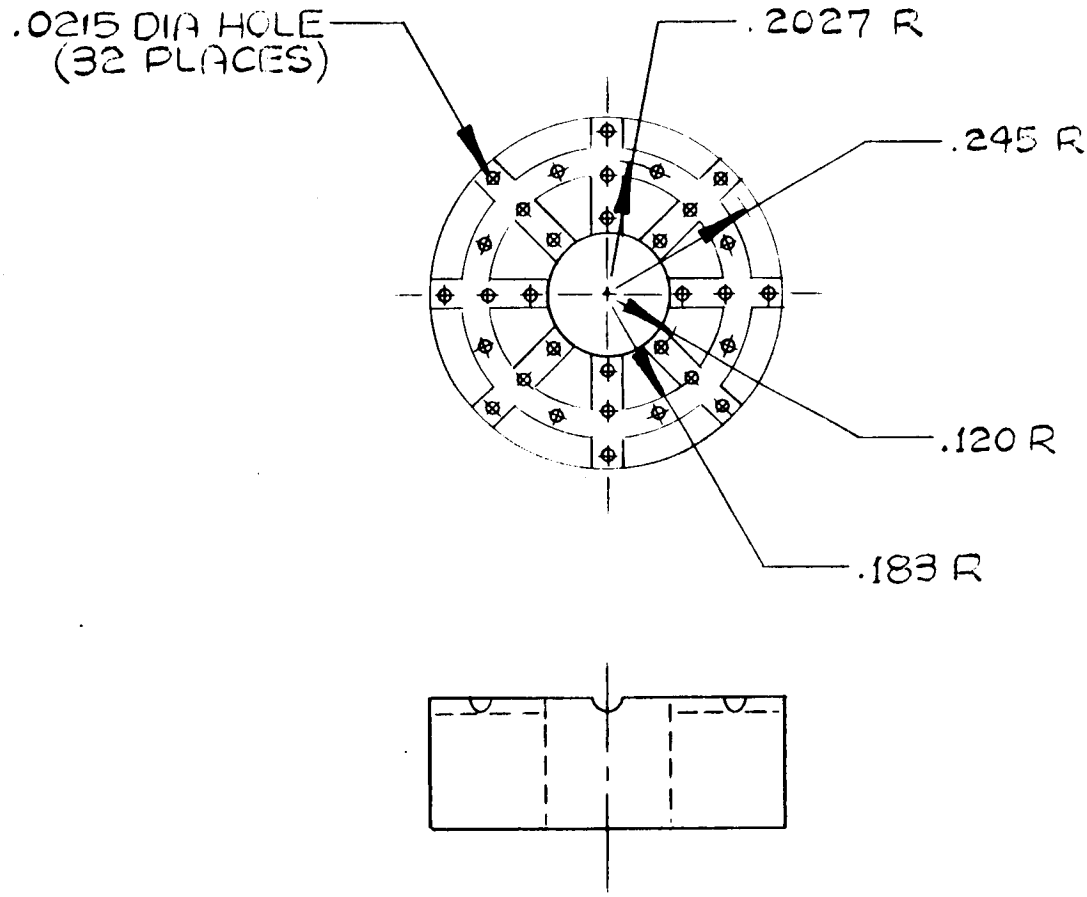

$\frac{A}{V}$ = 17.5613 IN^{-1} OR 6.9139 CM^{-1}

Fig. 2.52(c)--(C-RD) (Gp-1) Fuel configurations used in experiment No. 62-13-R2

The first was to excercise rigid control of the moisture content in the oil medium in which the electrical discharge machining was carried out and to minimize the exposure of the sample to air or to solvents having a finite solubility of water. The second was to increase the carbon content of carbon-deficient 50UC-50ZrC samples by carburization. Three approaches were tried in the carburization experiments. The first was to carburize the sample in a fluidized bed containing pyrocarbon coated uranium dicarbide particles for 8-10 minutes at 1400-2100°C and then to homogenize the carburized sample in vacuum for 2 hours at 2000°C. This approach was abandoned after it was found that the particles in the fluidized bed tended to chip the edge of the sample. The second approach was to enclose the sample in a graphite crucible and to carburize the sample by carbon transport through the vapor phase in the temperature range 1850-2080°C for 3-5 hours. No detectable increase in carbon content, however, was observed. The third approach was to pack the sample in 30 micron size graphite flour and to carburize the sample at 2150-2300°C for 2-5 hours; this was followed by vacuum homogenization at 2200-2300°C for 16 hours. For the limited number of experiments carried out, no reproducible increase in carbon content was established and cracks were observed in some of the samples studied. The carburization experiments were terminated after improvements made in the electrical-discharge-machining operation resulted in samples of acceptable carbon to uranium ratios.

(C-RD)(Gp-1) Characteristics of fuel samples prepared. – The characteristics of the fuel samples prepared are summarized in Table 2.10. The arrangements of these samples in the fuel cups of Capsules V-2C and V-2D are shown in Fig. 2.53. Samples were stacked in the fuel cup in the order of increasing geometric surface area to volume ratio in order to minimize the risk of blocking the fission gas venting holes if severe fuel swelling does occur in the samples of lower geometric surface area to volume ratio. Figures 2.54 and 2.55 show the typical microstructures of the 90UC-10ZrC and the 50UC-50ZrC samples respectively. In both cases, the matrix consists of the UC-ZrC phase containing a few weight percent of tungsten and the dispersions are the UWC_2 phase. The UWC_2 phase in 90UC-10ZrC is bigger than that in 50UC-50ZrC, and there seem to be more UWC_2 phases in the 90UC-10ZrC sample than in the 50UC-50ZrC sample.

Table 2.10

(U) CHARACTERISTICS OF FUEL SAMPLES USED IN IRRADIATION EXPERIMENT 63-12-R2

(This table is classified Confidential-Restricted Data-Group 1)

Capsule	Sample No.	Composition				U^{235} Enrichment	Configuration (See Figure 2.36)	Density (% Theoretical)	SRF	C/U	Remarks
		U	Zr	W	C						
V-2C	1 2	0.855	0.095	0.049	1.022	30 wt% of total uranium content	(a)	76.0	176	1.05	Test sample
	3 4	0.859	0.093	0.050	1.012	30 wt% of total uranium content	(b)	76.5	161	1.04	Test sample
	5 6	0.856	0.093	0.050	1.007	30 wt% of total uranium content	(c)	79.0	162	1.035	Test sample
	7 8 9	0.850	0.097	0.054	1.009	30 wt% of total uranium content	(c)	75.1	198	1.04	Thermal shield
V-2D	1 2	0.498	0.482	0.041	1.000	50 wt% of total uranium content	(a)	79.9	182*	1.04	Test sample
	3 4	0.475	0.481	0.044	1.000	50 wt% of total uranium content	(b)	78.0	200**	1.04	Test sample
	5 6	0.472	0.484	0.046	1.001	50 wt% of total uranium content	(c)	80.0	185	1.045	Test sample
	7 8 9	0.498	0.482	0.041	1.000	50 wt% of total uranium content	(c)	75.5	237	1.03	Thermal shield

*Determined by using a sample containing 24 holes instead of 16 holes. Since the 24 hole sample has the same volume (therefore the same amount of open porosities) but a longer geometric surface area than that of the 16 hole sample, it is believed that the SRF value of the 16 hole sample should be higher than 182.

**Determined by using half of a 24 hole sample. Since the full size sample has twice the amount of open porosities but less than twice the geometric surface area as that of the half size sample, it is believed that the SRF value of the test sample should be higher than 200.

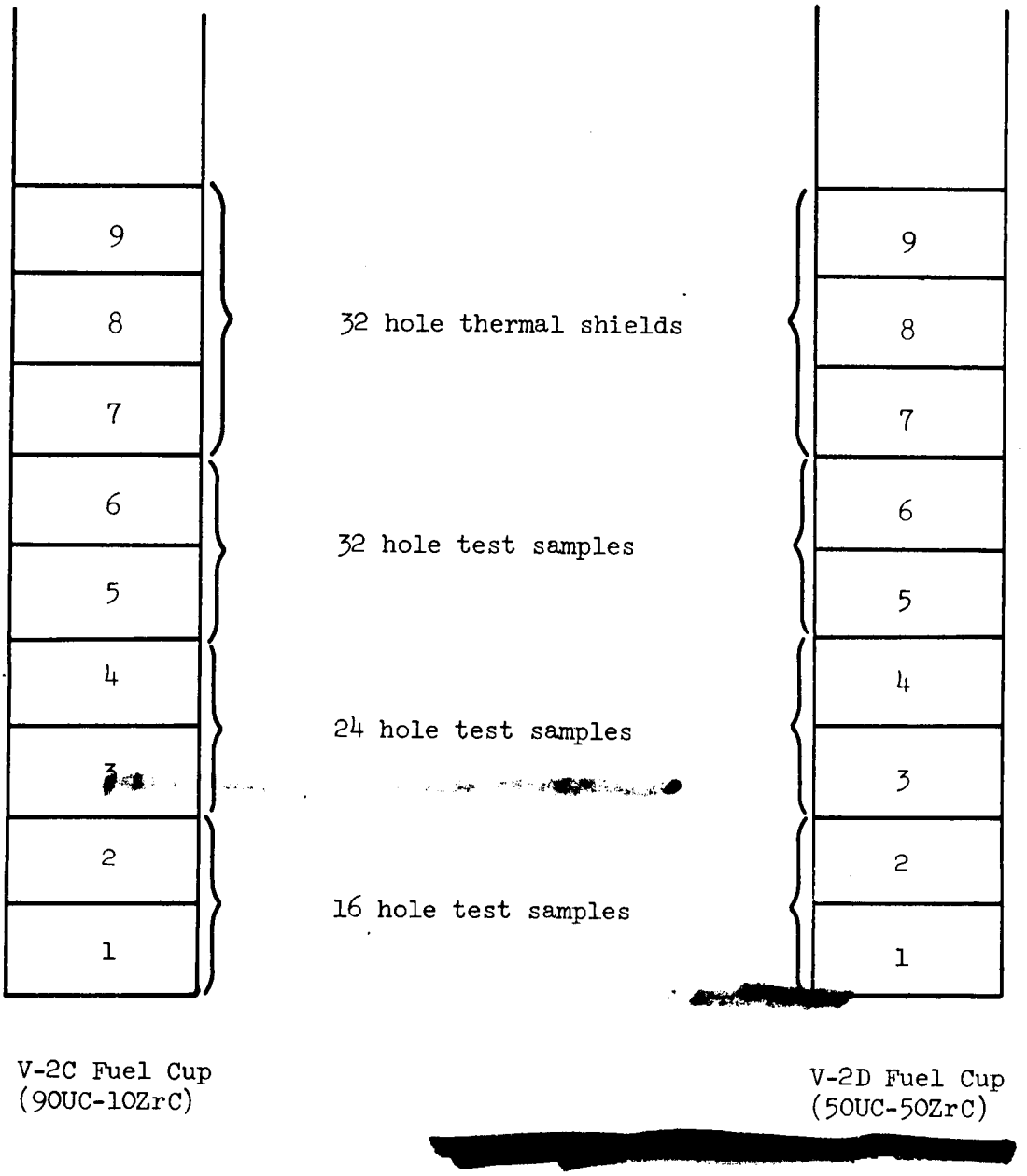

Fig. 2.53-- Arrangements of samples in the fuel cups of V-2C and V-2D fuel pins

(See Table 2.10 for characteristics of each sample)

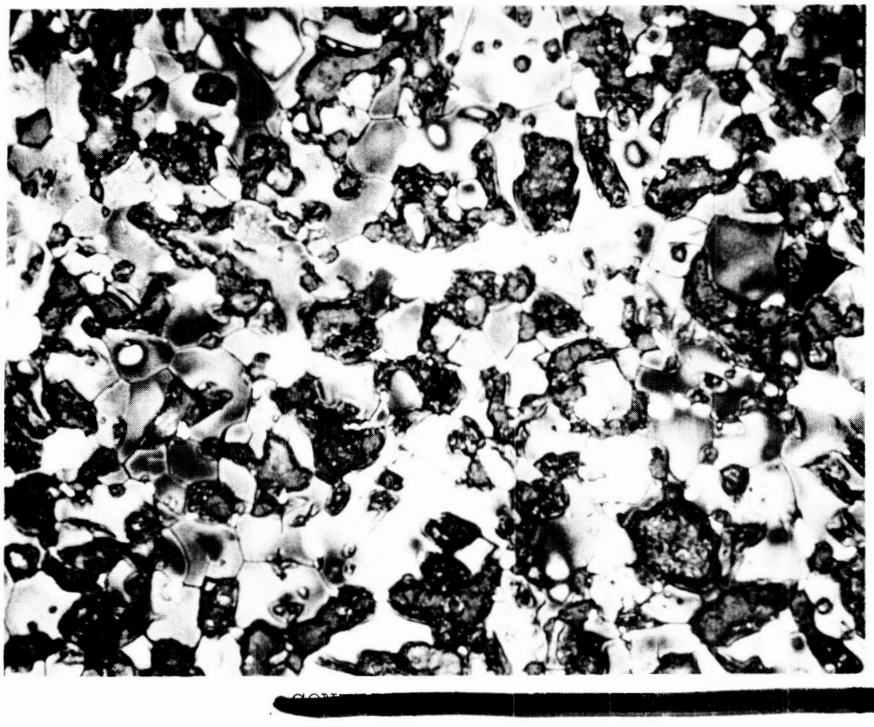

750X

Fig. 2.54--[redacted] Microstructures of 90UC-10ZrC fuel samples used in Capsule V-2C

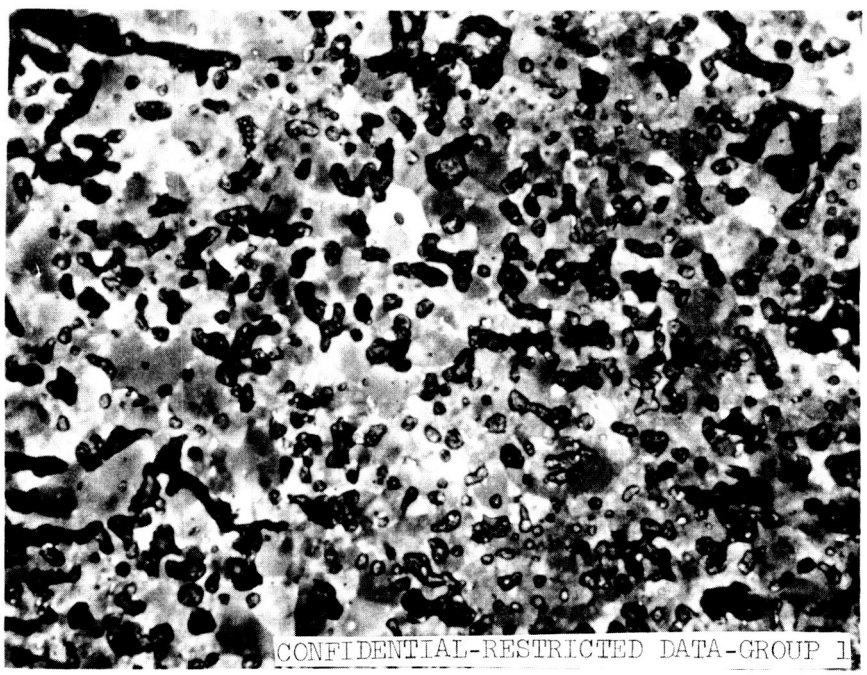

M-26170-1 750X

Fig. 2.55--(C-RD)(Gp-1) Microstructures of 50UC-50ZrC fuel samples used in Capsule V-2D

2.2.4. Capsule Assembly

2.2.4.1. Assembly of the Fuel Pin and the Fission Gas Containment Chamber

(U) The fuel samples, arranged in the proper order and supported on the tungsten thermocouple well with a tungsten spring holding them in position, were inserted into the tungsten cup. A stainless steel spring which was used to hold the tantalum transition of the thermocouple well inside the tantalum transition of the tungsten fuel cup, was then inserted through the copper pinch-off tube and held in position with a snap ring. The assembly was then placed in a vacuum environment, with the copper pinch-off tube connected to another vacuum system. The fueled region was then heated by high frequency induction at 1650°C until a vacuum of $\sim 10^{-7}$ torr was attained in the fuel cup. The assembly was then cooled to room temperature and pinch-off at the copper pinch-off tube. Figure 2.56 shows the appearance of the pinch-off fuel cup. Following the pinch-off, a weld was then made between the tantalum transition of the thermocouple well and the tantalum transition of the fuel cup by electron beam welding. The assembly was then gamma-graphed to insure that the fuel samples were in the proper positions. Figures 2.57(a) and (b) are the gamma-graphs taken of V-2C fuel cup and V-2D fuel cup respectively after the thermal contact welding.

(U) The fuel cup was then placed in an inert gas filled glove box and the copper pinch-off tube was removed mechanically. The high temperature thermocouple assembly (Fig. 2.58) was then inserted into the fuel pin. The Inconel fission gas containment tube was then slipped over the high temperature thermocouple assembly and welded to both units. The assembly was then attached to an ion pump and a helium leak detector which was used both for leak detection and for the starting of the ion pump. The complete unit with the ion pump attached, was installed in a bakeout station and outgassed at 600°C at a residual gas pressure of less than 1×10^{-5} torr in the bakeout station, and $\sim 10^{-7}$ torr in the assembled unit. After cooling to room temperature, the assembly was backfilled with high purity argon gas to 1.5 psia and the copper exhaust tube was pinched off and

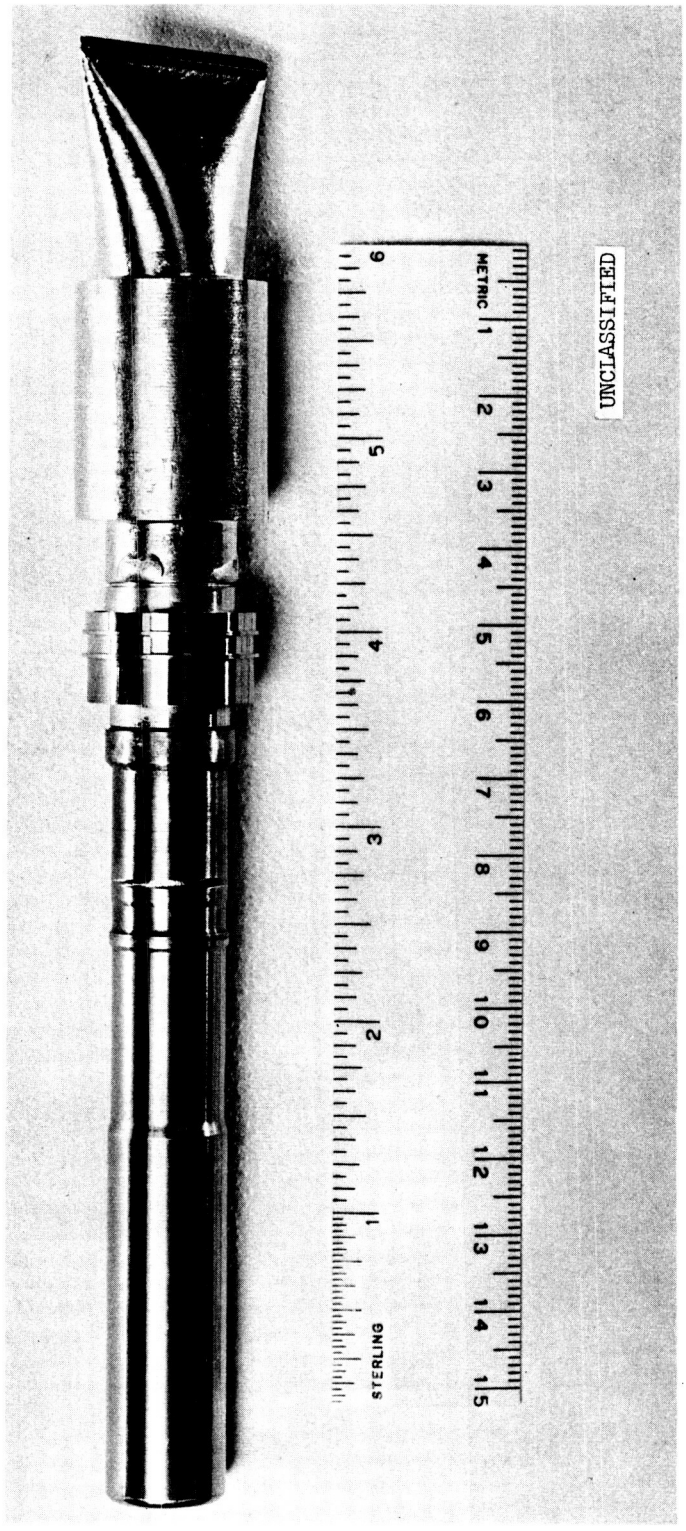

Fig. 2.56--(U) Fuel cup after pinch-off

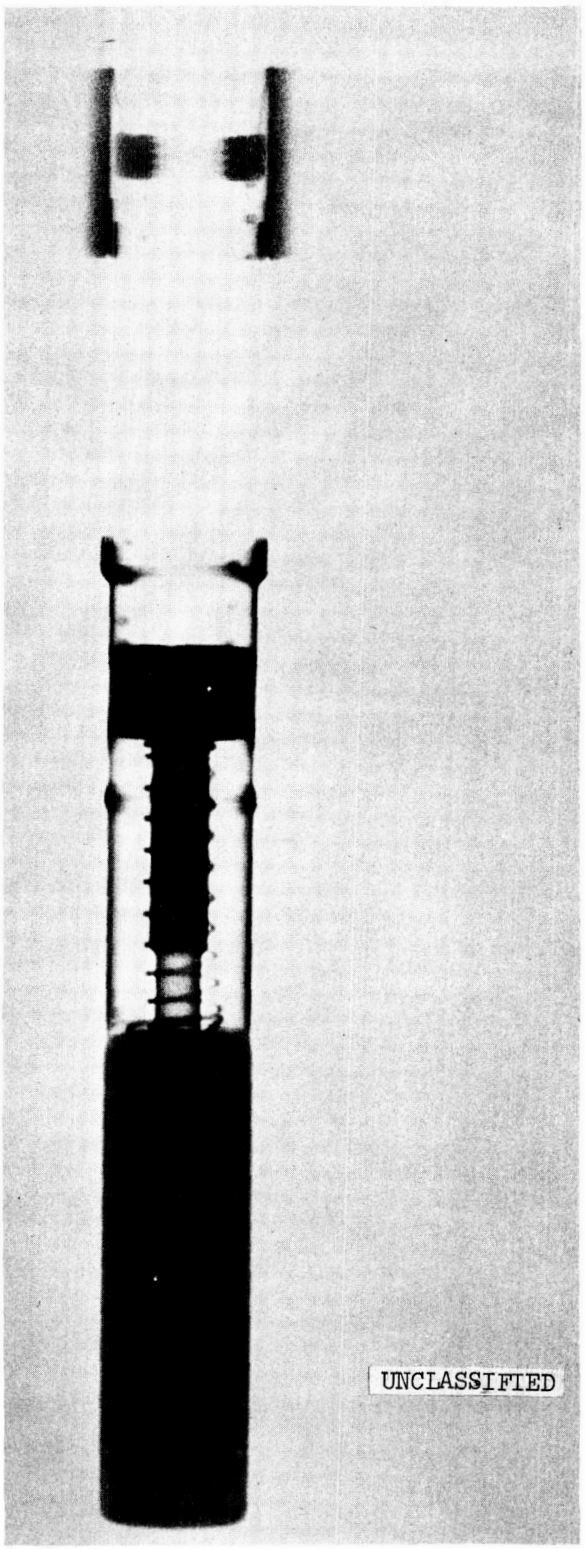

Fig. 2.57 (a)--(U) γ-graph of fuel cup for Capsule V-2C

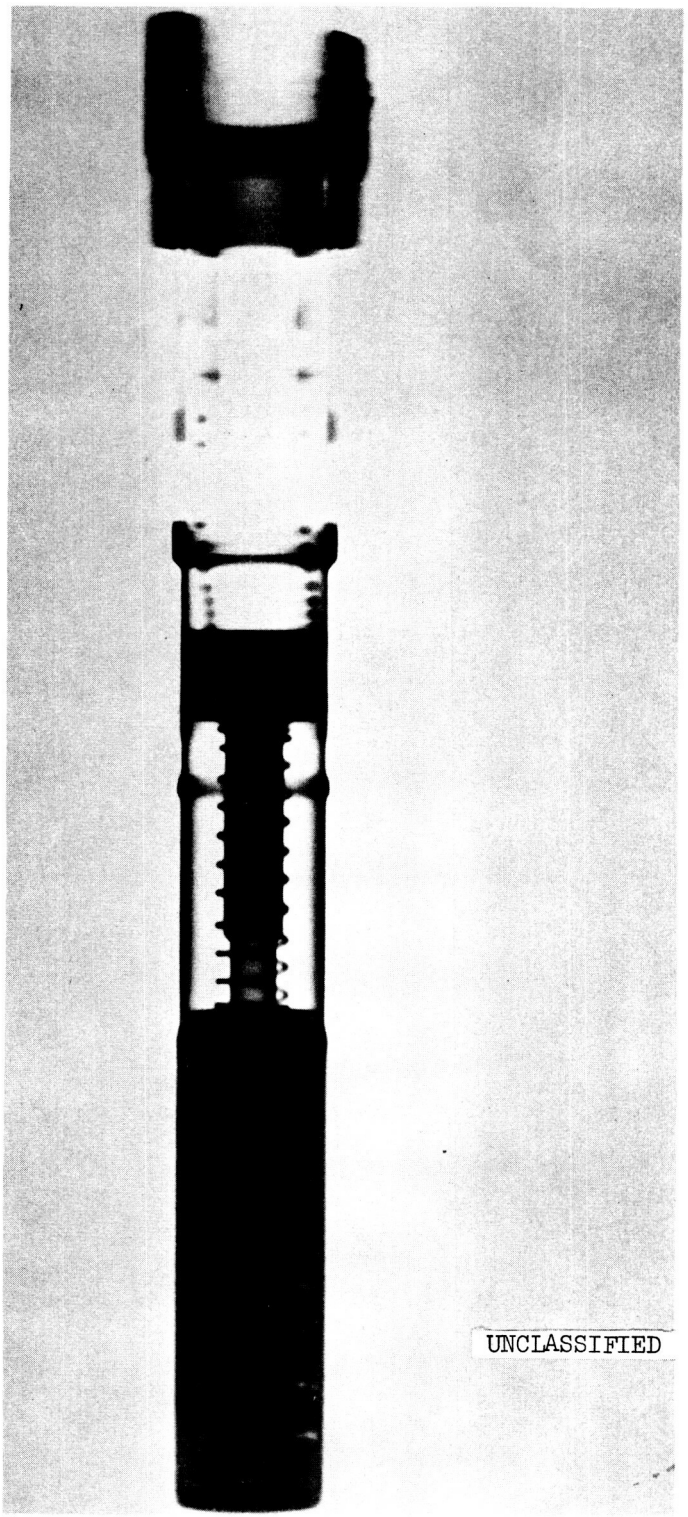

Fig. 2.57 (b)--(U) γ-graph of fuel cup for Capsule V-2D

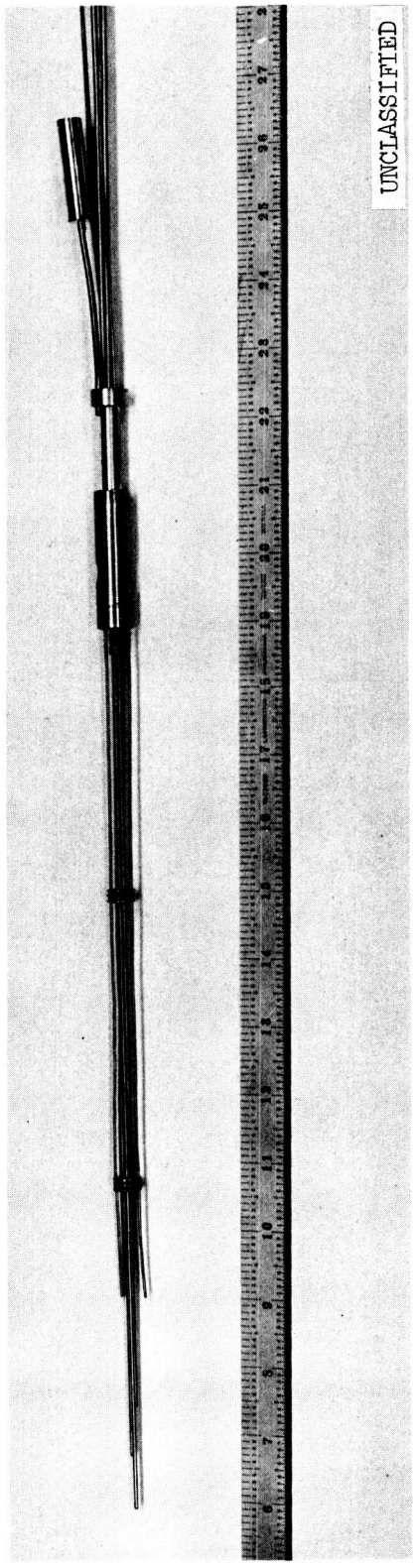

Fig. 2.58--(U) High temperature thermocouple assembly

backwelded (Fig. 2.59). The assembly was then gamma graphed to locate the positions of the high temperature thermocouples. The thermocouples were checked for both polarity and continuity.

2.2.4.2. Primary Containment Assembly

(U) The first step in the assembly of the primary containment was the welding of the center sleeve to the fuel cup and fission gas chamber assembly described above, while maintaining equal gap size between the fuel cup and the tungsten pins held in the sleeve. The gamma heat meter and the Chromel-Alumel radial thermocouples were then installed into the primary containment can components and brazed into the feedthrough. The primary containment can components were then welded to the bottom of the center sleeve and the top of the Inconel transition of the fuel cup. (See Fig. 2.60.) The completed unit was helium leak checked. External heating tapes were then wrapped around the assembly and the latter was heated to 250°C for 4 hours at an internal residual gas pressure less than 4×10^{-6} torr. All the thermocouples were checked at this time. The assembly was then cooled to room temperature, leak checked and backfilled with neon gas to a pressure of one atmosphere. The copper exhaust tube was then pinched off and the pinch-off was then backwelded. The completed assembly is shown at the bottom of Fig. 2.61.

2.2.4.3. Outer Containment Assembly

(U) Assembly of the outer containment started by the brazing of the thermocouples into another feedthrough. The brazed unit was then inserted into the outer containment can. The feedthrough and the lower sleeve containing the final closure valve were then welded to the two ends of the outer containment can. (See Fig. 2.61.) The assembly was leak checked and then baked at 250°C, while pumped with a mechanical oil pump for four hours. After cooling to room temperature and backfilled to 165 psia of high purity helium gas, the final closure valve attached to the lower sleeve was tightly closed and welded to form a leak proof seal. The completed unit is shown on the top of Fig. 2.62.

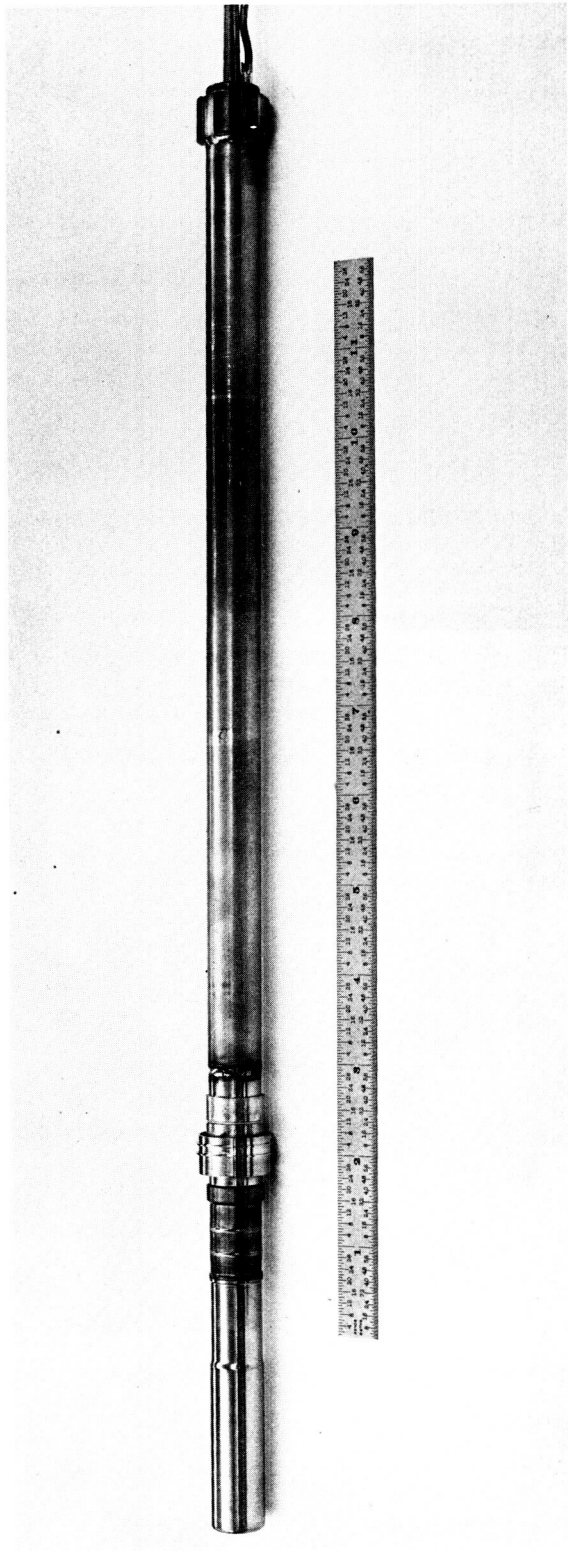

UNCLASSIFTED

Fig. 2.59--(U) Fuel cup and fission gas chamber assembly

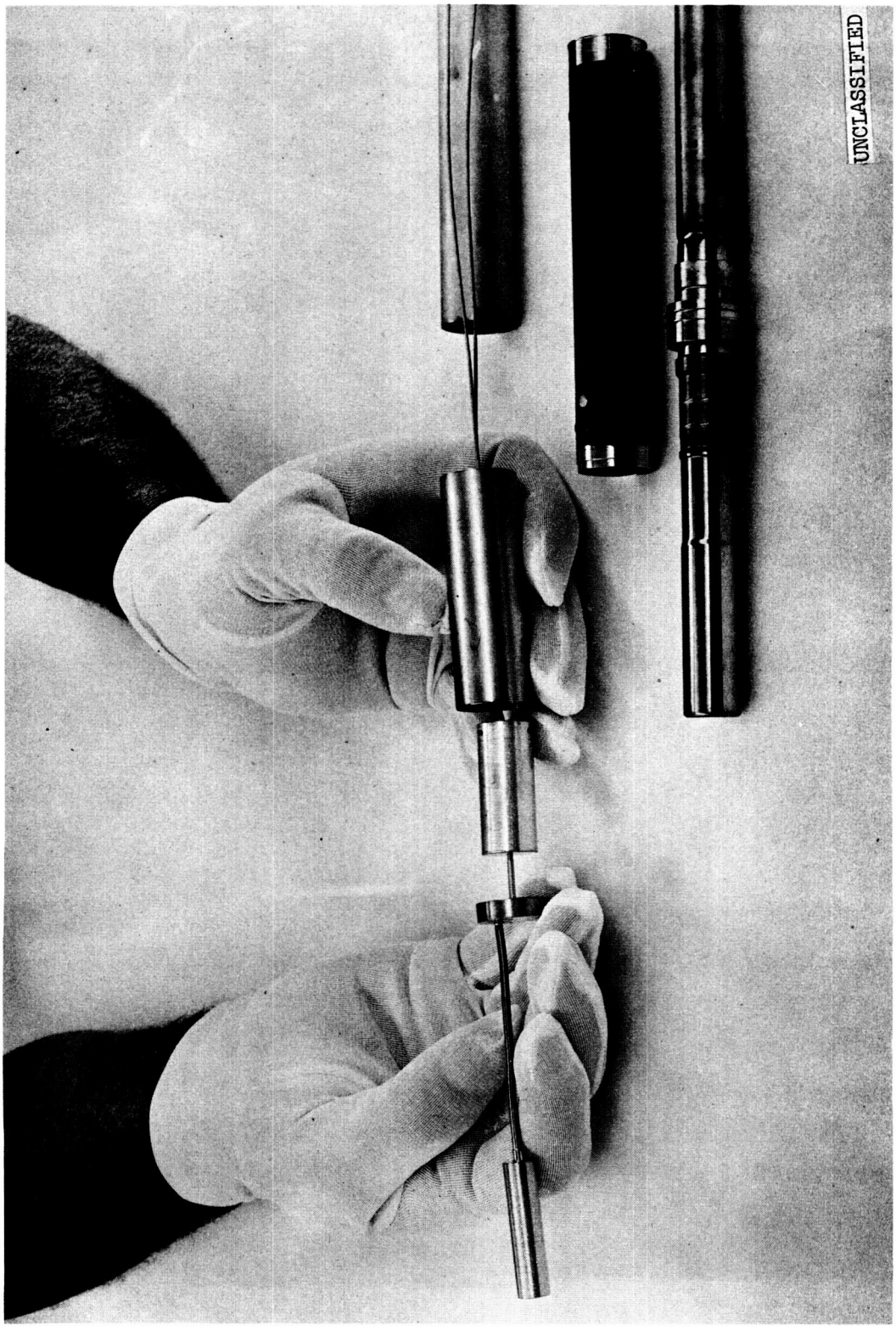

Fig. 2.60--(U) Components for primary containment can

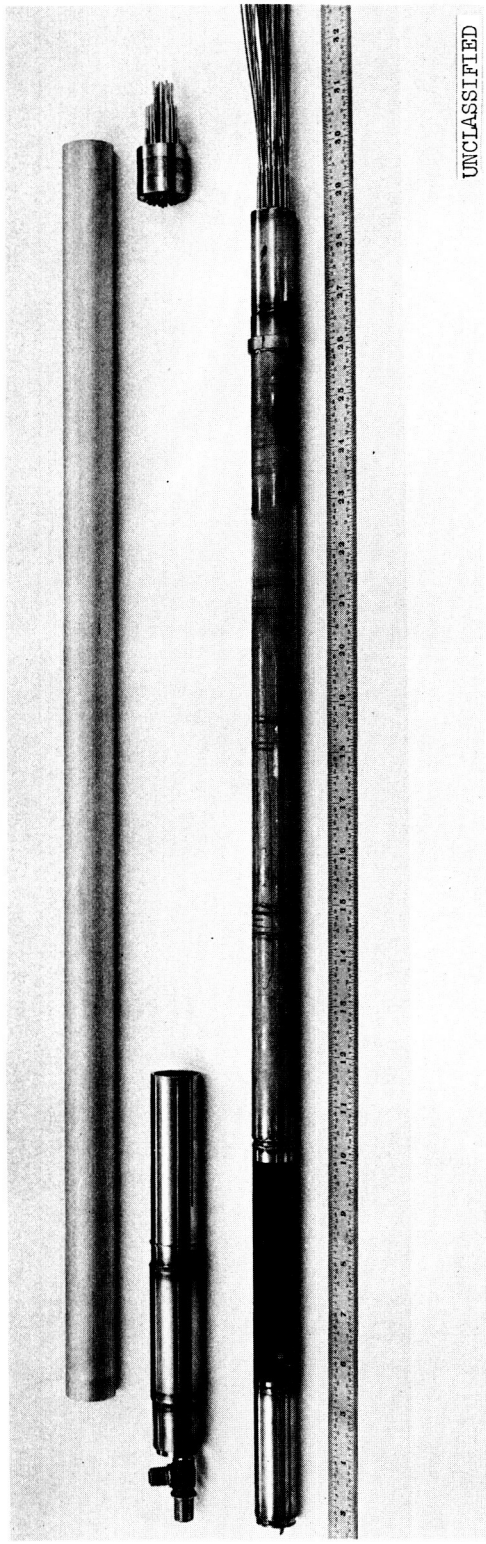

Fig. 2.61--(U) Components of outer containment can

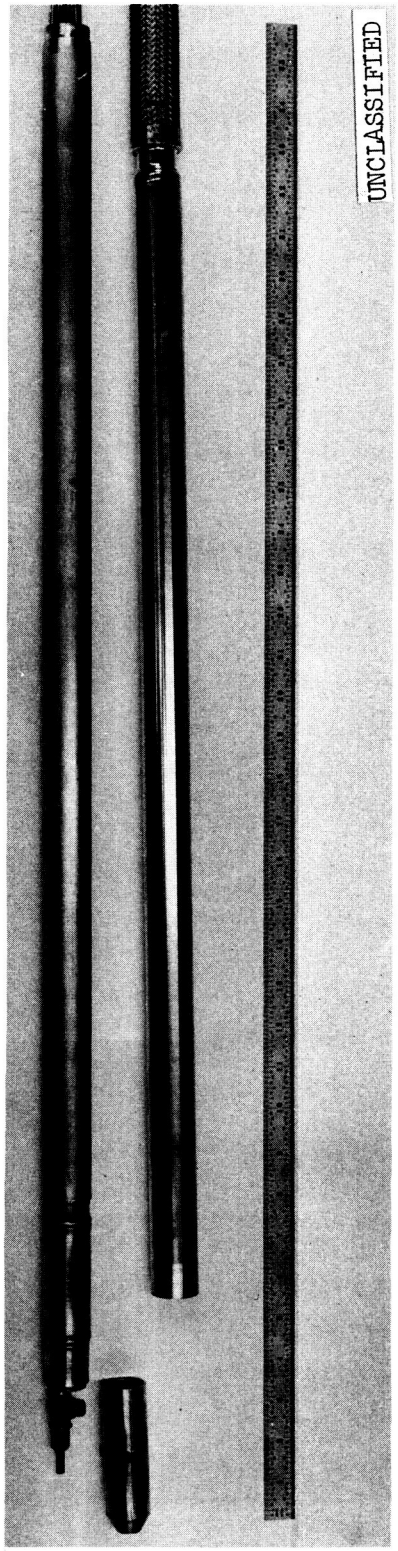

Fig. 2.62--(U) Assembled outer containment can and lead tube

2.2.4.4. Lead Tube Connection

(U) The thermocouples and the gamma heat meter leads were joined to the extension leads which were then potted and run through the flexible section of the lead tube (see Fig. 2.62) to its upper end. The thermocouples and the gamma heat meter heater were then checked out both before and after soldering to the cannon plug. The welds that make up this section (see Fig. 2.63) were then completed, dye penetrant checked and helium leak checked. The assembly was then pressurized to 225 psig with dry nitrogen and left under pressure for one hour. Afterwards, it was again helium leak checked. A mating connector was then joined to the cannon plug. A current was run through the gamma heat meter heater and the responses of the thermocouples were recorded, which were used to check the polarity and the locations in the capsule against the proper pin locations in the cannon plug. The capsule then was ready for shipment.

2.2.5. Packaging and Shipping

(U) The capsules were shipped to the Plum Brook Reactor Facility in an Electronic Air Ride van. This is the method normally used by Gulf General Atomic to ship electronic consoles that are sensitive to vibration and shock. An analysis of the maximum possible dynamic loads was conducted for the capsule based on the following:

(1) The ability of the capsule to withstand up to 20 G's of shock in any axis without sustaining damage.

(2) The ability of the capsule to withstand transportation's vibrations of 5 C.P.S. (cycles per second)

(Natural frequencies of truck bed during transport are 11 to 15 C.P.S.) Although no data are available, it is reasoned that the lower frequency will result by the use of "Air Ride Van" for road transport.

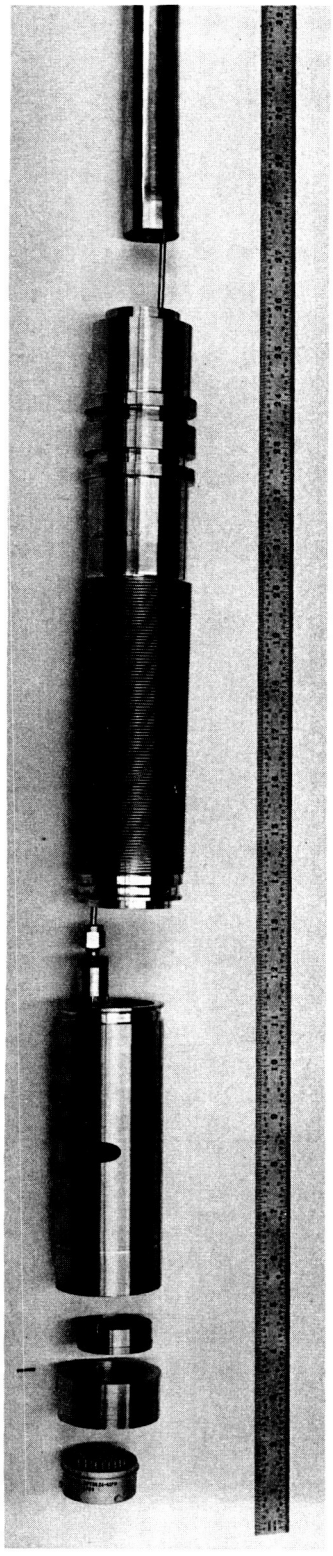

UNCLASSIFIED

Fig. 2.63--(U) Top of lead tube

(3) Protecting the packaged capsule from damage if dropped from a height of 36 inches. (This height was selected because of the distance from the truck freight door to ground level.)

(4) The possible deflection curve limitations of the capsule in a linear axis.

(5) A support collar of ample strength and stiffness will be secured to the capsule to prevent compression, elongation and deflection of the flexible hose section of the assembly.

Some of the symbols used in the analysis are:

dn = (normal travel distance of cushioned item receiving shock load of 20 G's.)

do = (cushion thickness required)

ko = (spring constant of the cushioning - 200 lb/in. for 2 lb. density polyurethane)

W = (weight of item cushioned - 90 lbs.)

h = (drop height anticipated - 36 inches)

G = (G Factor or shock item can experience without sustaining damage - 20 G's)

fn = material frequency of the part within the polyurethane cushioning.

(U) Normal distance item will travel at impact within 2# density polyurethane

$$dn = \frac{2h}{G} = \frac{2 \times 36}{20} = 3.6 \text{ inch.}$$

i.e. 3.6 inch of cushioning is required to stop item travel when item is subjected to 20 G shock load. (item will fully compress cushioning, bottom out and receive damage.)

(U) Cushioning thickness required for full shock dampening

$$do = \sqrt{\frac{2\ W\ h}{ko}} = \sqrt{\frac{2 \times 90 \times 36}{200}} = 5.6 \text{ inch}$$

i.e. 5.6 inch of cushioning required to protect item from damage.

(U) Transmissibility and dampening factor

$$fn = 3.13\sqrt{\frac{ko}{W}} = 3.13\sqrt{\frac{200}{90}} \approx 5 \text{ cycles/sec.}$$

F = 15 cycles/sec. forcing frequency of truck bed at 60 mph.

The frequency ratio is:

$$F/_{fn} = 15/_{5} = 3$$

Transmissibility is:

$$T_r = \frac{1}{(F/_{fn})^2 - 1} = \frac{1}{(3)^2 - 1} = \frac{1}{8} = .125$$

$$C_o = \text{Critical Dampening} = \frac{2\ W\ fn}{g} = \frac{2 \times 90 \times 5}{32} = 28 \frac{\text{lbs.}}{\text{ft.}} \text{ /sec.}$$

C = Actual amount of dampening provided.

$$d = \text{The dampening factor} = \frac{C}{C_o} = \frac{10.5}{28} = .375$$

Since transmissibility and dampening factor are below 1.0 good cushioning, protection is provided to the part for shipment. The results of the shock transfer analysis as a function absorption cushion thickness is shown in Fig. 2.64. For an allowable transfer of 20 G a cushion thickness of 5 inches of polyurethane foam was selected. This results in a static load of less than 0.5 psi.

(U) A cross section of the shipping package design is shown in Fig. 2.65. Both Capsules V-2C and V-2D have been successfully shipped using the packaging design and the shipping method described above.

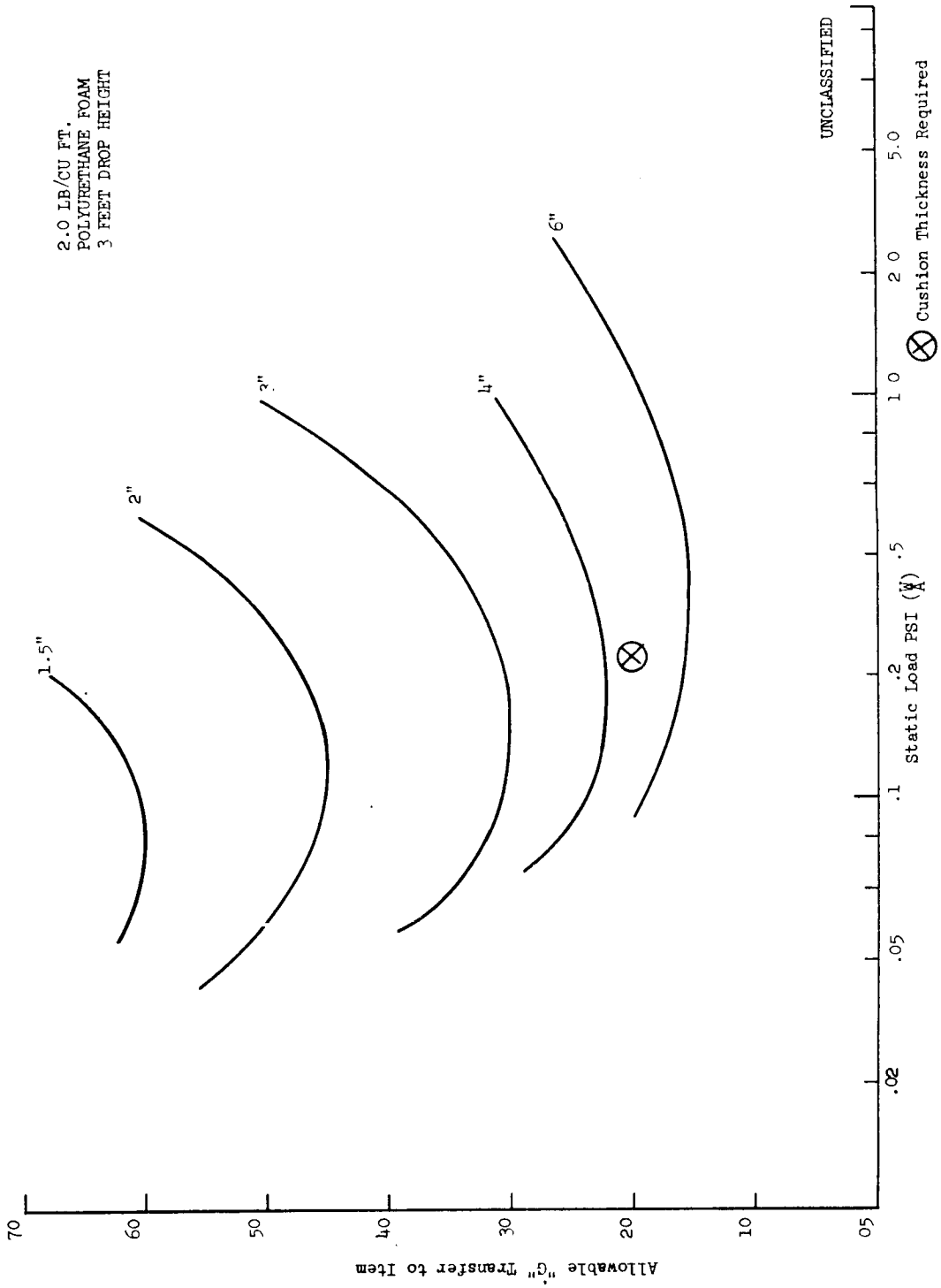

Fig. 2.64--(U) Results of shock transfer analysis

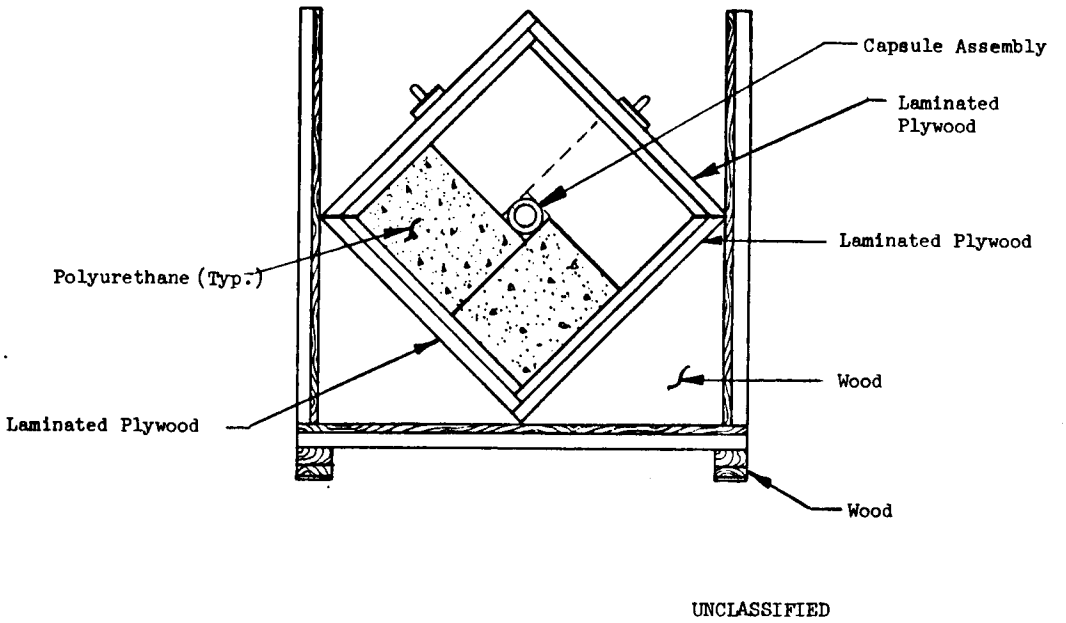

Fig. 2.65--(U) Cross section of capsule shipping container

REFERENCES

(1) "Studies of Thermionic Materials for Space Power Applications, Summary Report for the Period September 1, 1964 through November 23, 1965 (U)," National Aeronautics and Space Administration Report NASA-CR-54980, General Dynamics, General Atomic Division, May 6, 1966. (C/RD).

(2) Yang, L., et al., "Investigations of Carbides as Cathodes for Thermionic Space Reactors, Final Report," National Aeronautic and Space Administration Report NASA-CR-56280, General Dynamics, General Atomic Division, March 17, 1964, Part I. (U).

(3) "Studies of Thermionic Materials for Space Power Applications, Annual Summary Report for the Period September 1, 1963 through August 31, 1964 (U)," National Aeronautics and Space Administration Report NASA CR-54322, General Dynamics, General Atomic Division. (C/RD).

(4) "Experiment Design Manual and Hazard Analysis, Plum Brook Reactor Facility Experiment No. 62-13-R1," General Dynamics, General Atomic Division, unpublished data, September 1, 1964. (U).

(5) Tsederberg, N. V., Thermal Conductivity of Gases and Liquids, M.I.T. Press, Cambridge, 1965.

(6) Keys, F. G. and R. G. Vines, "Thermal Conductivity of Nitrogen and Argon, " J. Heat Transfer 87 No. 2, 177-83 (May 1965).

(7) Goldsmith, Alexander, Handbook of Thermophysical Properties of Solid Materials, Vol. II, The Macmillan Company, New York, 1961.

(8) Wood, W. D., H. W. Deem, and C. F. Lucks, "Thermal Radiative Properties of Selected Materials," Battelle Memorial Institute Defense Metals Information Center Report DMIC-177, Vol. I, November 15, 1962. (U).

(9) Gubareff, G. G., Shao-Yen Ko., and P. E. McNall, Jr., "Review of the Thermal Radiation Property Values for Metals and Other Materials," Minneapolis-Honeywell Regulator Co. Report GR 2462-R3, September 1958, p. 139. (U).

(10) "Studies of Thermionic Materials for Space Power Applications, Semi-Annual Report for the Period February 1, 1967 through July 31, 1967 (U)," National Aeronautics and Space Administration Report NASA CR-72327, Gulf General Atomic Incorporated, November 30, 1967. (C/RD).

(11) Kline, S. J., and F. A. McClintock, "Describing Uncertainties in Single-Sample Experiments," Mech. Eng. 75, 3 (1953).

(12) Forsythe, W. E., and E. Q. Adams, "Radiating Characteristics of Tungsten and Tungsten Lamp." J. Opt. Soc. Am. 35, 2 (1945).

(13) Yang, L., A. F. Weinberg, and J. R. Lundgren, "Investigation of Carbides as Cathodes for Thermionic Space Reactors, Final Report (U)," National Aeronautics and Space Administration Report NASA CR-71336, General Dynamics, General Atomic Division, N.D., Part II. (C/RD).

APPENDIX A: HAZARDS ANALYSIS

A.1. MAXIMUM CREDIBLE ACCIDENT

(U) From the hazards evaluation of the capsule and experiment, the maximum credible accident has been determined to be the rupture of all three fuel containment cans. This accident is analyzed in Section A.4.3, Case 8.

A.2. LOSS OF SYSTEM COOLANT FLOW

(U) No hazard is involved with the loss of system coolant flow since the flow passes through a turbine flow meter which sets up a fast-out condition when the flow drops below the set point. This is a fail-safe condition in that normally open contacts are used and the CPM control system will not function, other than in the fast-out condition, until the flow exceeds the set point. After a low flow signal, the CPM control must be manually reset before CPM movement can occur as required.

A.3. LOSS OF SYSTEM COOLANT PRESSURE

(U) The coolant system water is taken from the reactor primary system through an opening in the V-tube. Loss of system pressure due to rupture is covered in Section A.7.4.

A.4. SYSTEM RUPTURE

A.4.1. Coolant and CPM System Rupture

A.4.1.1. Inside Pressure Vessel

(U) There are several areas where the coolant system lines could rupture inside the pressure vessel. If the coolant discharge line should fail, the capsules would fail to be cooled adequately. The CPM may not go

into a fast-out condition due to low flow since the flow meter could still indicate at least a normal flow rate. However, once the capsule loses the coolant flow, temperatures would start rising immediately. If the temperature rises above appropriate set points, either the EDLAS or the safety channel will initiate a fast-out condition. A further increase in temperature will result in an automatic reactor power reduction via the safety channel. In any ruptures of water lines inside the reactor vessel, the reactor would have to be shut down. The capsules would have to be removed and the facility repaired or replaced.

A.4.1.2. Outside Pressure Vessel

(U) The coolant discharge line outside the pressure vessel contains primary water. A rupture in this line could result in primary water being discharged under the missile shield. However, tubing has been bought to Specification MIL-T-8808 which requires hydrostatic test at approximately 4000 psi. Danger of rupture is remote. If the rupture is upstream of the flow meter in the discharge line, a low flow condition would exist if the leak was large enough. No other method of leak detection is proposed other then pre-irradiation and between cycle pressure checks if required.

A.4.2. Gas System Ruptures

(U) The capsule lead line is pressurized with helium to 165 psig. If the lead line ruptures inside the pressure vessel, helium would leak into the reactor water from the PBRF gas pressurization system for lead capsule experiments. A leak would be detected by large usage of helium, although this would not pinpoint the rupture area. If the leak is outside the reactor, it can be easily repaired. If it is inside the pressure vessel, it may be possible to raise the capsule enough to repair the leak if the induced activity in the capsule materials is not severe. Otherwise, the capsule must be discharged.

A.4.3. Capsule Rupture

(U) The capsules are constructed with triple containment of the fuel so that three cans must rupture before the fuel would be exposed to

the reactor water. Table A.1 lists the types of ruptures that can occur and the results of such ruptures.

A.5. LOSS OF ELECTRICAL POWER

(U) The experiment console is supplied with commercial power. The two safety channels, TR-3 and TR-4, receive their power the guaranteed power circuit. On loss of commercial power to the console, low flow, low temperature, high temperature, high fuel temperature alarms will be summary on XCR annunciator; however, the capsules will still be protected by safety channels.

A.6. REACTOR EXCURSION TO 150 PERCENT FOR 60 MSEC FOLLOWED BY REACTOR SCRAM

(U) For a flux of 7.5×10^{13} (approximately 1 inch in from V-tube center line) there is a power generation of 200 watts/cm^3 resulting in fuel temperatures of 1700°C. Power generation of 200 watts/cm^3 indicate an Inconel end cap temperature of 760°C. If the reactor power increases to 150 percent or a power generation of 300 watts/cm^3, the fuel temperature would rise to 1950°C and the Inconel to 897°C under steady state conditions.

(U) The melting temperature of the fuels is 2450 to 3100°C. Thus, the steady state condition can be tolerated, but is not desirable, hence no hazard is visualized in the transient case.

A.7. REACTOR OPERATION AT 120 PERCENT

(U) The CPM movement is designed to accommodate a factor of 4 change in flux in the capsules. Only when operating in the extreme out position, at 100 percent reactor power, would reactor operation at 120 percent be objectionable. This still would only result in a fuel temperature of 1760°C, and an Inconel end cap temperature of 820°C. Since this temperature could be tolerated, no hazard is present.

Table A.1

(U) ANALYSIS OF HAZARDS DUE TO CAPSULE RUPTURE

(This table is Unclassified)

Accident Postulated	Probability	Resulting Hazard And Detection Methods
1. Rupture of outer containment (no others)	Credible	Water enters outer gas annulus. Steam formation results and cools secondary containment wall. Will have minor effect on fuel temperature. Temperature distribution will be upset and observale on temperature recorders. Capsule will have to be discharged.
2. Rupture of primary containment (no others)	Credible No previous failures of this containment	Failure will result in exchange of Ne from primary containment with He from the outer containment. May have slight effect on temperature distribution and may be detected via gamma calorimeter. No hazard involved.
3. Rupture of fuel containment (no others)	Credible Previous broach of similar containment resulted from thermocouple sheath failure; however, no leakage from containment occurred until thermocouples were severed under water during discharge of experiment. This resulted in water leaking into fuel compartment. No hazard involved other than loss of experimental results.	Previous failure went undetected during operation due to secondary containment integrity. Ne from primary containment may exchange with A in fuel containment which would result in lower fuel temperatures. CPM will be adjusted to compensate.

Table A.1 (Continued)

Accident Postulated	Probability	Resulting Hazard And Detection Methods
4. Lead tube rupture (no others)	Credible	High rate of He gas usage. If water enters lead tube it may lead to shorting of thermocouples, but water cannot enter any of capsule containments.
5. Sequential rupture of outer containment followed by primary containment failure (no others)	Credible, but a remote possibility	Temperature distribution will be upset in capsule by entry of water. Steam formation will cool primary containment shell. Due to reactor primary water coolant pressure (165 psi), corresponding saturated steam temperature will be ~366°F (183.6°C). Consequently, Inconel primary containment will reach temperature equilibrium with steam and no greater ΔT across can wall should exist than during normal operation (~30°F). Therefore, the thermal stress will not increase to cause rupture. Calculated normal thermal stress is 4950 psi compared to yield strength of 26,500 psi at 1200°F (~649°C). Corrosion is not a problem over the short period in which water leakage into gas annulus may go undetected.
6. Leakage of fission gases from fuel containment along or through thermocouples	Credible, but a remote possibility	Requires the failure of tungsten thermocouple thimble plus three seal failures or the longitudinal splitting of the thermocouple sheath continuing for over a minimum lengthof 1-1/4 inches. Fission gases will then be detected during lead tube purge during first purging operation thereafter.

Table A.1 (Continued)

Accident Postulated	Probability	Resulting Hazard And Detection Methods
7. Fuel temperature TC's EMF degradation followed by similar action or complete loss of C/A TC's	Incredible	W/Re TC's may very likely fail or degrade in EMF output. However, C/A TC's at this temperature are extremely reliable and outnumber W/Re TC's by 3:1 ratio. Such an incredible failure could be detected by individual pod temperature comparisons and previously obtained correlations with respect to CPM position. Normal CPM movement is based on C/A thermocouples.
8. Sequential rupture of: 1) Fuel containment 2) Primary containment 3) Outer containment	Credible, but extremely remote possibility	Outer containment failure followed by primary containment already treated in 5 above. Same arguments apply here. Resulting hazard is the slow decomposition of UC-ZrC fuel to oxide with acetylene formation. Fission products will be given up slowly to the capsule coolant water which is a portion of the closed primary water system.

A.8. HANDLING ACCIDENTS

(U) No hazards are anticipated due to mishandling. Damage could occur to the V-tube, the CPM, and the capsule if not given reasonable care but this in itself does not represent any hazard.

A.9. INSTRUMENT FAILURE

(U) Instrument failure due to loss of electrical power is covered under Section A.5, Loss of Electrical Power. Instrument failure due to malfunction may present specific problems which are individually analyzed.

A.9.1. Annunciator Failure

(U) Alarm conditions may exist but are brought to the operator's attention via EDLAS. The annunciator has a test button and the instrument should be checked as often as deemed practical, probably once per shift.

A.9.2. Recorder Failure

(U) The four-pen recorder is used as an aid in adjusting the capsule temperature and its failure does not incur any hazard. The EDLAS can be used to note controlling temperatures if necessary.

A.9.3. CPM Failure

(U) Failure of the CPM can be categorized in three conditions:

(1) Insability to move CPM.
(2) Loss of position indication.
(3) Uncontrolled CPM movement.

(U) The loss of movement ability does not present any hazard even if a reactor excursion occurs. This condition is covered in Sections A.6 and A.7. If for any reason the capsule temperature does rise and the CPM cannot be moved, protection still exists with the safety channels.

(U) Loss of position indication will not affect the continuation of capsule irradiation, since the capsule temperature is the controlling parameter. The position indication is only for reference purposes and the faulty indicator can be replaced or repaired during a reactor shutdown.

(U) An uncontrolled movement of the CPM towards the core may occur due to sticking relays. This is not a hazardous condition since a mechanical stop is present to prevent movement of the capsule into a high flux position.

(U) The following tabulation (Table A.2) outlines various CPM failure conditions, their cause and affect on the experiment, and remedial action. The CPM has been designed so that all of the repairs may be accomplished without going inside the reactor, with the exception of pivot bearing repair.

A.9.4. Flow Meter Failure

(U) If the flow meter or readout failed such that a low flow rate was indicated, the CPM would experience a fast out. If the failure resulted in not receiving a low flow alarm when such a condition actually existed, capsule protection would still exist with the safety channels.

A.10. CONTROL SYSTEM FAILURE

(U) This was included as part of the instrument failure section, Section A.9.3.

A.11. CHEMICAL REACTIONS

(U) All materials in contact with reactor water are either stainless steel or aluminum. All joints are either welded or flanged, with no braze materials of any kind used inside the reactor vessel that could be in contact with the primary water. Should the capsule containment fail, there are brazed seals that would come in contact with the water. If all capsule containments fail, the fuel would react with the primary water. This hazard is analyzed in Section A.4.3.

Table A.2

(U) CPM FAILURE ANALYSIS

(This table is Unclassified)

Failure	Cause	Effect	Remedy
1. CPM power failure	Loss of commercial power	Reactor scram	-
2. Drive motor inoperative	Locked rotor, bearing failure, open motor windings	Unable to move CPM	Replace motor
3. Motor coupling slippage	Loose set screw and loss of shaft key	Uncontrolled movement of CPM between in and out	Replace applicable parts
4. Uncoupling of Jactuator rod from CPM beam	Loss of clevis pin	Unable to move CPM	Replace clevis pin
5. Pivot bearing failure	Particles embedded in bearing surfaces	Possible loss of CPM movement	Remove V-tube-CPM assembly from reactor and replace bearing
6. Position indicator	a. Open transducer circuit b. Uncoupling of transducer armature rod	No position indication	a. Check out circuit b. Repair during reactor shutdown
7. Uncontrolled CPM movement	Sticking relays	Could move capsule toward mechanical stop	Repair or replace faulty relay

A.12. ACCIDENTS PECULIAR TO SYSTEM

A.12.1. Excess Temperature

(U) The capsule is designed to operate at a steady-state maximum temperature of approximately 1700°C in the fuel. No hazard to the reactor is expected to occur if these temperatures are exceeded by as much as 300°C as indicated in Sections A.6 and A.7; however, reliable interpretation of the experimental data for the irradiated specimens depends on an accurate knowledge of the temperature history to which the specimens are subjected during irradiation. It is therefore important, from the standpoint of the reliability of the experiment, to exercise control over the temperature in the capsule during irradiation.

A.12.2. Release of Radioactive Products

(U) Some radioactive products will be produced during the irradiation of these materials capsules. Parts of the irradiation capsule will become activated as a result of neutron bombardment. However, these are not expected to present any hazards from the standpoint of uncontrolled escape from the experiment during irradiation.

(U) The hazards associated with the activation products in the parts of the capsule will occur primarily during the discharge of the capsule from the reactor and subsequent handling.

A.13. SELECTION OF REACTOR POWER REDUCTION MODE

(U) The following modes of negative reactivity insertion are available:

(1) SCRAM - dropping of all shim safety rods.

(2) Junior SCRAM - dropping of one or more selected shim safety rods.

(3) Fast reverse - moving of all active shim safety rods at a speed of approximately 9 inches per minute.

(4) Slow reverse - moving all active shim safety rods at a speed of approximately 3 inches per minute.

(5) Fast setback - reduction in power on a 50 to 20-second period to 0.03 percent of full power.

(6) Slow setback - reduction in power on 110 to 55-second period of approximately 0.03 percent of full power.

(U) The following creiteria were used in selecting the appropriate shutdown mode:

(1) The selected mode should decrease the flux (and capsule power production) at a rate great enough to prevent an over-temperature and possible rupture of all three containments due to loss of capsule coolant flow.

(2) The mode should cause a minimum perturbation on reactor operation.

(U) Calculations were performed using the above criteria, and the results indicate that a reactor slow setback is adequate protection for the capsules under all rod positions.

APPENDIX B.I

FUEL TEMPERATURE UNCERTAINTY DETAILS

B.I.1. Fuel Thermocouple Calibration and Drift

(U) The calibration is felt to be accurate to ±25°C. Arbitrarily take the drift as 5% of 1650°C = ±85°C. For long term operation the thermocouple calibration uncertainty is:

$$\sqrt{85^2 + 25^2} = \pm 89^\circ C$$

B.I.2. Heat Meter Thermocouple Calibration and Drift

(U) Chromel-alumel thermocouples have a calibration accuracy of ±3°C to 650°C (Temperature - Its Measurement and Control in Science and Industry) with an estimated drift of ±1/2°C.

Or the long-term error is given by:

$$\sqrt{3^2 + 1/2^2} = \pm 3.0^\circ C = \pm 5.4^\circ F.$$

From the thermal analysis

$T_{Inc} = 459^\circ C = 857^\circ F$ (Inconel temperature)

$T_{SS} = 92^\circ C = 197^\circ F$ (stainless steel temperature)

$T_W = 1640^\circ C = 2975^\circ F$ (tungsten temperature).

For a typical location in the capsule.

By radial heat balance and linearizing the thermal radiation conductance:

$$\left.\begin{aligned} q' &= H_{He}(T_{Inc} - T_{SS}) \\ q' &= H_{Ne}(T_W - T_{Inc}) \end{aligned}\right\}$$

$$T_W = \frac{q'}{H_{Ne}} + T_{Inc}$$

$$T_W = \frac{H_{He}}{H_{Ne}} (T_{Inc} - T_{SS}) + T_{Inc}$$

$$T_W = T_{Inc} \left(1 + \frac{H_{He}}{H_{Ne}}\right) - \frac{H_{He}}{H_{Ne}} \times T_{SS}.$$

Let $H = \frac{H_{He}}{H_{Ne}}$,

substituting

$$2975 = 857 (1 + H) - 197H$$
$$2975 = 857 + 857H - 197H$$
$$2118 = 660H,$$
$$3.21 = H$$

or

$$T_W = 4.21\ T_{Inc} - 3.21\ T_{SS}$$

differencing

$$\Delta T_W = 4.21\ \Delta T_{Inc} - 3.21\ \Delta T_{SS}. \qquad (1)$$

(U) Equation (1) is the difference equation expressing the effects of errors in T_{Inc} and T_{SS} upon the determination of T_W through use of the heat meter. The error due to the T_{Inc} reading is

$$\Delta_{TW} = 4.21 \times \pm 5.4 = \pm 23^{\circ}F = \pm 12.6^{\circ}C,$$

and due to the T_{SS} reading,

$$\Delta T_W = 3.21 \times \pm 5.4 = \pm 17.3^{\circ}F = \pm 9.6^{\circ}C.$$

B.I.3. Thermal Radiation Properties

(U) For the neon gap, the radiant flux is 16.4 W/cm^2 or 36.5% of the total.

(U) For the helium gap, the radiant heat transfer is 2.7% of the total.

(U) If the effective emittance of the helium gap changes by a factor of 2.0, then we can be in error by as much as 1/2 x 2.7% = 0.0135 of the total flux.

(U) This will affect $(T_{Inc} - T_{SS}) = 660^{\circ}F$ by

$$660 \times 0.0135 = 9.9^{\circ}F.$$

This corresponds to an error in fuel temperature of

$$\Delta T_W = 4.21 \times 9.9 = 41.8^{\circ}F = 23^{\circ}C$$

according to equation (1).

(U) For the neon gap, assume the tungsten surface to remain unchanged with respect to radiation properties and the Inconel emittance to change by an arbitrary factor of 2.0.

(U) This will produce a change in fuel temperature of 64°C to maintain the same heat flux (45 W/cm^2 total).

B.I.4. Gas Composition Changes

(U) A maximum rate of 2×10^{-10} scc/sec of helium into the neon gap is specified. If the irradiation time is 2000 hours,

$$V = 2 \times 10^{-10} \times 2000 \times 3600 = 1.44 \times 10^{-3} \text{ scc.}$$

The neon volume is approximately 40 cm^3 or the volume dilution of the neon by helium is about 4×10^{-5}. This should produce a negligible change in the thermal transport properties of the neon. A similar result is obtained for leakage of the neon into the helium.

B.I.5. Angular Variations in Spacing (Eccentricity)

(U) The spacing pins will provide for a negligible distortion of the radial temperature profile (compared to the power skew).

B.I.6. Mode of Averaging of Axial and Radial Gradients

(U) The radial gradient for a 2:1 power skew at 45 W/cm^2 surface flux is estimated to be $108^\circ F$. We can take this as a variation about a mean temperature of $\pm 54^\circ F$.

For $T_{mean} = 2975^\circ F$, $T_{max} = 2975 + 54 = 3029^\circ F = 3489^\circ R$

$T_{min} = 2975 - 54 = 2921^\circ F = 3381^\circ R$.

Since the thermocouple is radiantly coupled to the fuel, the sensed temperature varies with the mean T^4.

$$\overline{T^4} = \frac{3489^4 + 3381^4}{2} = 139.5 \times 10^{12}.$$

Then

$$\sqrt[4]{\overline{T^4}} = 3435^\circ R = 2975^\circ F,$$

or there is no radial averaging error.

(U) The axial gradient in the fuel temperature produces a heat flow in the thermocouple which causes an error in temperature measurement.

(U) From the thermal analysis of the thermocouple well, at the center plane,

$$\frac{\Delta T}{\Delta X} = 2400^\circ F/ft \ ;$$

if we take the thermocouple as a fin exchanging heat with its surroundings,

$$\lambda = \sqrt{\frac{kA}{hP}} = \text{thermal relaxation length.}$$

Take

$$k = k_{BeO} = 9 \text{ Btu/hr-ft-}^{\circ}\text{R},$$

$$h = 4\epsilon\sigma T^3 = 4(0.25)0.171 \times 10^{-8}(3740)^3 = 87 \text{ Btu/hr}^2\text{-}^{\circ}\text{R}.$$

Then λ for an 0.040 o.d. thermocouple is:

$$\lambda = \sqrt{\frac{9\pi(0.04)^2}{12 \times 87\pi(0.04) \times 4}} = 9.3 \times 10^{-3} \text{ ft.}$$

Then ΔT (in λ) = $2400 \times 9.3 \times 10^{-3} = 22^{\circ}\text{F}$.

Refer to the figure

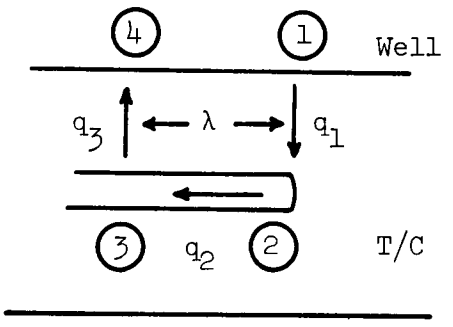

$$q_1' = hP(T_1 - T_2)$$

$$q_2' = \frac{kA}{\lambda}(T_2 - T_3)$$

$$q_3' = hP(T_3 - T_4)$$

$$q_1' = q_2' = q_3'$$

$$T_1 - T_4 = \Delta T \text{ (in } \lambda) = 22^{\circ}\text{F}.$$

Solving the above equations

$$T_1 - T_2 = 0.2^{\circ}\text{F} \approx 1^{\circ}\text{F}$$

or the error due to the axial gradient is less than 1°F.

B.I.7. Axial Heat Flow in the Inconel Can

(U) The Inconel containment can is 0.895 o.d. x 0.693 i.d. in the capsule region. The area, $A = \frac{\pi}{4}(0.895^2 - 0.693^2) = 0.251$ in.^{2} From the thermal analysis, the temperature gradients at the top and bottom of the capsule region were determined.

$$\frac{\Delta T}{\Delta X}_{top} = 5310^{\circ}F/ft.$$

$$\frac{\Delta T}{\Delta X}_{bottom} = 13{,}500^{\circ}F/ft.$$

The k_{Inc} is taken as 11.7 Btu/hr-ft-$^{\circ}$R.

Then

$$q_{top} = ka\frac{\Delta T}{\Delta X} = \frac{11.7(0.251)}{144}(5310) = 108 \text{ Btu/hr} = 32 \text{ W.}$$

$$q_{bottom} = \frac{11.7(0.251)}{144}(13{,}500) = 276 \text{ Btu/hr} = 81 \text{ W.}$$

$$\sum q_{axial} = 81 + 32 = 113 \text{ W.}$$

The total heat produced in the capsule is 1075 W, including gamma heat at 1 W/gm. The gamma heating of the Inconel produces 65.4 W at 1 W/gm, or the total heat coming through the Inconel without end losses is 65.4 + 1075 = 1140.4 W. The heat flux error would be 113/1140 = 9.9%. The ΔT_{error} is 0.099 (2975 - 857) = 210°F = 117°C. It will be necessary to make a correction for axial heat flow. Assume this correction to be good to ±20%; then

$$\Delta T_{error} = \pm 0.2(117) = \pm 23^{\circ}C$$

B.I.8. Thermocouple Radial Location Error

(U) The stainless steel (outer) containment can is 1.125 o.d. x 0.921 i.d. The heat flux coming to it from the Inconel is 338 W/cm = 35,200 Btu/hr-ft.

(U) The corresponding temperature drop is

$$\Delta T = \frac{q' \ln \frac{r_2}{r_1}}{2\pi k} = \frac{35{,}200 \ln \frac{1.125}{0.921}}{2\pi(11)} = 101^{\circ}F.$$

The gamma heat rate in the stainless steel is 18.2 W/cm.

So $$\Delta T_{\gamma} = 101 \times \frac{18.2}{338} \times \frac{1}{2} = 3^{\circ}F.$$

$$\sum \Delta T = 3 + 101 = 104^{\circ}F.$$

Assume the thermocouple junction can be located to within 10% of the wall thickness (± 0.010 in.),

then

$$\Delta T_{loc} = \pm 0.1 \times 104 = \pm 10.4^{\circ}F.$$

From equation (1)

$$\Delta T_{error} = 3.21 \times \pm 10.4 = \pm 33^{\circ}F = \pm 19^{\circ}C.$$

For the Inconel can, the through lineal heat rate is 224 W/cm = 23,300 Btu/hr-ft. This results in a ΔT of $81^{\circ}F$.

The gamma heat generated in the Inconel at 1 W/gm produces a ΔT of $2.5^{\circ}F$; then $\sum \Delta T = 81 + 3 = 84^{\circ}F = 47^{\circ}C$, for a 10% location uncertainty, this results in a temperature uncertainty of $\pm 5^{\circ}C$. According to equation (1),

$$\Delta T_{error} = \pm 5 \times 4.21 = \pm 21^{\circ}C.$$

B.I.9. Fuel Temperature Error Due to Gamma Heating of Thermocouple

(U) Each thermocouple junction terminates in a tantalum cylinder 0.040 in. in diameter. The thermocouple is enclosed in an 0.062 o.d. tungsten tube with an 0.009 in. wall. Gamma heating rate is 1 w/gm.

$$V'_{Ta} = \frac{\pi}{4} (0.04 \times 2.54)^2 \frac{cm^3}{cm} = 0.00814 \frac{cm^3}{cm} .$$

$$Q'_{Ta} = 0.00814 \frac{cm^3}{cm} \times 16.6 \frac{gm}{cm^3} \times 1 \frac{W}{gm} = 0.135 \text{ W/cm} .$$

$$V'_{W} = \pi(0.062)\ (0.009)\ (2.54^2) \frac{cm^3}{cm} = 0.0113 \frac{cm^3}{cm} .$$

$$Q'_{W} = 0.0113 \frac{cm^3}{cm} \times 19.4 \frac{gm}{cm^3} \times 1 \frac{W}{gm} = 0.219 \frac{W}{cm} .$$

$$\sum Q' = 0.219 + 0.135 = 0.354 \text{ W/cm} = 37.9 \text{ Btu/hr-ft.}$$

Estimate h_r for T = 1650°C = 3460°R.

$$\epsilon_W = 0.24 \text{ or } \epsilon_{effective} = 0.12 \text{ for 2, parallel surfaces.}$$

$$h_r = 4\sigma\epsilon T^3$$

$$h_r = 4(0.171)10^{-8}\ (0.12)(3460)^3 = 34 \text{ Btu/hr-ft}^2\text{-}^\circ\text{R}$$

(U) Assume that each thermocouple "sees" the inside of the well over 2/3 of its surface--

$$A' = \frac{2}{3} \frac{\pi(0.062)}{12} = 0.0108 \frac{ft^2}{ft} .$$

$$\Delta T = \frac{Q'}{h_r A'} = \frac{37.9}{34 \times 0.0108} = 10.3^\circ F = 6^\circ C.$$

Estimate the radial ΔT in the Ta block,

$$Q = 4\pi Lk\ \Delta T .$$

$$\Delta T = \frac{Q}{4\pi Lk} = \frac{0.135 \times 3.413 \times 2.54 \times 12}{4\pi \times 42} = 0.026^\circ F.$$

This is negligible.

(U) The radial clearance between the Ta block and the tungsten tube is 0.001 in. This is filled by argon with k = 0.038 Btu/hr-ft-°F.

$$Q = kA \frac{\Delta T}{\Delta r}$$

$$\Delta T = \frac{\Delta r\, Q}{kA} = \frac{0.001 \text{ in.} \times 0.135 \times 3.413 \times 2.54 \times 12 \frac{\text{Btu}}{\text{hr-ft}}}{0.038 \frac{\text{Btu}}{\text{hr-ft-}^\circ\text{F}} \times \pi\ (0.040)\ \frac{\text{in}^2}{\text{in.}}}$$

$$\Delta T = 3^\circ\text{F} = 1.7^\circ\text{C},$$

or the total temperature error is about [6 + 1.7 = 7.7] or 8°C.

B.I.10. Fuel Thermal Conductivity Uncertainty

(U) The temperature drop calculated across the fuel is 46°C. If we assume that the fuel conductivity is known to ±50%, then the uncertainty in the temperature drop is

$$\Delta T_F = \pm 0.5\ (46) = \pm 23^\circ\text{C}.$$

APPENDIX B.II

FISSION POWER UNCERTAINTY DETAILS

B.II.1. Capsule Heat Meter Thermocouple Calibration and Drift

(U) The long-term error in a single thermocouple reading is estimated to be $\pm 5.4^{\circ}F$. The probable error in reading the difference in two readings is

$$\pm \sqrt{2} \times 5.4 = \pm 7.6^{\circ}F.$$

Therefore,

$$\Delta q''_{error} = \frac{\pm 7.6}{857 - 197} = \frac{\pm 7.6}{660} = \pm 1.15\%.$$

B.II.2. Heat Transfer Gap Spacing

(U) The helium gap spacing, in operation, is nominally 0.011 in. radially. Manufacturing tolerances will be held to ensure that variations in gap spacing do not exceed 0.001 in. radially, including the effect of eccentricity. This results in

$$\Delta q''_{error} = \frac{\pm 0.001}{0.011} = \pm 9.1\%.$$

B.II.3. Gap Transport Properties

(U) It can be shown that a factor of 2.0 change in effective emittance changes T_{Inc} by $9.9^{\circ}F$. This results in

$$\Delta q''_{error} = \frac{\pm 9.9}{857 - 197} = \frac{\pm 9.9}{660} = \pm 1.5\% .$$

The gas composition change was shown above to have a negligible effect on gap transport properties.

B.II.4. Gamma Heat Meter Uncertainties

(U) The lineal gamma heating rates in the assembly components were estimated, at 1 W/gm gamma rate and 45 W/cm^2 surface flux, to be

Location	Lineal Heating Rate
Capsule	24.0 W/cm
Inconel Can	13.8
Stainless Steel Can	18.2
Fission Heat	200.0
	256.0 W/cm Total

of this $\frac{q_{fission}}{q_{total}} = \frac{200}{256} = 78\%$.

(U) Or gamma heating accounts for 22% of the total heat. Because of this, any error in determining gamma heat cannot affect the total heat measured by more than 22% of the amount measured.

(U) The electric heater in the gamma heat meter is used for calibration. There is an uncertainty associated with measurement of the electrical power input. Assume that the voltage and current can each be measured to ±3%. This gives an uncertainty in the power of ±6%. Since this error applies to 22% of the total heat,

$$\Delta q''_{error} = \pm 6\% \times 0.22 = \pm 1.3\%.$$

For the gamma heat meter, thermocouple calibration and gap size are eliminated as sources of uncertainty because of the ability to recalibrate electrically as often as desired.

(U) Reproducibility of the temperature recorder reading is taken as ±1% of full scale, assumed to be 800°F. The uncertainty here is, then, ±8°F. The temperature drop in the heat meter gap is 110°F; so,

$$\Delta q''_{error} = \frac{\pm 8}{110} \times 0.22 = \pm 1.6\%.$$

Activation of the heat meter material is estimated to produce 0.18 W/gm or less.

Then,

$$\Delta q''_{error} = \frac{0.18}{1.18} \times 0.22 = 3.3\% = \pm 1.7\% \text{ about some mean.}$$

(U) End losses from the heat meter represent an unmeasurable source of error. These are calculated to be less than 1% of the gamma heat at 1 W/gm.

B.II.5. Axial Heat Loss Uncertainty

(U) There is axial heat flow in the Inconel can and from the fuel capsule. Axial heat flow in the stainless steel can is negligible.

(U) The axial heat flow in the Inconel can is estimated to be 113 W. Assume that these axial losses can be calculated to ±20% uncertainty; or 113 x ±20% = ±23W. Since the capsule heat is about 1075 W,

$$\Delta q''_{error} = \frac{\pm 23}{1075} = \pm 2.1\% \ .$$

(U) The heat loss from the bottom of the capsule by radiation is estimated to be 10 W. The stem gradient is 23,200 ^{o}F/ft from the thermal analysis.

$$A_{stem} = \frac{\pi}{4} (0.595^2 - 0.545^2) = 0.0448 \text{ in.}^2$$

Take

$$k_{stem} = 60 \text{ Btu/hr-ft-}^{o}\text{R} \ ;$$

then,

$$q_{stem} = \frac{60(0.0448)(23{,}200)}{144} = 434 \text{ Btu/hr} = 127 \text{ W.}$$

$$q_{stem} + q_{bottom} = 127 + 10 = 137 \text{ W.}$$

Assume that these end losses from the capsule can be estimated to ±50%; then,

$$\Delta q''_{error} = \frac{\pm 137}{1075} \times 0.50 = \pm 6.4\%.$$

B.II.6. Radial Location Uncertainty for Heat Meter Thermocouples

(U) The location errors are $\pm 10^{\circ}F$ for the thermocouples in stainless steel and $\pm 5^{\circ}F$ for thermocouples in the Inconel containment can. The probable error in their difference is:

$$\Delta T_{error} = \sqrt{10^2 + 5^2} = \pm 11.2^{\circ}F.$$

This is equivalent to

$$\Delta q''_{error} = \frac{\pm 11.2}{660} = \pm 1.7\%.$$

DISTRIBUTION LIST

1. NASA Lewis Research Center
Attn: Librarian
21000 Brookpark Road
Cleveland, Ohio 44135
For: J. E. Dilley, MS 302-1 (1)
J. W. R. Creagh, MS 49-2 (1)
J. R. Smith, MS 49-2 (1)
R. Breitwieser, MS 302-1 (1)
R. Mather, MS 500-309 (1)
N. Saunders, MS 105-1 (1)
Technology Utilization Office, MS 3-19 (1)
R. Migra, MS 49-2 (1)
J. Ward, MS 309-1 (1)
R. Forman, MS 302-1 (1)
B. Lubarsky, MS 500-201 (1)
T. A. Moss, MS 500-201 (1)
Report Control, MS 5-5 (1)
Library, MS 3-7 (1)
V. Hlavin, MS 3-14 (1)

2. NASA Washington
Attn: Document Control
600 Independence Avenue, S.W.
Washington, D. C. 20546
For: James J. Lynch, Code RNP (1)
Fred Schulman, Code RNP (1)

3. Jet Propulsion Laboratory
California Institute of Technology
Attn: Central Document Control
4800 Oak Grove Drive
Pasadena, California 91103
For: Jerry Davis (1)
Peter Rouklove (1)

4. NASA Manned Spacecraft Center
Attn: Technical Information Program Division
Houston, Texas 77058
For: Bobby Bragg (1)

5. NASA Electronics Research Center
Attn: Librarian
575 Technology Square
Cambridge, Massachusetts 02139
For: F. C. Schwarz, Code CP (1)

6. NASA Ames Research Center
Attn: Document Control Section
Moffett Field, California 94035
For: Library (1)

7. NASA Goddard Space Flight Center
Attn: Security Officer 236
Greenbelt, Maryland 20771
For: Joseph Epstein (1)
Library (1)

8. NASA Langley Research Center
Attn: Librarian
Langley Field, Virginia 23365
For: Library (1)

9. NASA Marshall Space Flight Center
Attn: Library
Huntsville, Alabama 35812
For: Library (1)

10. NASA Scientific Technical Information Facility
Attn: NASA Representative
P. O. Box 33
College Park, Maryland 20740
For: NASA Representative (2 + Repro)

11. Battelle Memorial Institute
Columbus Laboratories
Attn: Security Officer
505 King Avenue
Columbus, Ohio 43201
For: Don Kizer (1)
Don Keller (1)

12. Battelle Memorial Institute
Pacific Northwest Laboratories
Attn: Technical Information Center
P. O. Box 999
Richland, Washington 99352
For: Library (1)

13. The Boeing Company
Attn: Aerospace Library 8K38
P. O. Box 3999
Seattle, Washington 98124
For: Library (1)

14. Naval Ship Systems Command
Department of the Navy
Washington, D. C. 20360
For: B. B. Rosenbaum, Code 3422 (1)
E. P. Lewis, Code 08 (1)

15. McDonnell Douglass Aircraft Corporation
Missile & Space Engineering Nuclear Research (A-260)
Attn: Library
3000 Ocean Park Boulevard
Santa Monica, California 90405
For: Library (1)

16. Electro-Optical Systems, Inc.
Attn: Security
300 North Halstead Avenue
Pasadena, California 91107
For: A. Jensen (1)

17. General Electric Company
Missile & Space Division
Attn: Document Control Center
P. O. Box 8555
Philadelphia, Pennsylvania 19101
For: ANSE (1)

18. General Electric Company
Knolls Atomic Power Laboratory
Attn: Document Custodian
P. O. Box 1072
Schenectady, New York 12301
For: R. Ehrlich (1)

19. General Electric Company
Nuclear Systems Programs
Attn: J. W. Stephenson
P. O. Box 15132
Cincinnati, Ohio 45215
For: J. A. McGurty (1)

20. General Electric Company
Research Development Center
Attn: Document Control Center
P. O. Box 8
Schenectady, New York 12301
For: Volney C. Wilson (1)

21. General Electric Company
Electronic Components Division
Attn: Document Control
One River Road
Schenectady, New York 12301
For: D. A. Wilbur, Mgr., Tube Research (1)

22. General Electric Company
Atomic Power Equipment Department
Attn: Alleen Thompson
P. O. Box 1131
San Jose, California 95108
For: J. Danko (1)
B. G. Voorhees (1)
J. Van Hoomissen (1)

23. North American Aviation, Inc.
S&ID Division
Attn: Document Control
12214 Lakewood Boulevard
Downey, California 90241
For: C. L. Gould (1)

24. North American Aviation, Inc.
Atomics International
Attn: Document Control
P. O. Box 309
Canoga Park, California 91304
For: Robert C. Allen (1)
Charles K. Smith (1)

25. Oak Ridge National Laboratory
Attn: Library
Oak Ridge, Tennessee 37831
For: Library (1)

26. Office of Naval Research
Power Branch
Department of the Navy
Attn: Code 429
Washington, D. C. 20360
For: CDR O. J. Loper (1)

27. United Aircraft Corporation
Pratt & Whitney Division
Attn: Document Control
400 Main Street
East Hartford, Connecticut 06108
For: Library (1)

28. The Rand Corporation
Attn: Correspondence Cpntrol
1700 Main Street
Santa Monica, California 90406
For: Ben Pinkel (1)

29. Republic Aviation Corporation
Fairchild Hiller Division
Attn: Engineering Library
Farmingdale, L. I., New York 11735
For: Alfred Schock (1)
B. Wolk (1)

30. Aerojet General Corporation
San Ramon Plant
Attn: Sandra Johnson
P. O. Box 86
San Ramon, California 94583
For: Library (1)

31. Aerospace Corporation
Attn: Reports Acquisition Group
P. O. Box 95085
Los Angeles, California 90045
For: Library (1)

32. AF Cambridge Research Laboratory
Attn: Chief S&TIS
L. G. Hanscom Field
Bedford, Massachusetts 01730
For: CRZAP (1)

33. AFWL (WLIL)
Kirtland AFB New Mexico 87117
For: WLIL (1)

34. Flight Vehicle Power Branch
AF Aero Propulsion Laboratory
Wright-Patterson AFB Ohio 45433
For: A. E. Wallis (1)

35. Headquarters
Space & Missile Systems Org. (SMTS)
AF Unit Post Office
Los Angeles, California 90045
For: SMTS (1)

36. General Motors Corporation
Research Laboratories
Attn: Security Officer
P. O. Box 866
Warren, Michigan 48090
For: F. E. Jamerson (1)

37. Institute for Defense Analyses
Attn: Document Control
400 Army-Navy Drive
Arlington, Virginia 22202
For: R. C. Hamilton (1)

38. Radio Corporation of America
Attn: Master Document Control
P. O. Box 1140
Lancaster, Pennsylvania 17601
For: Fred Block (1)

39. Babcock & Wilcox Company
Boiler Division
Attn: Document Custodian
5061 Fort Avenue
Lynchburg, Virginia 24505
For: Library (1)

40. Los Alamos Scientific Laboratory
Attn: Mail & Records Group
P. O. Box 1663
Los Alamos, New Mexico 87544
For: G. M. Grover (1)
R. Salmi (1)

41. Marquardt Corporation
Attn: Document Control Station
16555 Saticoy Street
P. O. Box 2013
Van Nuys, California 91409
For: A. N. Thomas (1)

42. Lockheed Missile & Space Company
Attn: Document Control Station
P. O. Box 504
Sunnyvale, California 94088
For: H. H. Greenfield (1)

43. TRW Systems
Attn: Manager Technical Information Center
One Space Park
Redondo Beach, California 92078
For: M. N. Sloane, Chief Librarian (1)

44. U. S. Army ERDL
Attn: Security Officer
Fort Monmouth, New Jersey 07703
For: Emil Kittl (1)

45. Mr. Donald S. Beard
Space Nuclear Systems Division
U. S. Atomic Energy Commission
Washington, D. C. 20545 (1)

46. Mr. Patrick O'Riordan
Space Nuclear Systems Division
U. S. Atomic Energy Commission
Washington, D. C. 20545 (1)

47. Mr. J. M. O'Leary
U. S. Atomic Energy Commission
Technical Reports Library
Washington, D. C. 20525 (3)

48. U. S. Atomic Energy Commission
Division of Technical Information Extension
P. O. Box 62
Oak Ridge, Tennessee 37831 (3)

49. Varian Associates
Attn: Document Control
611 Hansen Way
Palo Alto, California 94303
For: Ira Weismann (1)

50. Westinghouse Electric Corporation
Astro-Nuclear Laboratory
Attn: Document Custodian
P. O. Box 10864
Pittsburgh, Pennsylvania 15236 (1)

51. Thermo Electron Engineering Corporation
Attn: Security Officer
P. O. Box 482
Waltham, Massachusetts 02154
For: George Hatsopoulos (1)
Robert Howard (1)